UNIVERSITÉ DU QUÉBEC À MONTRÉAL

THÈSE PRÉSENTÉE À L'UNIVERSITÉ DU QUÉBEC À CHICOUTIMI
COMME EXIGENCE PARTIELLE
DU DOCTORAT EN RESSOURCES MINÉRALES
OFFERT À
L'UNIVERSITÉ DU QUÉBEC À MONTRÉAL
EN VERTU D'UN PROTOCOLE D'ENTENTE AVEC
L'UNIVERSITÉ DU QUÉBEC À CHICOUTIMI

PAR

GABRIEL VOICU

GÉOLOGIE, GÉOCHIMIE ET METALLOGÉNIE DU GISEMENT D'OR
OMAI, BOUCLIER GUYANAIS, AMÉRIQUE DU SUD

GEOLOGY, GEOCHEMISTRY AND METALLOGENY OF THE OMAI
GOLD DEPOSIT, GUIANA SHIELD, SOUTH AMERICA

MAI 1999

0-612-43281-5

Canada

RÉSUMÉ

La mine d'or d'Omai est située dans le Supergroupe Barama-Mazaruni, qui fait partie de la ceinture paléoprotérozoïque de roches vertes du Bouclier guyanais. La séquence stratigraphique se compose de cycles de roches volcaniques mafiques (et de corps mafiques-ultramafiques sous-volcaniques génétiquement reliés) à felsiques, intercalées avec des sédiments terrigènes. La séquence volcano-sedimentaire a été percée par un stock quartzo-monzodioritique (le stock d'Omai), ainsi que par plusieurs filons de porphyres quartzo-feldspathiques et rhyolitiques de formes irrégulières. Des dikes et des sills mafiques post-minéralisation se sont mis en place au Mésoprotérozoïque et au Trias. La séquence volcano-sédimentaire de Barama-Mazaruni a été métamorphisée au sous-faciès des schistes verts inférieur. La structure locale est relativement simple et consiste en deux phases de déformation (D1 et D2). La phase D1 a produit une foliation régionale fortement pentée ayant une direction ESE-ONO ainsi que des cisaillements ductiles sub-parallèles à la foliation régionale. La phase D2 a plutôt produit une fracturation cassante/ductile a pendage modéré et disposée perpendiculairement aux zones de cisaillement de la phase D1. Les structures D2 représentent les principales voies d'accès des fluides minéralisateurs.

Le gisement d'Omai se compose de deux zones aurifères distinctes, exploitées depuis 1992 dans des fossees à ciel ouvert appelées *Fennell* et *Wenot*. La minéralisation de *Fennell* est reliée principalement au stock d'Omai et, en moindre volume, dans les roches volcaniques encaissantes (basaltes tholéiitiques et andésites calco-alcalines). La minéralisation de *Wenot* est principalement associée à des dikes tabulaires de porphyres quartzo-feldspathiques et de rhyolites fortement silicifiés, et localement à des andésites et métapelites.

Les caractéristiques géologiques et les données géochronologiques des deux zones minéralisées suggèrent qu'elles sont reliées génétiquement et représentent un même évènement métallogénique corrélable à la dernière phase de déformation cassante-ductile associée à l'orogénèse trans-amazonienne il y a 2.0 Ga.

Les veines aurifères sont subhorizontales et subverticales. Les veines subhorizontales ont été divisées en trois systèmes: 205°-215°/15-35°NO, 120°-140°/15°-35°SO et un système à direction variable et pendage de 5-15° qui longe le contact nord du stock d'Omai. Ces systèmes de veines sont essentiellement confinés aux roches magmatiques felsiques (le stock d'Omai, les dikes de porphyres quartzo-feldspathiques et de rhyolites), à l'exception du troisième système qui se propage uniquement dans les basaltes tholéiitiques de la zone *Fennell*. La majorité des veines se pincent abruptement au contact des roches volcano-sédimentaires encaissantes plus

ductiles. L'épaisseur des veines varie de quelques millimètres à 0.8 m. Dans la zone *Fennell*, les veines subhorizontales montrent peu de variation de direction et pendage, tandis que dans la zone *Wenot* elles ont des directions et pendages aléatoires décrivant l'aspect typique en "stockwork".

Les veines subverticales recoupent tous les contacts stratigraphiques. Elles sont moins abondantes que les veines subhorizontales. Les relations de recoupement en alternance entre les veines subhorizontales et subverticales suggèrent que leur mise en place était simultanée. Les réseaux de veines sont de type fentes de tension ("crack-seal" et "cisaillement") et de type brèches. Certaines caractéristiques texturales des veines à Omai sont comparables avec celles décrites dans les gisements d'or orogénique archéens, tandis que d'autres sont semblables aux textures décrites dans les gisements épithermaux cénozoïques des régions circum-pacifiques.

La minéralogie des veines comprend principalement, en ordre d'abondance relative, du quartz, carbonates (calcite, ankérite), scheelite, or natif, et plusieurs espèces de sulfures et tellurures. La plupart des phases métalliques et de gangue ont précipités à basse température (entre 120 et 260°C), dans un milieu chimique situé à la limite entre oxydant et réducteur. Les premiers fluides hydrothermaux enrichis en CO_2, W, et Na ainsi que les fluides subséquents enrichis en S ont joués un rôle important dans le transport et dépôt de l'or. Les mécanismes probables qui ont influencés le dépôt de l'or incluent: 1) le refroidissement des fluides minéralisateurs; 2) la composition chimique des épontes et; 3) la perméabilité de l'éponte. L'efficacité de l'intéraction fluide-roche et la diminution graduelle de la fO_2 et du H_2S dans les solutions hydrothermales ont favorisé le dépôt de l'or et des sulfures/tellurures.

Les scheelites des veines aurifères ont des rapports isotopiques $^{87}Sr/^{86}Sr$ variant entre 0.7019-0.7021 et des valeurs $\delta^{18}O$ entre 3.8 et 4.8‰, qui suggèrent des températures et des compositions isotopiques constantes des solutions hydrothermales. Les isotopes d'oxigène mesurés dans le quartz varient entre 13.2 et 14‰ et sont identiques aux rapports isotopiques mesurés dans des carbonates (moyenne de 13.8‰ pour la calcite et 14.4‰ pour l'ankérite). Les isotopes du carbone des carbonates varient entre +1.7 et 4.7‰. Les valeurs de $\delta^{18}O$ des fluides hydrothermaux se situent entre +5.3 et −2.7‰ et les valeurs de δD entre −52 et +18‰.

Les isotopes radiogéniques et stables des deux principaux types de veines suggèrent que les fluides minéralisateurs proviennent de deux sources différentes: 1) d'origine mantéllique et/ou en provenance de la partie inférieure de la croûte continentale, qui ont interragit avec les roches volcaniques mafiques locales et; 2) d'origine superficielle (eau marine ou météorique). Les conditions physico-chimiques de

dépôt de la minéralisation à Omai (basse température, pression, salinité, et contenu en CO_2, pH légèrement acide à neutre, fugacités modérées de l'oxygène et du soufre, fugacité élevée des tellurures), l'implication de l'eau de surface, la présence des structures hôtes de la minéralisation de nature essentiellement cassante et la localisation dans un terrain faiblement métamorphisé sont autant de critères permettant de classer Omai dans la catégorie des gîtes épithermaux. D'autres caractéristiques majeures tels que: le style d'altération; le cadre géodynamique; l'emplacement tardi-orogénique/syn- à tardi-tectonique; la présence des fluides d'une source profonde et; de manière moins directe, la paragénèse minéralogique se rattachent à la définition des gîtes mésothermaux plus profonds. La superposition des caractéristiques épi- et mésothermales d'Omai correspond donc à la partie supérieure du "continuum model" proposé pour les gisements archéens de type "gold-only" et définie comme le domaine crustal dit épizonal. Omai serait donc **un premier exemple de gîte orogénique aurifère d'âge paléoprotérozoïque de type épizonal associé aux granitoïdes et aux roches vertes**. Il représente un équivalent de ce type de gîte ayant été décrit uniquement dans certains cratons archéens (Yilgam et Zimbabwe).

Mots clé: Guyana, Paléoprotérozoïque, or, géochimie, métallogénie

ABSTRACT

The Omai gold mine is located in the Barama-Mazaruni Supergroup, part of the Paleoproterozoic greenstone belt of the north-central Guiana Shield. The lithological sequence consists of mafic volcanic (and genetically related subvolcanic mafic-ultramafic bodies) to felsic volcanic cycles with intercalated sediments. The volcano-sedimentary unit was intruded by a quartz monzodiorite plug (the Omai stock) and several irregularly-shaped quartz-feldspar porphyry and rhyolite dikes. Post-mineralization mafic dikes and sills were intruded discontinuously from Mesoproterozoic to Triassic. The Barama-Mazaruni volcano-sedimentary sequence has been metamorphosed to lower greenschist facies. The local structure is relatively simple and consists of two deformational phases (D1 and D2). D1 phase resulted in the ESE-WNW trending/steeply dipping regional scale foliation and ductile shear zones, whereas the D2 event caused brittle±ductile fracturing with moderate dips, oriented perpendicularly to D1 shear zones. D2 structures provided the main pathways for the mineralizing fluids.

The Omai deposit consists of two gold mineralized zones exploited in open pit operations referred to as *Fennell* and *Wenot*. *Fennell* mineralization is mainly hosted by the Omai stock and to a lesser extends by the volcanic rocks (tholeiitic basalts and calc-alkaline andesites). *Wenot* mineralization is mainly hosted by tabular quartz-feldspar porphyry dikes as well as by strongly silicified rhyolite dikes, and subordinately by andesites and metapelites.

The geological features and geochronological data of these ore zones suggest that they are genetically related and represent a contemporaneous metallogenetic event related to the last brittle-ductile phases of the Trans-Amazonian orogeny at about 2.0 Ga).

The gold-bearing veins are subhorizontal and subvertical. Subhorizontal veins have been divided in three sets: 205°-215°/15-35°NW, 120°-140°/15°-35°SW and a vein set with variable strike and 5-15° dip that follows the northern contact of the Omai stock. They are generally restricted to felsic rock types (the Omai stock, quartz-feldspar porphyry and rhyolite dikes), except the third vein set that occurs only in the tholeiitic basalts of the *Fennell* zone. Commonly, these veins pinch out abruptly at the contact with more ductile intermediate/mafic volcanic and/or sedimentary country rocks. The thickness of veins ranges from a few millimetres up to 0.8 m. In the *Fennell* zone, the subhorizontal veins display little structural variation, whereas in the *Wenot* zone the veins display random strikes and dips, which result in a typical stockwork aspect.

The subvertical veins are not confined to certain rock types, but they cut across all stratigraphical contacts. They are less frequent than the subhorizontal veins. The relationships between all vein types suggest that they are contemporaneous. The vein systems at the Omai mine can be classified as extensional (including crack and seal tensional and shear veins) and breccia veins. Some features of the vein textures at Omai are comparable to those described in Archean orogenic gold deposits, whereas other are closer to the vein textures described in the circum-Pacific Tertiary epithermal deposits.

Vein mineralogy includes mainly quartz, carbonates (ankerite, calcite), scheelite, native gold, and various sulfides/tellurides. The bulk of ore and gangue minerals precipitated at low temperatures (between 120 and 260°C) from hydrothermal fluids characterized by a gradual transition from oxidizing to reducing conditions. The early hydrothermal fluids were CO_2, W, and Na-rich, whereas subsequent S-rich fluids played an important role in gold transport and deposition. Possible mechanisms of gold deposition have been: 1) fluid cooling; 2) chemical composition of wallrocks, and; 3) wallrock permeability. High efficiency of fluid/rock interaction and gradual decrease of fO_2 and H_2S content in the hydrothermal solutions have directly influenced gold and sulfide±telluride deposition.

Vein-forming scheelite has $^{87}Sr/^{86}Sr$ ratios between 0.7019-0.7021 and $\delta^{18}O$ values between 3.8 and 4.3‰, which suggest both consistent temperature and isotopic composition of the hydrothermal solutions during its deposition. Oxygen isotopes measured in vein quartz vary between 13.2 and 14‰, similarly to the $\delta^{18}O$ values of carbonates (average 13.8‰ for calcite and 14.4‰ for ankerite). The carbon isotopes of carbonates range between +1.7 and +4.7%. The $\delta^{18}O$ values of the mineralizing fluids vary between +5.3 and -2.7‰ and the δD values between -52 and +18‰.

The radiogenic and stable isotopes suggest the presence of two different fluid sources: 1) mantellic and/or lower crustal origin , which interacted with the local mafic volcanic rocks and; 2) surface-derived (seawater or meteoric water). The physicochemical conditions of ore deposition at Omai (low temperature, pression, salinity, low CO_2 content, slightly acidic to neutral pH, moderate O and S fugacities, high Te fugacity), surface-water involvement, presence of dominant brittle ore-hosting structures, and location in low metamorphic terranes are more like those of epithermal deposits. Other major features (alteration style, geodynamic setting, late-orogenic/syn- to late tectonic emplacement, the presence of deeply sourced fluids, and partially the mineral paragenesis) are characteristic to deeper-level mesothermal deposits. These overlapping features between epi- and mesothermal corresponds to the upper part of the continuum model proposed for the Archean 'gold-only' deposits, which was defined as epizonal. The Omai deposit represents a first example of a Paleoproterozoic granitoid-

and greenstone-hosted equivalent of the Archean epizonal orogenic gold deposits described in Yilgarn and Zimbabwe Cratons.

ACKNOWLEDGMENTS

TABLE OF CONTENTS

LIST OF FIGURES

CHAPTER II

CHAPTER III

(mq) represents a latter filling phase; py = pyrite; B. Crack and seal shear vein (H3 vein system, Wenot pit). Several mm-thick ribbons are parallel to the axial plane of the vein. They formed by successive episodes of opening and mineral deposition; C. Single-stage breccia vein (H3 system in basalts, Fennell pit). Subrounded to angular, unaltered (except pyritization) wallrocks (wr) are trapped within the quartz matrix (mq). The wallrock fragments have no alteration rim (marker as scale); D. Multi-stage breccia vein (V3 vein system, Wenot pit). Angular, subrounded or rounded altered wallrock fragments (wr) are surrounded by later mineral (mostly ankerite, ank) rims and cemented with milky quartz (mq). Quartz stringers crosscut locally the breccia fragments .109

CHAPTER IV

CHAPTER V

APPENDIX 1

APPENDIX 2

LIST OF TABLES

CHAPTER III

CHAPTER IV

CHAPTER V

INTRODUCTION

The Omai deposit represents a large tonnage/low grade world class deposit located in the Paleoproterozoic greenstone belt of north-central Guyana. South America (Fig. 1). The deposit contains 84 million tonnes grading at 1.5 g/t Au (including past production and proven reserves). The Omai mine represents the only major producing mine in the Guiana Shield. but. what is more important. it proves the huge potential for gold exploration in this Paleoproterozoic greenstone terrane.

Very little research has been undertaken in the Guiana Shield in the last 30 years. This is due in part to the poor infrastructure. thick laterite/sand cover. dense tropical rainforest and in part due to the lack of confidence of the exploration companies in the mining potential of this region. The situation has changed drastically since 1991. when the Omai mine started operating. Many companies started constant exploration projects. which resulted in the discovery of important gold deposits (Las Cristinas. Venezuela: Gross Rosebel. Suriname: Dorlin. Yaou. French Guiana: Eagle Mountain. Guyana).

The Omai open pits represent one of the few zones in the Guiana Shield where fresh bedrock can be studied. The purpose of this thesis is to present and discuss the geologic and metallogenic environment of the Omai gold mine based on: a) Petrologic and mineralogical studies of both bedrock and weathering profile: b) Whole-rock geochemistry: c) Structural and textural evidence of the mineralized veins and their host rocks: and d) Radiogenic and stable isotope studies. It is therefore intended that this work will provide a geologic and metallogenic base for further studies of the orogenic gold deposits in Guyana and will serve as a guide to gold exploration in the Guiana Shield.
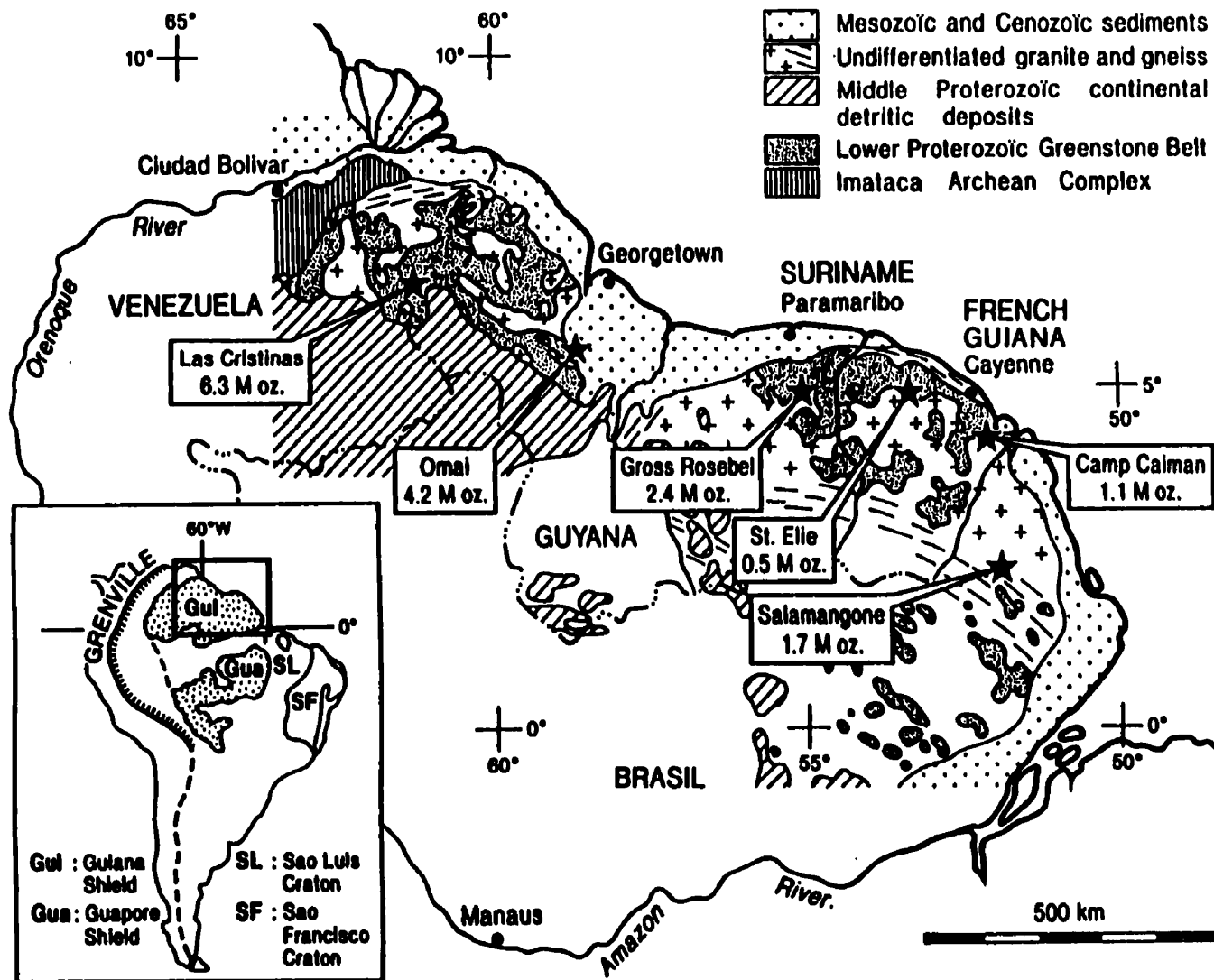
Figure 1   Simplified geological map of the Guiana Shield showing the principal gold deposits.

The research work of the Omai deposit was initiated in late 1994. as a result of an agreement between Adjunct Professor Marc Bardoux of l'Université du Québec à Montréal and Chief Geologist Robert Crépeau and Director of Mine Geology François Viens of Omai Gold Mines/Cambior.

Fieldwork consisted of detailed mapping/sampling of the open pits and concession area and logging/sampling the drill cores. More than 500 samples were collected and analysed by various methods at UQÀM. McGill University. Université Laval. Stellenbosch University (South Africa). and Krueger Enterprises (USA).

More than 400 thin/polished sections were studied. including more than 50 by scanning electronic microscopy and electron-microprobe. About 40 samples were analysed by X-ray diffractometry. The geochemical work consisted of 82 whole-rock chemical analyses for 10 major oxides. 32 trace elements and 7 rare-earth elements (REE). The REE analyses were performed by the author. under the supervision of Dr. Luc Harnois at UQÀM. 24 whole-rock samples were analysed for Sm-Nd isotopes and 8 samples of scheelite for Sm-Nd and Sr isotopes. The radiogenic isotope analyses were performed by the author. under the supervision of Dr. Ross Stevenson at UQÀM. 40 samples were analysed for oxygen isotopes. 15 for carbon isotopes. and 5 for hydrogen isotopes.

The thesis comprises 5 chapters. each of them representing papers/manuscripts that have been submitted to scientific journals with editorial boards.

Chapter I describes the geological. petrographical. and geochemical features of the Omai rock types in order to define the tectono-magmatic history of this part of the Guiana Shield. The paper was published by Exploration and Mining Geology. v. 6. no.

2, p. 153-170 (1997). The co-authors are M. Bardoux (UQÀM), L. Harnois (UQÀM), and R. Crépeau (Cambior Inc.).

Chapter II presents textural details and analytical data for Omai telluride minerals. Furthermore, the telluride-bearing mineral assemblage was used to constrain the physicochemical parameters of ore deposition, as well as the transport and deposition mechanisms. The co-authors are M. Bardoux and M. Jébrak (UQÀM). The paper was accepted and will be published in The Canadian Mineralogist, vol. 37, 3, june 1999.

Chapter III contains the structural, textural, mineralogical and geochemical characteristics of the Omai gold deposit. This chapter includes also the stable isotope results, a proposed genetic model, and a brief comparison between Omai and other Precambrian orogenic gold deposits. The co-authors are M. Bardoux (UQÀM), M. Jébrak (UQÀM), and R. Crépeau (Cambior Inc.). The manuscript was submitted to Economic Geology.

Chapter IV presents and discusses the Sm-Nd and Sr isotope of vein-forming scheelite and host rocks. The radiogenic isotope data were used to constrain the source of the igneous rocks and the path and source of mineralizing fluids. The co-authors are M. Bardoux, R. Stevenson, and M. Jébrak (UQÀM). The manuscript was submitted to Mineralium Deposita.

Chapter V describes and includes a computer program for the mineralogical norm calculations of the weathering profiles from the tropical regions. Applications for several types of weathering profiles, including Omai, are presented. The paper was published in Mineralogical Magazine, v. 61, p. 185-196 (1997). The co-authors are M. Bardoux (UQÀM) and D. Voicu (Université de Montréal).

Appendix 1 contains the extended abstract presented at Geocongress'98. The Geological Society of South Africa. 8-10 July 1998. The abstract has attached the chemical composition of the fluid inclusions in the main vein-forming mineral phases. The authors are D.K. Hallbauer (Stellenbosch University. South Africa) and G. Voicu.

Appendix 2 contains a presentation of Guyana's mineral resources. The mineral resources of Guyana were divided into metallogenic provinces. based on specific tectono-magmatic evolution of each major lithostratigraphic unit. which could represent the host rocks for different ore deposit models. The ore deposit models that could apply to Guiana Shield are described. The aim is to provide the reader with an overall view of Guyana's resources and to provide a guide to mineral exploration.

Parts of the thesis were presented at the following international meetings:

- International Conference on Tectonics & Metallogeny of Early/Mid Precambrian Orogenic Belts. Montreal. Canada. August 28-September 1. 1995. Program with Abstracts. p. 213:
- Winnipeg96. GAC/MAC Annual Meeting. Winnipeg. Canada. May 27-29. 1996. Program with Abstracts. v. 21. p. A-99:
- 30th International Geological Congress. Beijing. China. August 1-12. 1996: published in Qui et al. (eds.). v. 2. 1. p. 101-114.
- 39th Geological Congress. Geological Society of Brazil. Salvador (Bahia). Brazil. September 1-6. 1996. Extended Abstracts. p. 43-46:
- Ottawa97. GAC/MAC Annual Meeting. Ottawa. Canada. May 21-23. 1997. Program with Abstracts. v. 22. p. A-154:

- Northwest Mining Convention. Spokane. WA. USA. December 1-6. 1997. Short Course Notes - The Geology. Geochemistry. Geophysics. and Mineral Deposits of the Guiana and West African Shields. 42 p.

- Geocongress'98. The Geological Society of South Africa. 8-10 July 1998. Extended Abstracts. p. 213-215.

CHAPTER I

LITHOLOGICAL AND GEOCHEMICAL FEATURES OF IGNEOUS AND SEDIMENTARY ROCKS AT THE OMAI GOLD MINE, GUYANA, SOUTH AMERICA

1.1 INTRODUCTION

In comparison to other Precambrian greenstone belts and their related gold mineralization. the Guiana Shield has been the subject of few geological and geochemical studies. Tropical conditions have severely weathered the rocks. transforming most to saprolite to depths of more than 50 m. Fortunately. certain streams and major rivers have incised the saprolite and provide sufficient exposures of primary rock units to produce a general picture of the geology of the Guiana Shield.

The Omai gold deposit. located 200 km southwest of Georgetown. Guyana. on the west bank of the Essequibo River. is one of the largest gold deposits in South America. Gold showings have been known in this area for more than a hundred years. and were exploited sporadically on a small scale. In 1990. a joint venture between Cambior Inc. and Golden Star Resources initiated a large-scale mining operation. resulting in the first hardrock open pit to be developed on the Guiana Shield. The current mineable reserves (including past production) are 83 million tonnes at 1.6 g/t Au. representing 130.5 tonnes (4.2 million ounces) of Au. At present. two open pit mines. the Fennell and Wenot pits. are in production. which provide access for examination and study of the Proterozoic basement.

The present paper is the first part of a study of the geologic and metallogenic environment at Omai. The aims are threefold: first. to review the geology and to constrain the geochemical characteristics of the Omai rock types in order to decipher the local setting: second. to propose a possible tectonic environment for the Omai area in a regional context: and third. to compare the lithological and geochemical features of the greenstone belt at Omai with other Precambrian greenstone terranes.

1.2 REGIONAL GEOLOGY

The current lithostratigraphic. geochronological and tectonic data for the northern Guyana allow division of the rock types into six main assemblages (Williams et al.. 1967: Choudhuri. 1980: Walrond. 1980. 1987: Gibbs and Barron. 1983. 1993: Gibbs. 1987a). These are briefly described below. from oldest to youngest.

1) High-grade metamorphic rocks referred to as the Bartica Formation. which represent high-grade equivalents of overlying low-grade greenstone belts. Similar high-grade metamorphic rocks in Venezuela and Brazil have yielded Sm-Nd ages of 2.2 Ga (Teixeira et al.. 1989: Gibbs and Barron. 1993) and in French Guyana have given ages of 2.23 Ga (U-Pb method on zircons: Milési et al.. 1995) and 2.0 Ga (Rb-Sr method: Gruau et al.. 1985).

2) Low-grade metavolcanic and metasedimentary rocks of the Barama-Mazaruni Supergroup considered to represent a Paleoproterozoic equivalent of the Archean greenstone belts. Zircons from metagraywacke and acid volcanics of the northern part of the Barama-Mazaruni greenstone belt in Guyana have been dated by U-Pb method at 2.25 ± 0.10 Ga (Gibbs and Olszewski. 1982).

3) Paleoproterozoic syn- to late-tectonic intrusions of intermediate to acid composition termed the Older and Younger Granites. In Guyana. even though the granitoids are divided into two distinct groups. the available geological studies and maps (Williams et al.. 1967: Snelling and McConnell. 1969: Walrond. 1980. 1987: Gibbs and Barron. 1983. 1993: Gibbs. 1987a: Renner and Gibbs. 1987: and unpublished local geological maps). together with geochronological data (ages between 2.1 and 1.8 Ga given by K-Ar and Rb-Sr methods: Williams et al.. 1967: Snelling and McConnell. 1969). suggest that the granitoids are probably related to protracted plutonic events

during the Trans-Amazonian orogeny (2.25 - 1.9 Ga: Montgomery. 1979: Gibbs and Olszewski. 1982: Teixeira et al.. 1989: Gibbs and Barron. 1993). As is the case in other regions of the Guiana Shield. there are insufficient data available to divide the Paleoproterozoic granitoids (Bosma et al.. 1984: Cox et al.. 1993: Milési et al.. 1995). Thus. the term Granitoid Complex is proposed for the Paleoproterozoic intrusions of northern Guyana. analogous to the terminology suggested by Bosma et al. (1984) for Suriname and by Milési et al. (1995) for French Guiana.

4) Small mafic/ultramafic sills and dikes referred to as the Older and Younger Basic Groups are described as being associated. respectively. with the Paleoproterozoic volcanic and plutonic rocks. as well as the Mesoproterozoic Roraïma Formation. The Older Basic Group has been described as gabbroic-hornblenditic bodies related to the Barama-Mazaruni Supergroup and to the Granitoid Complex (Williams. 1967: Renner and Gibbs. 1987: Gibbs and Barron. 1993). At Omai. these bodies may represent subvolcanic equivalents of the overlying mafic volcanic rocks (Voicu and Bardoux. 1995). Younger Basic Group rocks yielded ages between 1.6 and 1.8 Ga by K-Ar and Rb-Sr methods (Snelling and McConnell. 1969). similar to ages of the Mesoproterozoic Avanavero Suite. which has been described throughout the Guiana Shield (Hawkes. 1966: Choudhuri. 1978: Gibbs. 1987b: Teixeira. 1990: Choudhuri et al.. 1990).

5) Mesoproterozoic anorogenic felsic lavas (Iwokrama Formation) and continental sedimentary rocks of the Roraïma Group.

6) Permo-Triassic mafic dike swarms of the Apatoe Suite. related to the opening of the Atlantic Ocean (Oliveira et al.. 1990: Dossin et al.. 1995).

In the Omai-Potaro-Mariaba region (Fig. 1.1). the Bartica Formation consists of leucocratic biotite-gneiss. amphibolitic gneiss and coarse-grained hornblende-biotite

GEOLOGICAL MAP OF THE POTARO-OMAI-MARIABA REGION
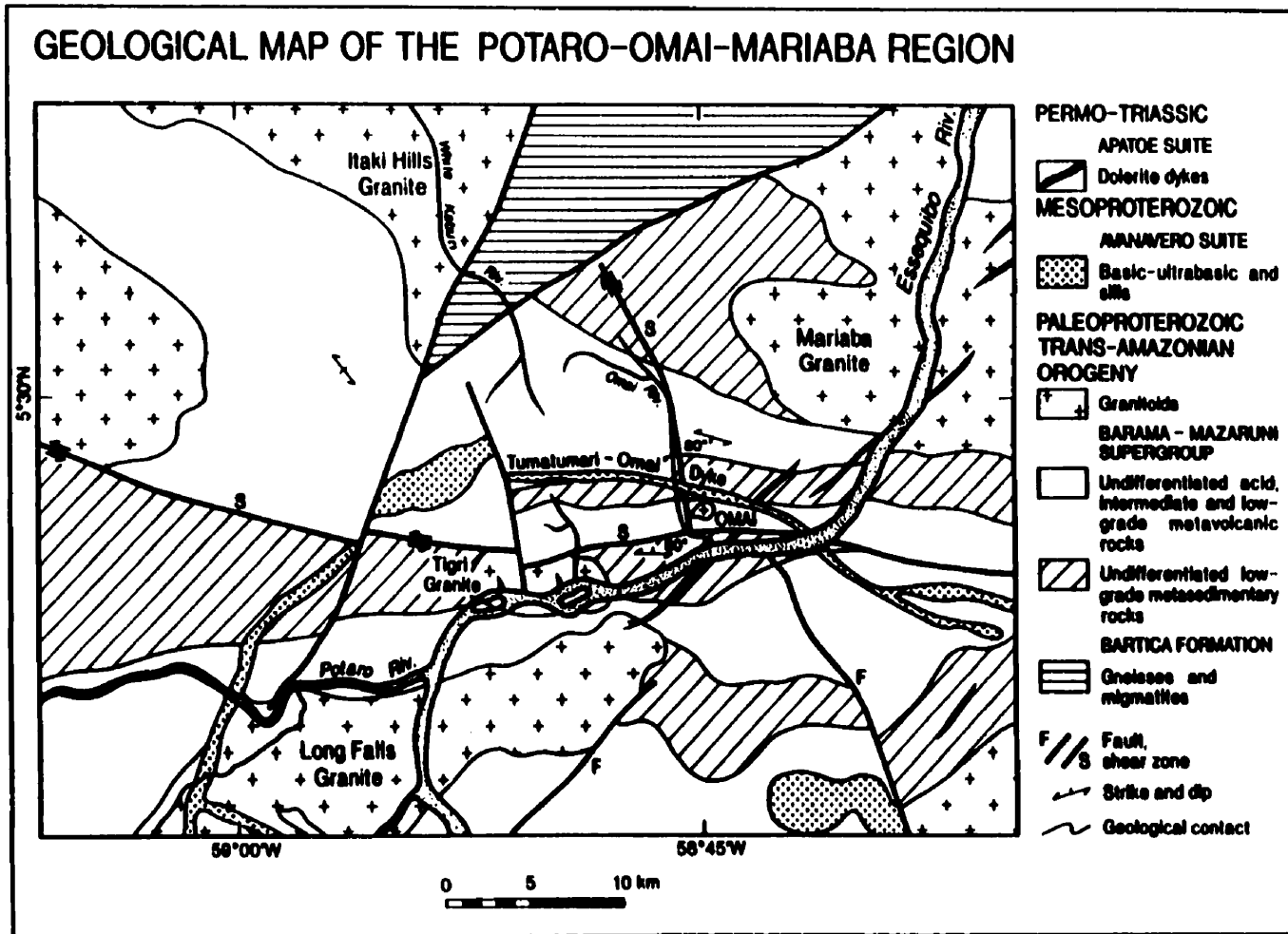
Figure 1.1   Bedrock geology of the Omai-Potaro-Mariaba area. Data compiled from Bateson (1961), Cannon (1963), Hawkes (1966), Collings (1969), Guardia (1969), Bertoni et al. (1991), Gibbs and Barron (1993), and Voicu et al. (1996).

gneiss (Bateson. 1961). The Barama-Mazaruni Supergroup comprises alternating felsic. intermediate and mafic metavolcanic rocks and immature sedimentary rocks (greywacke. volcanoclastic conglomerates. tuffs and phyllites). metamorphosed in the prehnite-pumpellyite to lower greenschist facies. These units strike E-W to NW-SE. and dip steeply and mainly to the north (Guardia. 1969: Collings. 1969: Bertoni et al.. 1991: Elliott. 1992: Voicu et al.. 1996). The detailed petrography. stratigraphy. and structure of these units are poorly known.

The Granitoid Complex comprises several plutons and stocks (Omai. Mariaba. Tigri. Long Falls. Itaki Hills). which range from granite to granodiorite. trondhjemite. adamellite. and quartz-monzodiorite (Guardia. 1969: Elliott. 1992). The Tigri granite provided an age of 1.945 Ga (K-Ar method on hornblende). whereas the Mariaba granite yielded an age of 1.71 Ga (K-Ar method on biotite: Snelling and McConnell. 1969). The granitoids are usually medium to coarse grained. with weakly porphyritic textures locally (Guardia. 1969: Collings. 1969: Bertoni et al.. 1991: Elliott. 1992: Bhatt. 1995: Voicu and Bardoux. 1995). They intrude the volcanic and sedimentary rocks of the Barama-Mazaruni Supergroup. but no extensive metamorphic aureoles have been reported.

Sills and dikes of the Avanavero Suite form prominent ridges detectable on air photographs and radar images. The largest is the Tumatumari sill. an unmetamorphosed layered intrusion. which is composed of gabbro. hornblende pyroxenite and granophyre (Hawkes. 1966). The central part of the sill has been dated at 1.66 Ga (K-Ar method on plagioclase: Williams et al.. 1967). Based on C-band synthetic aperture radar images. this sill was correlated with the gabbroic sill that outcrops north of the Omai stock.

The Permo-Triassic Apatoe tholeiitic dike swarms are widespread in the region and cut all other lithological complexes.

1.3 STRUCTURE AND METAMORPHISM

Facing directions at Omai can be interpreted from sedimentary structures and pillow shapes. Statistical data on the asymmetry of re-entrants in pillow lobe outlines measured in both the Fennell and Wenot pits yield a younging direction to the south. As the dip is generally steeply to the north, the units may be overturned. Near the Omai stock, two principal sets of strikes and dips were measured for the volcanic rocks, with means of $252^\circ/80^\circ$ NW and $345^\circ/75^\circ$ NE, respectively. These different attitudes probably reflect local perturbations caused by the emplacement of the Omai stock and surrounding intrusive bodies. Farther away from the stock, and in the Wenot pit area, the mean strike/dip values for volcanic and sedimentary sequences are $280^\circ/80^\circ$ NE. Subsidiary discrete anticline and syncline folds were observed in the saprolite profile in the Wenot pit, but in general the rocks dip steeply to the north-east. Regional scale foliation (D1) is well developed in the sedimentary sequence from the southern part of the Wenot pit and less so in the volcanic rocks. It has a general trend of $100-110^\circ$ with steep dips (mean $= 73^\circ$) in either direction, and it is typically parallel to bedding. Generally, only one foliation is developed in the volcanic rocks, but in the sedimentary sequence, two discrete superimposed cleavages can be observed in several drill cores. These cleavages may reflect the overprint of later deformational events, but they may also be the result of localised recrystallization under a weak stress regime during gold mineralization. The D1 event was associated to development of ductile shear zones, broadly oriented WNW-ESE.

Regional metamorphism in subgreenschist to greenschist facies followed, with associated development of brittle fractures between the main shear zones. The subhorizontal, northeast-striking extensional zone is thought to have determined the dominant orientation of the vein sets hosted by the Omai stock, as well as porphyry and rhyolite dikes. The extensional zone is pre-mineralization and is the result of the brittle

response of these lithotypes to the regional stress field. A last structural post-mineralization event is recorded by N-S fractures (Omai River fault and several faults in the Wenot pit), which are probably related to the Permo-Triassic Apatoe dike swarm emplacement.

At Omai, and elsewhere in the Barama-Mazaruni Supergroup (Gibbs and Barron, 1983, 1993), the metamorphic grade varies between pumpellyite-prehnite and sub-greenschist facies. A chlorite-albite-epidote assemblage, locally associated with pumpellyite, indicates that the metamorphism of most rocks is confined to the chlorite zone of the greenschist facies, possibly superimposed on an earlier pumpellyite-prehnite regional burial stage, as in the Abitibi subprovince (Spooner and Barrie, 1993) and in Birimian greenstone belt of the West African Craton (Leube et al., 1990).

1.4 LITHOLOGICAL DESCRIPTION AND CLASSIFICATION

The Omai mine area consists of a typical greenstone belt sequence, represented by various volcanic and sedimentary rocks, which have been intruded by a granitoid stock (Omai stock) and several generations of mafic to felsic dikes and sills (Fig. 1.2). The volcanic sequence consists mainly of massive to pillowed tholeiitic basalts and calc-alkaline andesites, commonly showing amygdaloidal/fluidal textures, and evidence of spilitic alteration. Also present are lesser proportions of rhyolites, quartz-feldspar porphyries of rhyodacitic composition and thin tuffaceous levels. Although all rock classes are present, the gap in SiO_2 content between 60 and 70% suggests that the suite is bimodal (Fig. 1.3), similar to the northern part of the Barama-Mazaruni greenstone belt (Gibbs, 1987a).

15
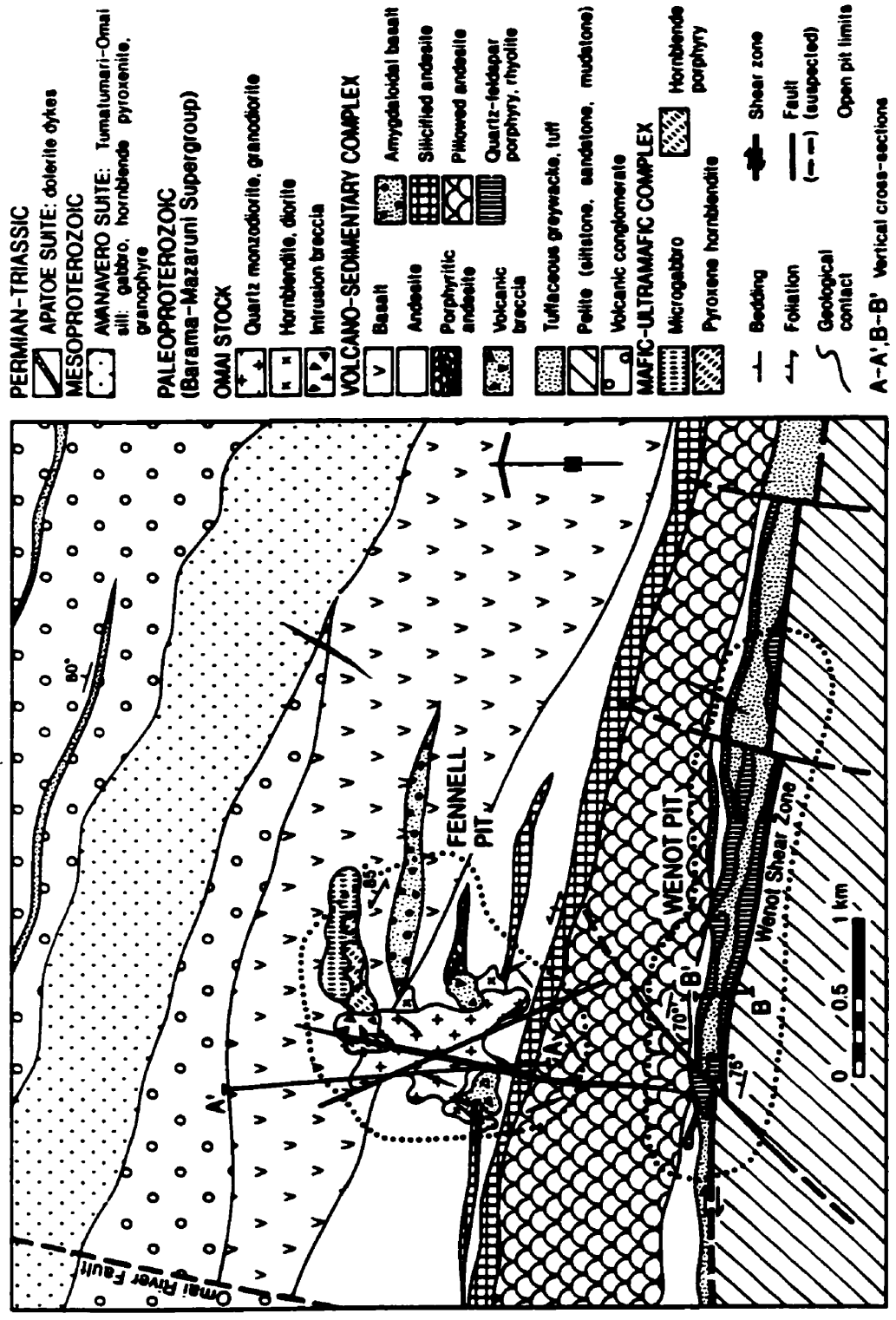
Figure 1.2   Simplified geological map of the Omai area.

PERMIAN-TRIASSIC
APATOE SUITE: dolerite dykes

MESOPROTEROZOIC
AMANAVERO SUITE: Tumatumari-Omai sill: gabbro, hornblende pyroxenite, granophyre

PALEOPROTEROZOIC
(Barama-Mazaruni Supergroup)

OMAI STOCK
Quartz monzodiorite, granodiorite
Hornblendite, diorite
Intrusion breccia

VOLCANO-SEDIMENTARY COMPLEX
Basalt
Andesite
Porphyritic andesite
Volcanic breccia
Amygdaloidal basalt
Silicified andesite
Pillowed andesite
Quartz-feldspar porphyry, rhyolite
Tuffaceous greywacke, tuff
Pelite (siltstone, sandstone, mudstone)
Volcanic conglomerate

MAFIC-ULTRAMAFIC COMPLEX
Microgabbro
Pyroxene hornblendite
Hornblende porphyry

Bedding
Foliation
Geological contact
Shear zone
Fault (suspected)
Open pit limits
A-A';B-B' Vertical cross-sections

Figure 1.3   SiO$_2$ *vs* Zr/TiO$_2$ classification diagram (Wincester and Floyd. 1977) for the Omai igneous rocks. Symbols: squares: tholeiitic basalts and basaltic andesites: crosses: calc-alkaline andesites: triangles: quartz-feldspar porphyries: open circles: rhyolites: closed circles: Omai stock: half-filled squares: Mesoproterozoic (Tumatumari-Omai gabbro dike) and Permo-Triassic (Apatoe) tholeiitic dikes.

Due to the regional deformation. the pillowed lavas are slightly flattened. except in the central/southern part of the Wenot pit. where they are strongly streched close to the east-west striking shear zone. The pillows are closely packed. with diameters ranging from 0.5 to 2.5 m. The pillows have distinctly darker. chilled rims and massive interiors. Locally. tensional cracks and ropy wrinkled surfaces are visible. Lack of vesicles and of multiple-rind structure may be considered as arguments for pillow emplacement in relatively deep water. Large pillow size suggests low lava viscosity. generally related to high eruption temperature (cf. McPhie et al.. 1993). The interpillow spaces. which were initially filled with hyaloclastite derived from spalled glassy rinds. or with other sediment. are now represented by fine-grained semi-opaque material composed of epidote. chlorite. opaque and argillaceous minerals. Locally. the interpillow spaces are filled with chert. which seems to be associated with mafic lavas. a characteristic feature in many Precambrian greenstone belts. Beds of intermediate pyroclastic rocks (tuffs) are observed in the Wenot area. and to a lesser extend in the Fennell area.

Two quartz-feldspar porphyry (QFP) dikes striking N100-110° and dipping 75-85° to the north are intercalated within the volcanic sequence in the Wenot area. The thickness of the QFP dikes varies between 5 to 25 m. and they can be traced for more than 2 km along strike and at least 250 m downdip. The QFP is of rhyodacitic composition and consists of albite. K-feldspar. quartz. chlorite (replacing biotite). calcite. and traces of apatite. rutile and pyrite. Locally. fragments of extrusive felsic volcanic material and tuffaceous fabrics were observed. The relationship of the QFP dikes with the host volcanic flows is somehow ambiguous. Both extrusive and intrusive contacts have been observed. suggesting that the porphyries were emplaced contemporaneously with. or shortly following extrusive activity. at or near the seafloor surface. Ambiguous contact relationships also characterize some quartz-feldspar porphyries related to gold deposits in the Superior Province of Canada (Hodgson and MacGeehan. 1982: Hodgson.

1990). In the Wenot area, late rhyolite dikes crosscut the lithological contacts. Their average thickness is about 5 m. The rhyolites are strongly silicified, massive, and aphanitic to very fine-grained. They have typical granophyric texture, resulting from graphically intergrown quartz and alkali feldspar. Chemically, the rhyolites have a prominent negative Eu anomaly, indicating cotectic or eutectic crystallization of a final residual melt (cf. Nabelek, 1986). Rhyolite dikes are crosscut by the stockwork-type gold-quartz veins and stringers (described later).

An irregular, mafic/ultramafic body consisting of gabbro, pyroxene hornblendite and hornblende porphyry was mapped in the northern part of the Fennell pit. Its contact with the associated basalts is generally gradational, but sharp contacts are locally present. The mafic/ultramafic body is of tholeiitic affinity and could represent a deeper-seated equivalent of the basaltic part of the volcanic sequence.

The Omai stock represents an irregularly-shaped intrusion, with moderate plunge (70-80°) to the northeast. It intrudes mainly along the contact between tholeiitic basalts (and related mafic-ultramafic body) and the calc-alkaline andesites and was not affected by the regional-scale deformation (D1 event). The weak orientation of the mafic minerals in places near the border of the stock is considered to be a primary magmatic feature rather than foliation induced by deformation. Petrographic types within the stock include quartz-monzodiorite, granodiorite, diorite and hornblendite. These lithotypes appear to be consanguineous phases with gradual transitions from one another, but they are in sharp contact with the volcanic sequence. The felsic/intermediate lithologies are fine- to medium-grained and locally weakly porphyritic, whereas the hornblendite which forms a rim to the stock is very coarse-grained, with hornblende crystals up to 6 cm in length.

Sedimentary rocks consist of siltstones. sandstones and greywackes (phyllitic tuffs in mine terminology). locally with carbonate porphyroblasts. A sequence more than 2 km thick of poorly-sorted cobble conglomerate. interlayered with thin basaltic flows and beds of lithic tuff. outcrops north of the Fennell Pit.

Several pre- and post-mineralization dikes have been mapped in the Omai area. Highly irregular dikes and sills of alkali basaltic composition postdate the volcanic sequence and the Omai stock. but predate the emplacement of the gold-bearing quartz veins. Post-mineralization Mesoproterozoic Tumatumari-Omai gabbro dike (Avanavero suite) occurs north of the Fennell pit and truncates all rock types and veins. Because it dips to the south ($30°$ to $40°$) and its thickness is ~140m. it will ultimately form the natural bottom of the Fennell pit. Triassic Apatoe dikes intrude all exposed lithotypes and mineralized veins in the Omai region. These dikes. which occur in swarms. range in width from a few centimeters to about 4 m. strike roughly north-south. and dip steeply eastward. They are characterized by closely spaced jointing which is perpendicular to strike. and in their thicker parts by aphanitic margins. suggesting emplacement at shallow levels into relatively cold country rock. Although preexisting fault zones may have facilitated the emplacement of these dikes. only a few seem to occur along or close to faults.

1.5 THE OMAI GOLD VEINS

Two types of gold-bearing veins can be distinguished at Omai: vein sets (=stockworks) and lode veins. These vein types have been observed in both the Fennell and Wenot pits.

Vein sets are essentially restricted to the Omai stock. quartz-feldspar porphyry and rhyolite dikes. Even though veins are present up to 10 m beyond the intrusive

margins of these rock types. their frequency diminishes rapidly away from them. Usually. the vein sets pinch out abruptly at the contact with more ductile intermediate/mafic volcanic and sedimentary country rocks. The thickness of veins ranges from a few millimeters up to 0.8 m and is related to the volume of the felsic host rock. Veins are generally thicker in the Omai stock relative to veins hosted by thinner porphyry and rhyolite dykes. Other differences are observed between vein sets from the Omai stock (Fennell pit) and those hosted by porphyries and rhyolites (Wenot pit). In the Omai stock. most veins display a swarm style with little variation in strike and dip. mainly striking N 205° to 215° and dipping 25° to 40° NW. A subordinate vein system strikes N 140° to 160° and dips 25° to 40° SW. A random distribution of thin veins and stringers occurs locally. mainly along the lithological contacts between the Omai stock and host andesite/basalt. The vein sets can be traced several tens of meters. sometimes crosscutting the whole stock. but commonly the veins are boudinaged and their lengths are less than 20 m. In the Wenot pit. the vein sets display random strikes and dips. resulting in a typical stockwork aspect. Generally. these veins dip more steeply than those hosted by the Omai stock. The thickness of the veins is usually less than 10 cm. but their frequency is increased relative to veins in the Omai stock.

Lode veins generally overprint the stockwork veins. but the inverse situation also exists. suggesting a quasi-contemporaneous emplacement of the vein types. Lode veins strike N 200° to 220° and dip between 0° and 30° NW or SE. Relative to the vein sets. they are generally thicker (between 0.3 and 1.3 m) and cut across all rock types (except late gabbro and diabase dikes).

Both vein sets and lode veins have formed by successive episodes of crack and seal. as a result of several pulses of a protracted hydrothermal system. The process was similar to that described by Robert and Brown (1986) for Archean gold-bearing quartz

veins at the Sigma mine in the Abitibi greenstone belt. Two principal textures - 'ribbon' and 'breccia' - have been noted in both vein types from all lithological complexes.

Even where the vein mineralogy is complex. the metallic minerals generally form <1% of the veins. although up to 5% pyrite is locally present. Vein filling minerals include quartz. ankerite. scheelite. calcite. chlorite. epidote. white and green mica. pyrite. various Au-Ag-Pb-Bi-Hg tellurides. galena. chalcopyrite. molybdenite. sphalerite. tetradymite. and native Au. Bi. and Cu (Bertoni et al.. 1991: Elliott. 1992: Bhatt. 1995: Voicu and Bardoux. 1995).

The Fennell and Wenot deposits display a similar alteration paragenesis. Extensive zones of pervasive alteration associated with the stockwork-style mineralization were noted. especially in the Omai stock (Fennell pit) and quartz-feldspar porphyries/rhyolites (Wenot pit). In basalts. the gold-bearing lode-type veins display narrow (few mm to 1 cm) alteration zones and mineral pseudomorphs. In other lithotypes. tension veins have alteration patterns similar to those associated with vein sets/stockwork-type mineralization. The hydrothermal alteration includes carbonatization. phyllitization. silicification and sulfidization. The importance of wallrock chemical composition and the efficiency of fluid-wallrock interaction played a major role during the alteration processes at Omai. as has been also suggested for Archean lode gold deposits (Böhlke. 1989: Ridley et al.. 1996). Within the Omai deposit. lateral alteration zonation around veins is on a scale varying from few centimetres to metres. In stockwork-style mineralization. the increased vein density leads to an overlapping of the alteration envelopes. commonly resulting in a complete transformation of the primary mineralogy of the host rock types. The lateral zonation can be viewed as the result of dispersion and diffusion of a dominantly channelised fluid flow. which modifies the chemistry of the wallrock (cf. Ridley et al.. 1996). Dispersion into the wallrock has resulted in the formation of alteration zones parallel to the veins.

whereas diffusion has created a series of narrow alteration zones perpendicular to the main direction of fluid flow. No alteration zonation with depth has been observed. indicating limited temperature gradients and little change in fluid chemistry along the flow path. The alteration envelopes are superimposed on a sub-greenschist facies metamorphic assemblage. and also. in the case of the mafic volcanic rocks. on a earlier low-temperature sea-floor spilitic alteration assemblage.

At Omai. the quartz-feldspar porphyry a U-Pb isochron age of 2120 ± 2 Ma. while the Omai stock has an age of 2094 ± 1 Ma (Norcross. 1997). The vein-forming scheelite has given an age of 1994 ± 140 Ma (Sm-Nd method. Voicu et al.. unpublished data). As stockwork-related scheelite is contemporaneous with or predates the bulk of gold deposition. and the stockwork veins generally predate the lode veins. the age of scheelite is considered as representing the maximum age for the Omai mineralization. The interval between 2.12 and 1.99 Ga therefore seems to bracket the main phases of magmatic. metamorphic. deformational and hydrothermal evolution of the Omai area. Following this interval. only late faulting and sporadic basic magmatism affected the area.

1.6 GEOCHEMISTRY OF THE HOST ROCKS

1.6.1 Analytical Methods

Representative samples of the Omai host rocks were analysed for major. trace. precious and rare-earth elements (Table 1.1). In order to obtain representative primary magmatic compositions. we selected those samples considered to be least altered for chemical analyses.

Major oxides and most trace elements were analyzed by X-ray fluorescence techniques at the Geochemical Laboratories. McGill University. Montreal. Total iron is

Table 1.1   Representative whole-rock chemical analyses of the igneous and sedimentary rocks at Omai, Guyana

Table 1.1   Representative whole-rock chemical analyses of the igneous and sedimentary rocks at Omai, Guyana (continuation)

given as Fe_2O_3. U. Th. Ta. Cs. Hf. and the rare earth elements were determined by neutron activation analysis at Université du Québec à Montréal and École Polytechnique Montréal. Precious metals Au. Pt. Pd. and Ag were analyzed at McGill University using fire assay techniques. with detection limits of 1. 5. 3. and 0.2 ppb. respectively.

1.6.2 Results

Selected chemical features of the Omai rock types are presented in Table 1.2. Although least altered samples were selected. many show weak carbonate and phyllic alteration under the microscope. Thus. the CaO. K_2O and LOI values may not reflect primary contents of these components in every case.

An AFM diagram (Irvine and Baragar. 1971) suggests that the mafic/ultramafic body and associated basalts/basaltic andesites of the northern part of the Fennell Pit are tholeiitic. whereas plutonic rocks of the Omai stock and intermediate/acid volcanic rocks are calc-alkaline (Fig. 1.4). Most volcanic rocks are subalkaline. with low Na_2O+K_2O values at a given silica content. but few samples appear to be weakly alkaline. due either to fractional crystallization and accumulation of feldspar or to metasomatism related to the emplacement of the Omai stock.

1.6.2.1 Tholeiitic volcanic and subvolcanic rocks

Tholeiitic rocks are dominated by basalts of the volcanic sequence and by the mafic-ultramafic subvolcanic body north of Fennell Pit. On a chemical basis. no distinction can be made between these rocks. possibly suggesting a common origin. The mafic volcanic rocks have similar SiO_2. MgO. and Fe_2O_3 contents typical of high-Fe

Table 1.2   Main chemical characteristics (minimum-maximum; mean) of the igneous and sedimentary rocks at Omai, Guyana

Chemical trend Complex	Tholeiitic		Calc-alkaline				
	MUR	VR-B	VR-A	VR-QP	VR-R	OS	Sed
SiO_2	45-52; 49	44-56; 49	51-60; 56	71-76; 73	77-78; 77	50-68; 60	50-69; 62
Zr/Nb	8-17; 14	8-22; 13	10-20; 15	10-19; 14	9-15; 13	12-28; 22	8-22; 16
Zr/Y	2-5; 4	2-5; 3	5-9; 7	14-16; 15	3-4; 3.2	5-94; 13	4-9; 7
Ti/V	36-41; 39	30-128; 55	34-56; 42	36-110; 73	20-22; 21	35-86; 66	48-77; 66
Nb/Y	0.2-0.3; 0.3	0.2-0.3; 0.3	0.3-0.7; 0.5	0.9-1.5; 1.2	0.2-0.3; 0.25	0.3-4; 0.6	0.3-0.5; 0.45
La_n	27-48; 9	12-55; 38	37-147; 80	62-170; 115	146-339; 225	45-315; 169	87-245; 128
La_n/Yb_n	2-6; 3	1-5; 2	4-9; 5.5	23-29; 26	2-4; 2.5	6-13; 10.4	6-12; 9
Lu_n	8-30; 17	11-36; 20	9-25; 14	2-5; 3.5	73-94; 81	7-27; 15	8-32; 14
Al_2O_3/TiO_2	7-17; 11	5-18; 11	19-44; 30	38-52; 45	113-121; 117	13-58; 39	8-42; 21
Eu/Eu*	0.9-1.2; 1.1	0.8-1.3; 1	0.9-1.4; 1.1	0.96-1.02; 0.99	0.3-0.4; 0.32	0.7-1; 0.94	0.6-1.1; 0.8
Ce/Ce*	1.1-2.1; 1.5	0.7-3; 1.6	0.9-1.8; 1.2	0.7-0.9; 0.8	0.8-1.6; 1.3	0.7-1.9; 1.2	0.5-1.7; 1.2

Tholeiitic: MUR: Mafic/ultramafic rocks; VR-B: Volcanic rocks, basalts and basaltic andesites; Calc-alkaline: VR-A: Volcanic rocks, andesites; VR-QP: Volcanic rocks, quartz feldspar porphyries; VR-R: Volcanic rocks, rhyolites; OS: Omai stock; Sed: Sedimentary rocks.

FeOT

THOLEIITIC

CALC-ALKALINE

Na₂O+K₂O   **MgO**
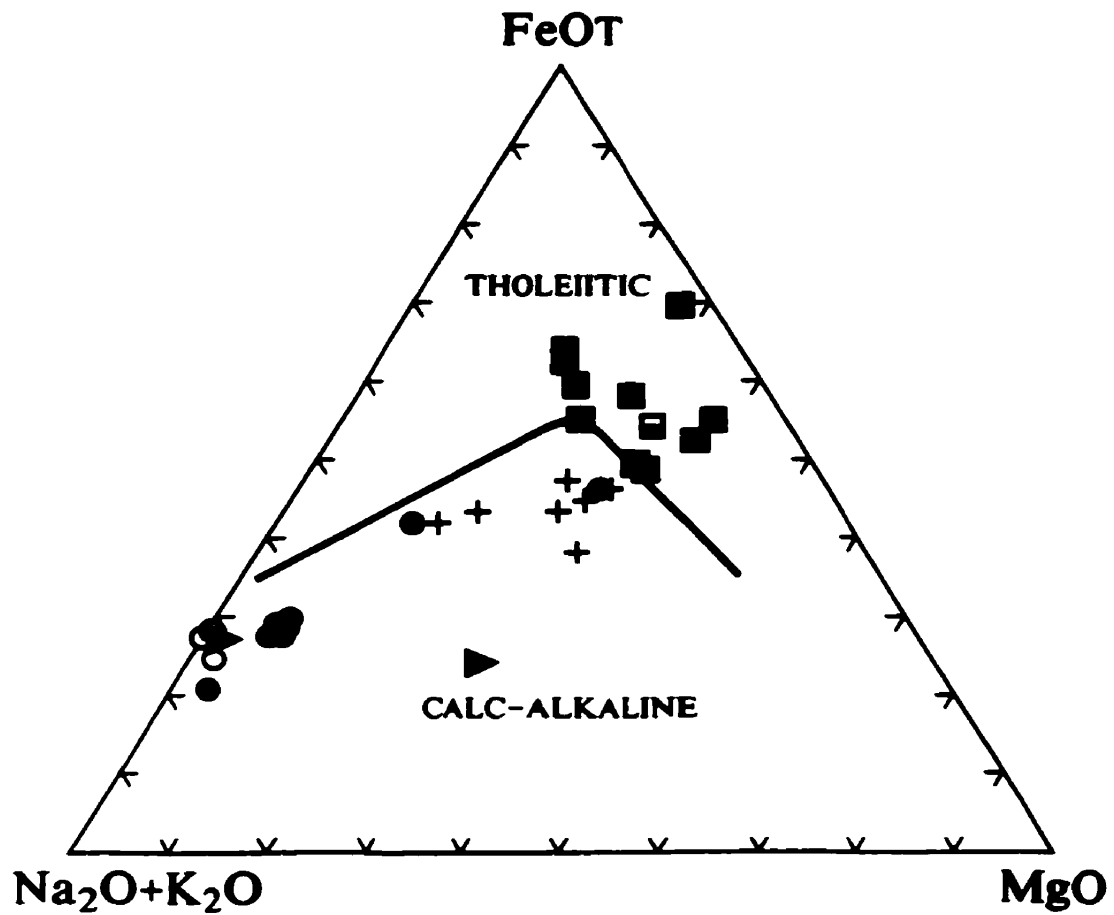
Figure 1.4   AFM diagram (Irvine and Baragar, 1971) for the Omai volcanic and plutonic rocks, showing the tholeiitic to calc-alkaline affinities. Symbols as in Figure 1. 3.

basalts. and low to moderate Mg-numbers (50-60) and Ni contents (28-162 ppm. mean of 88 ppm). A few samples with K_2O < 0.5% are likely least-altered rocks and could be classified as low-K tholeiites.

On chondrite-normalized REE plots. tholeiites (Fig. 1.5A) show slight to moderate LREE/HREE ratios (La_n/Yb_n = 0.9-5.5: mean = 2.3) with nearly flat HREE slopes (Tb_n/Lu_n = 0.7-1.5: mean = 1.1). The tholeiites with the highest Mg numbers tend to have the lowest REE contents. Several samples have small negative or positive Eu and Ce anomalies. which suggests a mobilization of these elements during metamorphism or alteration.

On a MORB-normalized incompatible element diagram (Fig. 1.6A). the large-ion lithophile elements (LILE) excluding Th are generally enriched. whereas the high- field-strength elements (HSFE) have values close to those of MORB. Th varies from notably depleted to enriched. Nb and Y display weak troughs. while Ti shows moderate but variable enrichment.

1.6.2..2 Calc-alkaline volcanic rocks

Andesites. rhyolites and quartz feldspar porphyries are calc-alkaline. They have generally higher Sr. K_2O. and Ba than the tholeiitic rocks.

On chondrite-normalized plots. andesites (Fig. 1.5B) show moderate LREE/HREE enrichment (La_n/Yb_n = 4-9). with nearly flat HREE segments (Tb_n/Lu_n = 1-2). Three samples have positive Ce anomalies. On a MORB-normalized incompatible
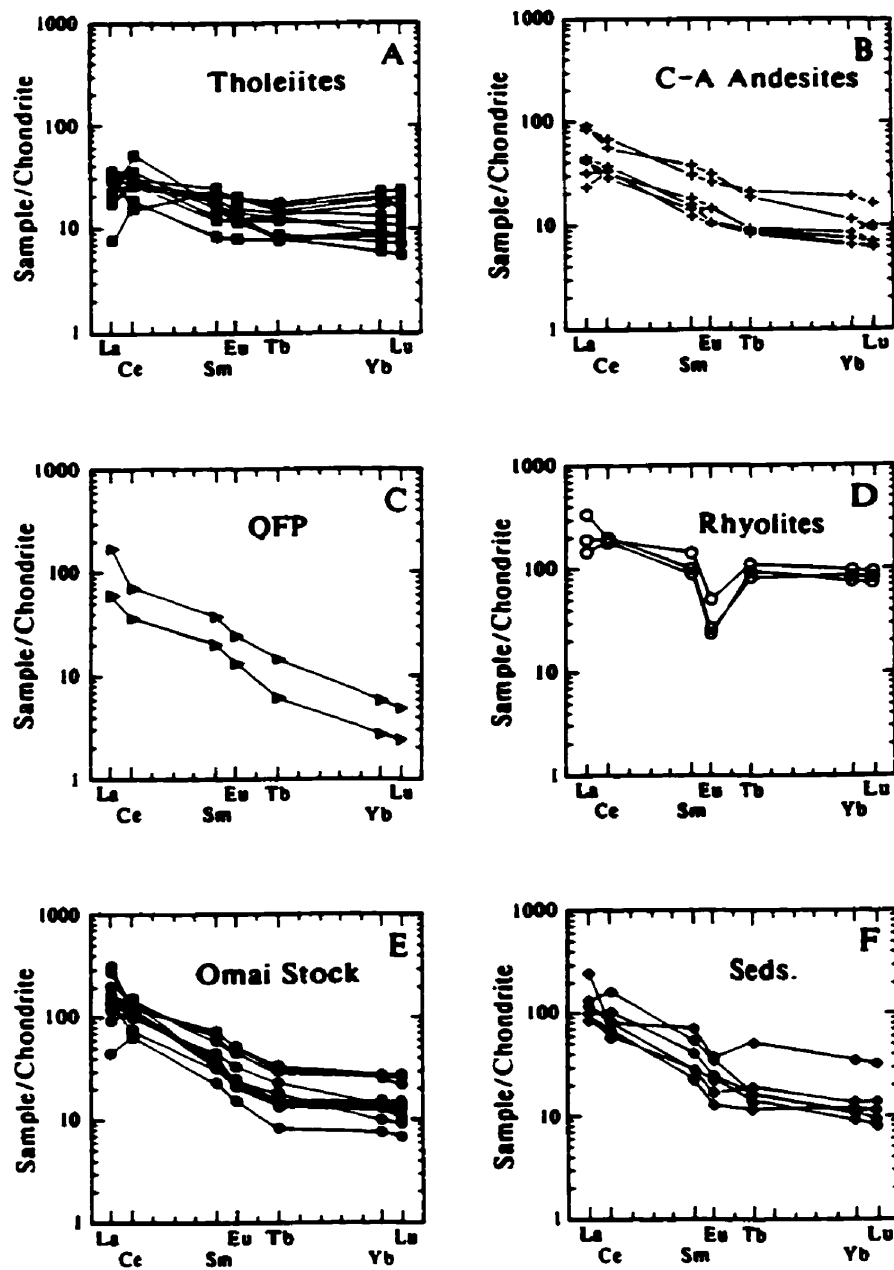
Figure 1.5   Chondrite-normalized REE patterns for Omai rock types. Normalizing values from Sun and McDonough (1989). A - tholeiites: B - calc-alkaline andesites: C - quartz-feldspar porphyries: D - rhyolites: E - Omai stock: F - sedimentary rocks.
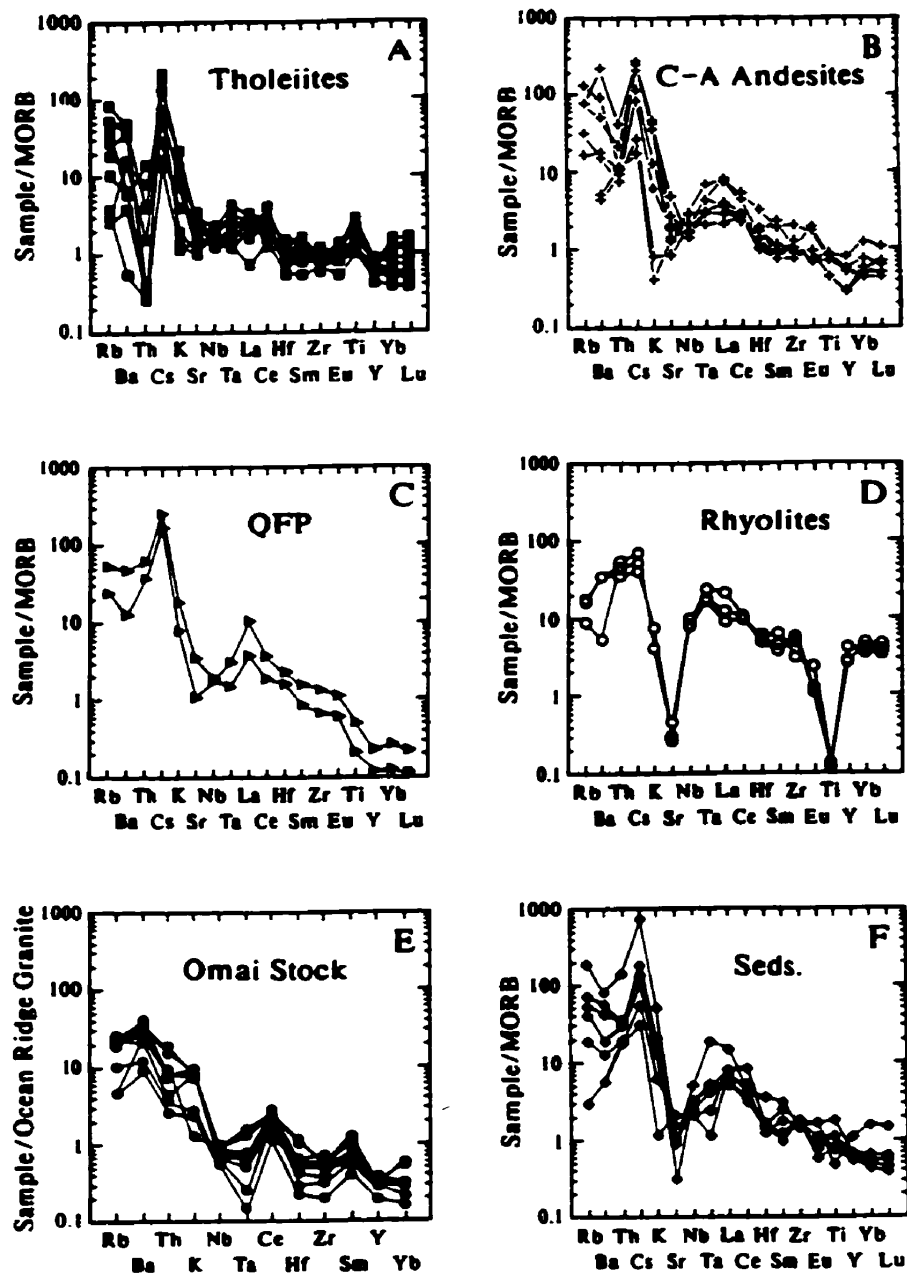
Figure 1.6   Incompatible element diagrams normalized to MORB (for volcanic and sedimentary rocks) and to ocean-ridge granite (for the Omai stock). MORB values are from Sun and McDonough (1989) and ORG values from Harris et al. (1986). A: tholeiites: B: calc-alkaline andesites: C: quartz-feldspar porphyries: D: rhyolites: E: Omai stock: F: sedimentary rocks.

element diagram. andesites (Fig. 1.6B) show variable LILE enrichment. and HFSE depletion (with pronounced Nb-Ta-Y-Ti troughs).

Quartz-feldspar porphyries have high LREE to HREE ratios (La_n/Yb_n = 23-29), but compared to andesites. they are depleted in HREE (Fig. 1.5C). The MORB-normalized diagram (Fig. 1.6C) indicates that the quartz-feldspar porphyries are strongly depleted in the HFSE.

A special case is represented by the rhyolitic rocks. They are high-Na (up to 5.8% Na_2O). corundum-normative peraluminous rhyolites. with a differentiation index > 91. The rhyolites have rare-earth and incompatible element patterns which are distinctive relative to other rocks of the volcanic sequence. The rhyolites have slightly sloping. chondrite-normalized REE patterns (La_n/Yb_n = 2-3.5). high REE contents. and strongly negative Eu anomalies (Eu/Eu* = 0.26) (Fig. 1.5D). On a MORB-normalized diagram. the rhyolites show Cs and Th enrichments (60 x MORB values). pronounced Ti and Sr troughs. and a general enrichment in the incompatible immobile elements (Nb. Y. Zr. Ta. Hf) (Fig. 1.6D).

1.6.2.3 Calc-alkaline plutonic rocks (Omai stock)

SiO_2 in the Omai stock varies from 49.5% in hornblendites to 68% in granodiorites. with a mean value of 60.1%. The granodioritic core is sodic (Na_2O/K_2O ratio = 13.7). whereas the intermediate phases (quartz monzodiorite and diorite) show variable K_2O enrichment (Na_2O/K_2O ratios of 7.9 to 1.1). Although some of the high K_2O values(>3%) may reflect gold-related sericite alteration. there is a general lack of

correlation between K_2O and LOI contents which suggests that the K_2O values are generally primary.

The Omai stock has an agpaitic index (molar alkali/alumina ratio) of <1. and is diopside-normative (up to 38% in hornblendites). which is typical of intermediate to weakly evolved metaluminous I-type granitoids. Na_2O and K_2O increase in abundance with SiO_2 content. suggesting a progressive evolution toward a more peraluminous. granitoid end member. TiO_2. Fe_2O_3. MnO. MgO. CaO. and P_2O_5 decrease with increasing SiO_2 content. indicating extraction of mafic phases during differentiation processes. There is no correlation between alumina and SiO_2 contents. The Nb/Ta ratios (8-53) in the Omai stock are similar with other I-type granites (Blevin and Chapell. 1995: Green. 1995).

Chondrite-normalized REE patterns for the Omai stock (Fig. 1.5 F) show pronounced LREE enrichment (La_n = 44 -315). moderate LREE/HREE ratios (La_n/Yb_n = 6-13). and nearly flat HREE segments (Tb_n/Lu_n = 1.2). The lack of negative Eu anomalies. and the generally parallel REE patterns of the Omai stock suggest that REE behaviour was not controlled by plagioclase fractionation. but rather by minerals such as sphene and apatite which have similar mineral/melt partition coefficients for the REE. Incompatible element distributions normalized to ocean-ridge granites (Fig. 1.6F) suggest a typical arc-like signature. with enrichment of the LILE (Ba. Rb. K. Th) and depletion of the HFSE (Nb. Ta. Y. Yb).

1.6.2.4 Sedimentary rocks

Metasedimentary rocks at Omai comprise tuffs and pelites, with alumina contents ranging between 12 and 18% (mean=14.3%). The silica content is highly variable (50-70%), but the mean of 62% is close to the mean of calc-alkaline volcanic rocks from Omai. The median K_2O/Na_2O ratio of 0.5 for pelites and tuffs is comparable to the ratio for sediments in other regions of the Barama-Mazaruni Supergroup (mean=0.8) and to that of modern sediments of arc terranes (Gibbs et al., 1986: Condie, 1993). The REE patterns of the Omai sedimentary rocks (Fig. 1.5E) show strong enrichment of LREE (La_n = 87-132), and moderate LREE/HREE ratios (La_n/Yb_n = 6-13) and resemble those of the calc-alkaline andesites and to a degree the quartz-feldspar porphyries. The sedimentary rocks thus appear to contain a dominantly calc-alkaline rather than tholeiitic volcaniclastic component. This is also shown by the incompatible element signature of the sediments (Fig. 1.6E), which is similar to that of the calc-alkaline andesites.

1.7 TECTONIC SETTING

Tholeiitic rocks at Omai have incompatible and rare-earth element distributions that are characteristic either of a volcanic island arc or of E-MORB basalts affected by a strong arc signature, a feature commonly reported from back-arc basin basalts (LeRoex, 1987: Stern et al., 1995a,b). The low abundance of Nb, Ta, and Ti in arc-related rocks has been explained by their retention in residual phases in a hydrated mantle source region (Condie, 1993). The enrichment of LILE is frequently attributed to their mobility in aqueous solutions generated by dewatering of the subducted oceanic slab (Pearce, 1982). The tholeiites are unlikely to be the product of melting of continental crust, but rather by melting peridotites. Although this indicates that the tholeiites have not

assimilated older. Archean. continental crust. some assimilation of Paleoproterozoic crustal material cannot be ruled out.

Th/Nb ratios are considered to be a useful monitor of LILE/HFSE variations in greenschist facies basalts due to the immobility of these elements and their different concentrations in juvenile magmas (Th/Nb in N-MORB <0.07: E-MORB <0.1) relative to the upper continental crust (Th/Nb in volcanic arc basalts > 0.1. Sun and McDonough. 1989: Stern et al.. 1995b). At Omai. the Th/Nb ratios of the tholeiites vary between 0.01 and 0.6. consistent with the occurrence of initially primitive basalt magma. some of which were partially contaminated by Paleoproterozoic crustal material in a back-arc environment. The pillowed nature of the tholeiitic volcanic rocks at Omai. together with the presence of immature sedimentary beds within the stratigraphic succession and tectonic setting diagrams (see below). is also consistent with an oceanic setting.

Calc-alkaline andesites at Omai are also pillowed. The calc-alkaline suite. which includes mainly andesites and subordinately rhyolites and quartz-feldspar porphyries. is characterized by large negative Nb-Ta anomalies and high LREE/HREE ratios. In the FeO^T-MgO-Al_2O_3 diagram of Pearce (1982) (not shown). most of the calc-alkaline rocks plot in the volcanic arc field. whereas the tholeiitic rocks are dispersed between ocean-island and continental fields. In the Hf-Th-Nb diagram of Wood (1980). all calc-alkaline rocks plot in the volcanic arc field. whereas most tholeiites plot in the E-MORB field. with a few in the volcanic arc field (Fig. 1.7).

The tectonic setting of the Omai stock also can be constrained by using major and trace element relations and multivariate discriminant analysis. Plots of SiO_2 vs $FeO^T/(FeO^T+MgO)$ (Maniar and Piccoli. 1989; not shown) and Rb vs Y+Nb (Fig. 1.8A) indicate that the Omai stock is a typical volcanic arc granitoid. The R1-R2 diagram of
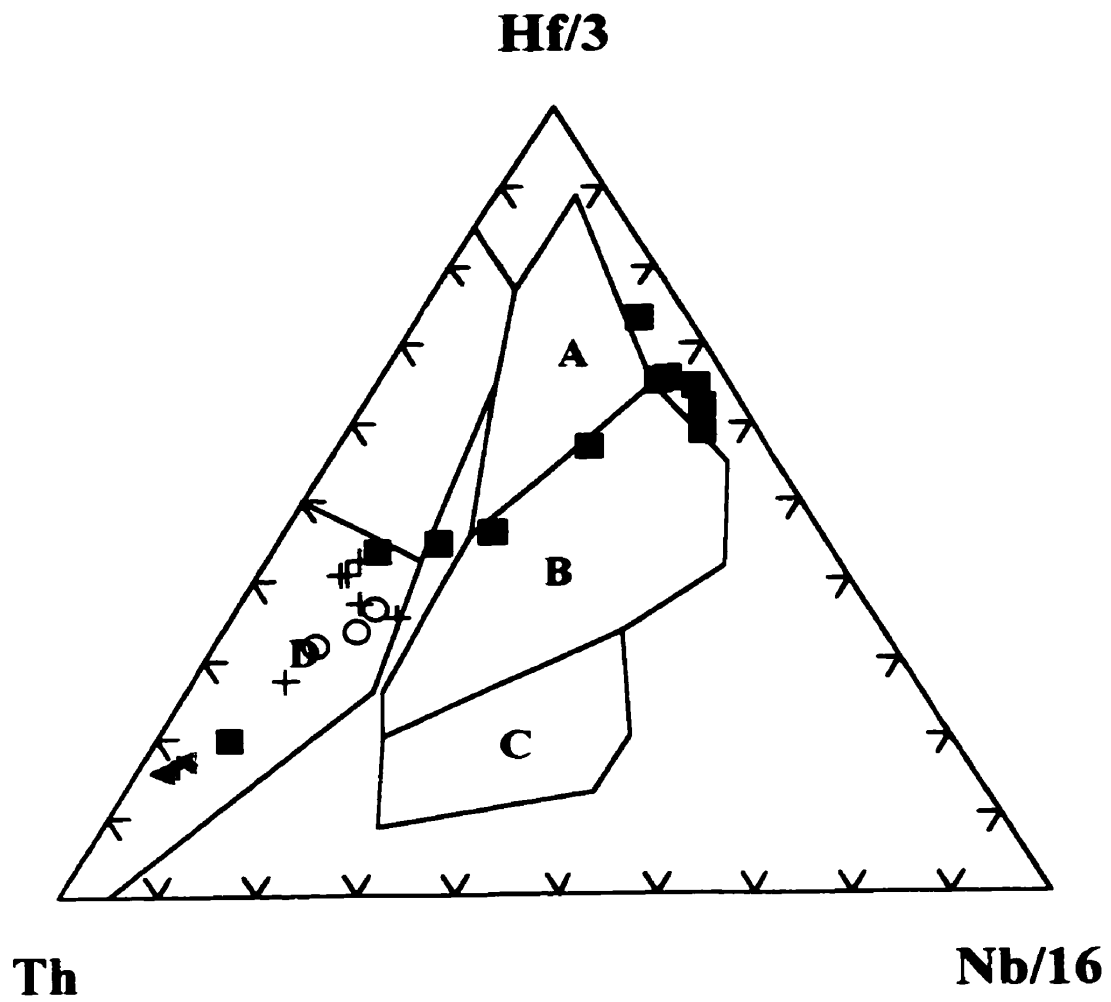
Figure 1.7   Hf-Th-Nb tectonic discrimination diagram (Wood. 1980) for the Omai volcanic rocks: A: N-MORB basalts: B: E-MORB basalts: C: within plate basalts: D: destructive plate-margin basalts. Symbols as in Figure 1.3.
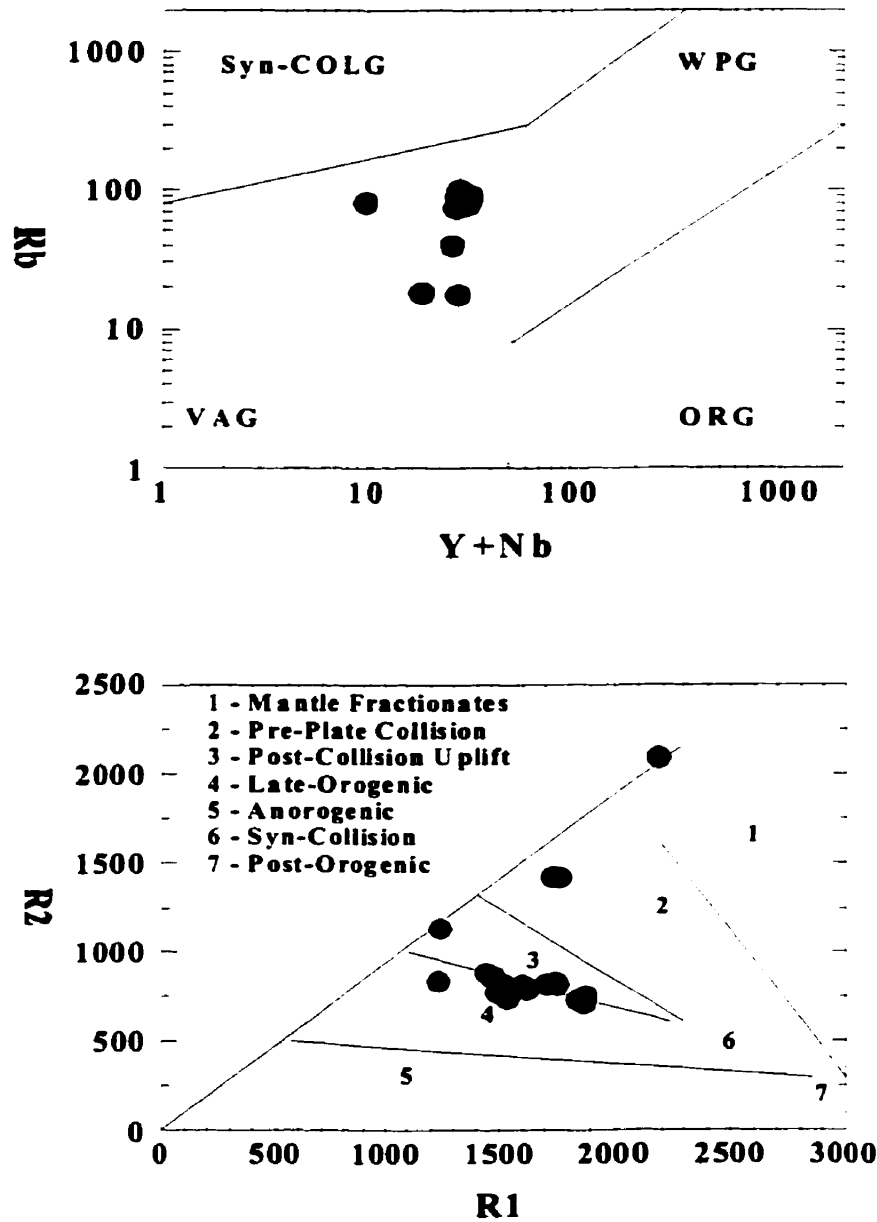
Figure 1.8   Tectonic discrimination diagrams for the Omai stock. A. Rb vs Y+Nb diagram (Pearce et al., 1984); VAG - volcanic arc granites; ORG - ocean ridge granites; WPG - within plate granites; Syn-COLG - collision granites; B. R1 vs R2 diagram (Batchelor and Bowden, 1985).

Batchelor and Bowden (1985) suggests that the stock is mainly a late-orogenic intrusion (Fig. 1.8B).

Rogers and Greenberg (1990) have classified granitoids into categories: (1) orogenic granitoids. which are subdivided into late-orogenic varieties (LO) associated with subduction-related. large calc-alkaline batholiths or small isolated stocks. and post-orogenic varieties (PO) that occur as isolated diapiric plutons: and (2) anorogenic granitoids. which are subdivided into anorthosite/rapakivi complexes (AR) and alkalic ring-complexes (RC). A discriminant score (D) for a granitoid can be obtained from the following linear discrimination equation (Agrawal. 1995):

$$D_i = B_1X_1 + B_2X_2 + \ldots + B_pX_p + B_0 \qquad (1)$$

where X is the major oxide value. B is the discriminant function coefficient. B_0 is a constant. and i = 1. 2. and 3. respectively. for the orogenic vs anorogenic. LO vs PO. and AR vs RC pairs of groups. The discriminant rule (R) for a granite group can be calculated using the equation:

$$R = (D_i - C_i)/(M_i - C_i) \qquad (2)$$

where C_i is the cut-off value. and M_i is the mean discriminant score for the first group in a two-group (orogenic-anorogenic. LO-PO. AR-RC) discriminant analysis with i = 1. 2. and 3. The results obtained for the Omai stock using the multivariate discriminant analysis are as follows:

A. Orogenic vs anorogenic pair: D_1 = -1.46: R = 2.24. As R is >0. the Omai stock is assigned to the first group (orogenic) from the two-group pair.

B. Late orogenic (LO) vs post-orogenic (PO) pair: D_2 = -2.61: R = 2.23. As R is > 0. the Omai stock is assigned to the first group (late orogenic) from the two-group pair.

The classification of the Omai stock as late orogenic is in good agreement with the geochronological data and the geological history of the Omai area.

1.8 DISCUSSION

The spread of geochemical patterns of the volcanic and plutonic rocks in a small sampled area at Omai suggests that the rocks represent more than one tectonic setting. Many back-arc basalts from modem ocean basins plot within both MORB and island-arc fields (Gaskarth and Parslow. 1987: Stern et al.. 1995b and references therein). These authors have noted that mafic rocks from back-arc basins commonly are enriched in LILE and depleted in the HFSE. At Omai. the occurrence of a tholeiitic basalt-basaltic andesite sequence. associated with calc-alkaline andesites. rhyodacites. rhyolites and intermediate-acid plutonic rocks. supports the hypothesis that the volcanic eruptions took place in both extensional and compressional environments. Similar relations have been described from the southern Abitibi Archean greenstone belt (Jackson et al.. 1994). from Proterozoic sequences in the southwestern United States and the Grenville Province. and from Tertiary sequences in central Chile (as discussed in Smith and Holm. 1987). The contrasting calc-alkaline and tholeiitic rocks in these areas are interpreted as the result of. respectively. successive back-arc closure and Andean-type orogenies. However. at Omai. geochemical and isotopic patterns for the calc-alkaline rocks suggest that they represent a relatively primitive island arc rather than a mature Andean-type arc. In

general. alternating periods of extension and compression could result in the migration of loci of magmatism and periodical changes in the chemical character of the magmas. This appears to have occurred both at the local scale (as at Omai). as well as in other parts of Guyana greenstone belts (Gibbs. 1987a: Renner and Gibbs. 1987: Elliott. 1992). It is proposed that the dominant tholeiitic volcanism at Omai formed in a back-arc basin. with a geochemically distinct arc signature. during extensional periods. whereas the calc-alkaline eruptions and intrusions reflect compressional periods. The locus of arc volcanism may have migrated with time across this part of the Guiana Shield. Syn- to post-volcanic accretion of this region to the margin of a continent. or to another crustal terrane. resulted in juxtaposed sequences composed of primitive mafic tholeiites. associated with more geochemically evolved intermediate to acid calc-alkaline magmas.

The occurrence of calc-alkaline as well as tholeiitic igneous rocks at Omai contrasts with the main tholeiitic trend of the Issineru Formation of the Barama-Mazaruni Supergroup (Renner and Gibbs. 1987). but is analogous to the majority of greenstone belts of the Guiana Shield (Veenstra. 1983: Gibbs. 1987a: Wirth et al.. 1990: Cox et al.. 1993: Gibbs and Barron. 1993: Milési et al.. 1995: Vanderhaeghe et al.. 1998). In the Abitibi Subprovince. similar trends occur in the greenstone sequence of the Blake River Group which ranges in composition from basalt to rhyolite and includes rocks of broadly alternating tholeiitic and calc-alkaline affinity (Thurston. 1990).

The moderate LREE enrichment of the Omai tholeiites contrasts with the flat (unfractionated) REE patterns commonly described for tholeiites in greenstone belts (for example. the Flin Flon belt. Canada: Stern et al.. 1995b). but has been described in the Archean Nondweni greenstone belt (Riganti and Wilson. 1995). This implies the involvement of a LREE-enriched mantle source in the generation of the tholeiitic lavas. La/Ta. Hf/Ta. and La/Yb ratios of the Omai tholeiites are lower than those of Paleoproterozoic basalts (Condie. 1990). and of Issineru Formation basalts (Renner and

Gibbs. 1987). but higher than those of Birimian greenstone basalts of the West African Craton (Sylvester and Attoh. 1992). suggesting relative inhomogenous source regions during the Paleoproterozoic time.

The mafic-ultramafic body north of the Fennell Pit shares many of the petrographic and geochemical characteristics of the Paleoproterozoic De Goeje gabbroic suite in Suriname (Bosma et al.. 1984). However. more geochemical data are needed to assess the regional extend of the ultramafic bodies and their structural and temporal relationships with the surrounding rock types.

The calc-alkaline andesitic rocks at Omai have trace element and REE patterns similar to those described for the calc-alkaline andesitic rocks of the Paramaca Formation (the equivalent to the Barama Mazaruni Supergroup) in northern French Guiana (Milési et al.. 1995: Vanderhaeghe et al.. 1998). which are both consistent with volcanism related to the development of magmatic arcs in a subduction context.

The trace element and REE patterns of the Omai rhyolites. as well as R1-R2 diagram (not shown) of Batchelor and Bowen (1985) suggest that they are post-orogenic. Thick Mesoproterozoic rhyolitic flows of the Iwokrama Formation occur about 40 km south of the Omai area (Walrond. 1987). The rhyolites occur at Omai as dikes crosscut by gold-bearing veins. suggesting that they have been emplaced before 1.99 Ga. the age of the mineralization. Furthermore. the geochemical characteristics of intra-continental rhyolitic flows of the Uatuma Supergroup of Venezuela and Brazil (Montalvao and Santarem. 1984). which is equivalent to the Iwokrama Formation of Guyana. indicate that there is a pronounced difference in their alkali contents compared to Omai rhyolites: Uatuma rhyolites have between 2 and 7% K_2O and < 1.5% Na_2O. whereas the Omai rhyolites have low K_2O (< 0.7%) and high Na_2O contents (up to 5.8%). The high-K

affinity generally reflects a progressive thickening of the crust. whereas the high-Na content characterizes early periods of crustal development. Thus, the Omai rhyolites can be considered as contemporaneous or slightly post-dating the early phases of crustal growth

The general petrological and geochemical characteristics of the Omai stock are similar to those of the Archean MMGS (late-syntectonic to late-tectonic monzodiorite-monzonite-granodiorite-syenite) series in the Pontiac subprovince. and the SMG (late-tectonic quartz-syenite-monzonite-granite) series in the Abitibi subprovince. Superior Province (Feng and Kerrich. 1992). These plutons range from large batholiths to small stocks and usually were emplaced at shallow levels at pressures of around 1 kbar. In a diagram of SiO_2 vs (CaO/Na_2O+K_2O) (Fig. 1.9A). the Omai stock plots in the SMG-MMGS field. In a Na_2O vs K_2O diagram (Fig. 1.9B). the stock plots between the SMG-MMGS field and Phanerozoic Lachan and Californian I-type granites.

The composition of the Paleoproterozoic Omai stock is consistent with the secular change (Sylvester and Attoh. 1992: Feng and Kerrich. 1992: Martin. 1993) documented elsewhere from high-Na trondhjemitic granitoids to lower Na/higher K post-Archean granitoids (Fig. 1.10).

At Omai. the relationship between the gold mineralization and its host rocks does not seem to be genetic. but rather. the emplacement of mineralization was strongly influenced by the rheological contrasts between the intrusive/subvolcanic bodies and the volcanic/sedimentary country rocks. These contrasts may have helped to focus the regional stress upon the more competent plutonic/subvolcanic bodies. resulting in brittle fracturing. and therefore in greatly enhanced permeability for the hydrothermal fluids.
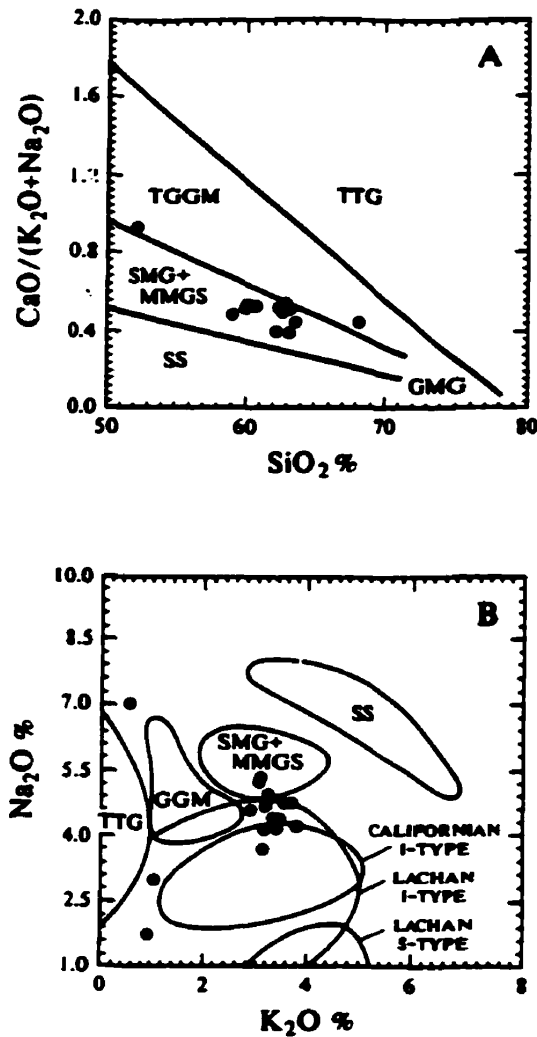
Figure 1.9   A. CaO/(K₂O+ Na₂O) *vs* SiO₂ diagram (modified from Feng and Kerrich. 1992). comparing the Omai stock with Archean granitoids of the Superior Province. Canada: TTG = synvolcanic trondhjemite-tonalite-granite series (Abitibi subprovince): TGGM = syntectonic tonalite-granodiorite-granite-quartz monzonite series (Abitibi): SMG = late-tectonic quartz syenite-monzonite-granite series (Abitibi): SS = post-tectonic alkali feldspar syenite series (Abitibi): MMGS = late syntectonic to late tectonic monzodiorite - monzonite - granodiorite - syenite series (Pontiac subprovince): GMC - syncollisional garnet - muscovite granite series (Pontiac). B. Na₂O *vs* K₂O diagram (modified from Feng and Kerrich. 1992) comparing the Omai stock with other Precambrian and Phanerozoic granitoids. Abbreviations as in A.
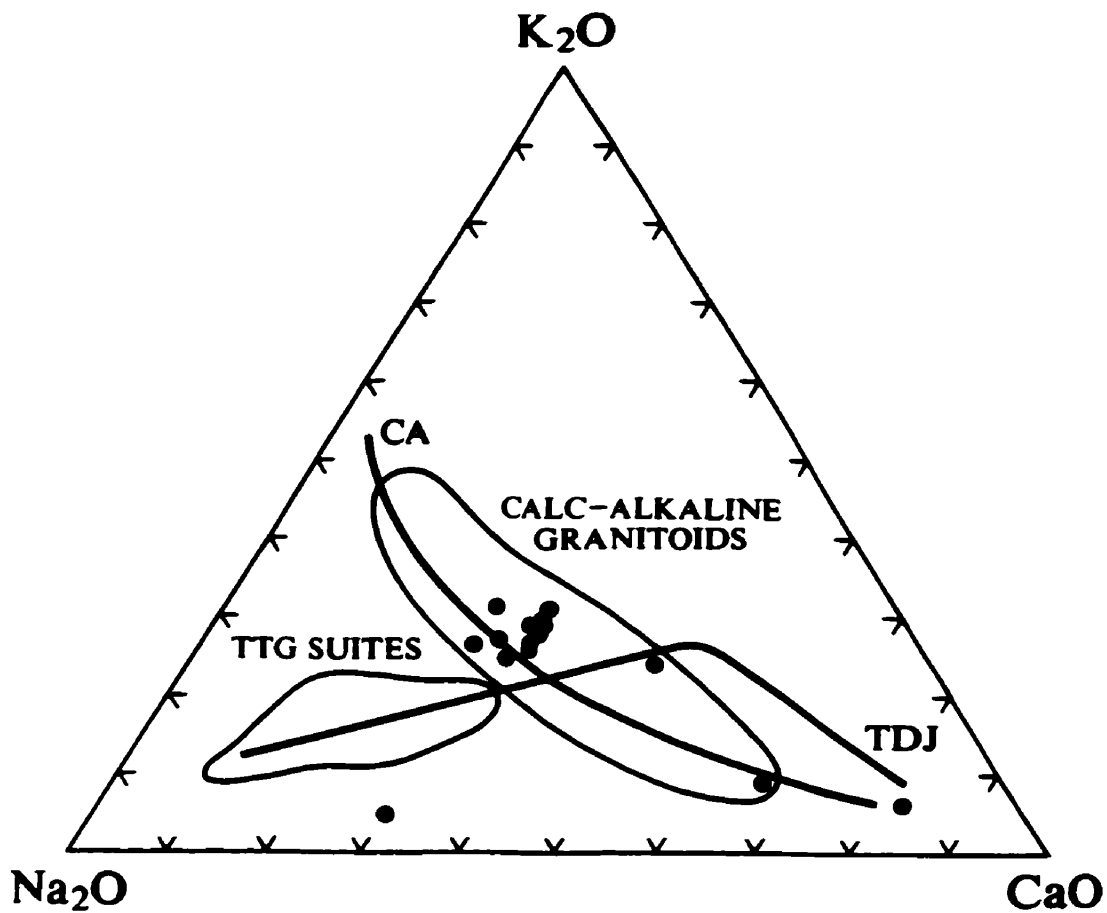
Figure 1.10 K_2O-Na_2O-CaO diagram (modified from Martin. 1993). showing that the Omai stock (closed circles) has a typical calc-alkaline affinity. which is similar to that of other Precambrian granitoids. but which contrasts with the Archean TTG trondhjemitic trend.

Using the tectonic classification scheme proposed for French Guiana by Milési et al. (1995), the Omai mineralization can be classified as late tectonic. Its emplacement was controlled by the last brittle to brittle-ductile stages (2.12-1.99 Ga) of the Trans-Amazonian orogeny. Features similar to those associated with the gold mineralization at Omai have been described for the gold deposits at LouLouie and Adieu-Vat in French Guiana (Milési et al. 1995). Las Cristinas in Venezuela (Cox et al.. 1993). and Hiré and Poura on the West African Craton (Milési et al.. 1992).

1.9 CONCLUSIONS

The volcanic complexes at Omai most likely originated within immature island arcs which were built on oceanic crust. in association with small marginal basins. Subsequently. during the compressional phases of the Trans-Amazonian orogeny. the sequences were accreted. producing a succession of marginal basin tholeiitic mafic lavas alternating with island arc calc-alkaline intermediate/felsic flows. The occurrence of calc-alkaline in addition to tholeiitic series may reflect the presence of a crustal component at depth during closure of a marginal ocean basin. Regional deformation (D1) resulted in E-W striking and steeply dipping structures. probably accompanied by low-grade (prehnite-pumpellyite) metamorphism. These events were closely followed by compressional peak of regional metamorphism in the subgreenschist to greenschist facies. which induced development of ductile-brittle shear zones. Granitoid plutonism and uplift followed shortly after closure of the ocean basin. as is the case for many modern subduction zones. The late tectonic phases were synchronous with the reactivation of shear zones. development of brittle fractures. and subsequent emplacement of the gold-bearing veins. Post-tectonic. intra-continental magmatism in the Omai area is represented by the Mesoproterozoic Tumatumari-Omai dike and Permo-Triassic Apatoe Suite.

1.10 REFERENCES

Agrawal. S.. 1995. Discrimination between late-orogenic. post-orogenic. and anorogenic granites by major element compositions. Journal of Geology. v. 103. p. 529-537.

Batchelor. R.A.. and Bowden. P.. 1985. Petrogenetic interpretation of granitoid rocks series using multication parameters. Chemical Geology. v. 48. p. 43-55.

Bateson. J.H.. 1961. Geological map. Potaro NE sheet. Geological Survey of British Guyana.

Bertoni. C.H.. Shaw. R.P.. Singh. R.. Minamoto. J.. Richards. J.M.. and Belzile. E.. 1991. Geology and gold mineralisation of the Omai property. Guyana. *In* Brazil Gold '91: The Economics. Geology. Geochemistry and Genesis of Gold Deposits. *Edited by* E.A. Ladeira. Balkema. Rotterdam. p. 767-773.

Bhatt. B.J.. 1995. Geology. geochemistry. and origin of the Proterozoic gold-quartz vein mineralization and igneous intrusions. Omai mines. Guyana. Unpublished report. 45 p.

Blevin. P.L.. and Chapell. B.W.. 1995. Chemistry. origin. and evolution of mineralized granites in the Lachlan fold belt. Australia: The metallogeny of I- and S-type granites. Economic Geology. v. 90. p. 1604-1619.

Böhlke. J.K.. 1989. Comparison of metasomatic reactions between a common CO_2-rich vein fluid and diverse wall rocks: intensive variables. mass transfers and Au mineralization at Alleghany. California. Economic Geology. v. 84. p. 291-327.

Bosma. W.. Kroonenberg. S.B.. van Lissa. R.V.. and de Roever. E.W.F.. 1984. An explanation to the geology of Suriname. Contributions to the Geology of Suriname. v. 8. p. 31-82.

Choudhuri. A.. 1978. Geochemical trends in tholeiite dykes of different ages from Guyana. Chemical Geology. v. 22. p. 79-85.

Choudhuri. A.. 1980. The early Proterozoic greenstone belt of the northern Guiana shield. South America. Precambrian Research. v. 13. p. 79-85.

Choudhuri. A.. Sial. A.N.. and Oliveira. E.P.. 1990. Unmetamorphosed Proterozoic tholeiite dykes from the northern Amazon Craton. Guiana. in the evolution of basaltic magmatism. *In* Mafic Dykes and Emplacement Mechanisms. *Edited by*

A.J. Parker. P.C. Rickwood and D.H. Tucker. IGCP Project 257. Publication Number 23. Balkema. Rotterdam. p. 275-284.

Collings. S.P.. 1969. Geology and geochemistry of the Omai Mine area. Omai. Guyana. Unpublished MSc thesis. Colorado School of Mines. 223 pp.

Condie. K.C.. 1990. Geochemical characteristics of Precambrian basaltic greenstones. In Early Precambrian Basic Magmatism. Edited by R.P. Hall and D.J. Hughes. Blackie. Glasgow. London. p. 40-56.

Condie. K.C.. 1993. Chemical composition and evolution of the upper continental crust: Contrasting results from surface samples and shales. Chemical Geology. v. 104. p. 1-37.

Cox. R.P.. Wynn. J.C.. Sidder. G.B.. and Page. N.J.. 1993. Geology of the Venezuelan Guayana Shield. In Geology and Mineral Resource Assessment of the Venezuelan Guayana Shield. Edited by U.S. Geological Survey and Corporation Venezolana de Guayana. Técnica Minera. C.A.. U.S. Geological Survey Bulletin 2062. p. 9-15.

Dossin. T.M.. Dossin. I.A.. Charvet. J.. and Bonhomme. M.G.. 1995. K-Ar chronology of a Mesozoic dyke swarm from southern Espinfaço region (SE Brazil). Journal of South American Earth Sciences. v. 8. no. 1. p. 47-53.

Elliott. R.G.. 1992. The Geology and the Geochemistry of the Omai Goldfield. Guyana. Ph.D. thesis. Oxford Brookes University. Oxford. 230 p.

Feng. R.. and Kerrich. R.. 1992. Geochemical evolution of granitoids from the Archean Abitibi Southern Volcanic Zone and the Pontiac subprovince. Superior Province. Canada: Implications for tectonic history and source regions. Chemical Geology. v. 98. p. 23-70.

Gaskarth. J.W.. and Parslow. G.R.. 1987. Proterozoic volcanism in the Flin Flon greenstone belt. east-central Saskatchewan. Canada. In Geochemistry and Mineralization of Proterozoic Volcanic suites. Edited by T.C. Pharaoh. R.D. Beckinsale and D. Rickard. Geological Society Special Publication. 33. Blackwell. Oxford. p. 183-200.

Gibbs. A.K.. 1987a. Proterozoic volcanic rocks of the northern Guyana Shield. South America. In Geochemistry and Mineralization of Proterozoic Volcanic Suites. Edited by T.C. Pharaoh. R.D. Beckinsale and D. Rickard. Geological Society of London Special Publication. 33. Blackwell. Oxford. p. 275-288.

Gibbs. A.K.. 1987b. Contrasting styles of continental mafic intrusions in the Guiana Shield. *In* Mafic Dykes Swarms. *Edited by* H.C. Halls and W.F. Fahrig. Geological Association of Canada Special Paper. 34. p. 457-465.

Gibbs. A.K.. and Olszewski. W.J.. 1982. Zircon U-Pb ages of Guiana greenstone-gneiss terrane. Precambrian Research. v. 17. p. 199-214.

Gibbs. A.K.. and Barron. C.N.. 1983. The Guiana Shield reviewed. Episodes. v. 2. p. 7-14.

Gibbs. A.K.. and Barron. C.N.. 1993. Geology of the Guiana Shield. Oxford Monographs on Geology and Geophysics. v. 22. Clarendon Press. Oxford. 246 p.

Gibbs. A.K.. Montgomery. C.W.. O'Day. P.A.. and Erslev. E.A.. 1986. The Archean-Proterozoic transition: Evidence from the geochemistry of metasedimentary rocks of Guyana and Montana. Geochimica et Cosmochimica Acta. v. 50. p. 2125-2141.

Green. T.H.. 1995. Significance of Nb/Ta as an indicator of geochemical processes in the crust-mantle system. Chemical Geology. v. 120. p. 347-359.

Gruau. G.. Martin. H.. Leveque. B.. and Capdevilla. R.. 1985. Rb-Sr and Sm-Nd geochronology of Lower Proterozoic granite-greenstone terrains in French Guiana. South America. Precambrian Research. v. 30. p. 63-80.

Guardia. F.J.. 1969. The Omai Mine area - report on geological and geochemical surveys Sept.-Dec. 1967. Geological Survey of Guyana. unpublished report. 46 p.

Harris. N.B.W.. Pearce. J.A.. and Tindle. A.G.. 1986. Geochemical characteristics of collision-zone magmatism. *In* Collision Tectonics. *Edited by* M.P. Cowed and A.C. Ries. Geological Society of London. Special Publication. v. 19. p. 67-81.

Hawkes. D.D.. 1966. Differentiation of the Tumatumari-Kopinang dolerite intrusion. British Guyana. Geological Society of America Bulletin. v. 77. p. 1131-1158.

Hodgson. C.J.. 1990. An overview of the geological characteristics of gold deposits in the Abitibi subprovince. University of Western Australia Geology Department Extension Publication. v. 24. p. 63-100.

Hodgson. C.J.. and MacGeehan. P.J.. 1982. A review of the geological characteristics of 'gold-only' deposits in the Superior province of the Canadian Shield. *In*

Geology of Canadian Gold Deposits. *Edited* by R.W. Hodder and W. Petruk. CIMM Special Volume 24. p. 211-227.

Irvine. T.N.. and Baragar. W.R.A.. 1971. A guide to the chemical classification of the common volcanic rocks. Canadian Journal of Earth Sciences. v. 8. p. 523-548.

Jackson. S.L.. Fyon. J.A.. and Corfu. F.. 1994. Review of Archean supracrustal assemblages of the southern Abitibi greenstone belt in Ontario. Canada: products of microplate interaction within a large-scale plate-tectonic setting. Precambrian Research. v. 65. p. 183-205.

Leube. A.. Hirdes. W.. Mauer. R.. and Kesse. G.O.. 1990. The Early Proterozoic Birimian Supergroup of Ghana and some aspects of its associated gold mineralization. Precambrian Research. v. 46. p. 139-165.

LeRoex. A.P.. 1987. Source regions of mid-ocean ridge basalts: evidence for enrichment processes. *In* Mantle Metasomatism. *Edited by* M.A. Menzies and C.J. Hawkesworth. Academic Press. p. 389-422.

Maniar. P.D.. and Piccoli. P.M.. 1989. Tectonic discrimination of granitoids. Geological Society of America Bulletin. v. 101. p. 635-643.

Martin. H.. 1993. The mechanisms of petrogenesis of the Archean continental crust - Comparison with modern processes. Lithos. v. 30. p. 373-388.

McPhie. J.. Doyle. M.. and Allen. R.. 1993. Volcanic textures. A guide to the interpretation of textures in volcanic rocks. University of Tasmania. 196 p.

Milési. J-P.. Ledru. P.. Feybesse. J-L.. Dommanget. A.. and Marcoux. E.. 1992. Early Proterozoic ore deposits and tectonics of the Birimian orogenic belt. West Africa. Precambrian Research. v. 58. p. 305-344.

Milési. J-P.. Egal. E.. Ledru. P.. Vernhet. Y.. Thiéblemont. D.. Cocherie. A.. Tegyey. M.. Martel-Jantin. B.. and Lagny. P.. 1995. Les minéralisations du Nord de la Guyane française dans leur cadre géologique. Chronique de recherche minière. v. 518. p. 5-58.

Montalvao. R.M.G.. and Santarem. P.C.. 1984. Parametros estatisticos para oxidos (elemenos maiores das rochas vulcanicas e piriclasticas do supergrupo Uatuma): parte I. DNPM. Anais. II Symposium Amazonico. Manaus. Brazil. p. 179-212.

Montgomery. C.N.. 1979. Uranium-lead isotopes of the Archean Imataca series. Venezuelian Guiana Shield. Contributions to Mineralogy and Petrology. v. 69. p. 167-176.

Nabelek. P.I.. 1986. Trace element modelling of the petrogenesis of granophyres and aplites in the Noatch Peak granitic stock. Utah. American Mineralogist. v. 71. p. 460-471.

Oliveira. E.P.. Tarney. J.. and João. X.J.. 1990. Geochemistry of the Mesozoic Amapá and Jari dyke swarms. northern Brazil: Plume-related magmatism during the opening of the central Atlantic. In Mafic Dykes and Emplacement Mechanisms. Edited by A.J. Parker. P.C. Rickwood and D.H. Tucker. IGCP Project 257. Publication Number 23. Balkema. Rotterdam. p. 173-184.

Pearce. J.A.. 1982. Trace element characteristics of lavas from destructive plate boundaries. In: Andesites: Orogenic Andesites and Related Rocks. Edited by R.S. Thorpe. John Wiley. New York. p. 524-548.

Renner. R.. and Gibbs. A.K.. 1987. Geochemistry and petrology of metavolcanic rocks of the early Proterozoic Mazaruni greenstone belt. northern Guyana. In Geochemistry and Mineralization of Proterozoic Volcanic Suites. Edited by T.C. Pharaoh. R.D. Beckinsale and D. Rickard. Geological Society Special Publication. 33. Blackwell. Oxford. p. 289-314.

Ridley. J.. Mikucki. E.J.. and Groves. D.I.. 1996. Archean lode-gold deposits: fluid flow and chemical evolution in vertically extensive hydrothermal systems. Ore Geology Reviews. v. 10. p. 279-293.

Riganti. A.. and Wilson. A.H.. 1995. Geochemistry of the mafic/ultramafic volcanic associations of the Nondweni greenstone belt. South Africa. and constraints on their petrogenesis. Lithos. v. 34. p. 235-252.

Robert. F.. and Brown. A.C.. 1986. Archean gold-bearing quartz veins at the Sigma Mine. Abitibi greenstone belt. Quebec: Part II. Vein paragenesis and hydrothermal alteration. Economic Geology. v. 81. p. 593-616.

Rogers. J.J.W.. and Greenberg. J.K.. 1990. Late-orogenic. post-orogenic. and anorogenic granites: distinction by major-element and trace-element chemistry and possible origins. Journal of Geology. v. 98. p. 291-309.

Smith. T.E.. and Holm. P.E.. 1987. The trace element geochemistry of metavolcanics and dykes from Central Metasedimentary Belt of the Grenville Province. southeastern

Ontario. Canada. *In* Geochemistry and Mineralization of Proterozoic Volcanic Suites. *Edited by* T.C. Pharaoh. R.D. Beckinsale and D. Rickard. Geological Society Special Publication. 33. Blackwell. Oxford. p. 453-470.

Snelling. N.J.. and McConnell. R.B.. 1969. The geochronology of Guyana. Geologie en Mijnbouw. v. 48. p. 201-213.

Spooner. E.T.C.. and Barrie. C.T.. 1993. A special issue devoted to Abitibi ore deposits in a modern context. Preface. Economic Geology. v. 88. p. 1307-1322.

Stern. R.A.. Syme. E.C.. Bailes. A.H.. and Lucas. S.B.. 1995a. Paleoproterozoic (1.90-1.86 Ga) arc volcanism in the Flin Flon Belt. Trans-Hudson Orogen. Canada. Contributions to Mineralogy and Petrology. v. 119. p. 117-141.

Stern. R.A.. Syme. E.C.. and Lucas. S.B.. 1995b. Geochemistry of 1.9 Ga MORB- and OIB-like basalts from the Amisk collage. Flin Flon Belt. Canada: Evidence for an intra-oceanic origin. Geochimica et Cosmochimica Acta. v. 59. p. 3131-3154.

Sun. S-S.. and McDonough. W.F.. 1989. Chemical and isotopic systematics of oceanic basalts: implication for mantle composition and processes. *In* Magmatism in the Ocean Basins. *Edited by* A.D. Saunders and M.J. Norry. Geological Society Special Publication. 42. Blackwell. Oxford. p. 313-345.

Sylvester. P.J.. and Attoh. K.. 1992. Lithostratigraphy and composition of 2.1 Ga greenstone belts of the West African Craton and their bearing on crustal evolution and the Archean-Proterozoic boundary. Journal of Geology. v. 100. p. 377-393.

Teixeira. W.. 1990. The Proterozoic mafic dyke swarms and alkaline intrusions in the Amazonian Craton. South America. and their tectonic evolution based on Rb-Sr. K-Ar and Ar-Ar geochronology. *In* Mafic Dykes and Emplacement Mechanisms. *Edited by* A.J. Parker. P.C. Rickwood and D.H. Tucker. IGCP Project. Publication 23. Balkema. Rotterdam. p. 285-294.

Teixeira. W.. Tassinari. C.C.G.. Cordani. U.G.. and Kawashita. K.. 1989. A review of the geochronology of the Amazonian Craton: tectonic implications. Precambrian Research. v. 42. p. 213-227.

Thurston. P.C.. 1990. Early Precambrian rocks of the Canadian Shield. *In* Early Precambrian Basic Magmatism. *Edited by* R.P. Hall and D.J. Hughes. Blackie. Glasgow. London. p. 221-247.

Vanderhaeghe. O.. Ledru. P.. Thiéblemont. D.. Egal. E.. Cocherie. A.. Tegyey. M.. and Milési. J-P.. 1998. Contrasting mechanism of crustal growth. Geodynamic evolution of the Paleoproterozoic granite-greenstone belts of French Guiana. Precambrian Research. v. 92. p. 165-193.

Veenstra. E.. 1983. Petrology and geochemistry of sheet Stonbroeke. Sheet 30. Suriname. Contributions to the Geology of Suriname. v. 7. p. 1- 112.

Voicu. G.. and Bardoux. M.. 1995. Petrography. geochemistry. and tectonic transitions in the evolution of the Omai zone. Guyana. South America. Unpublished report. 185 p.

Voicu. G.. Bardoux. M.. Harnois. L.. Stevenson. R.. and Crépeau. R.. 1996. Geochemical evolution of the Paleoproterozoic volcanic and igneous rocks from Omai area. Guyana. South America: Implications for tectonic history and source regions. 30th International Geological Congress. Beijing. China. Abstracts. v. 2. p. 324.

Walrond. G.W.. 1980. A metallogenetic scheme for the Guyana Shield. In Metalogenesis en Latinoamerica. Edited by J.L.L. Moreno. Simposium Internacional. Mexico. p. 141-164.

Walrond. G.W.. 1987. Geological map of Guyana. Guyana Geology and Mines Commission.

Williams. E.. Cannon. R.T.. McConnell. R.B.. and Snelling. N.J.. 1967. The folded Precambrian of northern Guyana related to the geology of the Guiana Shield. Geological Survey of Guyana Records. v. 5. 60 p.

Wincester. J.A.. and Floyd. P.A.. 1977. Geochemical discrimination of different magma series and their differentiation products using immobile elements. Chemical Geology. v. 20. p. 325-343.

Wirth. K.R.. Oliveira. E.P.. Silva. J.H.. and Tarney. J.. 1990. Early Precambrian basic rocks of South America. In Early Precambrian Basic Magmatism. Edited by R.P. Hall and D.J. Hughes. Blackie. Glasgow and London. p. 379-404.

Wood. D.A.. 1980. Major and trace element variations in the Tertiary lavas of eastern Iceland and their significance with respect to the Iceland Geochemical Anomaly. Journal of Petrology. v. 19. p. 393-436.

CHAPTER II

TELLURIDES FROM THE PALEOPROTEROZOIC OMAI GOLD DEPOSIT, GUIANA SHIELD

2.1 INTRODUCTION

The Omai gold deposit is the first primary gold mine in the Guiana Shield and contains more than 120 tonnes of gold that occurs almost exclusively in quartz±carbonate±scheelite veins. The deposit is located in the Paleoproterozoic Barama-Mazaruni Supergroup of north-central Guyana (Fig. 2.1), a greenstone sequence consisting of alternating mafic/felsic volcanic rocks and sedimentary rocks, intruded by granitoid batholiths and stocks (Gibbs and Barron, 1993). At Omai, the gold-bearing veins occur within an epizonal, quartz-monzodioritic stock (Omai stock - Fennell pit), as well as within quartz-feldspar porphyry and rhyolite dikes and, to a lesser extent, in surrounding andesite and basalt flows and metapelitic rocks (Wenot pit) (Voicu et al., 1997a,b). The veins are undeformed and occupy the extensional fractures between WNW-ESE striking shear zones. The wallrocks and vein selvages commonly show discrete sheared planes, with both dextral and sinistral senses of movement. In the immediate vicinity of the quartz veins, the host rocks are altered to an assemblage of carbonate, quartz, sericite, chlorite, albite, pyrite, and pyrrhotite. The hydrothermal assemblages are superimposed on earlier phases of alteration related to the spilitization of the volcanic rocks and to the lower greenschist facies metamorphism that affected all rock types.

In the Omai stock (Fennell pit), the veins are subparallel and their thickness may vary from a few centimeters up to about 1.5 m. They chiefly strike $025°-035°$ and dip $15-35°$ northwest. A subordinate vein set, which strikes $300°-320°$ and dips $15°-35°$ southwest occurs locally. The intersections of these two vein sets are strongly enriched in gold. A third set, represented by thin (several cm thick) quartz veins, strikes generally $330°$ and dips steeply ($75°-85°$ in either direction). These vein sets are contemporaneous, resulting in complex crosscutting relationships. Few veins cut across the entire width of the stock, but commonly the veins define en echelon patterns.
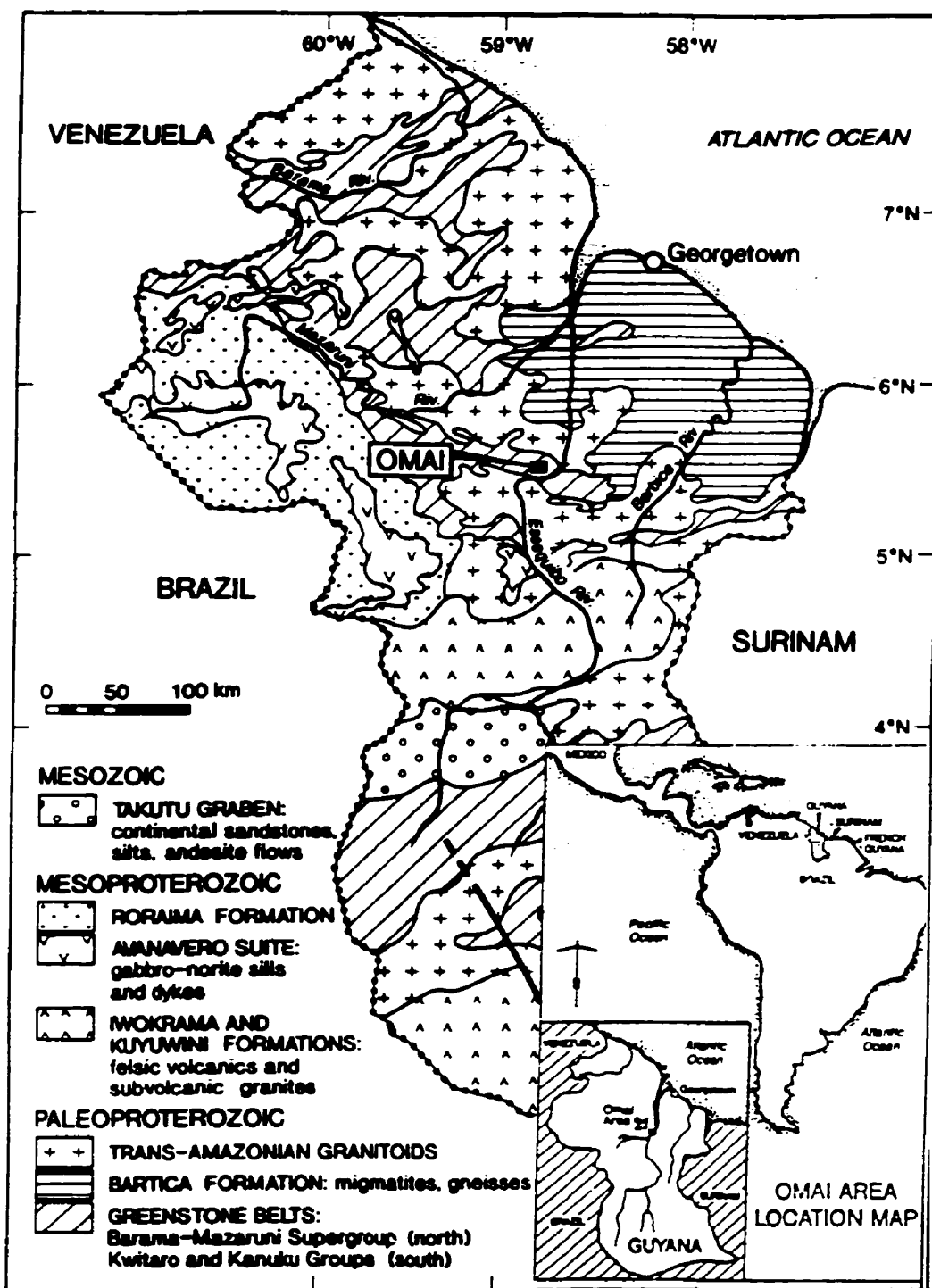
Figure 2.1   Simplified geological map of Guyana. modified after Walrond (1987) and Gibbs and Barron (1993). showing location of Omai mine.

In the Wenot pit. most mineralized veins are located in the east-west striking porphyry and rhyolite dikes and less frequently in andesites and metapelites. The veins have highly variable strikes and dips. which result in a stockwork aspect. However. there are three principal strike and dip sets: $020°-040°/70°-85°$. $020°-040°/30°-40°$. and $090°-110°/70°-90°$. The thickness of these veins is usually less than 0.3 m. while their frequency is significantly greater when compared to those in the Omai stock.

The gold-bearing veins appear to have formed by one or several crack and seal episodes of fracturing and vein formation caused by a protracted hydrothermal event. Two principal textures have been observed. namely 'ribbon' and 'breccia'. Ribbons are defined by individual mineral layers. which vary in thickness between several mm to more than 10 cm. The layers can be symmetrical about the vein central plane. indicating that opening of the veins took place on both walls of the vein. or asymmetrical. caused by reopening along one selvage. The core of the veins is generally occupied by quartz. but veins consisting mainly of ankerite or scheelite. with minor quartz and pyrite. occur locally in the Omai stock. Single- or multiple-stage brecciated veins contain angular or subrounded fragments of wallrocks reaching up to 0.8 m. Even if the fragments are poorly sorted. the largest tend to cluster toward the basal contacts of the veins. The wallrock fragments are usually near their location of origin. but transported fragments up to several meters from their original locations have been observed.

The telluride minerals for this study were collected from the ribboned and breccia veins located in the Omai stock and in surrounding andesites/basalts. Tellurides were not observed in the gold-bearing veins from the Wenot pit. This study is particularly concerned with the telluride mineral description and their relationships with co-existing metallic and gangue assemblage for each hydrothermal stage. These observations have been further used to establish the physico-chemical parameters of the environment of gold deposition. Using the telluride-bearing assemblages in relationship with the

thermodynamic data available for other mineral species may provide narrower limits on depositional conditions compared to the telluride-free assemblages. Furthermore, the knowledge of mineral assemblage and the physico-chemical conditions of ore deposition at Omai can contribute to a better understanding of the Paleoproterozoic greenstone-hosted gold deposits in the Guiana Shield and West African Craton. where only few of them such as Ashanti are well studied.

2.2 VEIN MINERALOGY

Table 2.1 summarises the vein mineralogy for the three mineralizing stages at Omai. Ore minerals and gangue are represented by silicates (quartz. sericite. chlorite. epidote. albite). carbonates (ankerite. calcite). tungstates (scheelite). sulfides (pyrite. galena. chalcopyrite. pyrrhotite. sphalerite. molybdenite). oxides (hematite. magnetite. rutile). borosilicates (tourmaline). native elements (Au. Cu). tellurides. and sulfosalts. Table 2.2 shows the chemical composition of the principal tellurides. sulfides. and native elements.

Quartz is the main vein-filling phase forming between 65 and 98% of vein volume. Two different types of quartz are related to mineralization. smokey and milky quartz. Scheelite and carbonates occur as semicontinuous coatings along the vein selvages.

Gold appears relatively early in the ore paragenesis. although the main gold mineralization is associated with sulfide and telluride deposition during stages II and III. It occurs both as free gold. as macroscopic irregular-shaped coarse grains (up to 4 mm) or dendritic fracture filling in milky quartz. scheelite. and carbonates. or as refractory ore. as small globular inclusions in pyrite (Fig. 2.2A) and pyrrhotite. usually in symplectitic intergrowths with sulfides and tellurides (Fig. 2.2G). The gold has high

Table 2.1   Mineral assemblage of the mineralized veins at Omai

Stage I	Stage II	Stage III	Post-mineralization
smokey quartz. calcite. ankerite. chlorite. epidote. albite. scheelite. rutile. tourmaline. pyrite. magnetite. chalcopyrite. melonite. native gold	milky quartz. calcite. ankerite. white mica. pyrite. pyrrhotite. sphalerite. galena. chalcopyrite. hematite. calaverite. hessite. petzite. altaite. coloradoite. tellurobismuthite. native gold	milky quartz. calcite. white mica. pyrite. sphalerite. galena. chalcopyrite. molybdenite. calaverite. hessite. petzite. tellurobismuthite. native copper. native gold	translucent quartz. calcite

Table 2.2   Representative compositions (in weight %) of native elements.

tellurides and common sulfides

Mineral	Stage	Au	Ag	Pb	Bi	Fe	Pt	Ni	Zn	Te	S	Sb	Hg	Total
Native gold	Au I	92.80	5.40	0	0	0.62	0	0	0	0.01	0.07	0	na	98.99
	Au I	90.44	8.71	0	0.11	1.91	0	na	0	0.08	0.31	0	1.11	102.67
	Au II	97.01	2.78	0	0	0.01	0	0	0	0	0.02	0	na	99.82
	Au III	92.80	5.37	0	0	0.62	0	na	0	0.01	0.06	0	na	98.89
	Au III	92.81	5.99	0	0	0.42	0	na	Na	0.04	0.07	0	1.22	100.58
Petzite	Ptz II	24.01	42.10	0	0.05	0.44	0.01	0	0	32.43	0.10	0.16	na	99.39
(AuAg;Te;)	Ptz II	20.82	46.37	0	0	0.58	0	na	Na	32.52	0.09	0.17	0.14	100.35
	Ptz II	22.33	43.54	0	0	0.91	0	na	Na	32.09	0.15	0.16	0.10	99.31
	Ptz II	24.45	44.14	0	0	0.17	0.01	0	0	30.17	0.10	0.16	na	99.22
	Ptz III	25.30	45.64	0	0	0.07	0	0	0	29.94	0.10	0.15	na	101.21
Calaverite	Cal II	41.68	0.71	0	0.19	0.35	0	na	Na	54.41	0.01	0.36	0.58	98.38
(AuTe;)	Cal II	41.69	0.75	0	0.07	0.76	0	na	Na	54.27	0.02	0.32	0.45	98.39
	Cal II	41.55	0.04	0	0.16	0.80	0	0	0	55.09	0.04	0.31	na	98.08
Hessite	Hes II	0.68	60.48	0.07	0	0.19	0	0	0	37.17	0.09	0.18	na	98.82
(Ag;Te)	Hes II	0.67	59.13	0	0	0.33	0	0	0	37.38	0.09	0.22	na	97.78
Telluro-	Tb II	0	0	0	53.15	0.32	0.01	0	0	44.79	0.28	0.28	na	98.86
Bismuthite	Tb III	0	0	0.04	51.76	0.14	0	0	0	45.25	0.05	0.23	na	97.56
(Bi;Te;)	Tb III	0	0	0	51.58	0.37	0	0	0	45.78	0.01	0.33	na	98.10
Melonite		0	0	0	0.01	0.80	0	20.82	0	79.18	0.23	0	na	101.04
(NiTe;)		0	0.05	0	0.16	5.88	0	15.38	0	69.82	8.24	0.47	0	100.06

na - not analyzed; 0 = below detection limit; Mineral compositions were determined on a JEOL electron-microprobe at McGill University in Montreal. Operating conditions were an accelerating voltage of 15 kV and a sample current of 20 nA on a Faraday cup. On-line ZAF corrections were performed by the MAGIC IV program. The following standards were used (in weight %): for Pd. Te and Hg - Pd;HgTe; (synthetic). Pd = 35.37, Hg = 22.22, Te = 42.41: for As - arsenopyrite. Fe = 33.05. Co = 0.58. Ni = 0.21. As = 45.61. Bi = 0.88. S =19.67: for Bi - Bi$_2$S$_3$. Bi = 81.29. S = 18.71: for Pb - galena. Pb = 86.60. S = 13.40: for Fe - pyrite. Fe = 46.55: S = 53.45: for Au. Ag. Pt. Sb - pure metals. Composition of electron-microprobe standards was obtained by EPMA

Table 2.2   Representative compositions (in weight %) of native elements. tellurides and common sulfides (continuation)

Mineral	Stage	Au	Ag	Pb	Bi	Fe	Pt	Ni	Zn	Te	S	Sb	Hg	Total
Altaite		0.00	0.16	57.25	0.15	0.59	0.01	na	Na	35.60	0.05	0.24	na	94.06
(PbTe)		0.04	0.08	58.14	0.10	1.24	0.05	na	Na	35.52	0.38	0.22	na	95.78
Coloradoite		0.04	13.34	0	0	1.54	0.08	na	Na	34.75	0.25	0.17	51.41	101.15
((Hg.Ag)Te)														
Galena	Gal III	0.01	0	83.93	0	0.10	0.08	na	Na	0.15	12.92	0	na	97.27
	Gal III	0	0	83.59	0	0.19	0.01	na	Na	0.06	13.11	0	na	96.94
	Gal II	0.00	0	86.57	0	0.52	0.00	na	Na	0.03	13.20	0	na	100.42
Sphalerite	Sph II	0.00	0	0	0	1.59	0	na	67.04	0	30.70	na	na	99.33
Pyrite	Py III	na	na	na	na	51.35	na	na	0	na	48.63	na	na	99.96
		na	na	na	na	51.29	na	na	0	na	49.07	na	na	100.32
Pyrrhotite		0	na	na	na	62.67	na	1.43	0	na	34.32	na	na	98.40
		0	na	na	na	61.20	na	na	Na	na	36.53	na	na	97.72

na- not analyzed; 0 = below detection limit; Mineral compositions were determined on a JEOL electron-microprobe at McGill University in Montreal. Operating conditions were an accelerating voltage of 15 kV and a sample current of 20 nA on a Faraday cup. On-line ZAF corrections were performed by the MAGIC IV program. The following standards were used (in weight %): for Pd. Te and Hg - Pd$_3$HgTe$_3$ (synthetic). Pd = 35.37. Hg = 22.22. Te = 42.41: for As – arsenopyrite. Fe = 33.05. Co = 0.58. Ni = 0.21. As = 45.61. Bi = 0.88. S =19.67: for Bi - Bi$_2$S$_3$. Bi = 81.29. S = 18.71: for Pb – galena. Pb = 86.60. S = 13.40: for Fe – pyrite. Fe = 46.55: S = 53.45: for Au. Ag. Pt. Sb – pure metals. Composition of electron-microprobe standards was obtained by EPMA

fineness (950-990) and electrum has not been detected. This suggests that the formation of Ag-Te-Au mineral phases instead of Ag-Au alloys was greatly influenced by Te concentration in the hydrothermal fluids.

Pyrite. the main gold-bearing sulfide phase. is widespread at Omai and is characterized by brittle deformation. typically shown by fractured grains. The size of the pyrite grains varies between a few mm up to 5 cm. Frequently. the pyrite grains are veined/replaced along fractures/grain boundaries by a later generation of gold. tellurides and sulfides.

Pyrrhotite always occurs in basalts as pseudomorphs after pyrite. Perfect cubes of pyrrhotite. formed by partial or total replacement of pyrite are observed in milky quartz and wallrocks. Pyrrhotite pseudomorphs represent a principal depositional site of gold. as coatings on the grain boundaries or as filling of pyrrhotite fractures.

Other silicate. sulfide. oxide. and borosilicate minerals represent minor phases. which occur locally.

2.3 TELLURIDE MINERALS

Tellurides represent minor phases within the quartz veins. They form complex aggregates in ribbon- and breccia-texture veins in the Omai stock. Telluride minerals occur randomly. in contrast with the zoned distribution described by Bowell et al. (1990) for the Paleoproterozoic tellurides at the Ashanti gold mine. Ghana. Three distinct generations of tellurides (I. II. and III) occur at Omai. The first generation is represented by melonite. which is associated with native gold. rutile. and chalcopyrite in altered basalts. although its paragenetic position is still uncertain. Tellurides II occur as small inclusions in pyrite II. whereas tellurides III occur as replacement of pyrite III along
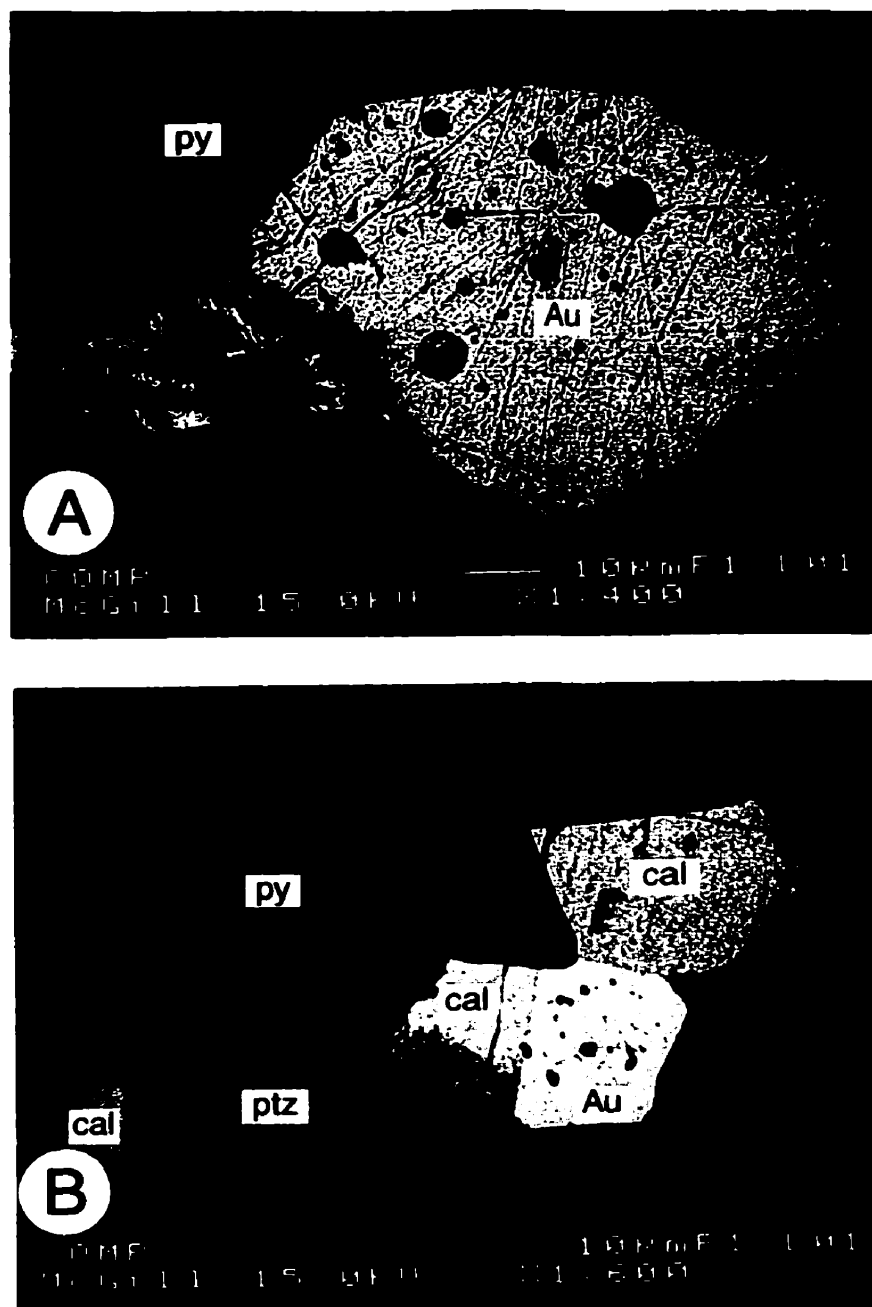
Figure 2.2   Back-scattered electon images of polished sections of gold inclusions in pyrite (A) and of symplectitic intergrowths among tellurides. sulfides. and gold (B-H). Abbreviations: Au = native gold; alt = altaite: cal = calaverite; col = coloradoite; gal = galena: hs = hessite: py = pyrite: ptz = petzite: tb = tellurobismuthite.

61
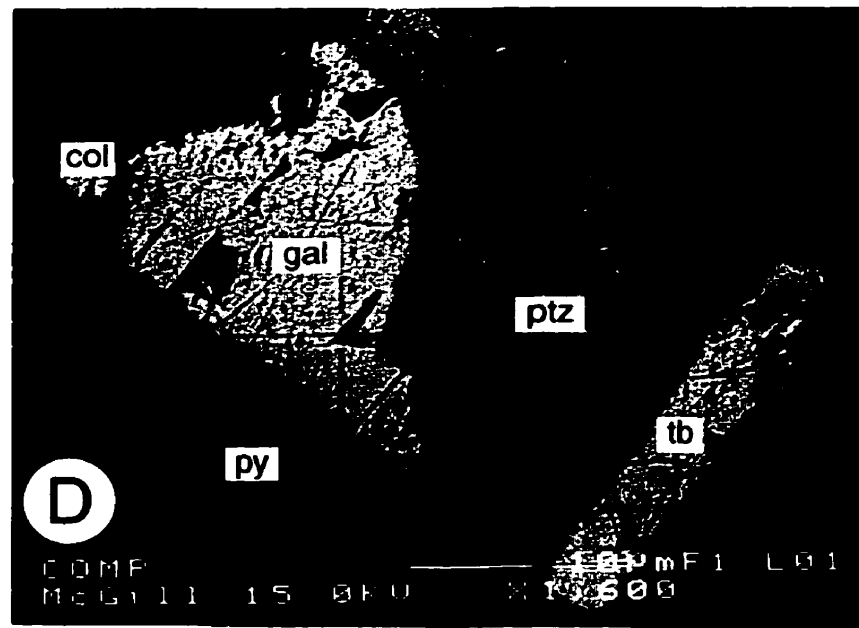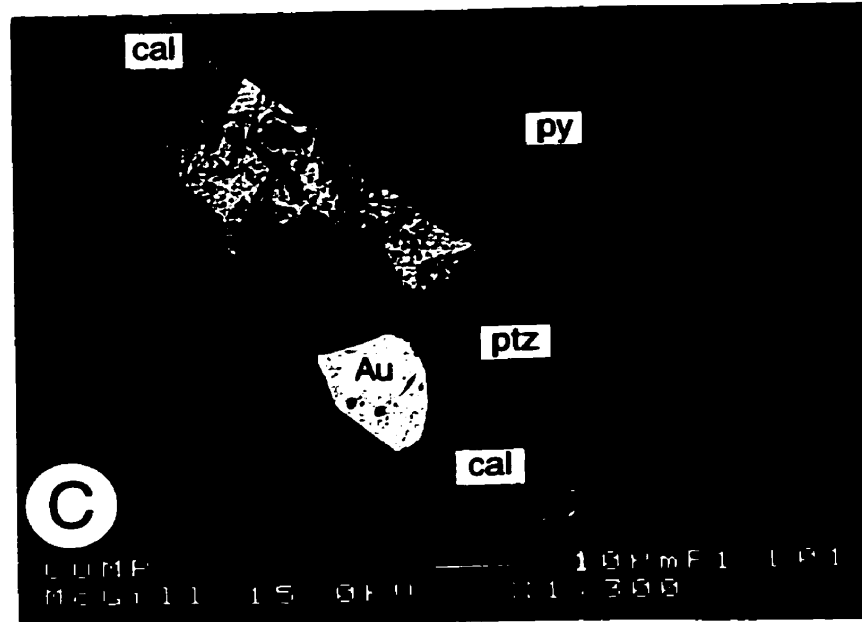
Figure 2.2   (continuation)
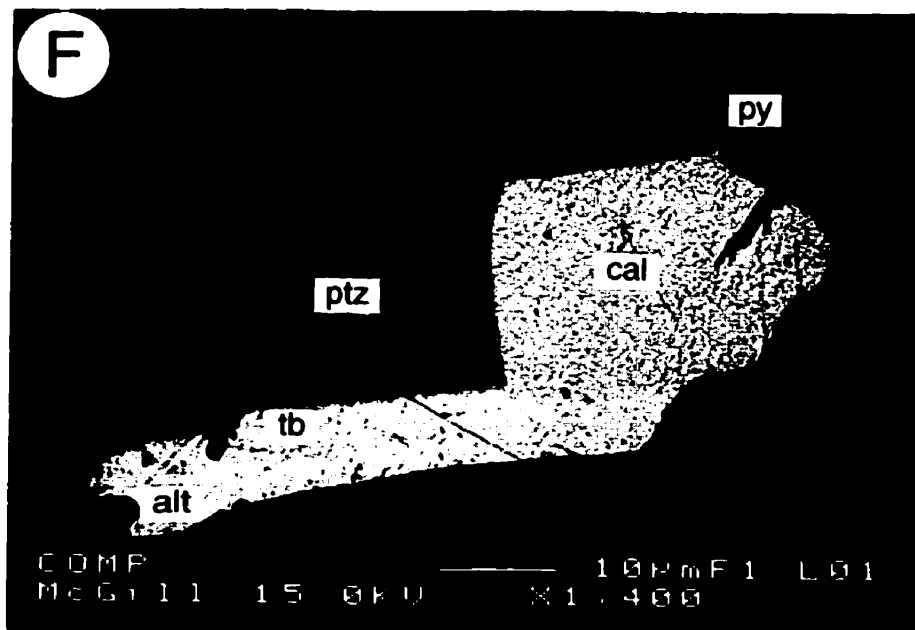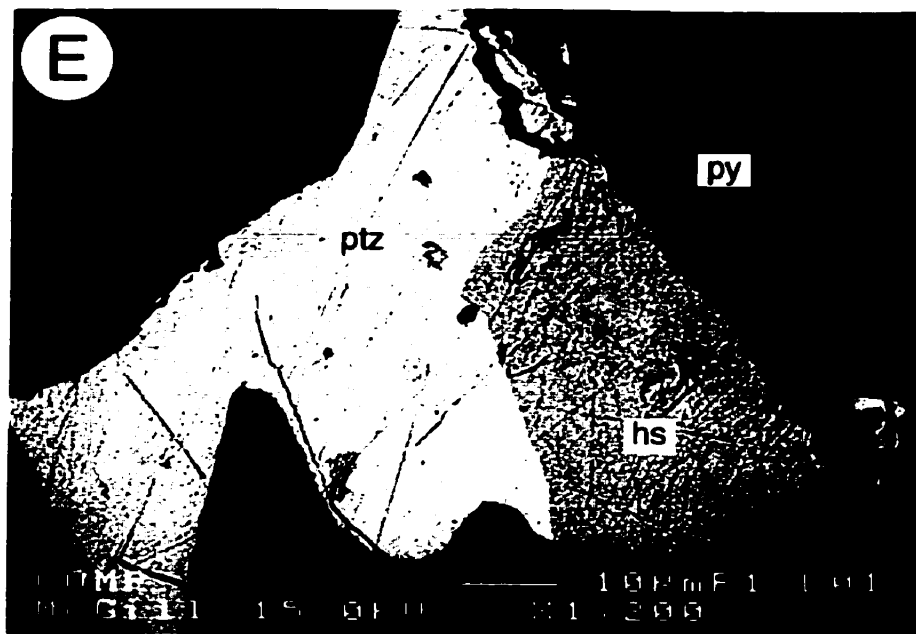
Figure 2.2   (continuation)
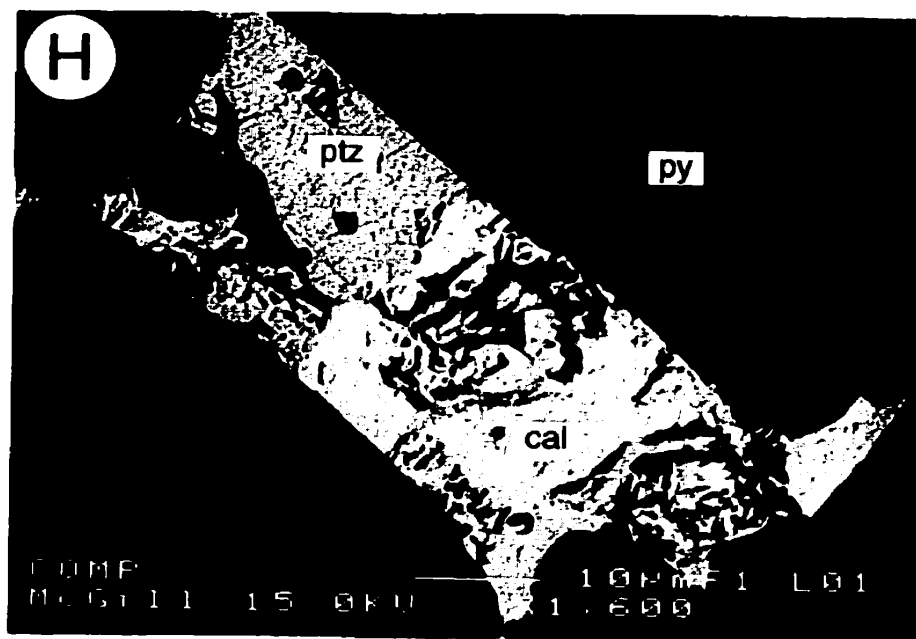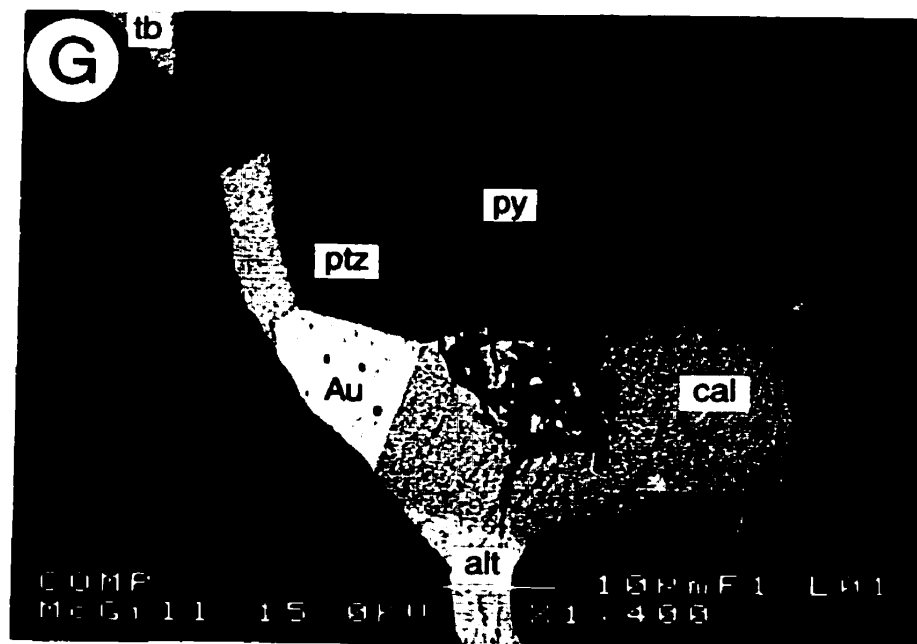
Figure 2.2 (continuation)

healed fractures and as thin (1-2 mm) fracture-filling veinlets in quartz. carbonates and scheelite. All telluride generations are associated with gold. The telluride II and III mineralogy is similar (except coloradoite and altaite. related only to the second generation). although a significant increase in sulfide minerals with the third telluride generation suggests a progressive change in the Te and S fugacities of fluids.

Au and Ag tellurides are represented by calaverite (AuTe$_2$). petzite (AuAg$_3$Te$_2$). and hessite (Ag$_2$Te). The most common is petzite. which varies from anhedral grains (Fig. 2.2B.C.D.E.H) to prismatic-shaped crystals up to 2 mm in length. The sharp contacts between petzite and other Au/Ag tellurides and the complex paragenesis indicate their coeval precipitation from the ore fluid. However. in several samples. the association petzite-hessite has many characteristics similar to those described by Kelly and Goddard (1969). which suggest that they are the product of decomposition of the χ phase at 120°C (Cabri. 1965; Affifi et al.. 1988; Cooke et al.. 1996). Therefore. probably two different petzite and hessite generations exist at Omai. the first as primary mineral phases and the second as a low-temperature decomposition product of χ phase.

At Omai. calaverite coexists with primary hessite (Fig. 2.3) and confirms the experimental data which suggest that these two minerals may form at similar fO_2-pH conditions at temperatures less than about 300°C (Legendre et al.. 1980; Jaireth. 1991; Zhang and Spry. 1994). Their association is in contradiction with the predicted occurrence in nature of calaverite-γ phase (Ag$_{1.89-1.97}$Te; Cabri. 1965; Pohl and Beaty. 1990). instead of the calaverite-hessite assemblage. Our observations should be interpreted to mean that either the γ phase cannot exist in nature. or that the hessite-γ phase reaction is above the native gold-calaverite transition and very close to the γ phase-stuetzite (Ag$_{5-x}$Te$_3$) reaction (at higher Te fugacity). In the latter situation. the stability of the γ phase between hessite and stuetzite formation is related to a narrow
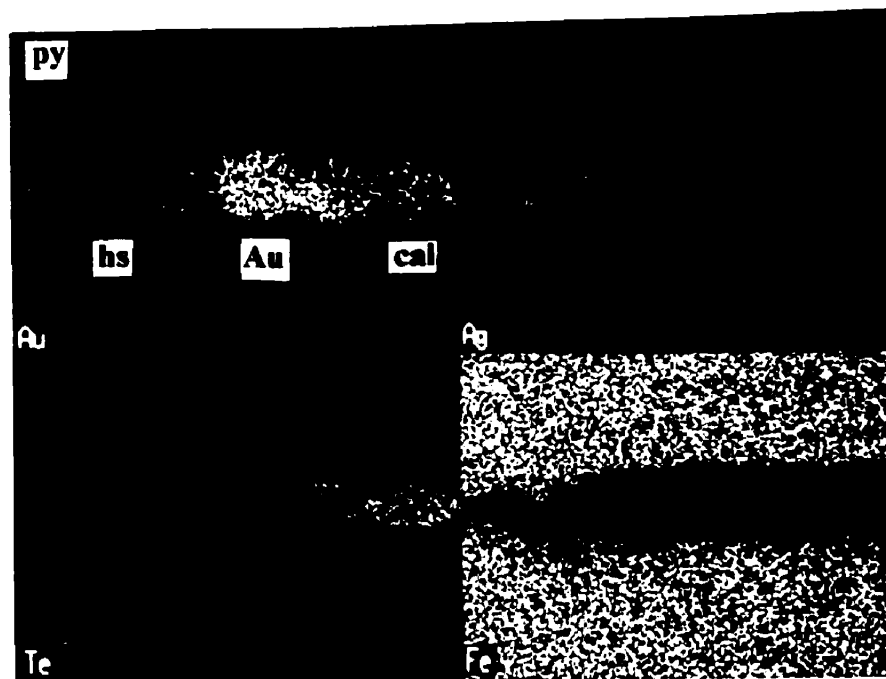
Figure 2.3   Single-element scanning electron micrograph for Au. Ag. Te. and Fe of the gold - calaverite - hessite association in pyrite. Abbreviations are the same as in Figure 2.2.

variation range of fTe_2. drastically diminishing the chances of finding the γ phase in natural assemblages. The calaverite-hessite association has been also described by Cooke et al. (1996) at Acupan. Philippines. Bowell et al. (1990) at Ashanti. Ahmad et al. (1987) at Emperor. Fiji. Siddeley and Araneda (1986) at El Indio. Chile. and Thompson et al. (1985) at Cripple Creek. Since the presence of the γ phase. although with atomic composition similar to hessite ($Ag_{1.95-1.97}Te$). was claimed only by Pohl and Beaty (1990). we postulate a direct hessite-stuetzite reaction in natural samples. The synthetic γ phase is thus considered to be a metastable intermediate phase within a very narrow temperature and Te fugacity range between hessite and stuetzite. This interpretation can only be verified once thermodynamic data for stuetzite become available.

Tellurobismuthite (Bi_2Te_3) represents the most common telluride at Omai (Fig. 2.2D.F). It is frequently associated with native gold. petzite. altaite and galena. Bertoni et al. (1991a.b) also identified native bismuth. tetradymite (Bi_2Te_2S). and wehrlite (originally described as BiTe: Brown and Lewis. 1962). Elliott (1992) also reported wehrlite. although its chemical composition is similar to pilsenite (Bi_4Te_3). in agreement with the fact that wehrlite actually represents a mixture of pilsenite and hessite (Ozawa and Shimazaki. 1984: Dobbe. 1993). However. it is of interest to note a gradual variation of Te/Bi. Te/S and Bi/S ratios. which resulted in the precipitation of various Bi-bearing tellurides/=sulphosalts. Sb substitution for Bi for up to 0.08 wt% in tellurobismuthite is probably due to the isomorphic structures of Bi_2Te_3 and Sb_2Te_3 (tellurantimony). The absence of native Te. correlated with the presence of Bi-rich mineral phases. suggests that the Omai mineral paragenesis lies on the Bi-rich side of the single Bi-Te solid-solution phase (Dobbe. 1993). The hydrothermal fluids were telluride-undersaturated (cf. Ahmad et al.. 1987: Zhang and Spry. 1994). and characterized by neutral to acid pH and a redox state near the magnetite-hematite buffer (cf. McPhail. 1995).

Altaite (PbTe) and Ag-bearing coloradoite ((Hg.Ag)Te ?) are minor phases which occur in association with galena and tellurobismuthite (Fig. 2.2D.F.G). and probably formed by contemporaneous crystallization of Pb-Bi-Hg-Te-rich fluids. However, as galena can incorporate appreciable Te and Hg in its crystal lattice (>100 ppm Te. Dobbe. 1993: >300 ppm Hg. Schalamuk and Logan. 1994). the segregation of native bismuth and Hg-Te minerals and replacement of galena by altaite cannot be disregarded. As the analyzed coloradoite is very small and in contact with a petzite grain. it is possible that part of the Ag content detected in coloradoite belongs to petzite.

Melonite (NiTe$_2$) is very rare at Omai. Usually. melonite is associated with magmatic copper-nickel deposits related to mafic-ultramafic rocks (e.g. Rao et al.. 1980: Hudson. 1986: Garuti and Rinaldi. 1986). Phanerozoic epithermal veins (e.g. Shimada et al.. 1981: Ahmad et al.. 1987: Afifi et al.. 1988). and epi-/mesothermal quartz veins of several Precambrian greenstone terranes (e.g. Harris et al.. 1983: Tremlow. 1984: Phillips. 1986: Robert and Brown. 1986: Milési et al.. 1992). At Omai. melonite is disseminated in weakly carbonate altered basalts. associated with gold. chalcopyrite. and rutile (formed from ilmenite) (Fig. 2.4). However. it is difficult to assess if melonite has a genetic relationship with the pervasive ankerite alteration or if it represents a mineral phase crystallized from a relatively Te-enriched basic-intermediate melt that underwent subsequent subsolidus modification. Taking into consideration the general Te enrichment of the hydrothermal fluids at Omai and the low Te concentrations in the host rocks (Voicu et al.. 1997a). we favor a genetic relationship between melonite and the Te-bearing mineralizing fluids.

Johnston (1960). Bertoni et al. (1991b). and Elliott (1992) noted several tellurides and sulfosalts at Omai that have not been encountered during this study. These are volynskite (AgBi$_{1.6}$Te$_2$). nagyagite (Pb$_5$Au(Te.Sb)$_4$S$_{5-8}$). and aikinite (PbCuBiS$_3$).
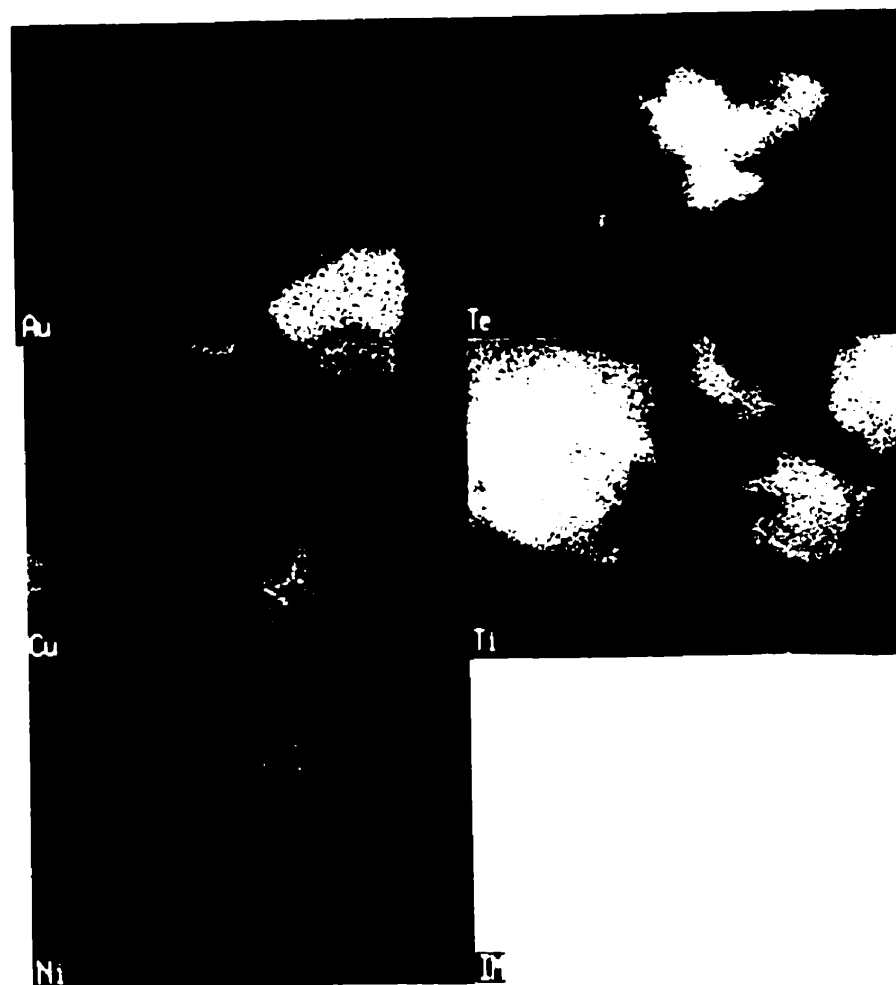
Figure 2.4   Single-element scanning electron micrograph for Ni-Cu-Au-Ti-Te and the analyzed area of the melonite - native gold - chalcopyrite - rutile assemblage. The rutile is formed from ilmenite.

Volynskite was determined by electronic microscopy (Elliott. 1992) and has a similar chemical composition to volynskite from the Yokozuru (Japan) and Ashley (Canada) gold deposits (Shimada et al.. 1981: Harris et al.. 1983). For nagyagite and aikinite. identified only by optical methods. their presence remains equivocal.

2.4 PHYSICOCHEMICAL CONDITIONS OF ORE FORMATION

Minerals in the system Au-Ag-Te commonly form in the last stages of epithermal and mesothermal gold-silver systems (e.g. Robert and Brown. 1986: Bowell et al.. 1990: Zhang and Spry. 1994). Thermodynamic data for this system are restricted to a few mineral species (calaverite. hessite. native gold. silver and tellurium). which do not allow the calculation of complete physicochemical conditions of ore formation. In contrast. using the telluride-bearing assemblages in relationship with the thermodynamic data available for other mineral species (sulfides. oxides. carbonates. and silicates) may provide narrower limits on depositional conditions compared to the telluride-free assemblages.

The conditions of ore formation at Omai can be estimated from the stability of telluride- sulfide-oxide-silicate minerals of each hydrothermal stage. Since all variables considered ($f\text{Te}_2$. $f\text{O}_2$. $f\text{S}_2$. temperature. and pH) cannot be represented simultaneously on one diagram. we have considered the temperature as the principal factor that influences and relates all other variables. The temperature data have been obtained using stable isotope geothermometers and the Na-K-Ca geothermometer of Fournier and Truesdell (1973) on cations analyzed from fluid inclusions in silicates. tungstates. carbonates. sulfides. and native gold by means of the crush/leach technique and capillary electrophoresis (Hallbauer. 1994: Hallbauer and Voicu. 1998). A summary of the temperature values of the vein-forming minerals is presented in Table 2.3. The three

Table 2.3   Temperature values of the vein-forming minerals at Omai

Mineral	Temperature (°C) Stage I	Temperature (°C) Stage II	Temperature (°C) Stage III
Scheelite	257-8[1]. n=7: 180-45[2]. n=7		
Quartz	257±8[1]. n=7: 175±22[2]. n=6: 215-300[3]	168±20[2]. n=13: 195-205[3]	170-185 [3]
Epidote	225±11[2]. n=4		
Ankerite		195±7[1]. n=6: 178±5[2]. n=4	
Calcite		198±10[1]. n=5: 190±13[2]. n=3	
Albite	213[2]. n=1		
Pyrite	243-8[2]. n=3	197±19[2]. n=2	
Galena			177[2]. n=1
Chalcopyrite		201±2[2]. n=2	
Native gold		198[2]. n=1	166[2]. n=1
Average T°C	225-25	192±8	172±5

n = number of samples; standard errors quoted as 2σ; [1] isotopic temperatures calculated by combining oxygen isotope fractionation equations between scheelite-water (Wesolowski and Ohmoto 1986), quartz-water (Clayton et al., 1972), and calcite-water (O'Neil et al., 1969); [2] calculated using Na-K-Ca geothermometer of Fournier and Truesdell (1973) (data from Hallbauer and Voicu, 1998); [3] homogenisation temperatures of the primary fluid inclusions (Elliott 1992)

main hydrothermal stages are considered to have formed at $220^\circ C$. $200^\circ C$. and $170^\circ C$. For stage I. an average temperature of $220^\circ C$ was used. due to discrepancies in temperature values for quartz and scheelite between isotopic and cationic geothermometers. Therefore. it is possible that the average temperature for this stage could be higher than $220^\circ C$. In order to better constrain the physicochemical conditions of mineral deposition. the following discussion considers each hydrothermal stage as a separate mineralizing event. However. the Omai deposit probably represents the result of a continuous hydrothermal process. where each fluid stage is characterized by gradual physical and chemical changes. This interpretation is supported by the sequential deposition of several mineral phases (quartz. carbonates. sericite. gold. pyrite. chalcopyrite. galena. tellurides) and by the overlap in range of fS_2. fTe_2. fO_2. and pH of the hydrothermal fluids (see below).

2.4.1 Tellurium and sulphur fugacities

The mineral paragenesis observed for each mineralization stage. superimposed on experimental data in the Au-Ag-Te. Cu-Fe-S-O and Bi-Pb-Hg-Ni-Te-S systems (Barton and Skinner. 1979; Afifi et al.. 1988; Zhang and Spry. 1994) allows an estimate to be made of the variation in Te_2 and S_2 fugacities. Because there are no significant changes to the location of stability fields at temperatures as high as $220^\circ C$. and as low as $170^\circ C$. an average temperature of $200^\circ C$ was chosen. This temperature value is representative for the Omai mineralization. as well as a likely temperature of stage II mineralization. The main characteristics of each hydrothermal stage are the following (Fig. 2.5):

Stage I: Coexisting pyrite and magnetite suggest that early sulfides were deposited between the reactions: pyrrhotite + S_2 = pyrite +magnetite and magnetite + S_2
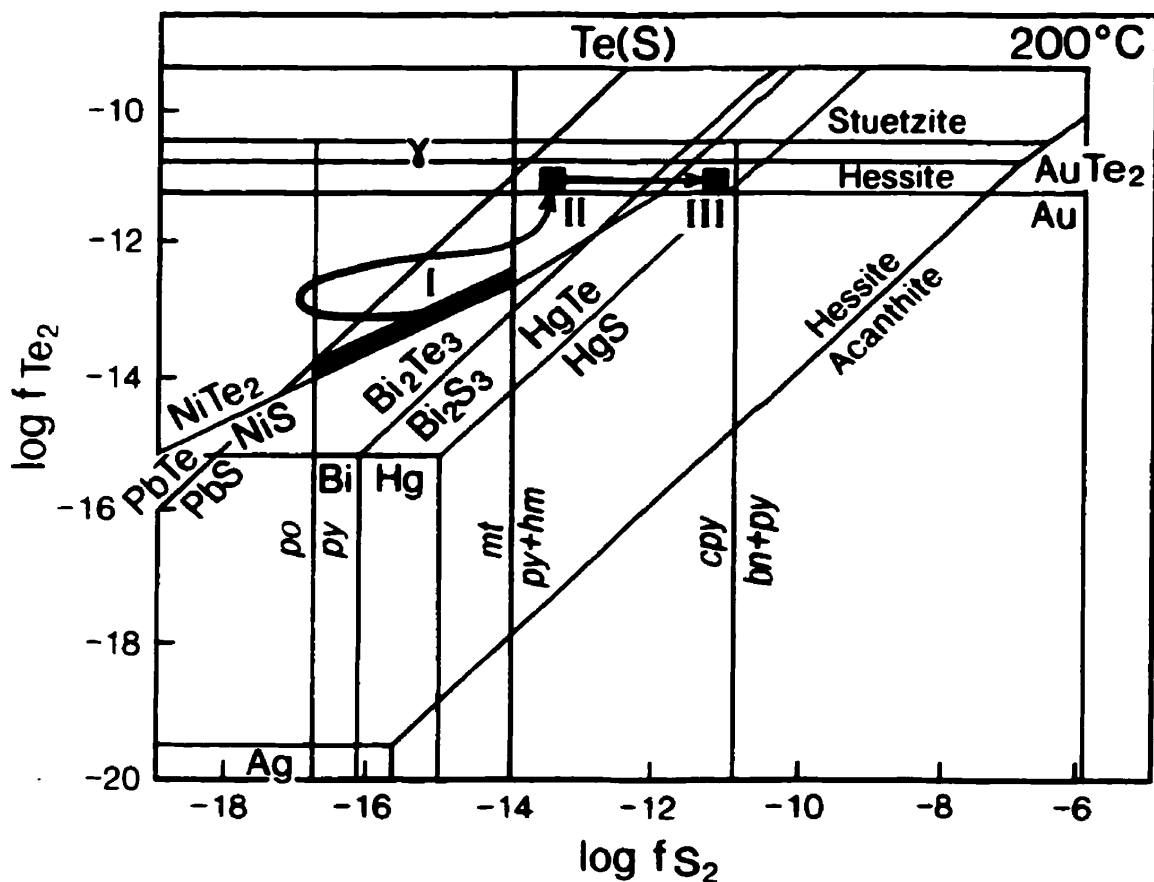
Figure 2.5   Variations of Te_2 and S_2 fugacities with respect to selected telluride-sulfide assemblages at a temperature of 200°C (modified after Afifi *et al.* 1988). Hessite-γ phase reaction was modified in order to accommodate the calaverite-hessite assemblage observed at Omai. Arrows show fugacity variations during the hydrothermal stages (I. II. and III) of the Omai gold deposit. Abbreviations: bn = bornite: hm = hematite: mt = magnetite: py = pyrite: po = pyrrhotite.

= hematite + pyrite. The presence of melonite indicates that the fTe_2 at a given fS_2 was above the hessite-acanthite reaction, which defines the minimum fTe_2 for the stability of tellurides. The absence of Au-Ag-Pb-Bi tellurides/sulfides is thus due to the absence of these elements in the hydrothermal brines during this mineralizing stage, rather than to the physico-chemical conditions of deposition. The presence of melonite and absence of millerite indicates that fTe_2 were above the millerite-melonite reaction. The construction of a fS_2 - fTe_2 diagram at an average temperature of 200°C shows a variation range of log fS_2 between -14 and -17, and a log fTe_2 value higher than -14.

Stage II: The presence of coloradoite instead of cinnabar/native Hg indicates that fugacities were above the coloradoite-cinnabar and coloradoite-native Hg reactions. The complex Bi telluride and sulfide association suggests a gradual change in the fTe_2/fS_2 ratios, which probably initially increased compared to stage I, allowing the gradual formation of pyrrhotite, galena, and altaite, followed by an increase of fTe_2 and fS_2 forming tellurobismuthite, pilsenite (and possibly hessite), and galena. This behavior explains the abundance of galena compared to other Bi-Pb tellurides and sulfides. A further increase of the fTe_2 resulted in the deposition of petzite, hessite and calaverite. The presence of hematite indicates that fS_2 was on the high fS_2 side of the reaction magnetite + S_2 = hematite +pyrite. The sulphur fugacity can be determined for this stage from the FeS content of sphalerite coexisting with pyrite. The mole percent FeS content of sphalerite from Omai is generally less than 2. Using an average value of 1 mole percent FeS in sphalerite, a temperature of 200°C, and the equation of Barton and Skinner (1979):

$$\text{Log } X_{Fe(Sphalerite)} = 7.16 - 7730/T - 1/2 \log fS_2 \quad (1)$$

where T is in Kelvin. the calculated log fS_2 is -18.3. However. the presence of ditellurides. hematite instead of magnetite and galena instead of altaite indicates that the final part of this stage is characterized by an increase of log fS_2 up to <-14 associated with an increase of log fTe_2. The upper and lower limits of fTe_2 can be defined by the absence of stuetzite (log fTe_2 < -10.5) and the presence of calaverite (log fTe_2 > -11.2).

Stage III: The predominance of sulfide over tellurium minerals indicates lower Te_2/S_2 ratios of the hydrothermal fluids compared to the previous stage. This is probably due to the increase of fS_2 rather than the decrease of fTe_2. as suggested by the continued presence of ditellurides such as calaverite in this hydrothermal stage. Therefore. the log fTe_2 probably varies over the same range as for stage II (between -11.2 and -10.5). The limits of fS_2 variation are constrained by the absence of magnetite and altaite and the presence of chalcopyrite instead of bornite. The log fS_2 during this stage vary between -13.5 and -11. Similar to the previous fluid stage. the mineral assemblage shows that mineralizing fluids were saturated with tellurides. but undersaturated with respect to native tellurium. As the mineral deposition of this stage took place at lower temperatures. the cooling paths of the fluids were associated with an almost constant tellurium fugacity.

The native gold-sulfide-telluride assemblage suggests that stage II and III are the main mineralizing events at Omai. All available tellurium from fluids has been deposited during these hydrothermal stages. Post-mineralization fluids are barren of tellurium-bearing minerals.

2.4.2 Oxygen fugacity and pH

The fO_2-pH values of the mineralizing fluids can be constrained for stages II and III. For stage I. the mineral assemblage does not give enough information to define pH and fO_2 conditions. The salinity data used here are based on a fluid inclusion study by Elliott (1992). A representative salinity of the hydrothermal fluids is taken to be 0.5 wt% NaCl. which corresponds to a concentration of 0.08 m Na$^-$ and an ionic strength (I) of 0.4. Assuming that the Na/K ratio was of 1:1. the K$^-$ concentration was 0.08 m. The calculated concentrations were converted to activities (log a $_{Na^-}$ = log a $_{K^-}$ = - 1.4) using the extension of the Debye-Hückel equation (Helgeson. 1969; Cooke et al.. 1996) in order to calculate K mineral fields as a function of pH. Total dissolved gold (ΣAu). silver (ΣAg) and tellurium (ΣTe) = 1 ppb has been assumed and represents the common amount for hydrothermal fluids that form at low temperature (Zhang and Spry. 1994; McPhail. 1995).

Using a temperature of 200°C and the mutual stability of the hessite-calaverite-pyrite-chalcopyrite-sericite assemblage during stage II. the values obtained for log fO_2 vary between -36 and -38. while for pH the values range between 4.2 and 5.4 (Fig. 2.6). The oxidation condition is above the hematite-magnetite buffer. but below the necessary oxidation conditions for hematite saturation.

Stage III is characterized by an almost similar mineral paragenesis. but a lower temperature (170°C) than stage II. Using similar fluid conditions as those of stage II. the log fO_2 value ranges between -39 and -43 and pH ranges between 4 and 5.2.
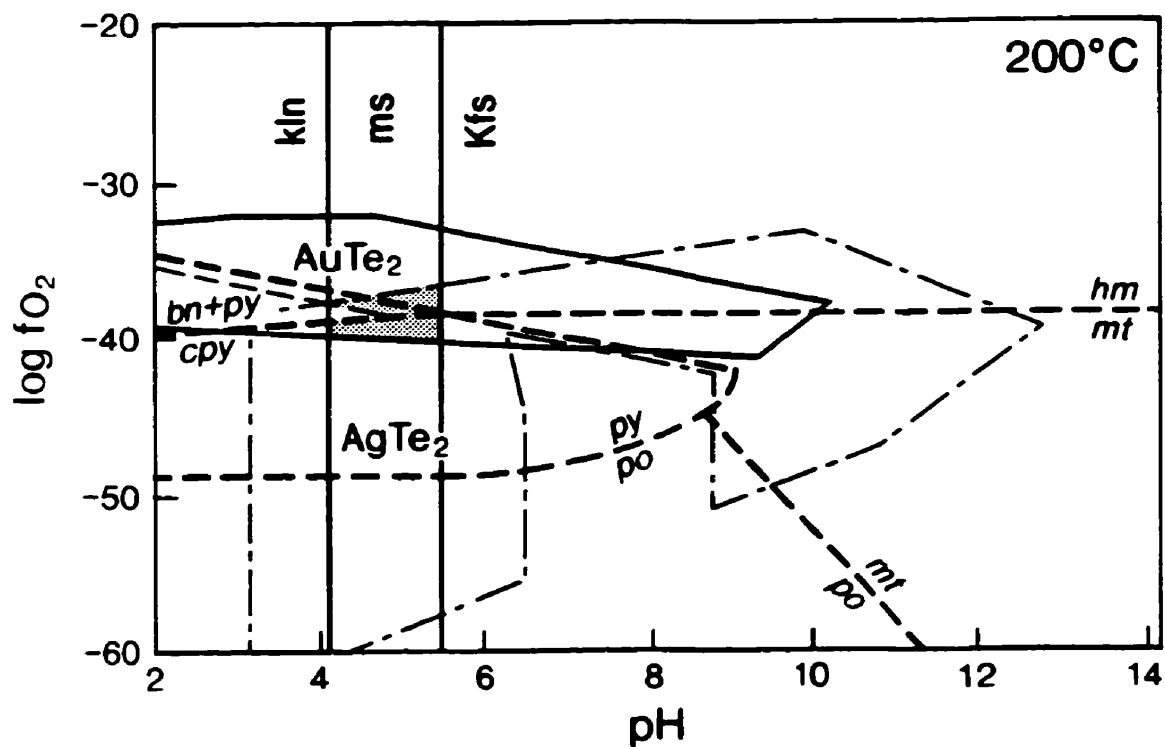
Figure 2.6   Diagram showing the fugacity of oxygen versus pH and the environment of deposition at Omai in stage II. The stability boundaries of calaverite (solid lines) and hessite (dashed-single dotted lines) (data from Zhang and Spry 1994) are superimposed onto the systems Fe-S-O. Cu-Fe-S. and K-Al-Si-O-H (calculated using SUPCRT software. Johnson et al. 1992) for the following conditions: T = 200°C: 1 = 0.4: ΣS = 0.01 m: ΣAu = 1 ppb; ΣAg = 1 ppb: ΣTe = 1 ppb: K^- = 0.08 m (see text for discussion of concentration estimates). Abbreviations: kln = kaolinite: ms = white mica: Kfs = potassium feldspar. The other abbreviations are the same as in Figure 2.5.

Relatively high oxygen fugacities in the mineralizing fluids at Omai are also confirmed by the negative $\delta^{34}S$ values (between -7.6 and -4.5‰. mean -5.6-0.9‰. n=4) of Au-related pyrite and galena (Bhatt. 1995). which can be attributed to mixing between deep-seated reduced fluids and surface oxidized waters or to H_2O-CO_2 phase separation.

The pH range between 4 and 5.4 for stages II and III is slightly more acidic than that of the typical greenschist-facies mesothermal gold deposits (pH ~ 5.2 to 6.2). but it is similar to that of shallow-level Archean gold deposits (pH between 4.1 and 5.2) at an equivalent temperature (~200°C) (Gebre-Mariam et al.. 1993: Hagemann et al.. 1994).

2.5 METAL TRANSPORT AND DEPOSITION

At Omai. scheelite and albite are related to stage I of mineralization. WO_4 anions were only found in fluids from scheelite. A good positive correlation could be observed between Na and WO_4. negative correlations between Ca/WO_4 and Sr/WO_4 and lack of correlation between Na and Cl (see Appendix 1). This could indicate a hydrothermal transport of W and Na as sodium tungstate and later precipitation as scheelite and albite (Hallbauer and Voicu. 1998). These data differ from the fluid inclusion data of the tungsten deposits worldwide which indicate that CO_2- and Cl-rich fluids are involved in the transport of tungsten at high and low temperatures and pressures. respectively (Foster. 1977: Higgins. 1980: Higgins and Kerrich. 1982: Heinrich. 1990).

Gold is usually transported either as chloride or sulfide species. The physico-chemical conditions at Omai (temperatures less than 220°C. low salinity. low pressure. weakly acid to neutral pH) suggest that the major Au-bearing species are most likely to have been $Au(HS)_2^-$ and $Au(HS)^0$ or $HAu(HS)_2^0$ (cf. Seward. 1991: Hayashi and

Ohmoto. 1991: Benning and Seward. 1994: Ridley et al.. 1996: Cooke et al.. 1996). The stability field for Au(HS)$_2$ is largely coincident with the stability field for pyrite. indicating that gold may be transported and deposited in equilibrium with pyrite (Shenberger and Barnes. 1989). Au(HS)^0/ HAu(HS)$^0_2$ complexes are important when gold is precipitated in equilibrium with sericite from weakly acidic to neutral conditions (pH ≤ 5.5). as at Omai. On the other hand. the analysis of fluid inclusions in sulfides (pyrite. chalcopyrite. and galena) and native gold from Omai by capillary electrophoresis detected significant quantities (up to 1130 ppm) of thiosulphate complexes ($S_2O_3^{2}$) (see Appendix 1: Hallbauer and Voicu. 1998). As suggested by Kucha et al. (1994). assemblages that contain pyrite and complexes with intermediate sulphur valencies may be a product of polysulphide-thiosulphate-sulfide-bearing fluids. These fluids form by the interaction between reduced. higher temperature fluids and oxygenated. low temperature. near surface groundwaters (Groves and Foster. 1991: Kucha et al.. 1994). They are very efficient at transporting gold at temperatures of around 200°C and may account for the association of gold and thiosulphate complexes identified at Omai.

Telluride minerals are volumetrically minor at Omai. but their presence is useful in working out the depositional processes. Using the equilibrium constants for reactions at 200°C. fO_2 between -36 and -38 and pH = 4.3-5.4 (for stage II) and fO_2 between -39 and -43 and pH = 4-5.2 (for stage III). in the system Au-Ag-Cl-S-O-H (Zhang and Spry. 1994). superimposed onto Te-O-H (McPhail and Bloom. 1993: McPhail. 1995: Cooke et al.. 1996) and Fe-S-O (Barton and Skinner. 1979) systems (Fig. 2.7). the predominant aqueous tellurium species are calculated to be H_2TeO_3 (for stage II) and H_2TeO_3. Te^{2}_2 and HTe (for stage III). These aqueous tellurium species occur under oxidizing
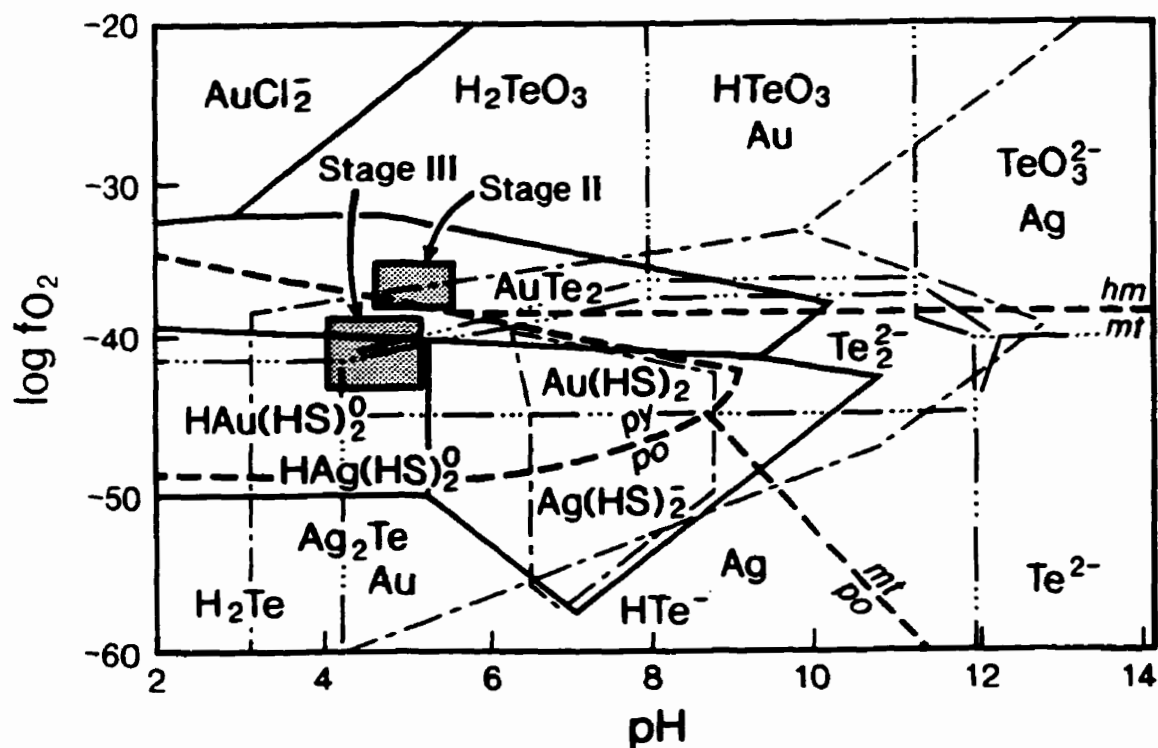
Figure 2.7   Diagram showing log fO_2 vs pH for the system Te-O-H (dashed-triple dotted lines), superimposed onto Au-Te-Cl-S-O-H (solid lines), Ag-Te-Cl-S-O-H (dashed-single dotted lines), and Fe-O-S (dashed lines) systems at the following conditions: $T = 200°C$: $\Sigma S = 0.01$ m: $\Sigma Au =$ 1 ppb: $\Sigma Ag = 1$ ppb: $m_{Cl^-} = 0.1$. Contours of the predominance of Te^-_2 are drawn at log $fTe_2 = -11$. Thermodynamic data are from Barton and Skinner (1979), Zhang and Spry (1994), McPhail (1995), and Cooke et al. (1996). The dark solid rectangles represent the estimated composition of the hydrothermal fluids (stages II and III) responsible for the mineralization at Omai. Abbreviations are the same as in Figure 2.5.

conditions in stage II (higher than the hematite-magnetite buffer). whereas for stage III there is a gradual transition from oxidizing to reduced conditions. The diagram also confirms that the most important aqueous gold-silver-bearing species responsible for the formation of gold-silver telluride minerals are $Au(HS)^0$ or $HAu(HS)^0_2$ and $Ag(HS)^0$ or $HAg(HS)^0_2$. Thiosulphate complexes have not been considered in the diagram. $Au(HS)_2$. $Ag(HS)_2$ and chloride species seem to have played a minor role. if any. in the transport and deposition of gold-silver tellurides in the temperature. pH. and fO_2 range of the Omai deposit.

Mechanisms of gold deposition include pH change. fluid cooling. H_2S loss from the fluid due to wallrock sulfidation reactions or to phase immiscibility (boiling). and reduction of the fluid due to interaction with graphite or ferrous mineral-rich reducing wallrocks (e.g. Phillips. 1986: Hayashi and Ohmoto. 1989: McCuaig and Kerrich. 1994: Ridley et al.. 1996). A brief discussion of these possible scenarios for transporting and depositing ore minerals at Omai follows.

Changes in fluid pH are inconsistent with the relatively constant pH during the whole mineralizing event at Omai. There is no mineralogical evidence for systematic changes in pH. neither for gangue nor ore minerals. The pH of the hydrothermal fluids was controlled by the mutual stability of quartz-sericite-K feldspar and ankerite/calcite reactions. which are present in all mineralizing stages. Furthermore. telluride precipitation cannot be explained by changes in pH. since the concentration of Te in solution is insensitive to pH at acidic to basic conditions (pH = 2 to 7: McPhail. 1995). Therefore. a small decrease of pH cannot be considered the most effective process for gold precipitation.

Fluid cooling represents an effective precipitation mechanism at temperatures less than $250°C$ (Hayashi and Ohmoto. 1991). At Omai. the progressive cooling with the evolution of the hydrothermal system suggests that temperature could have played a role in mineral precipitation. but probably associated with other simultaneous depositional mechanisms. The decrease of temperature may have been the result of gradual mixing of deeply sourced fluids with surface derived water. as suggested by stable isotopes and by presence of NO_3 anions. acetate and propionate in the fluid inclusions (Hallbauer and Voicu. 1998). Mixing resulted in gradual oxidation of the fluid. decrease in $H_2S_{(aq)}$ content and the beginning of gold+telluride deposition (stage II). Subsequent H_2S loss from the fluid was probably due to the efficiency of fluid-rock interaction associated with strong wallrock sulfidation and/or sulfide-bearing veinlets and gradual decrease of fO_2. hence directly contributing to the gold. sulfide and telluride precipitation (stage III). At Omai. gold grades generally correlate with the total sulfide content of the adjacent wallrocks. suggesting that this depositional mechanism may be dominant (cf. McCuaig and Kerrich. 1994).

The wallrock chemical composition has probably been another important factor for ore precipitation. especially in the mafic volcanics and sedimentary rocks. Iron-rich andesites and basalts. and graphite-bearing metapelites interacted with ore-forming fluids. resulting in local increase in $a_{H2(aq)}$ (i.e. decrease in fO_2). which could reduce the stability of gold-sulfide-species.

2.6 SUMMARY AND CONCLUSIONS

The Omai gold deposit is located at in the Paleoproterozoic Barama-Mazaruni greenstone belt. At local scale. the gold is found in quartz veins mainly located within intermediate and felsic plutonic and subvolcanic bodies. The veins are undeformed and

affected by brittle fracturing. Quartz forms up to 98% of vein volumes and is associated with a wide variety of metallic and gangue minerals. Gold is free or occurs as inclusions in pyrite and pyrrhotite. Telluride minerals are frequently associated with gold in the Omai stock. suggesting their common evolution during the mineralization process. Telluride metallic inventory includes Au. Ag. Bi. Pb. Hg. and Ni.

The mineral assemblage represented by various sulfides and tellurides can be used to constrain the chemical conditions of ore transport and deposition. The physicochemical parameters of the Omai hydrothermal system can be summarized as follows:

- gradual. but limited cooling of the mineralizing fluids. characterized by mesothermal temperatures during the early stage. followed by temperature intervals which are similar to those of the epithermal deposits:

- variable fS_2/fTe_2 ratios of each hydrothermal stage. which allowed the deposition of various sulfide and telluride minerals. The solutions were Te-undersaturated. allowing ditelluride deposition. while inhibiting the native tellurium and stuetzite formation. An increase of sulphur and tellurium fugacities during the last mineralizing stages allowed complete deposition of sulfides. tellurides. and gold. Post-mineralization fluids are barren of metallic minerals.

- pH conditions show constant values (between 4 and 5.4) for both main mineralizing stages. A slightly oxidizing environment in stage II could be explained by mixing with surface-derived waters or by phase immiscibility. Gradual transition from oxidizing conditions to a reducing environment could be the result of fluid-rock interaction associated with strong wallrock sulfidation.

- scheelite and albite were probably transported as sodium tungstate. the sulfides as sulfide or thiosulphate complexes. whereas Te was transported as aqueous H_2TeO_3. Te^{2-}_2. and HTe^- complexes.

- possible mechanisms of metal deposition include H_2S loss from the fluid due to wallrock sulfidation reactions or to phase immiscibility. fluid cooling. and interaction of mineralizing fluids with reducing wallrocks.

2.7 REFERENCES

Afifi. A.M.. Kelly. W.C.. and Essene. E.J.. 1988. Phase relations among tellurides. sulfides. and oxides: II. Applications to telluride-bearing ore deposits. Economic Geology. v. 83. p. 395-404.

Ahmad. M.. Solomon. M.. and Walshe. J.L.. 1987. Mineralogical and geochemical studies of the Emperor gold telluride deposit. Fiji. Economic Geology. v. 82. p. 345-370.

Barton. P.B.Jr.. and Skinner. B.J.. 1979. Sulfide mineral stabilities. In Geochemistry of hydrothermal ore deposits: 2nd edition. Edited by H.L. Barnes. Wiley Interscience. New York. p. 278-403.

Benning. L.G.. and Seward. T.M.. 1994. Hydrosulphide complexes of gold(I) at high pressures and temperatures: equilibrium and kinetic problems. Mineralogical Magazine. v. 58A. p. 75-76.

Bertoni. C.H.. Shaw. R.P.. Singh. R.. Minamoto. J.. Richards. J.M.. and Belzile. E.. 1991a. Geology and gold mineralization of the Omai property. Guyana. In Brazil gold '91: The economics geology geochemistry and genesis of gold deposits. Edited by E.A. Ladeira. Balkema. Rotterdam. p. 767-773.

Bertoni. C.H.. Shaw. R.P.. Singh. R.. Belzile. E.. Minamoto. J.. Richards. J.M.. and Morgan. R.. 1991b. Geology and gold mineralization of the Omai property. Guyana. Unpublished report. 111 p.

Bhatt. B.J.. 1995. Geology. geochemistry. and origin of the Proterozoic gold-quartz vein mineralization and igneous intrusions. Omai gold mine. Guyana. South America. Unpublished report. 50 p.

Bowell. R.J.. Foster. R.P.. and Stanley. C.J.. 1990. Telluride mineralization at Ashanti gold mine. Ghana. Mineralogical Magazine. v. 54. p. 617-627.

Brown. A.. and Lewis. B.. 1962. The systems bismuth-tellurium and antimony-tellurium and the synthesis of the minerals hedleyite and wehrlite. Physics and Chemistry of Solides. v. 23. p. 1597-1604.

Cabri. L.J.. 1965. Phase relations in the Au-Ag-Te system and their mineralogical significance. Economic Geology. v. 60. p. 1569-1606.

Clayton. R.N.. O'Neil. J.R.. and Mayeda. T.K.. 1972. Oxygen isotope exchange between quartz and water. Journal of Geophysical Research. v. 77. p. 3057-3067.

Cooke. D.R.. McPhail. and D.C.. Bloom. M.S.. 1996. Epithermal gold mineralization. Acupan. Baguio district. Philippines: Geology. mineralization. and the thermochimical environment of ore deposition. Economic Geology. v. 91. p. 243-272.

Dobbe. R.. 1993. Bismuth tellurides (joseite-B. bismuthian tsumoite) in a Pb-Zn deposit from Tunaberg. Sweden. European Journal of Mineralogy. v. 5. p. 165-170.

Elliott. R.G.. 1992. The geology and geochemistry of the Omai goldfield. Guyana. Unpublished Ph.D. thesis. Oxford Brookes University. 230 p.

Foster. R.P.. 1977. Solubility of scheelite in hydrothermal chloride solutions. Chemical Geology. v. 20. p. 27-43.

Fournier. R.O.. and Truesdell. A.H.. 1973. An empirical Na-K-Ca geothermometer for natural waters. Geochimica et Cosmochimica Acta. v. 37. p. 1255-1275.

Garuti. G.. and Rinaldi. R.. 1986. Mineralogy of melonite-group and other tellurides from the Ivrea-Verbano basic complex. western Italian Alps. Economic Geology. v. 81. p. 1213-1217.

Gebre-Mariam. M.. Groves. D.I.. McNaughton. N.J.. Mikucki. E.J.. and Vearncombe. J.R.. 1993. Archean Au-Ag mineralization at Racetrack. near Kalgoorlie. Western Australia: A high crustal-level expression of the Archean lode-gold continuum. Mineralium Deposita. v. 28. p. 375-387.

Gibbs. A.K.. and Barron. C.N.. 1993. Geology of the Guiana Shield. Oxford Monographs on Geology and Geophysics. v. 22. Oxford. Clarendon Press. 246 p.

Groves. D.I.. and Foster. R.P.. 1991. Archean lode gold deposits. *In* Gold Metallogeny and Exploration. *Edited by* R.P. Foster. Blackie. p. 63-103.

Hagemann. S.G.. Gebre-Mariam. M.. and Groves. D.I.. 1994. Surface-water influx in shallow-level Archean lode-gold deposits in Western Australia. Geology. v. 22. p. 1067-1070.

Hallbauer. D.K.. 1994. Geochemical trace element analysis for ionic species by capillary electrophoresis. Mineralogical Magazine. v. 58A. p. 362-363.

Hallbauer. D.K.. and Voicu. G.. 1998. A geochemical assessment of the hydrothermal systems at the Omai gold mine. Guyana. from the composition of fluid inclusions in ore minerals and gangue. Geocongress'98. The Geological Society of South Africa. 8-10 July 1998. Extended Abstracts. p. 213-215.

Harris. D.C.. Sinclair. W.D.. and Thorpe. R.I.. 1983. Telluride minerals from the Ashley deposit. Bannockburn township. Ontario. Canadian Mineralogist. v. 21. p. 137-143.

Hayashi. K.. and Ohmoto. H.. 1991. Solubility of gold in NaCl- and H_2S-bearing aqueous solutions at 250° - $350^\circ C$. Geochimica et Cosmochimica Acta. v. 55. p. 2111-2126.

Heinrich. C.A.. 1990. The chemistry of hydrothermal tin (-tungsten) ore deposition. Economic Geology. v. 85. p. 457-481.

Helgeson. H.C.. 1969. Thermodynamics of hydrothermal systems at elevated temperatures and pressures. American Journal of Science. v. 267. p. 729-804.

Higgins. N.C.. 1980. Fluid inclusion evidence for the transport of tungsten by carbonate complexes in hydrothermal systems. Canadian Journal of Earth Sciences. v. 17. p. 823-830.

Higgins. N.C.. and Kerrich. R.. 1982. Progressive [18]O depletion during CO_2 separation from a carbon-dioxide-rich hydrothermal fluid: evidence from the Grey River tungsten deposit. Newfoundland. Canadian Journal of Earth Sciences. v. 19. p. 2247-2257.

Hudson. D.R.. 1986. Platinum-group minerals from the Kambalda nickel deposits. Western Australia. Economic Geology. v. 81. p. 1218-1225.

Jaireth. S.. 1991. Hydrothermal geochemistry of Te. Ag,Te. and AuTe, in epithermal precious metal deposits. Economic Geology Research Unit. v. 37. James Cook University of North Queensland. Australia.

Johnston. R.. 1960. The geology of the Omai Mine. British Guyana. Unpublished Ph.D. thesis. University of St. Andrews. Scotland. 126 p.

Johnson. J.W.. Oelkers. E.H.. and Helgeson. H.C.. 1992. SUPCRT92: A software package for calculating the standard molal thermodynamic properties of minerals. gases. aqueous species and reactions from 1 to 5000 bars and 0 to 1000°C. Computers & Geosciences. v. 18. p. 899-947.

Kelly. W.C.. and Goddard. E.N.. 1969. Telluride ores of Boulder Country. Colorado. Geological Society of America Memoir. v. 109. 237 p.

Kucha. H.. Stumpfl. E.F.. Plimer. I.R.. and Köck. R.. 1994. Gold-pyrite association - result of oxysulphide and polysulphide transport of gold?. Trans. Inst. Min. Metall. (Sect. B: Appl. earth sci.). v. 103. p. B197-B205.

Legendre. B.. Souleau. C.. and Hancheng. C.. 1980. Le système ternaire or-argent-tellure: Societé Chimica Française Bulletin. v. 1. p. 197-204.

McCuaig. T.C.. and Kerrich. R.. 1994. P-T-t-deformation-fluid characteristics of lode gold deposits: Evidence from alteration systematics. In Alteration and alteration processes associated with ore-forming systems. Edited by D.R. Lentz. Geological Association of Canada. Short Course Notes. v. 11. p. 339-379.

McPhail. D.C.. 1995. Thermodynamic proprieties of aqueous tellurium species between 25 and 350°C. Geochimica et Cosmochimica Acta. v. 59. p. 851-866.

McPhail. D.C.. and Bloom. M.S.. 1993. The behaviour of tellurium and silver in hydrothermal fluids at temperatures up to 300°C: Experimental and theoretical studies. GAC/MAC Annual Meeting. Programs with Abstracts. p. A-69.

Milési. J-P.. Ledru. P.. Feybesse. J-L.. Dommanget. A.. and Marcoux. E.. 1992. Early Proterozoic ore deposits and tectonics of the Birimian orogenic belt. West Africa. Precambrian Research. v. 58. p. 305-344.

O'Neil. J.R.. Clayton. R.N.. and Mayeda. T.K.. 1969. Oxygen isotope fractionation in divalent metal carbonates. Journal of Chemical Physics. v. 51. p. 5547-5558.

Ozawa. T.. and Shimazaki. H.. 1984. Pilsenite redefined and wehrlite discredited. American Mineralogist. v. 69. p. 215.

Phillips. G.N.. 1986. Geology and alteration in the Golden Mile. Kalgoorlie. Economic Geology. v. 81. p. 779-808.

Pohl. D.C.. and Beaty. D.W.. 1990. The mineralogy and petrology of telluride-sulfosalt-sulfide replacement deposits in the Leadville dolomite. Buckeye Gulch. Colorado. Economic Geology Monograph. v. 7. p. 407-416.

Rao. N.K.. Narasimhan. D.. and Rao. G.V.U.. 1980. The nickel telluride mineral melonite from the Jaduguda uranium deposit. Singhbhum shear zone. Bihar. India. Mineralogical Magazine. v. 43. p. 775-777.

Ridley. J.. Mikucki. E.J.. and Groves. D.I.. 1996. Archean lode-gold deposits: fluid flow and chemical evolution in vertically extensive hydrothermal systems. Ore Geology Reviews. v. 10. p. 279-293.

Robert. F.. and Brown. A.C.. 1986. Archean gold-bearing quartz veins at the Sigma Mine. Abitibi greenstone belt. Quebec: Part II. Vein paragenesis and hydrothermal alteration. Economic Geology. v. 81. p. 593-616.

Schalamuk. I.B.. and Logan. A.V.. 1994. Polymetallic Ag-Te-bearing paragenesis of the Cerro Negro district. Famatina Range. La Rioja. Argentina. Canadian Mineralogist. v. 32. p. 667-679.

Seward. T.M.. 1991. The hydrothermal geochemistry of gold. In Gold Metallogeny and Exploration. Edited by R.P. Foster. Blackie. p. 37-62.

Shenberger. D.M.. and Barnes. H.L.. 1989. Solubility of gold in aqueous sulfide solutions from 150 to 350°C. Geochimica et Cosmochimica Acta. v. 53. p. 269-278.

Shimada. N.. Miyahisa. M.. and Hirowatari. F.. 1981. Melonite and volynskite from the Yokozuru mine. Sannotake. north Kyushu. Japan. Mineralogical Journal. v. 10. p. 269-278.

Siddeley. G.. and Araneda. R.. 1986. El Indio-Tambo gold deposits. Chile. In Gold '86. Edited by A.J. Macdonald. Willowdale. Ontario. p. 445-456.

Thompson. T.B.. Trippel. A.D.. and Dwelley. P.C.. 1985. Mineralized veins and breccias of the Cripple Creek district. Colorado. Economic Geology. v. 80. p. 1669-1688.

Tremlow. S.G.. 1984. Archean gold-telluride mineralization of the Commoner mine. Zimbabwe. In Gold'82. Edited by R.P. Foster. Balkema. Rotterdam. p. 469-492.

Voicu. G.. Bardoux. M.. Harnois. L.. Stevenson. R.. and Crépeau. R.. 1997a. Geochemical evolution of the Paleoproterozoic volcanic and plutonic rocks from Omai area. Guyana. South America: Implications for tectonic history and source regions. 30th International Geological Congress. Beijing. China. August 1-12. 1996. v. 2. no. 1. p. 101-114.

Voicu. G.. Bardoux. M.. Harnois. L.. and Crépeau. R.. 1997b. Lithological and geochemical features of igneous and sedimentary rocks at the Omai gold mine. Guyana. South America. Exploration and Mining Geology. v. 6. no. 2. p. 153-170.

Walrond. G.W.. 1987. Geological map of Guyana. scale 1: 1 million. Guyana Geology and Mines Commission.

Wesolowski. D.. and Ohmoto. H.. 1986. Calculated oxygen isotope fractionation factors between water and the minerals scheelite and powellite. Economic Geology. v. 81. p. 471-477.

Zhang. X.. and Spry. P.G.. 1994. Calculated stability of aqueous tellurium species. calaverite. and hessite at elevated temperatures. Economic Geology. v. 89. p. 1152-1166.

CHAPTER III

STRUCTURAL, MINERALOGICAL AND GEOCHEMICAL STUDIES OF THE PALEOPROTEROZOIC OMAI GOLD DEPOSIT, GUYANA

3.1 INTRODUCTION

The granitoid- and greenstone-hosted Omai gold deposit is located in the Paleoproterozoic Barama-Mazaruni Supergroup of north-central Guyana. The greenstone sequence is located in the Guiana Shield and consists of alternating mafic/felsic volcanic and sedimentary rocks. intruded by granitoid batholiths and stocks (Gibbs and Barron. 1993). The gold at Omai occurs in quartz veins. which are located within the Omai stock (Fennell pit). quartz-feldspar porphyry and rhyolite dikes and. to a lesser extent. in andesitic/basaltic flows and metapelitic rocks (Wenot pit) (Bertoni et al.. 1991a. Voicu et al.. 1997b.c).

Omai is presently the largest gold mining operation in the Guiana Shield and one of the major gold deposits in South America. Gold occurrences in this area have been known for more than a century. being sporadically explored and exploited by small-scale miners and by several mining companies. A detailed history of exploration and mining in the Omai area can be found in Bertoni et al. (1991b) and Elliott (1992). The total mineable reserves (including past production plus reserves) in both the weathering profile and bedrock are of more than 120 tonnes gold.

Omai is the best documented of the gold occurrences in the Guiana Shield. However. to date there is no comprehensive description of the geological and metallogenic environment of the deposit.

The object of this study is fourfold: first. to provide an extensive description of the structural. textural and mineralogical features of the gold-bearing veins. as well as their temporal relationships with the regional evolution of the Omai zone; second. to present and discuss the stable isotope data. available for the first time for a gold deposit in the Guiana Shield; three. to contribute to the important question of the type of deposit

and whether Archean models are applicable to Paleoproterozoic granitoid- and greenstone-hosted gold deposits: four. to compare the Omai deposit with other gold occurrences from Paleoproterozoic greenstone terranes in the Guiana and West African Shields which share a similar geologic evolution.

3.2 REGIONAL GEOLOGY

The Omai gold deposit is hosted in the Paleoproterozoic Barama-Mazaruni Supergroup (Fig. 3.1). a greenstone terrane deformed and metamorphosed during the Trans-Amazonian orogeny. a tectonomagmatic event bracketed between approximately 2.3 and 1.9 Ga (Gibbs and Olszewski. 1982: Gibbs and Barron. 1993). The greenstone belt sequence comprises alternating felsic to mafic and ultramafic volcanic flows interlayered with thick sedimentary units. The base of the sequence is dominated by tholeiitic basalts and associated mafic-ultramafic bodies and sills. which are overlain by intermediate and felsic volcanic rocks interlayered with immature clastic sedimentary rocks (Gibbs and Barron. 1993). The metamorphic grade is generally to lower greenschist facies. although locally the volcano-sedimentary rocks are metamorphosed to prehnite-pumpellyite or amphibolite facies (Gibbs and Barron. 1993: Voicu et al.. 1997c).

The greenstone belt is associated with extensive felsic to intermediate intrusions. collectively referred to as the Granitoid Complex/Trans-Amazonian Granitoids (Gibbs and Barron. 1993: Voicu et al.. 1997c). They are syn- to late tectonic and range in composition from granite. to granodiorite. diorite. tonalite. and adamellite. The Tigri granodiorite batholith. which occurs at ~6 km SW of Omai. was dated at 1945 ± 45 Ma (K-Ar method on hornblende: Snelling and McConnell. 1969).
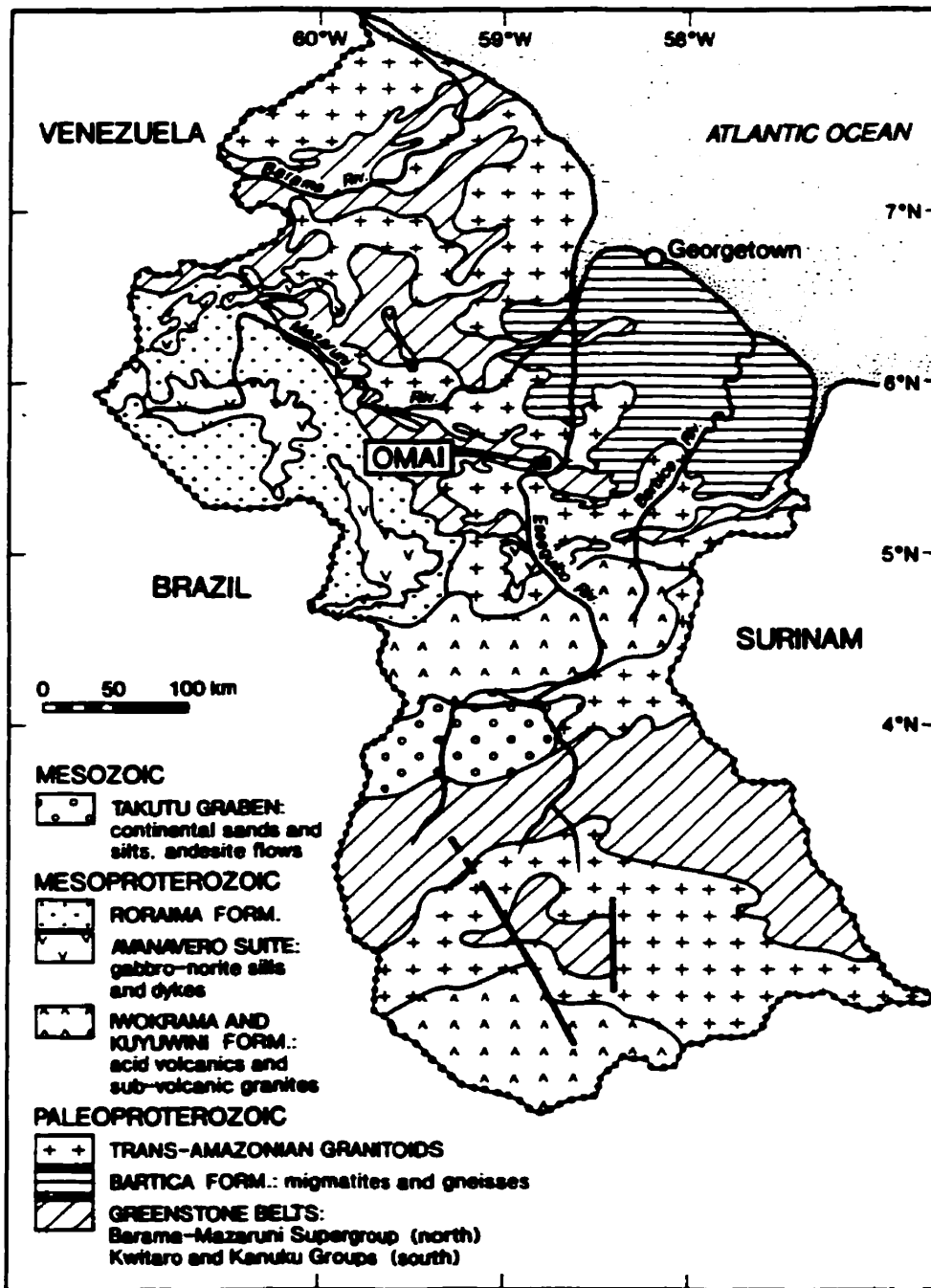
Figure 3.1   Simplified geological map of Guyana (modified from Walrond. 1987:
            Gibbs and Barron. 1993) showing location of the Omai mine.

The majority of gold occurrences in northern Guyana show an evident spatial correlation with the Paleoproterozoic greenstone terrane (Walrond, 1980, 1987; Elliott, 1992). Approximately 120t of gold (mines and placers) have been produced from this terrane during the period 1885-1995. The overall distribution of gold occurrences is structurally controlled by NW-trending major structural breaks referred to as the Makapa-Kuribrong (Walrond, 1980) and Issano-Appaparu (Elliott, 1992) shear zones (Fig. 3.2). The most comprehensive description of Guyana's goldfields (Macdonald, 1968) suggests that most of the historic mines are confined to gold-bearing stockwork veins hosted by strongly altered, small granitoid stocks within these crustal scale shear zones.

3.3 LOCAL GEOLOGY AND GEOCHRONOLOGY

Detailed Omai mine geology is presented in Voicu et al. (1997b,c) and is summarized below.

Rocks of the Omai mine consist of mafic and intermediate volcanic rocks underlain by polygenic conglomerates and overlain by fine grained sedimentary rocks. The volcanic rocks are intruded by quartz-feldspar porphyry and rhyolite dikes and by the Omai granitoid stock, and cut by several generations of mafic dikes and sills (Fig. 3.3). Volcanic rocks consist mainly of massive to pillowed tholeiitic basalts and calc-alkaline andesites, which are affected by strong spilitization. Pillows are usually well preserved, except in the central part of the Wenot area, where they are affected by ductile fabrics related to an east-west striking, 100 m wide shear corridor. Two quartz-feldspar porphyry dikes intrude the andesite unit of the Wenot pit. The southern dike is in tectonic contact with the metasedimentary rocks along the Wenot shear zone. This tectonic contact is marked by a discontinuous 1-2 m thick cataclastic breccia. The porphyry dikes follow the regional strike and they are generally vertical or steeply dip
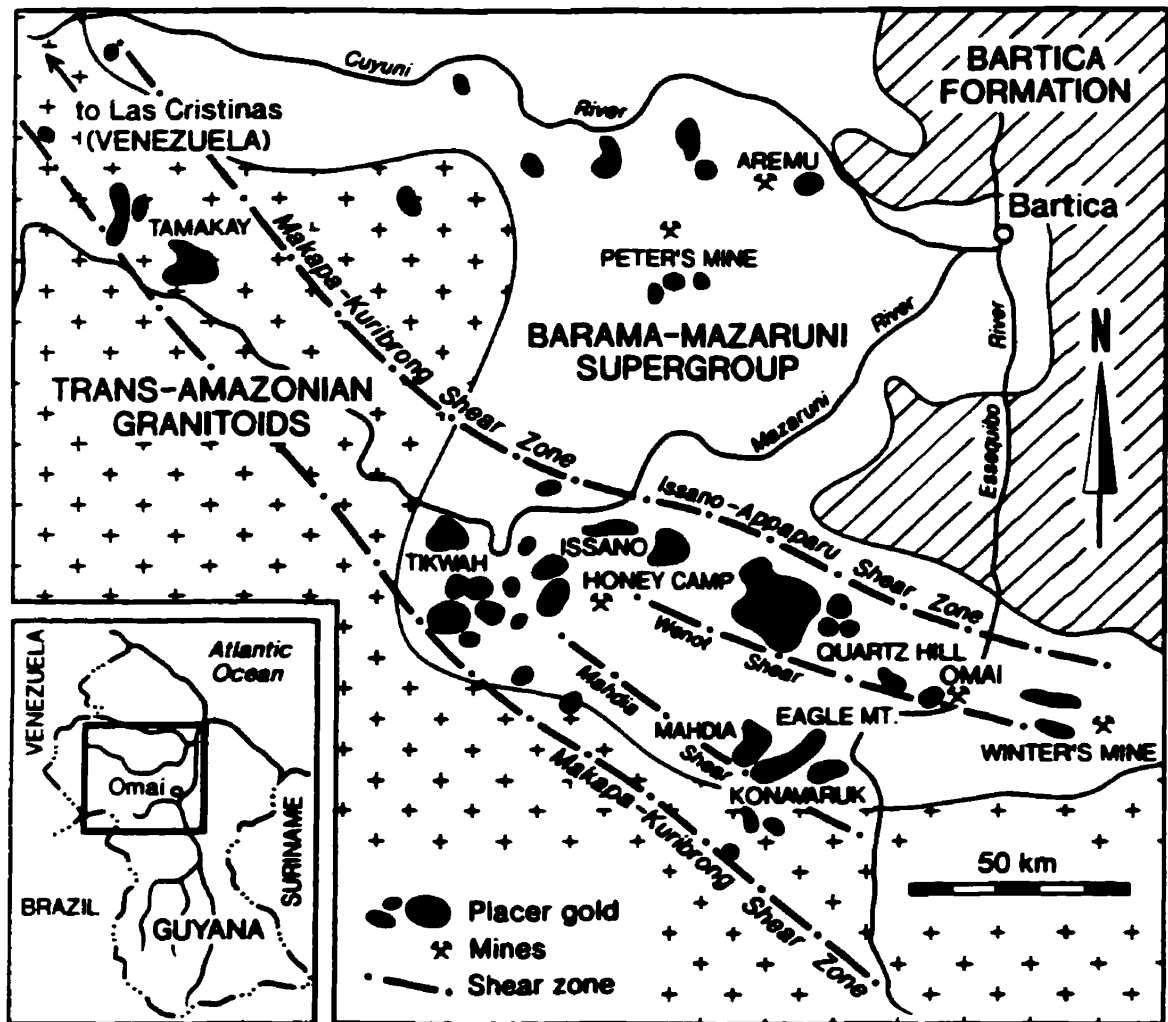
Figure 3.2   Regional map showing the spatial relationship between crustal-scale shear zones and distribution of gold occurrences and deposits in the Barama-Mazaruni greenstone belt of northern Guyana (modified from Elliott. 1992).

PERMIAN-TRIASSIC
APATOE SUITE: dolerite dykes
MESOPROTEROZOIC
AWANAVERO SUITE: Tumatumari-Omai sill: gabbro, hornblende pyroxenite, granophyre
PALEOPROTEROZOIC
(Barama-Mazaruni Supergroup)
OMAI STOCK
Quartz monzodiorite, granodiorite
Hornblendite, diorite
Intrusion breccia
VOLCANO-SEDIMENTARY COMPLEX
Basalt
Andesite
Porphyritic andesite
Volcanic breccia
Amygdaloidal basalt
Silicified andesite
Pillowed andesite
Quartz-feldspar porphyry, rhyolite
Tuffaceous greywacke, tuff
Pelite (siltstone, sandstone, mudstone)
Volcanic conglomerate
MAFIC-ULTRAMAFIC COMPLEX
Microgabbro
Pyroxene hornblendite
Hornblende porphyry
Shear zone
Fault (suspected)
Open pit limits
Bedding
Foliation
Geological contact
A-A',B-B' Vertical cross-sections

Omai River Fault
FENNELL PIT
WENOT PIT
Wenot Shear Zone
A'
B'
B

0   0.5   1 km

Figure 3.3   Simplified geological map of the Omai gold deposit.

in either direction. Their thickness averages 7 m and the dikes can be traced for more than 1.6 km along strike and at least 300 m downdip. Quartz-feldspar porphyry yielded a U-Pb zircon age of 2120 ± 2 Ma (Norcross et al.. 1998). Highly irregular and discontinuous rhyolite dikes. generally striking WNW-ESE and steeply dipping to the north. crosscut the volcanic rocks in the Wenot pit. The dikes range in thickness from 0.3 to 10 m. The rhyolites are strongly silicified. massive. aphanitic to very fine grained. and have granophyric texture.

Sedimentary rocks from the Wenot pit consist of siltstones. sandstones. and graywackes. A thick (more than 2 km) poorly-sorted cobble conglomerate sequence. interlayered with meter-thick beds of amygdaloidal basaltic flows and tuffs. outcrops north of the Fennell pit.

The Omai stock has in planview an irregular shape. whereas in vertical cross sections it shows a consistent steep plunge ($70°-80°$NE). The stock consists of fine to medium grained quartz-monzodiorite. granodiorite. and diorite in the center with a discontinuous. coarse-grained hornblendite rim at its contact with the volcanic host rocks. The Omai stock yielded an U-Pb zircon age of 2094 ± 1 Ma (Norcross et al.. 1998).

The vein-forming hydrothermal rutile and titanite yielded a Pb-Pb model age of 1999 ± 6 Ma (2σ) (Norcross et al.. 1998). whereas Sm-Nd age on hydrothermal scheelite yielded 1994 ± 140 Ma (Voicu et al.. 1997a). The time interval between 2.2 and 2.0 Ga loosely brackets the main phases of magmatism. metamorphism. deformation. and hydrothermal evolution of the Omai area. Post-mineralization brittle faulting. sporadic mafic magmatism. and erosion have only slightly modified the geometry of the mineralized zones by causing minor offsets and incision.

Post-mineralization mafic magmatism is represented at Omai by several dikes and sills. The Tumatumari-Omai gabbro dike (Avanavero suite), located north of the Fennell pit, was dated by U-Pb on zircon and baddeleyite at 1789 ± 2 Ma (Norcross, 1997).

3.4 STRUCTURAL RELATIONSHIPS AND GEOLOGICAL EVOLUTION OF THE OMAI AREA

The geological evolution of the Omai zone is summarized in Table 3.1. The mafic volcanic rocks, porphyry and rhyolite dikes, and the metapelitic rocks display a regional foliation which strikes 100-110° and steeply dips in either directions (Fig. 3.4A). Facing directions can be interpreted from sedimentary structures and pillow shapes. Statistical data on the asymmetry of re-entrants in pillow lobe outlines yield a younging direction to the south. As the dip is frequently steeply to the north, the volcanic units may be locally overturned. The volcanic sequence has been tilted to its vertical position and has not experienced polyphase deformation.

Ductile shear zones occur only in the Wenot pit, where a 100 m wide shear corridor consists of several 1-2 metre wide shear zones. Shear planar fabric is parallel to the regional foliation (Fig. 3.4A) and crosscuts the volcano-sedimentary and porphyry/rhyolite dikes, suggesting that both structural effects were induced by a single, contemporaneous event, which post-dates the emplacement of the volcano-sedimentary unit and the felsic dikes. The ductile shear zones do not contain mineralized veins.

The Omai stock was intruded after the Barama-Mazaruni lavas were tilted. Its contact with the host volcanic rocks is undeformed. Furthermore, the chlorite-albite-sericite-carbonate assemblage in the stock formed the hydrothermal alteration due to frequency of veins, but not a metamorphic mineral assemblage. Therefore, the Omai

Table 3.1   Geological evolution of the Omai zone

Geological events	Age (Ga)
Intrusion of Apatoe doleritic dikes	0.3 [4]
Intrusion of the Omai-Tumatumari gabbro sill (Avanavero suite)	1.79 [1]
Emplacement of gold-bearing vein swarms (+ stockworks) and lode gold mineralization	1.99 [2], [3]
Development of brittle fractures (mainly N20-40° 10-40°NW) between the main shear zones during a NW-SE tectonic compressional event (D2)	2.10 - 1.99
Intrusion of Omai stock	2.09 [1]
Regional deformation (D1), resulting in a general WNW-ESE striking and steeply dipping structures: development of ductile shear zones, broadly oriented WNW-ESE, accompagnied by low grade (prehnite-pumpelleyite to lower greenschist) metamorphism	2.12-2.09
Intrusion of quartz-feldspar porphyry and rhyolite dikes	2.12 [1]
Strong spilitic alteration of the mafic rocks, associated with hydrothermal pipes cemented with disseminated pyrite	>2.12
Emplacement of the tholeiitic basalts and mafic/ultramafic subvolcanic bodies, calc-alkaline andesites associated with sedimentary sequences	>2.12

[1] - U-Pb on zircon from Norcross et al., 1998; [2] - Pb-Pb on hydrothermal rutile and titanite from Norcross et al. 1998; [3] Sm-Nd data on scheelite (Voicu et al., 1997a); [4] K-Ar age from Gibbs and Barron (1993).
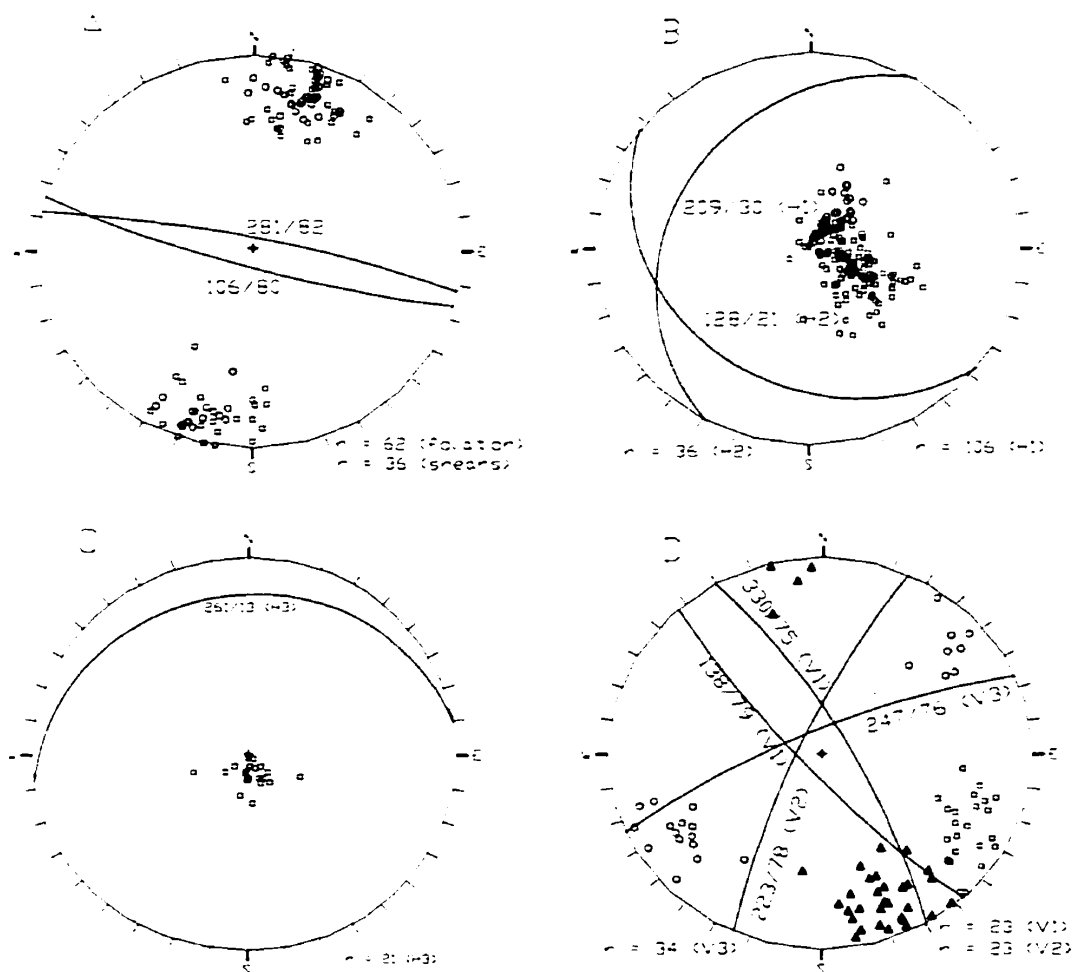
Figure 3.4   Equal area stereographic projections (lower hemisphere) of structural data from the Omai mine. A. Poles of foliation (squares) and ductile shear zones (circles) in the Wenot pit. Average orientation is also shown; B. Poles of subhorizontal H1 (squares) and H2 (circles) vein systems. Average orientation is also shown; C. Poles of suhorizontal H3 vein system. Average orientation is also shown; D. Poles of subvertical V1 (circles), V2 (squares), and V3 (triangles) vein systems. Average orientation is also shown. V3 vein system occupies the central part of the brittle shear zones in the Wenot pit. Therefore, the poles of V3 system represent also the orientation of the brittle shear zones.

stock post-dates the regional foliation and peak metamorphism. A late phase of brittle deformation affected the Omai stock and country volcanic rocks. This fracture network has represented the pathway for the emplacement of alkali basalt dikes. followed by mineralizing fluids.

A well developed brittle shear zone occurs in the Wenot pit and it contains one of the vertical vein systems discussed below.

3.5 VEIN STRUCTURE

Six main gold-bearing undeformed vein sets can be distinguished in the two ore zones (Fennell and Wenot) (Fig. 3.5 and Fig. 3.6). The vein sets can be divided in subhorizontal and subvertical.

3.5.1 Subhorizontal veins

Subhorizontal veins include three sets: $205°-215°/15-35°NW$. $120°-140°/15°-35°SW$ and a vein set with variable strike/$5-15°$ dip.

The 205°-215°/15-35°NW vein set (H1) is well developed in competent rock types (e.g. the Omai stock and porphyry/rhyolite dikes) and represents the main mineralized vein system at the Omai mine (Fig. 3.4B). Although the veins have been observed up to 10 m outside the felsic rocks. they pinch out abruptly at the contact with volcanic rocks and their frequency decreases rapidly from the intrusive contacts. The vein thickness ranges from a few mm up to 1.5 m. Significant differences are observed between the veins hosted by the Omai stock (in the Fennell pit) and those hosted by porphyries/rhyolites (in the Wenot pit).

H3 vein system

ELEV (Z)

454.79

H1 and H2 vein systems

Hornblendite rim

EAST (X)
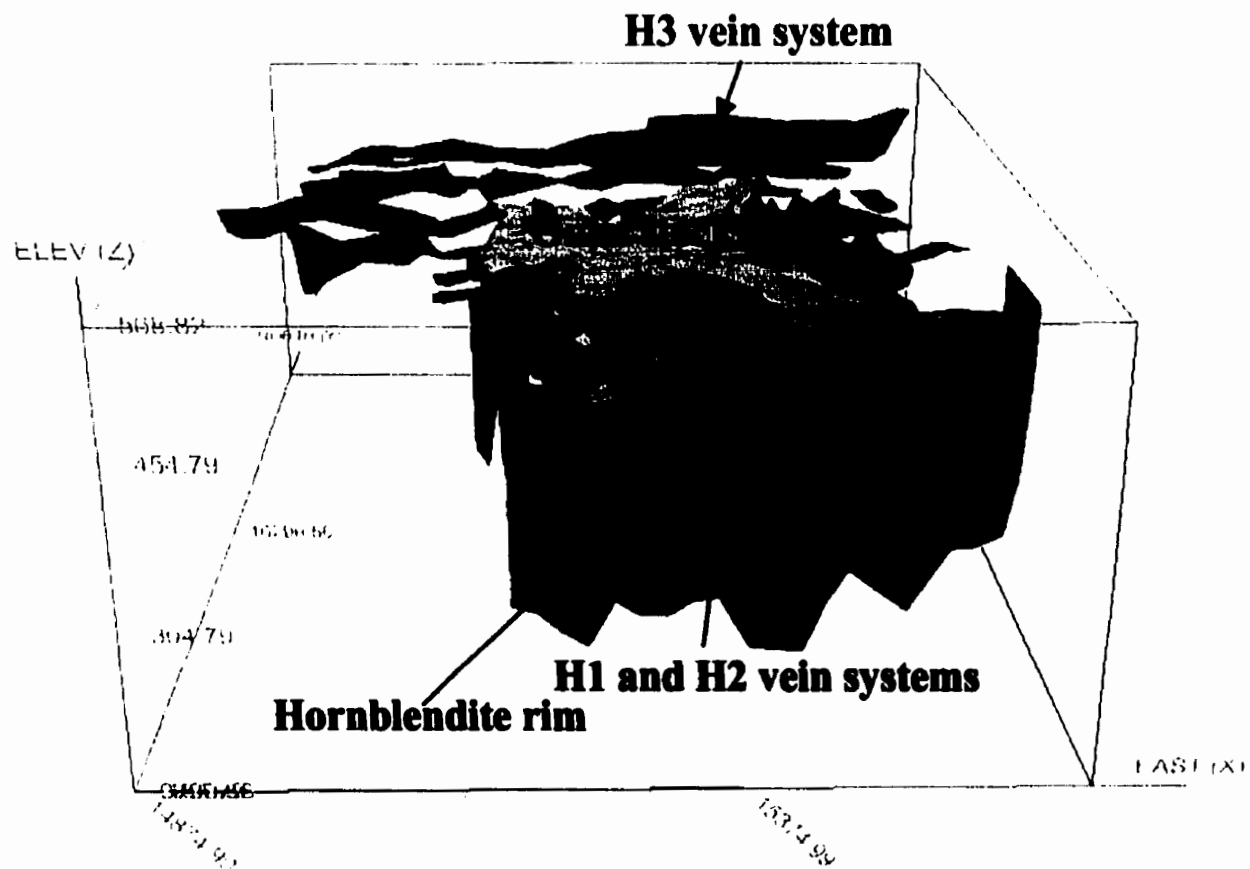
Figure 3.5   Model for mineralized veins and host rocks in the Fennell Pit (looking east). H1 and H2 vein systems have been cut away to show detail. Modeling by B. Westin, Omai Gold Mines Ltd., using the Gemcom ™ software.

Wenot shear corridor

EAS (X)

H1, H2 and V2
vein systems

Sediments

Quartz-feldspar
porphyry ELEV (_)

53-.
503.

408.
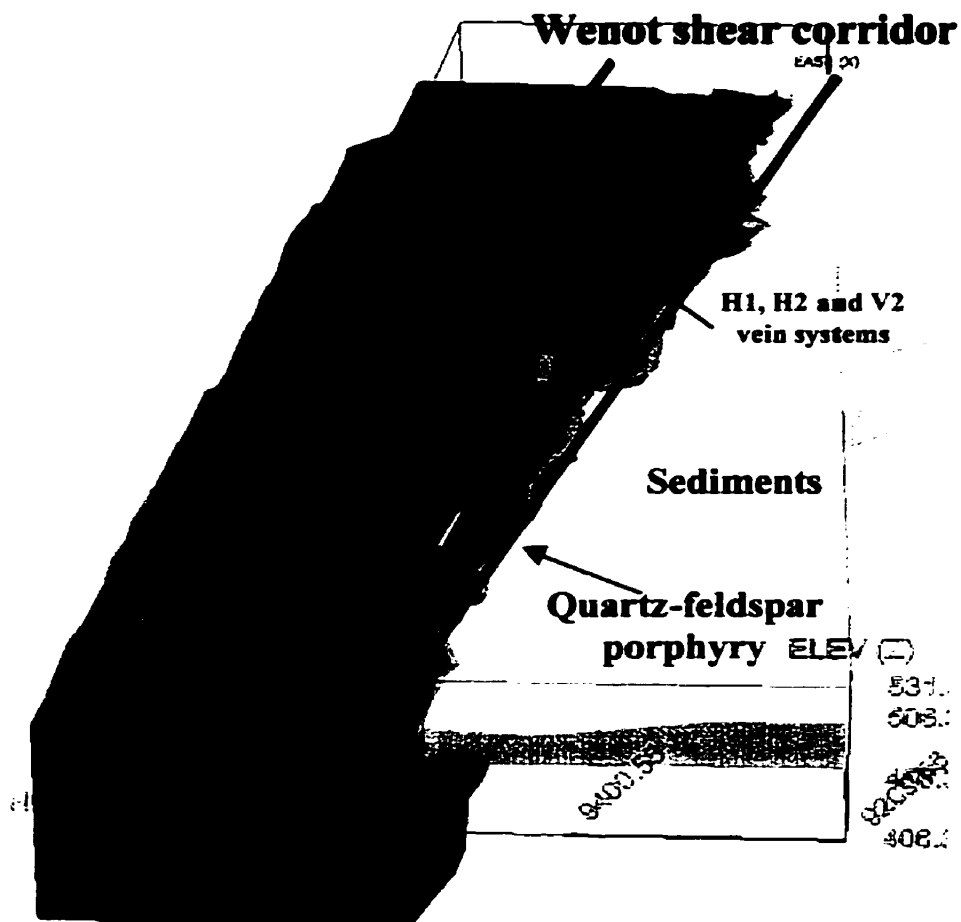
Figure 3.6   Model for mineralized veins and host rocks in the Wenot Pit (looking east). Modeling by B. Westin, Omai Gold Mines Ltd., using the Gemcom ™ software.

In the Fennell pit the veins form subparallel swarms spaced several to tens of meters apart defining *en echelon* patterns (Fig. 3.7A). The strike of this vein set can easily be recognized by the orientation of the high-grade ore shoots (Fig. 3.8A). Only a few master veins cut the entire Omai stock with an average dip of $35°$ and a thickness of approximately 1 m (Fig. 3.7B). The wallrocks and vein selvages commonly show discrete sheared planes. with both dextral and sinistral senses of movement. These master veins are commonly brecciated. in contrast with the *en echelon* veins which are crack and seal extension veins.

In the Wenot pit. the H1 veins have highly variable strikes and dips. producing a stockwork aspect (Fig. 3.7C). Most veins are hosted by the WNW-ESE striking porphyry/rhyolite dikes. and less commonly in andesites. Not all dikes are mineralized and one single dike can be only partially mineralized. The veins are generally perpendicular to the strike of dikes. but the mineralized zones follow the WNW-ESE strike of the dikes (Fig. 3.8B). The thickness of these veins is usually less than 0.3 m. while their frequency is significantly greater when compared to those in the Omai stock. The veins hosted by andesites are generally thin (up to 20 cm). with lengths of less than 10 m. Most of these veins formed in the immediate vicinity of the rhyolite/porphyry dikes.

Figure 3.7   Structural characteristics of the vein systems at Omai. A. Subhorizontal H1 vein system in the Omai stock (Fennell pit). The veins have gentle dips and are distributed subparallel to one another. They are irregularly spaced several to tens of meters apart and commonly define *en echelon* patterns: B. Subhorizontal H1 vein system: master vein that cuts the entire Omai stock (Fennell pit) or the andesite/porphyry/rhyolite contacts in the Wenot pit. This vein type can attain lengths of several hundreds of meters. The veins have an average dip of $35°$ and an average thickness of more than 1 m: C. H1 vein system in rhyolites (Wenot pit). which shows stockwork aspect (marker for scale): py = pyrite: D. V3 vein system in andesites (Wenot pit) showing horse tail aspect.

A
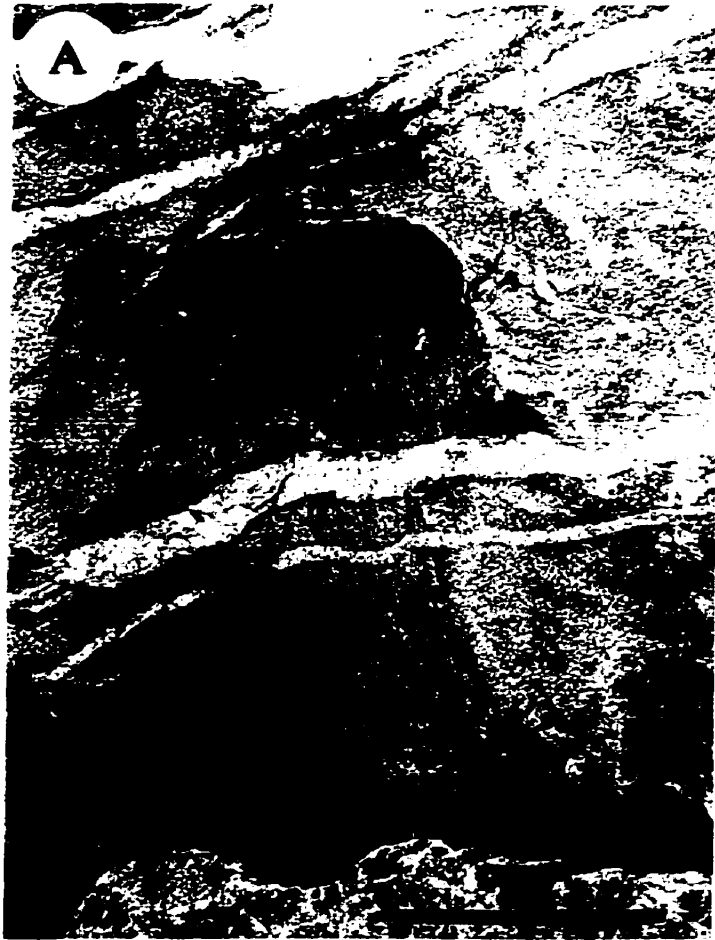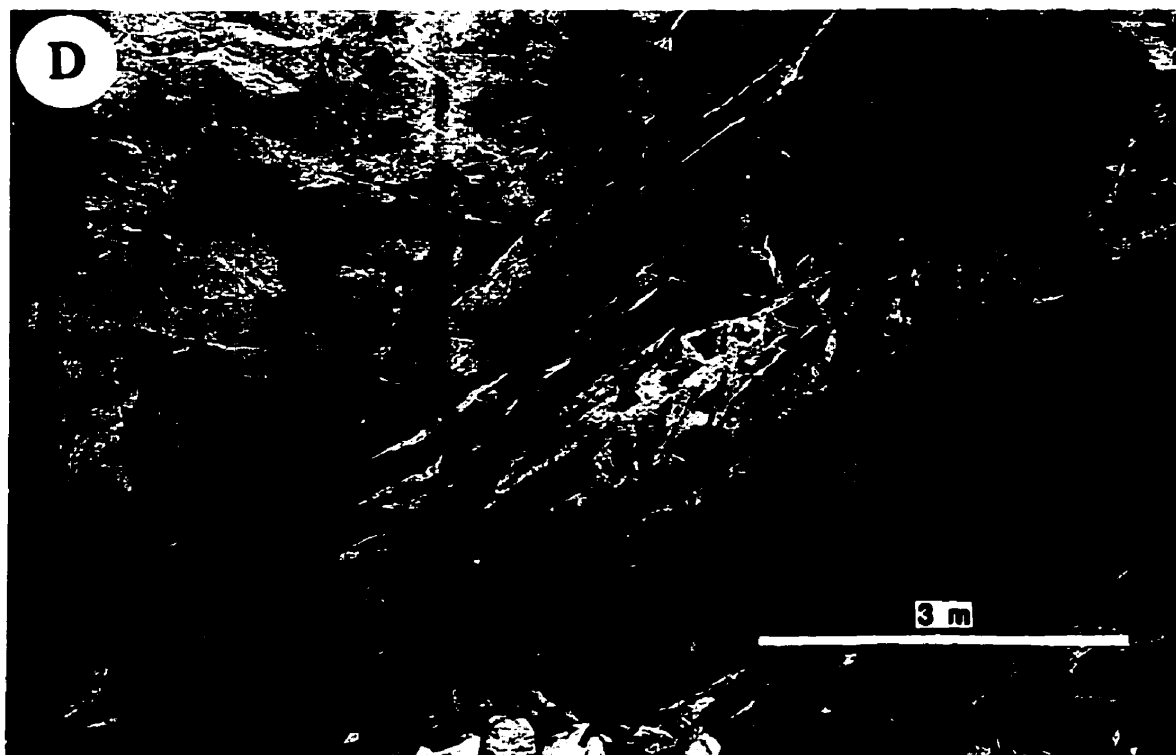
Fennell pit, 445 bench
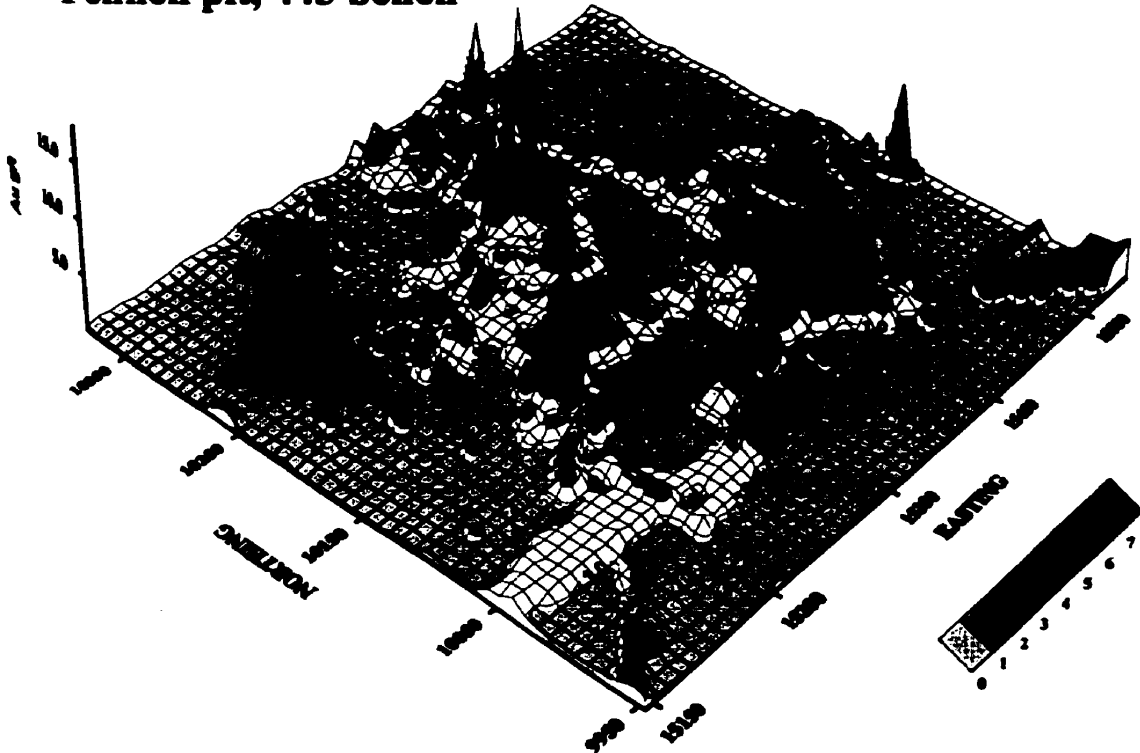
Figure 3.8   General distribution of gold grade. A. Fennell pit, 445 bench; the highest gold grade is related to the orientation of the H1 and H2 vein systems. Their intersections represent high-grade ore shoots; B. Wenot pit, 445 bench. The gold grade generally follows the WNW-ESE orientation of the felsic dikes. Gold grade is estimated from the production blastholes, for 5 m bench height. Contouring is done by Laplace method, with a smoothing factor of 1.

B

Wenot pit, 445 bench
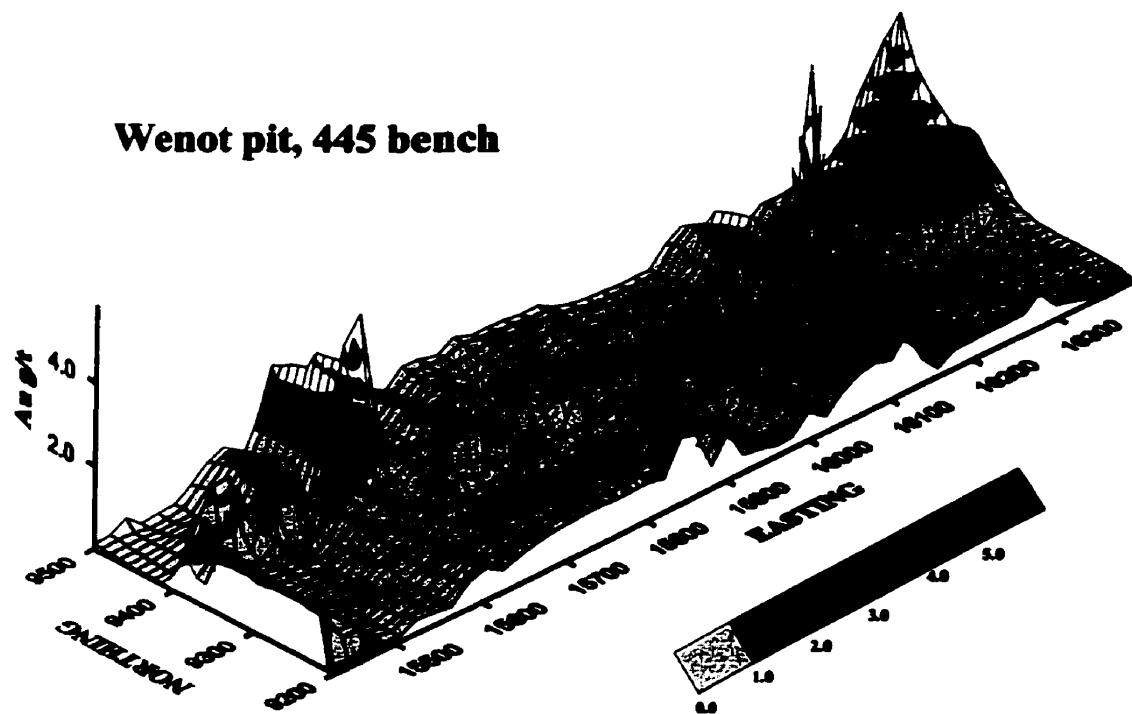
Figure 3.8   (continuation)

The 120 °-140 °/15 °-35 ° SW vein set (H2) occurs locally in the Fennell pit (Fig. 3.4B). The intersections of this vein set with previously described vein set are strongly enriched in gold. The overall features of this vein set are similar to the H1 vein system.

Variable strike/5 °-15 ° vein set (H3) occurs in the tholeiitic basalts north of Fennell pit and roughly follows the northern contact of the Omai stock. The veins have several tens of m length and an average thickness of about 10 cm. The veins gently dip to the north (5-15°) and are spaced tens of meters apart (Figure 3.4C). They occur above the Omai stock cupola and are located probably in fractures formed during the stock emplacement.

3.5.2 Subvertical veins

The 330 °/75 °-85 ° (in either direction) vein set (V1) is minor and occurs only in the Omai stock. It is represented by thin (several cm) quartz veins (Fig. 3.4D).

The 200 °-220 °/70 °-85 ° NW vein set (V2) occurs in the rhyolite/porphyry dikes, andesites, and pelitic rocks in the southern Wenot pit (Fig. 3.4D). The thickness of the veins is highly variable (several cm to 0.5 m), whereas their length is of several tens of m. They are irregularly spaced, generally several m apart.

The 240 °-260 °/70 °-90 ° vein set (V3) occurs only in the Wenot pit. It occupies the central part of the brittle shear zones (Fig. 3.4D). The vein thickness ranges between 0.5 m and 1.5 m and the length is up to 600 m. Commonly, the end of the veins shows a horse tail aspect, whereas the vein thickness can increase up to 3 m (Fig. 3.7D).

3.6 VEIN TEXTURES

The vein systems at Omai can be classified as extensional (including crack and seal tensional and shear veins), breccia veins, and fracture-filling veins. Some features of the vein textures are comparable to those described by Robert and Brown (1986) at the Sigma mine, in the Archean Abitibi greenstone belt, whereas others are closer to the vein textures described in the circum-Pacific Tertiary epithermal deposits (e.g. Cooke et al., 1996).

Crack and seal tensional veins

Individual ribbons of minerals deposited during one or more open space vein filling episodes characterize this type of veins (Fig. 3.9A). This textural aspect predominantly occurs within H1, H2, and V1 vein sets. Ribbons are defined by individual mineral layers that vary in thickness between several mm to more than 10 cm. The layers can be symmetrical about the vein central plane, indicating that opening of

Figure 3.9   Textural characteristics of the gold-bearing veins at the Omai mine. A. Crack and seal ribbon vein (H1 vein system, Fennell pit). Scheelite (sch) and ankerite I (ank) are deposited on vein selvages, whereas milky quartz (mq) represents a later filling phase: py = pyrite: B. Crack and seal shear vein (H3 vein system, Fennell pit). Several mm-thick ribbons are parallel to the axial plane of the vein. They formed by successive episodes of opening and mineral deposition: C. Single-stage breccia vein (H3 system in basalts, Fennell pit). Subrounded to angular, unaltered (except pyritization) wallrocks (wr) are trapped within the milky quartz (mq) matrix. The wallrock fragments have no alteration rim (marker for scale): D. Multi-stage breccia vein (V3 vein system, Wenot pit). Angular, subrounded or rounded altered wallrock fragments (wr) are surrounded by later mineral (mostly ankerite, ank) rims and cemented with milky quartz (mq). Quartz stringers crosscut locally the breccia fragments.
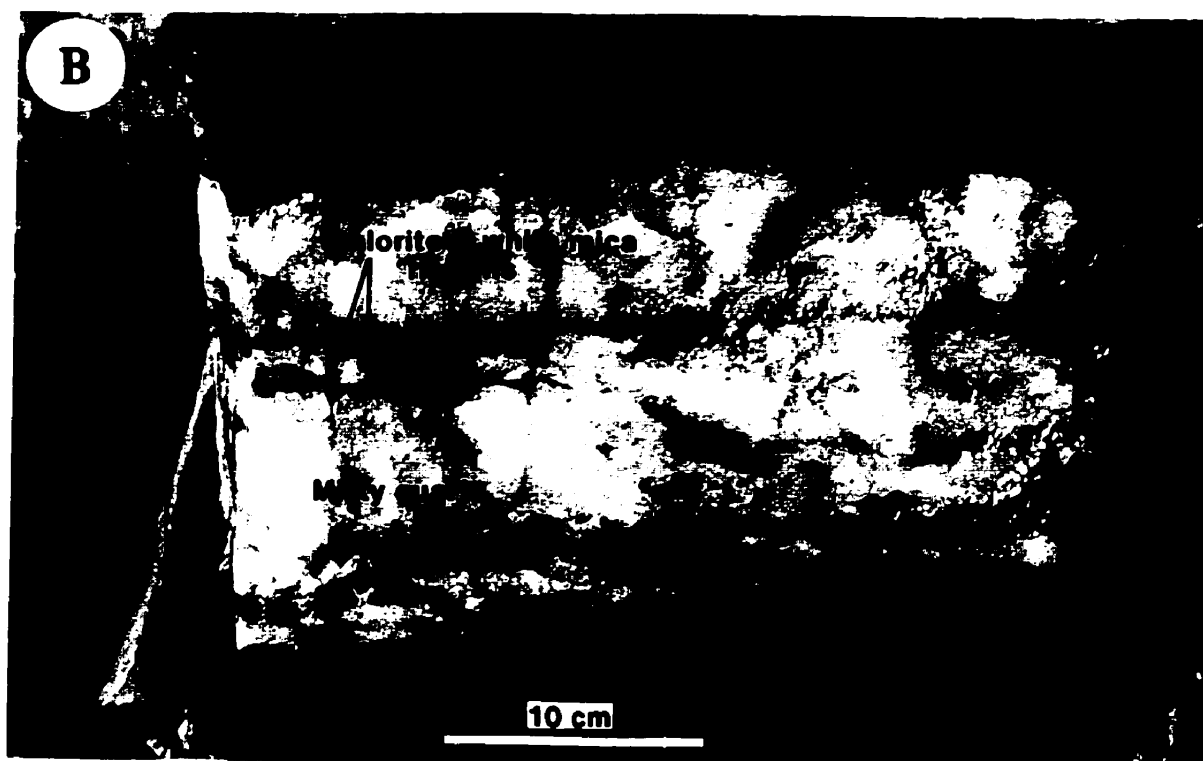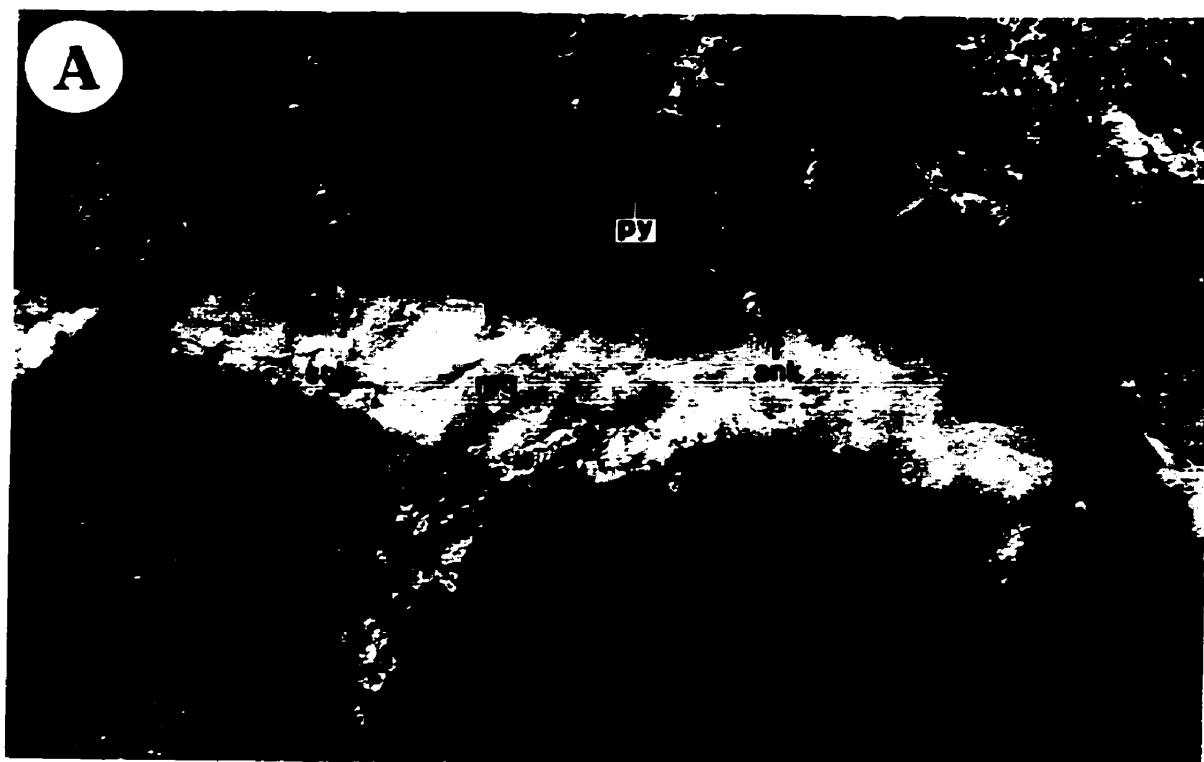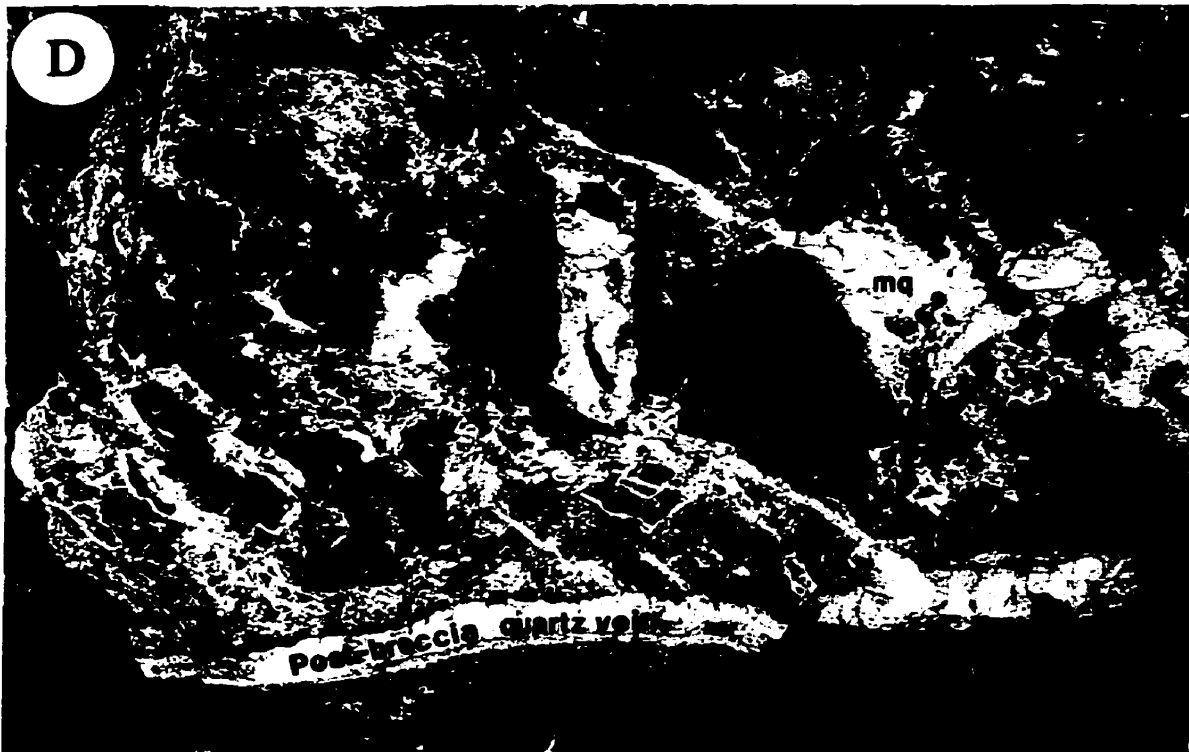
the veins took place on both walls of the vein. or asymmetrical. caused by re-opening along one selvage. No wallrock fragments occur within this vein type. The core of the veins is generally occupied by quartz. although veins consisting mainly of ankerite or scheelite. with minor quartz. occur locally in the Omai stock.

Crack and seal shear veins

They are characteristic for the H3 veins hosted by the tholeiitic basalts north of Fennell pit and. partially. for the V3 vein system in Wenot. These veins contain abundant ribbons of chlorite. sericite. epidote. and rarely ankerite or calcite. indicating successive vein opening and filling episodes. The ribbons are a few mm thick and are parallel to the vein central plan (Fig. 3.9B).

Breccia veins

This type of veins can be divided in single- and multi-stage brecciated veins. Single-stage breccia veins occur in the Omai stock and andesites (H1 vein type) and tholeiitic basalts (H3 type). They contain angular or subrounded fragments of wallrocks reaching up to 0.8 m.The breccia matrix is always represented by milky quartz. Even if the fragments are poorly sorted. the largest tend to cluster towards the basal contacts of the veins.The wallrock fragments are usually *in situ*. although transported fragments up to several m from their original locations have been observed. Locally. near the contact between the Omai stock and andesites. the breccia-texture veins within the stock contain andesite fragments. suggesting that the flow direction of the mineralizing fluid was from country rocks towards the Omai stock. The breccia fragments in the H1 vein set have undergone intense carbonate-sericite and pyrite alteration. which suggests that at least one phase of alteration pre-dates the introduction of the massive influx of silica-related

brecciation. In the H3 vein set. the breccia fragments are not altered (except pyritization) (Fig. 3.9C) and represent a preferred site of gold precipitation.

Multi-stage brecciated veins occur in the V3 vein set in the Wenot pit. Angular. subrounded or rounded altered wallrock fragments form between 60-90% of vein volume. They are generally rotated and surrounded by later mineral (mostly ankerite) rims and cemented with milky quartz. Quartz-only veinlets and stringers crosscut locally the breccia fragments (Fig. 3.9D).

Fracture-filling veins

The V2 vein set in Wenot is characterized by fracture-filling texture.The veins are planar and occur in irregular patterns.

3.7 RELATIONSHIPS BETWEEN VEIN SETS

In the Fennell pit. the veins that form a single vein set (H1) display complex crosscutting relationships. The master veins crossing the Omai stock generally overprint the *en echelon* veins. although the opposite relationship exists. Their crosscutting aspects are sharp. without formation of irregular material at the vein intersections. Similar complex crosscutting relationships exist between the H1. H2. and V1 vein sets. The H3 set generally cut across the H1 *en echelon* veins and the H2 set.

In the Wenot pit. the V3 vein system cuts across andesites and rhyolite dikes. No intersections have been observed between the V3 and V2 vein sets located in porphyry and metapelites. In the places where the V3 veins cut across rhyolites. they extend into H1 vein type. The opposite situation also exists. when H1 veins crosscut the V3 veins. Commonly. the H1 veins in Wenot consist only of milky quartz. although locally the veins display crack-seal tensional textures highlighted by ankerite=scheelite ribbons.

This aspect indicates that most of the H1 veins formed contemporaneously with the massive silica influx into crack-seal shear or multi-stage brecciated V3 veins. The strong competency contrast between andesites and rhyolites played a major role in the emplacement of the stockwork-like H1 veins. However. some H1 veins probably formed earlier. allowing the ribbon formation due to one or more opening and filling episodes. Furthermore. the H1 veins generally cut across the V2 veins. although the opposite relationship exists.

Field relationships suggest that vein systems of Fennell and Wenot are not overlapping and therefore do not allow to establish the genetic link that may exist between the two areas. However. their structural. textural. and mineralogical similarities suggest that the vein sets are contemporaneous.

3.8 VEIN MINERALOGY

Vein mineralogy is related to vein type and the chemical composition of the host rocks. The formation of most veins can be summarized by two filling stages (I and II) and a late fracture-filling stage (III) related to a protracted hydrothermal process. Stage I. II. and III do not represent generally distinct vein generations (i.e. crosscutting veins). but single veins that have been repeatedly opened and filled. The transition between stage I and II is represented by the deposition of milky instead of smokey quartz. and the presence of the second carbonate generation. There is no vertical zonation of vein minerals. Fig. 3.10 shows the paragenetic diagram for the vein systems and wallrocks.

Stage I

Translucent smokey quartz crystallized during stage I. It is commonly strained as shown by undulose extinction. deformation lamellae. and incipient recrystallization.
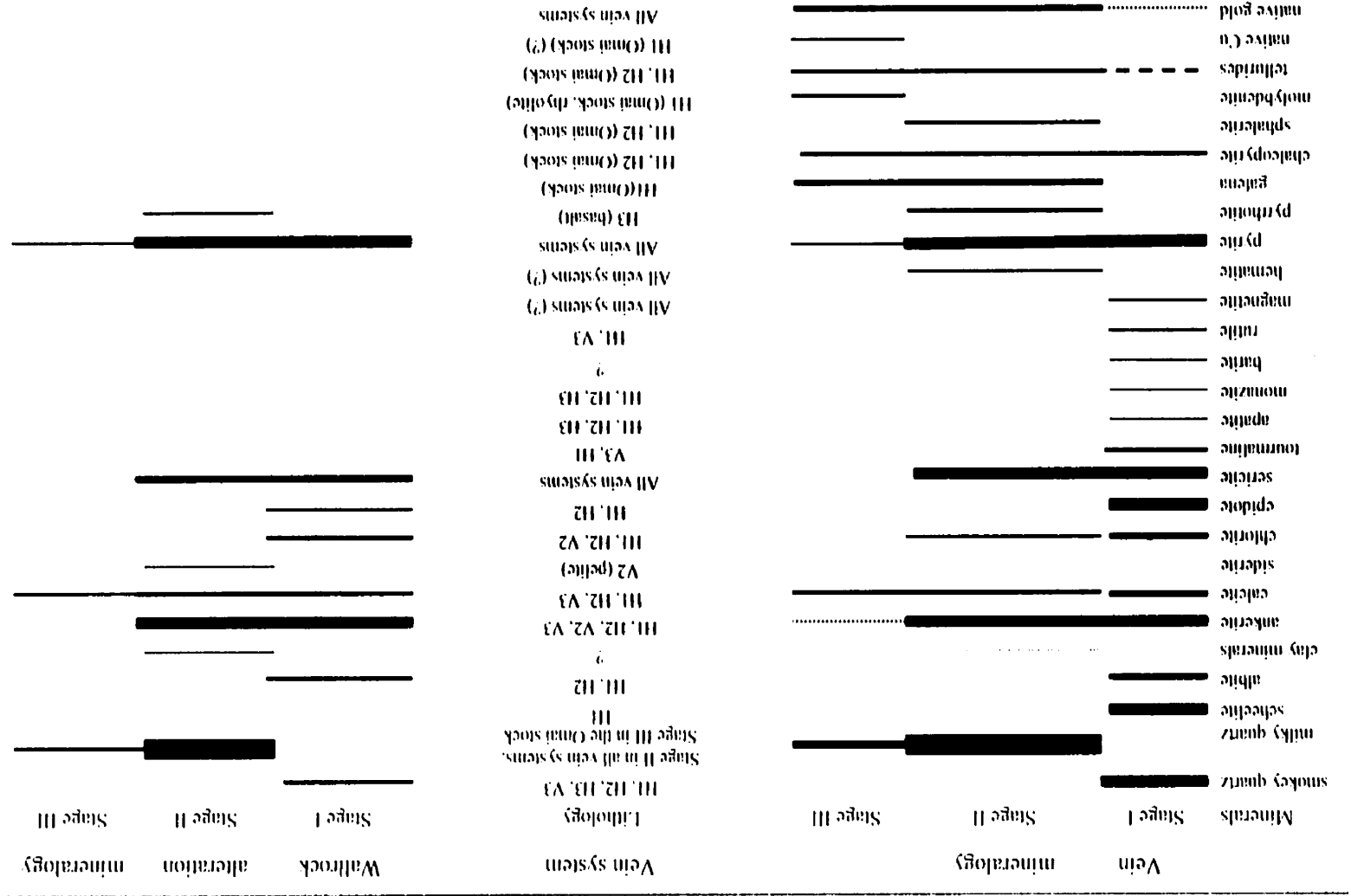
It is frequently associated with scheelite=carbonates (mainly ankerite). and occasionally contains visible gold inclusions. Scheelite is an important component of the veins hosted by the Omai stock and rhyolites. where it locally reaches up to 10% of vein volume. but it is a minor phase in the veins hosted by other rock types. Scheelite forms crystals up to 10 cm in size and occurs as 'pockets' or semicontinuous coatings on vein walls (Fig. 3.11A). Tourmaline. smokey quartz. gold and pyrite grains are surrounded by scheelite. which is also veined by these minerals. probably as the result of coeval precipitation. Carbonates are widespread at Omai. They occur as vein- or fracture-filling phases and as pervasive alteration in all rock types. Ankerite I occurs as dark gray patches which post-date scheelite. or as semicontinuous coatings on vein selvages when earlier formed minerals are not present. Ankerite I averages 5% of veins. but it is randomly distributed. Locally. smokey quartz-ankerite I veins are cut by milky quartz-bearing veins (Fig. 3.11B). Apatite. scheelite. and pyrite I are surrounded by ankerite I which. in turn. seems to be post-dated by all other mineral phases. Calcite I is represented by large. well crystallized light gray crystals. Sericite. chlorite. and epidote form cm wide coatings along the vein selvages. Acicular-prismatic crystals of epidote up to 1.5 cm long are common in the mafic volcanic rocks. Sericite is sparse. but it seems to represent a common gangue deposited during the whole mineralization process. Irregular masses of chlorite occur usually at the contacts with wallrock in veins hosted by andesites/basalts. but it is scarce in veins hosted by felsic rocks. Tourmaline (dravite) is rare and mostly associated with scheelite. No direct relationship has been observed between albite and tourmaline: however. the tourmaline-scheelite association suggests that tourmaline is post-albite. Smokey quartz veinlets crosscut scheelite but stop at the contact with tourmaline. suggesting that at least some tourmaline is post-scheelite/smokey quartz. Tourmaline typically forms small. randomly oriented needle-like black crystals clustered in irregular masses along scheelite grain boundaries. or as isolated crystals in scheelite. Albite forms several cm thick layers along vein selvages. Except apatite. rutile ±
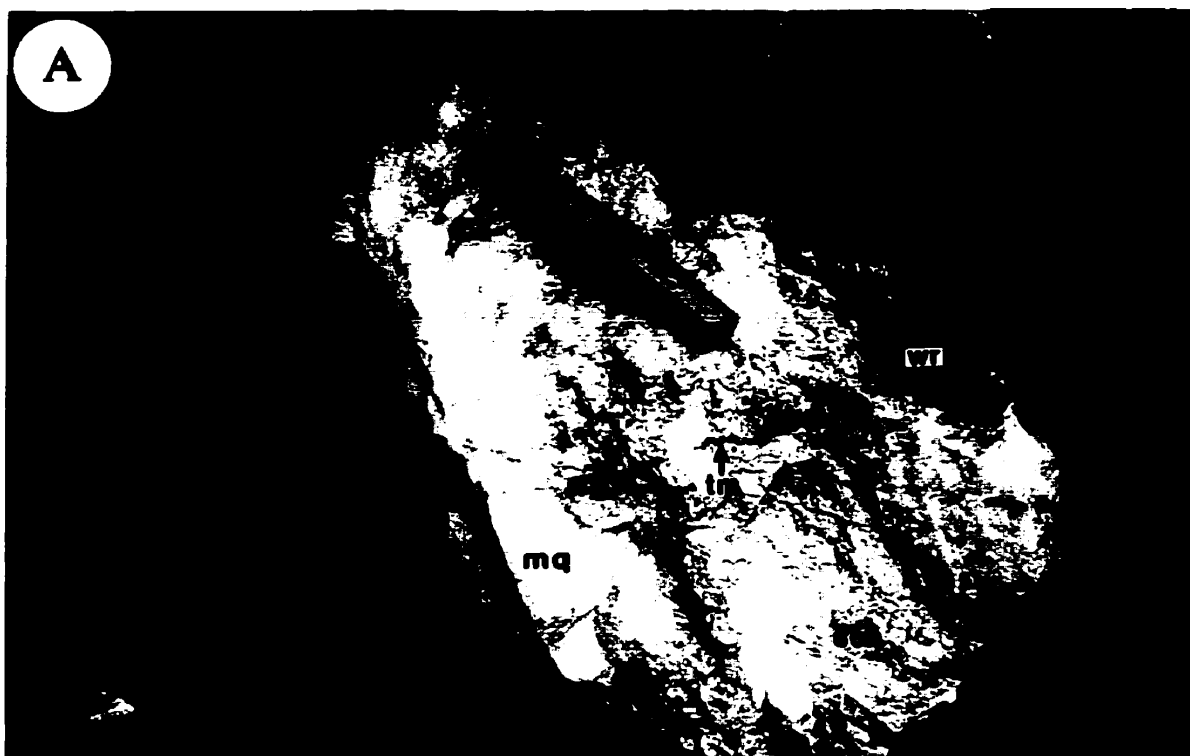
Figure 3.11   Mineral assemblages from the mineralized veins. A. Scheelite (sch) pockets and tourmaline (tm) in milky quartz (mq) in a breccia-textured (wr = wallrock fragment) vein: B. Smokey quartz and ankerite I (sq+ankI) (as continuous coatings on vein selvages) vein cut by milky quartz-ankerite II (mq+ankII) vein: C. Native gold (stage III) (Au) deposited as dendritic fracture fillings that can be traced for several cm in milky quartz or on the wallrock fragments (wr) within the single-stage breccia HI vein system (Fennell pit).
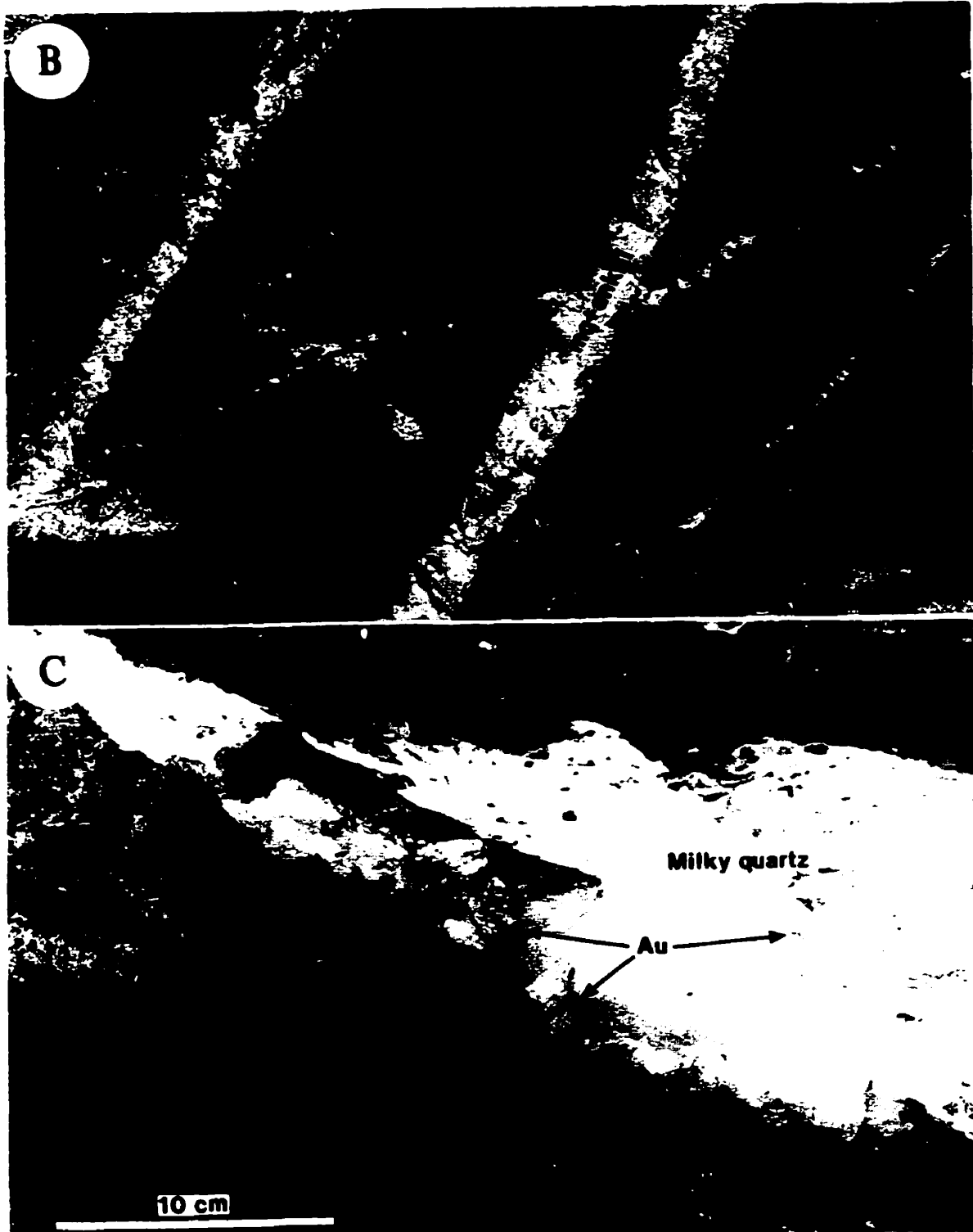
Figure 3.11   (continuation)

monazite. no other minerals seem to pre-date albite deposition. Apatite. rutile. monazite. and barite are minor phases in veins.

Pyrite is by far the most abundant metallic sulfide phase at Omai. It averages about 1% of the total vein volume. but locally reaches up to 5%. Pyrite I is principally distributed close to the vein walls. in alteration envelopes of veins. and in the wallrock fragments of the breccia-texture veins. Generally. the pyrite I abundance in veins is minor when compared to disseminated pyrite I in wallrocks. In the alteration envelope of the H3 veins. pyrite I is associated rarely with rutile. chalcopyrite. and melonite ($NiTe_2$). Magnetite is rare. and is generally associated with pyrite I.

Gold appears relatively early in the ore paragenesis. although the main gold mineralization is associated with sulfide and telluride deposition during stages II and III. In stage I. free gold occurs as irregular-shaped coarse grains.

Stage II

Milky quartz represents the most common vein-filling phase at Omai. It shows incipient crystallization and undulose extinction. but no deformation lamellae were observed. Locally. plumose textures with bladed habits may develop on the border of quartz crystals. Minor open cavities and vugs filled with microcrystalline quartz/opal occur locally. Ankerite II has similar chemical composition to ankerite I. It occurs in milky quartz from the ribbon and multi-stage brecciated veins. where it forms layers in the cores of the veins or envelopes wrapping wallrock fragments. respectively. Sericite and chlorite form mm wide layers within milky quartz from the crack-seal shear veins. Patches and aggregates of chlorite occurs in breccia veins and can represent chloritized wallrock fragments.

Pyrite II occurs as large euhedral crystals (up to 1.5 cm) in the cores of veins and in the alteration envelopes. Pyrite II frequently contains randomly distributed inclusions of chalcopyrite. gold. tellurides. galena. and. rarely. smokey quartz and ankerite. In the Omai stock. pyrite II is frequently veined/replaced along fractures/grain boundaries by later gold. tellurides and sulfides. Pyrrhotite was observed only in the H3 single-stage brecciated veins. always as pseudomorphs after pyrite I. Perfect cubes of pyrrhotite. formed by partial or total replacement of pyrite. occur in milky quartz and in adjacent wallrocks. The pyrrhotite pseudomorphs represent an important depositional site of gold II. which occurs as coatings on the grain boundaries or as fillings of pyrrhotite fractures. Galena occurs in the veins hosted by the Omai stock. Bertoni et al. (1991a,b) reported also galena in the Wenot pit. but it has not been observed in this study. Symplectic intergrowths of galena with gold and tellurides were observed as inclusions in pyrite II. Chalcopyrite is usually a minor phase associated with pyrite II. Sphalerite II contains inclusions of gold±tellurides and commonly is replaced along grain boundaries by a later gold-telluride-sulfide assemblage. Hematite is minor. and is generally associated with pyrite and sphalerite. Telluride minerals include tellurobismuthite. petzite. calaverite. hessite. altaite. and coloradoite.

Gold occurs as small globular inclusions in pyrite II. associated with galena and various Au-Ag-Pb-Bi tellurides in the veins hosted by all rock types. and as small ragged particles in milky quartz or deposited on pyrite I+II (in the Omai stock). wallrock fragments (in breccia veins. all rock types). and pyrrhotite (in basalts).

Stage III

Fine grained milky quartz and calcite III are associated with the last mineralizing fluids in the Omai stock.

Pyrite III represents a rare phase and is associated with the last pulse of gold-, telluride-, and sulfide-bearing mineralizing fluids. The Au-Te-S minerals are hosted by randomly oriented, thin fractures in smokey and milky quartz, and to a lesser extent in scheelite and ankerite I+II. Intergrowths of galena III with gold and tellurides (petzite, calaverite, hessite, and tellurobismuthite) occur as fracture-fillings in milky quartz. Chalcopyrite III usually forms irregular masses, although large chalcopyrite crystals (~4 cm), associated with gold and galena occur locally. Molybdenite is a minor phase in the Omai stock and rhyolite dikes. It forms either thin coatings on the slightly sheared contacts between veins and wallrocks, or is associated with the last generation of gold+tellurides+galena as thin coatings on the walls of the fracture system in milky quartz. Native copper was identified in several samples.

Gold III occurs as dendritic fracture fillings that can be traced for up to 3 cm in smokey and milky quartz-ankerite-scheelite (Fig. 3.11C). It is commonly associated with sulfides and tellurides. Gold III occurs only in the Omai stock. All three gold generations have high fineness (950-990), although a slight increase in Ag content (about 3%) was determined in gold I and III.

3.9 HYDROTHERMAL ALTERATION

Several alteration assemblages occur in association with the mineralized veins at Omai. There is an obvious association between the alteration assemblages, the vein internal textures and the chemical nature of the host rocks. The dominant alteration assemblages include carbonates, sericite, silica, chlorite, albite, epidote, and pyrite/pyrrhotite. Argillic minerals locally replace albite. Secondary biotite is absent at Omai. Generally, the alteration envelopes are fracture-controlled. Brittle quartz-vein sets are characterized by narrow (tens of cm) alteration zones, which frequently can overlap due to close spacing of veins (Fig. 3.12A). However, the primary wallrock texture is

preserved in the Omai stock and porphyry dikes. whereas strong silicification of the rhyolite dikes and carbonate-sericite alteration in andesites result in destruction of the original textures. The occurrence of alteration minerals both in veins and wallrocks suggests a close relationship between the emplacement of gold and alteration. The alteration assemblages are presented for each mineralizing stage. vein type and chemical nature of the wallrock. in order to establish the relationships between the mineralizing events. wallrock alteration and the influence of the host lithology (Fig. 3.10). The description of the alteration assemblages refers especially to the wallrocks. since the vein-forming minerals have been discussed in the previous section.

Stage I

Extensive and pervasive alteration. which occurs within the Omai stock (Fennell pit) and porphyries/rhyolites (Wenot pit) characterizes H1 and H2 vein sets. The intensity of alteration increases at the intersections of these two vein systems.

Figure 3.12   Features of the hydrothermal alteration at Omai. A. Example of fracture-controlled alteration. Smokey (light gray) and milky (white) quartz veins are characterized by narrow (cm to tens of cm) alteration zones. which frequently can overlap due to close spacing of veins (pencil for scale): B. Quartz (mq)-ankerite (ank) veins surrounded by partially overlapped alteration haloes. Adjacent to the veins. the alteration partially or totally obliterated the original wallrock texture. The result is formation of alteration haloes almost exclusively composed of various carbonates. sericite. rutile. and minor quartz. Note the strong pyritization (py) of the wallrocks (marker for scale): C. Strong pervasive silica alteration in rhyolites (Wenot pit): D. The influence of dispersion and diffusion alteration mechanisms displayed by andesites (Fennell pit).

C

Milky quartz

D

...SION

Quartz vein

...ERSION

Andesite
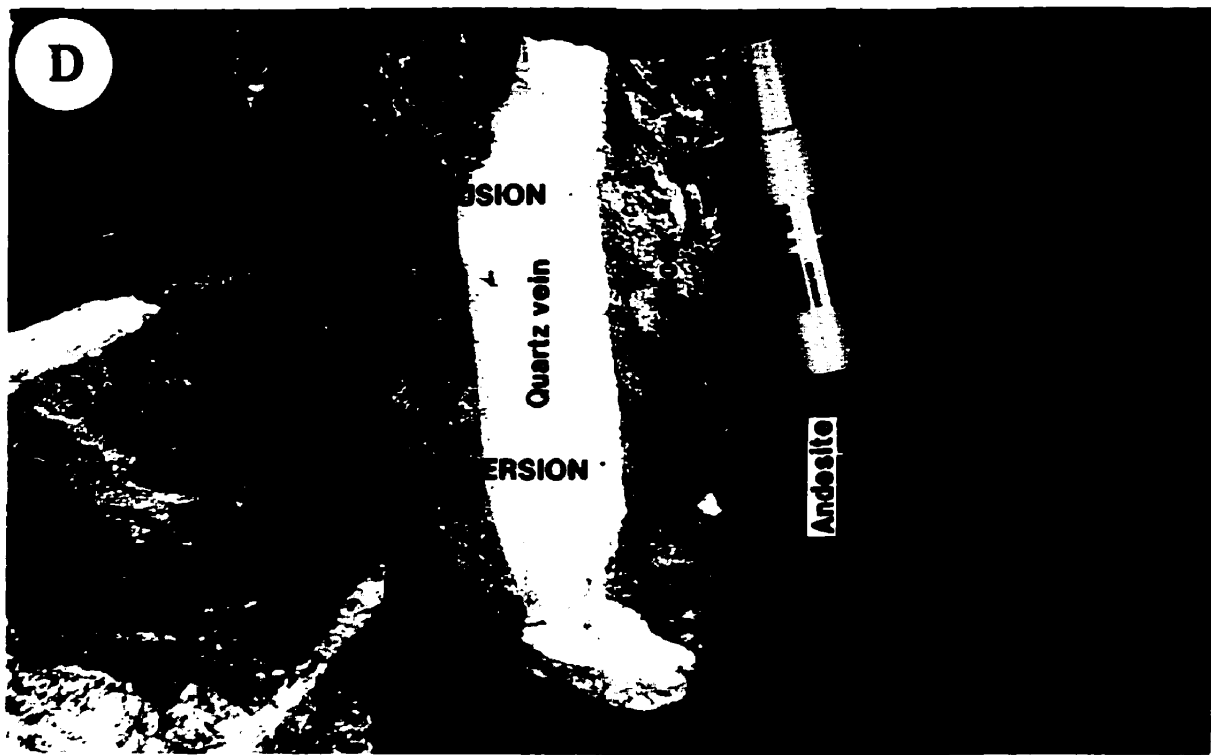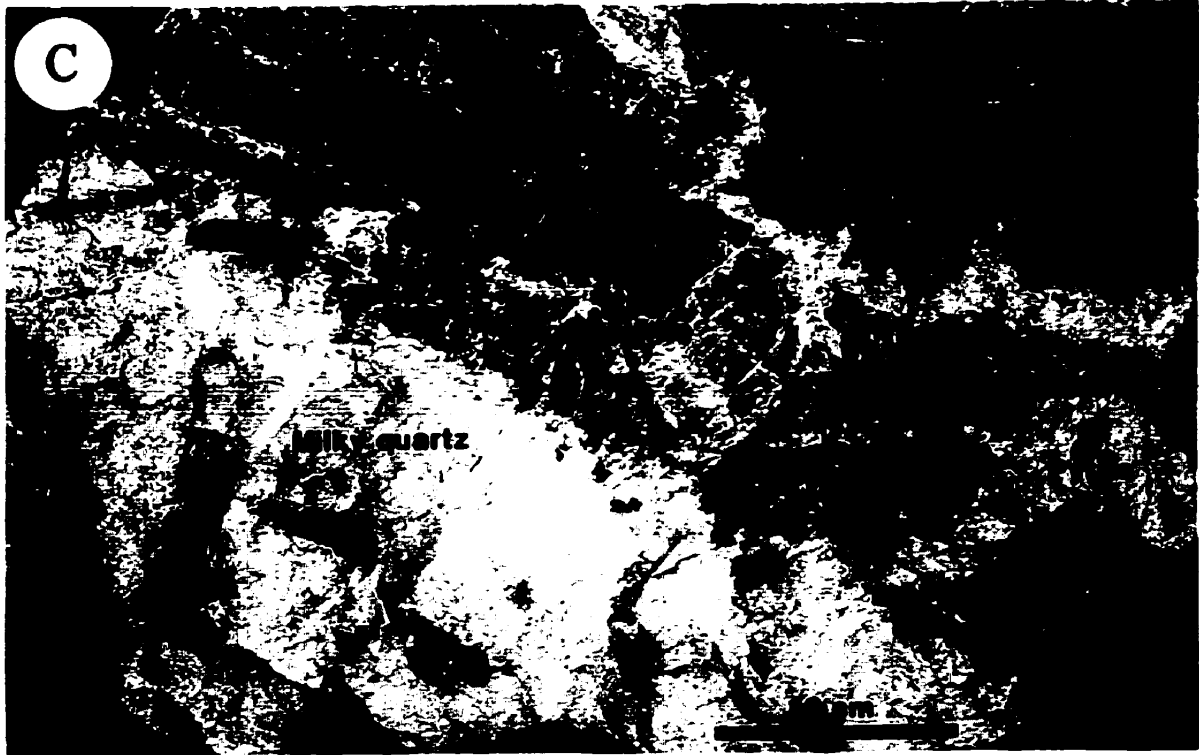
Albite is only locally present as coatings along the vein selvages and is always replaced by sericite±carbonates. Locally. albite is replaced by argillic minerals. which suggest that alteration continued to relatively low temperatures. There is no clear albitization front. but rather an albite halo surrounding parts of the veins. Sericite-carbonate (ankerite-calcite) assemblage represents the most widespread and pervasive alteration related to the H1 and H2 vein emplacement. Feldspars from the Omai stock and felsic rocks in the Wenot area are partially sericitized. whereas close to the veins it is completely replaced by sericite and carbonates. Additional calcite and ankerite was introduced as coatings along the vein selvages and grains or micro-veinlets in the matrix of the host rocks. The chlorite-epidote alteration assemblage forms by destruction of mafic magmatic minerals (mainly hornblende±pyroxene±biotite).

H3. V1. and V2 vein sets are characterized by the deposition of pyrite during the first mineralizing stage. For the V2 set. the pyritization is associated with pervasive chlorite and carbonate alteration. which results in several m wide. green or buff coloured halos surrounding the veins hosted by pelites in south Wenot.

V3 vein set has similar alteration assemblage to the H1 and H2 vein sets.

Stage II

H1. H2 and V3 vein sets are characterized by strong carbonate±sericite alteration. which shows several distinct aspects related to the vein internal texture. In the H1 and H2 veins. carbonate ribbons occur in the central part of veins. Carbonate rims surrounding wallrock fragments in the H1 and H2 breccia veins have not been observed. In andesites. the carbonate-sericite alteration forms the bleached zone. represented by less than 1 m thick envelopes around the veins. Several zones parallel to the vein given by different intensities of bleaching can be observed within the proximal alteration

envelope. which suggests that bleaching is the result of several alteration phases by fluids with comparable chemical compositions. The final result is the destruction of the original wallrock texture and formation of alteration haloes almost exclusively composed of various carbonates (calcite. ankerite. dolomite). sericite. rutile. and minor quartz (Fig. 3.12B). In the multi-stage breccia veins (V3 set). ankerite=calcite rims surround the wallrock clasts or replace the chlorite in the wallrocks. Locally. several carbonate rims overlap as a result of multiple reopenings of the veins.

In the felsic rocks. where there is a close spacing of veins. the alteration envelope overlapping results in zones of pervasive alteration. In these rock types. stage II mineralization is associated with strong. pervasive silica alteration (Fig. 3.12C). Generally. a broad correlation is observed between silicification and quartz vein volume. Quartz is predominant in the silicified haloes. and is usually accompanied by minor sericite and pyrite. Generally. there is a direct relationship between the vein texture and mineralogy and the intensity of silicification around the veins. The ribbon veins characterized by cm-thick pre-quartz carbonate/scheelite coatings show less pervasive silicification of the wallrocks due to the weak interaction between the silica-bearing fluids and the wallrocks. Conversely. wider. but more irregular silicification zones surround the breccia veins. characterized by an enhanced permeability for the fluids.

H3 vein set in basalts is characterized by the partial or total replacement of pyrite by pyrrhotite within the veins and in the wallrocks. Narrow (up to 1 cm) silicified zones occur in the vein selvages.

V1 vein set shows only discrete. several cm thick. silica alteration envelopes.

I2 *vein set* has a typical alteration feature in pelites. represented by the replacement of ilmenite and rutile by siderite. defining a pattern referred to as spotted alteration in mine terminology. Pyrite associated with stage II is rare (<0.5%).

Stage III

Hydrothermal alteration associated with stage III occurs only in H1 and H2 vein sets and is represented by minor silica and pyrite especially confined to the fractures within the veins.

3.10 SEQUENCE OF VEIN AND ALTERATION FORMATION

The relative timing of vein formation can be established using the textural. mineralogical. and alteration features presented in the previous sections.

Stage I is characterized by the deposition of the first mineral assemblage in the H1 and H2 vein sets and the first breccia-forming phase in the V3 veins. accompanied by wallrock alteration. represented mainly by albite-carbonates-sericite in felsic rocks. and chlorite-epidote-carbonates in mafic lavas. Further infiltration under low-pressure of the mineralizing fluids during stage II results in the deposition of milky quartz as the main filling mineral phase in the H1. H2. H3. and V2 vein sets. However. the vein sets (H3 and V3) with crack-seal shear textures formed by several episodes of opening and vein filling. which resulted in alternating bands consisting mainly of mm-thick silica minerals. On the other hand. fluids under higher pressure were emplaced into fractures which crosscut the lithological contacts. They formed single-stage breccia veins (H1) and. by several reopenings. the multi-breccia veins (V3). The intersections between the V3 set and the felsic dikes in Wenot played a major role in the formation of quartz-only H1 veins in these rock types. This stage is accompanied by a strong silicification.

together with carbonate and sericite alteration. Wallrock composition and the efficiency of fluid/wallrock interaction have played a major role during the alteration processes. The increased vein density in the felsic rocks has led to coalescence of the alteration envelopes. which locally results in the complete replacement of the primary mineralogy of the country rocks. Alteration zones resulted by the dispersion and diffusion of the channelized fluid flow. which modified both wallrock and fluid chemistry (cf. Ridley et al.. 1996). Dispersion into the wallrock has resulted in the formation of alteration haloes parallel to the vein. whereas diffusion has created relatively regular alteration zones at a high angle (usually close to 90°) to the major direction of fluid flow (Fig. 3.12D). Postfilling fracturing was subsequently filled by a sulfide-telluride assemblage. with minor quartz and carbonates. without evident alteration effects during stage III.

3.11 LIGHT STABLE ISOTOPE GEOCHEMISTRY

3.11.1 Methodology and analytical procedures

Oxygen isotopes were determined on silicates (quartz. epidote). tungstates (scheelite) and carbonates (calcite. ankerite). carbon isotope compositions on ankerite and calcite and hydrogen isotopes on silicates (epidote and sericite) (Table 3.2). In most cases replicates were analyzed from each sample. The O isotope ratios of silicates were analyzed in the Laboratoire de Géochimie Isotopique. Université Laval. Québec. The O and C isotopes on carbonates were analyzed at the Laboratoires GÉOTOP. Université du Québec à Montréal. Hydrogen isotope analyses were carried out by Krueger Entreprises. Cambridge. United States. For O isotopes on silicates and tungstates. the standard deviation (2σ) of NBS-28 and K1 (internal standard) is 0.09 (n = 13) and 0.11 (n = 21). respectively. The standard error of each analysis is ±0.05‰ for C and O isotopic ratios of carbonates.

Table 3.2   Radiogenic ($^{87}Sr/^{86}Sr$) and stable isotope (oxygen, carbon, and hydrogen) compositions of vein-forming minerals from Omai

sch = scheelite; qz = quartz; cc = calcite; ank = ankerite; chl = chlorite; ep = epidote; ser = sericite; Au = native gold; tel = tellurides; sl = sulfides; I - first stage; II - second stage. III - third stage. Stable isotope compositions are reported in ‰. Errors for Sr isotopes are quoted as 2σ. [1] temperature data for the vein-forming minerals of each sample from Hallbauer and Voicu (1998). [2] calculated using fluid inclusion temperatures (Hallbauer and Voicu, 1998). [3] isotopic temperature; [4] data from Voicu et al. (1997b). [5] calculated using isotopic temperatures. [6] average temperature for scheelite. [7] average temperature for quartz. [8] calculated from scheelite-water equation (Wesolowski and Ohmoto, 1986). [9] calculated from quartz-water equation (Clayton et al., 1972). [10] calculated from dolomite-water equation (Matthews and Katz, 1977). [11] calculated from calcite-water equation (O'Neil et al., 1969). [12] calculated from the estimated epidote curve of Bowers and Taylor (1985). [13] calculated from the estimated muscovite curve of Bowers and Taylor (1985).

Sr isotope ratios of scheelites from this study and from Voicu et al. (1997a) are also shown in Table 3.2. Sr isotope compositions were measured at the Laboratories GÉOTOP on a VG-Sector 54 multicollector mass spectrometer. using single Re filaments. Rb contents were not measured. but extremely low Rb/Sr ratios previously reported for scheelites (<0.001. Bell et al.. 1989: Mueller et al.. 1991) implies that correction for Rb decay is probably unnecessary. Sr isotope ratios were normalized to $^{86}Sr/^{88}Sr$ = 0.1194. The values of NBS-987 $SrCO_3$ standard for the laboratory was 0.710266 (2σ = 0.000035. n = 30).

3.11.2 Results

Silicate $\delta^{18}O$ isotopes

Oxygen isotope analyses were carried out on 18 silicate (quartz. epidote) samples from the hydrothermal veins from Fennell and Wenot pits (Fig. 3.13A). Values of $\delta^{18}O$ for both quartz generations (smokey and milky) show little variation. ranging between 13.2 and 14‰ (mean = 13.6±0.4‰). There is no significant difference between the $\delta^{18}O$ values of quartz from the six vein sets. or between quartz from the Fennell and Wenot zones. Epidote $\delta^{18}O$ values range from 7.7 at Fennell to 9.6‰ at Wenot.

Scheelite $\delta^{18}O$ isotopes

Seven scheelite samples were analyzed for oxygen isotopes. Values of $\delta^{18}O$ show a very narrow range. between 3.8 and 4.3‰ (mean 4±0.2‰). The narrow range in $\delta^{18}O$ and $^{87}Sr/^{86}Sr$ (0.7020-0.7021) values suggest both consistent temperature and isotopic composition of the hydrothermal solutions during scheelite deposition.
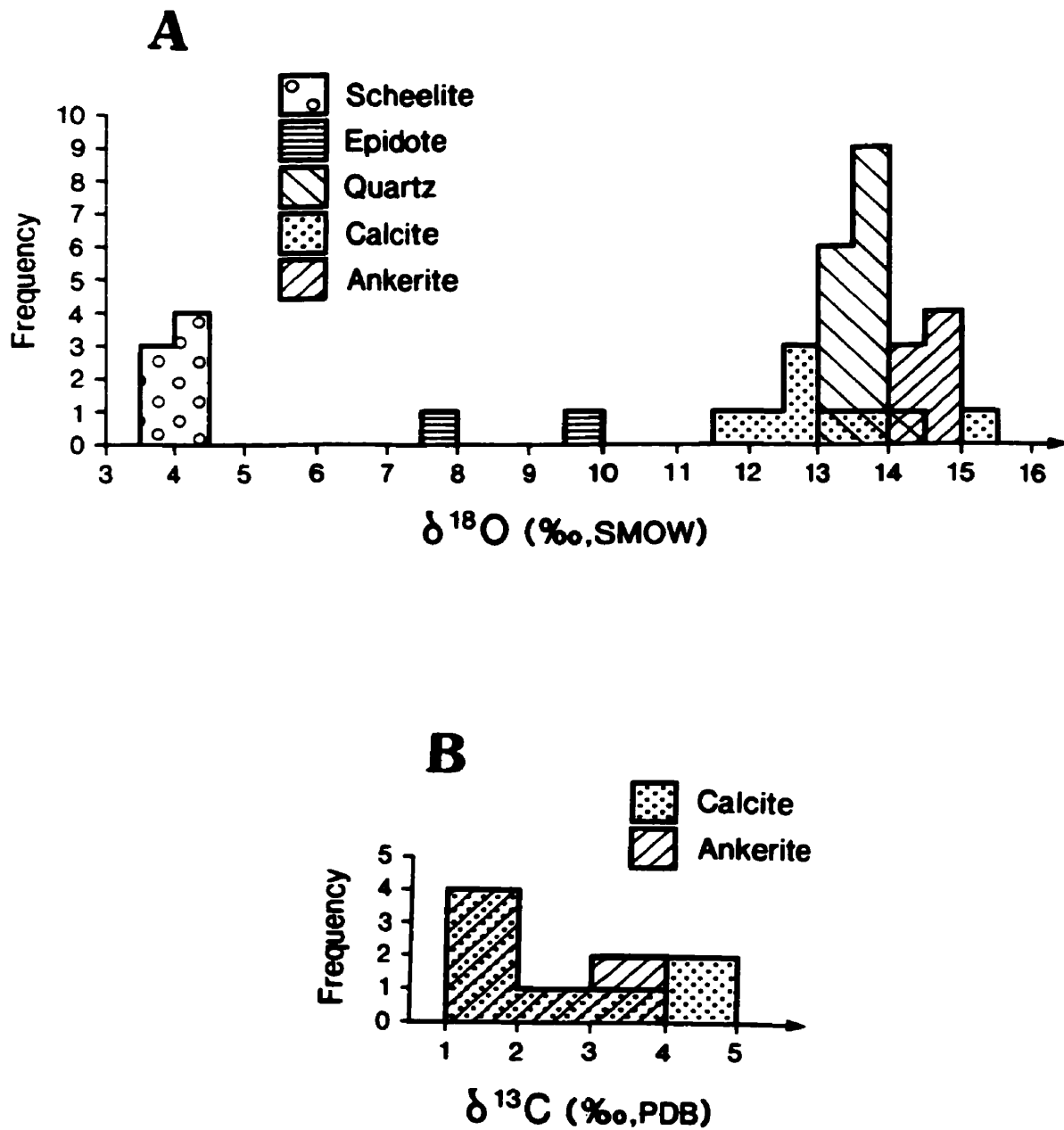
Figure 3.13   Histograms of stable isotope compositions of various vein-forming minerals of the Omai deposit: oxygen (A) and carbon (B) isotope data.

Carbonate δ¹⁸O and δ¹³C isotopes

Oxygen isotope compositions of vein-forming carbonates cluster tightly at $\delta^{18}O$ = +13.8 ± 1.4‰ for calcite and +14.4 ± 0.4‰ for ankerite. The general $\delta^{18}O$ average for Omai hydrothermal carbonates is +13.7 ± 0.8‰, which is similar to the $\delta^{18}O$ mean for quartz. Hydrothermal calcite and ankerite from the gold-bearing veins have $\delta^{13}C$ values between -1.3 and +4.7‰ (mean = +2.2‰), and +1.6 to +3.7‰ (mean = +2.3‰), respectively (Fig. 3.13B). The average $\delta^{13}C$ of carbonates is +2.2 ± 1‰. Generally, the O and C isotope variation in the analyzed samples is narrower for ankerite compared to calcite. Similar $\delta^{13}C$ and $\delta^{18}O$ results (+1.3 to +3.8‰ and +12.2‰ to +14.5‰, respectively) have been obtained for the Omai hydrothermal carbonates by Elliott (1992). However, Elliott (1992) also reported $\delta^{13}C$ values obtained from fluid inclusions in vein-quartz, which range from -13.2 to +0.6‰.

Epidote and sericite δD isotopes

Four epidote and one sericite sample were analyzed for the hydrogen isotope composition. The δD values for epidote range from -4 and -30‰, whereas the δD value for sericite is -57‰.

3.11.3 Isotopic temperatures

The rather constant isotopic fractionation values between quartz-scheelite (Δ = 9.3-10.0), quartz-calcite (Δ = 0.3-1.1), and ankerite-quartz (Δ = 0.05-1.2) suggest that isotopic equilibrium was probably attained. For the quartz-epidote pair (Δ = 3.8-5.8) the fractionation range is too large to consider that the fluids responsible for their deposition were in isotopic equilibrum. The fractionation values between quartz and carbonates are

small. and the isotopic temperatures between these mineral pairs have not been calculated. due to the uncertainties related to experimental errors. Absolute temperatures for quartz-scheelite were calculated by combining the scheelite-water fractionation equation of Wesolowski and Ohmoto (1986) and the quartz-water equation of Clayton et al. (1972). The following quartz-scheelite equation is obtained (Shieh and Zhang. 1991):

$$1000 \ln \alpha_{quartz-scheelite} = 2.47 + 1.99 \times 10^6/T^2$$

where temperature (T) is in Kelvin units. At Omai. the temperatures calculated from the $\Delta^{18}O_{quartz-scheelite}$ values range from 241 °C (for Δ = 10) to 266 °C (for Δ = 9.3). with a mean of 257 ± 7 °C. These values are higher by an average of 70 °C than those obtained by Hallbauer and Voicu (1998) using the Na-Ca-K geothermometer of Fournier and Truesdell (1973) on cations analyzed from fluid inclusions in quartz and scheelite by means of the crush/leach technique and capillary electrophoresis (Hallbauer. 1994) (see Appendix 1). The difference of temperatures between the two methods could be explained by the high concentration of Ca^{2+} in fluid inclusions due to common association between scheelite and carbonates.

By combining scheelite-water (Wesolowski and Ohmoto. 1986) and calcite-water (O'Neil et al.. 1969) equations. the following calcite-scheelite fractionation equation is obtained:

$$1000 \ln \alpha_{calcite-scheelite} = 2.48 + 1.39 \times 10^6/T^2$$

The three analyzed samples containing this mineral pair have Δ = 8.53 to 10.64. which would yield temperatures between 187 and 209 °C. $\Delta_{ankerite-scheelite}$ = 10.05 yields

a temperature of 183 °C (using the isotopic fractionation equation of Matthews and Katz. 1977). The isotopic temperatures for carbonates are in agreement with those obtained by Hallbauer and Voicu (1998) (see Appendix 1).

3.11.4 $\delta^{18}O$, δD, and $\delta^{13}C$ values of hydrothermal fluids

The $\delta^{18}O$ values of fluids responsible for the precipitation of the analyzed mineral phases in the Omai veins have been calculated from quartz. scheelite. carbonate and epidote data. using the range of temperatures calculated from the fractionation equations of these minerals and Fournier's geothermometer (Hallbauer and Voicu. 1998). Elliott (1992) recorded an average homogenization temperature in primary inclusions from vein-forming quartz of 207°C. which is closer to the temperatures obtained by Fournier's geothermometer than the calculated isotopic temperatures. A summary of the temperature data of the Omai deposit is shown in Table 3.3.

The $\delta^{18}O$ values of the mineralizing fluids range from +5.6 to -2.7‰ (mean = +2.0±2‰). Fluids responsible for scheelite deposition have $\delta^{18}O$ values between +5.3 and +3.2‰ (using isotopic temperatures) or between +4.1 and +1.4‰ (using temperature data from Hallbauer and Voicu. 1998). Fluids responsible for quartz and carbonate precipitation have $\delta^{18}O$ values between +5.3 and -2.7‰ and +5.3 and +1‰. respectively. $\delta^{18}O_{fluid}$ calculated for epidote varies between +5.6 and +3.2‰.

The δD_{fluid} was calculated using the estimated curves for epidote and muscovite at temperatures less than 220°C (Bowers and Taylor. 1985). The hydrothermal solutions responsible for precipitation of these two vein-forming minerals have δD values between -52‰ and +18‰.

Table 3.3   Temperature values of the vein-forming minerals at Omai

Mineral	Temperature (°C) Stage I	Temperature (°C) Stage II	Temperature (°C) Stage III
Scheelite	257±8[1]. n=7: 180±45[2]. n=7		
Quartz	257±8[1]. n=7: 175±22[2]. n=6: 215-300[3]	168±20[2]. n=13: 195-205[3]	170-185[3]
Epidote	225±11[2]. n=4		
Ankerite		195±7[1]. n=6: 178±5[2]. n=4	
Calcite		198±10[1]. n=5: 190±13[2]. n=3	
Albite	213[2]. n=1		
Pyrite	243±8[2]. n=3	197±19[2]. n=2	
Galena			177[2]. n=1
Chalcopyrite		201±2[2]. n=2	
Native gold		198[2]. n=1	166[2]. n=1
Average T C	225±25	192±8	172±5

n = number of samples: standard errors quoted as 2σ: [1] isotopic temperatures calculated by combining oxygen isotope fractionation equations between scheelite-water (Wesolowski and Ohmoto. 1986). quartz-water (Clayton et al.. 1972). and calcite-water (O'Neil et al.. 1969): [2] calculated using Na-K-Ca geothermometer of Fournier and Truesdell (1973) (data from Hallbauer and Voicu. 1998): [3] homogenisation temperatures of the primary fluid inclusions (Elliott 1992)

Assuming the hydrothermal fluids were in equilibrium with the average ankerite and calcite compositions (Bottinga, 1969), the calculated $\delta^{13}C_{CO_2}$ is $+1.5 \pm 1.2‰$.

3.11.5 Interpretation of oxygen, hydrogen and carbon isotope results

Fig. 3.14 shows the distribution of calculated fluid compositions on a $\delta^{18}O$ vs δD diagram. The calculated values for δD and $\delta^{18}O$ plot outside both metamorphic and magmatic water boxes. The combination of both depleted $\delta^{18}O$ and enriched δD is consistent with an influx of surface-water. The $\delta^{18}O$ data show a pronounced shift, varying from values closer to metamorphic waters for the early fluids (stage I) to values showing $\delta^{18}O$ depletion. For comparison purposes, data from several types of orogenic gold deposits are also shown. The calculated isotopic composition of hydrothermal fluids from Omai are different from the typical Archean and Paleoproterozoic mesozonal orogenic gold deposits. The variation range of $\delta^{18}O$ data is comparable to those of epithermal deposits, but at Omai δD values are higher. $\delta^{18}O$ and δD data of the Omai fluids are similar to the isotopic characteristics of Archean shallow-level gold deposits in Western Australia.

The carbonate $\delta^{18}O$ vs $\delta^{13}C$ diagram (Fig. 3.15) suggests that Omai carbonates have a similar isotopic composition to 2.0 Ga old limestones and marbles, characterized by heavy carbon compositions (Baker and Fallick, 1989; Melezhik et al., 1997). Such heavy carbon isotope compositions, when compared to other Precambrian gold deposits, associated with depleted $\delta^{18}O$ and enriched δD values of Omai ore-bearing fluids may result from a gradual addition of seawater or meteoric water to the mineralizing fluids. As Omai carbonates have $\delta^{13}C$ compositions enriched compared to seawater, the
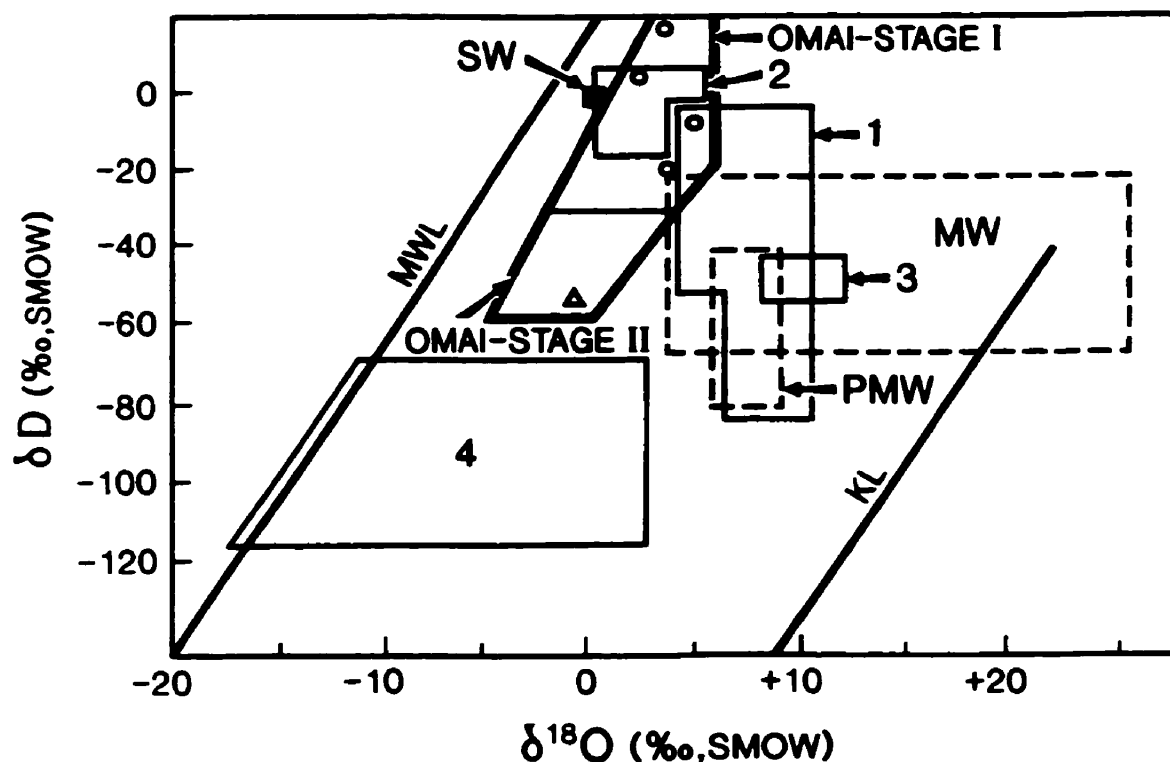
Figure 3.14   Hydrogen versus oxygen isotope diagram comparing stable isotope systematics of hydrothermal fluids from the Omai gold mine to those of other gold deposits. Triangle = sericite (calculated using the estimated muscovite curve of Bowers and Taylor, 1985); Circles = epidote (calculated using the estimated epidote curve of Bowers and Taylor, 1985); Seawater (SW), primary magmatic water (PMW), and metamorphic water (MW) from Taylor (1977); MWL = meteoric water line; KL = kaolinite line (from Rye, 1993); 1 = Archean mesozonal gold deposits; 2 = Archean shallow-level gold deposits; 3 = Paleoproterozoic mesozonal Ashanti (West African Craton) gold deposit; 4 = Tertiary epithermal gold deposits, mainly from Western United States and Korean Peninsula. Data from Shelton et al. (1990), deRonde et al. (1992), Rye (1993), Hagemann et al. (1994), Kerrich and Cassidy (1994), McCuaig and Kerrich (1994), and Oberthür et al. (1996).
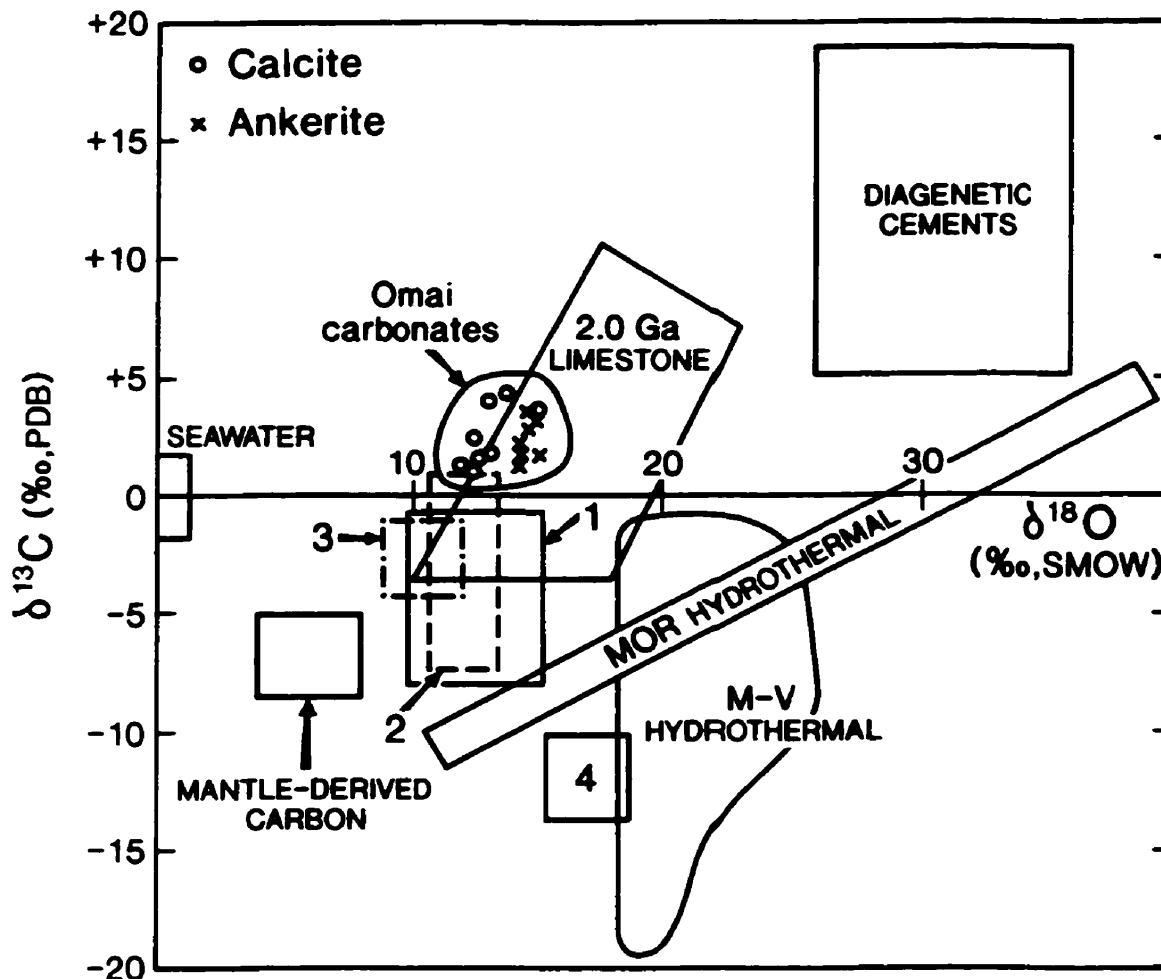
Figure 3.15   Carbon versus oxygen isotope diagram showing the isotopic composition of the Omai carbonates relative to carbonates of different origins and vein-forming carbonates of other Precambrian gold deposits. Abbreviations: MOR = mid-ocean ridge: M-V = Mississippi Valley-type deposits (data from Rollinson. 1993). Precambrian gold deposits: 1 - Abitibi Subprovince: 2 - Yilgarn Craton: 3 - Yilgarn Craton. shallow-level deposits: 4 - West African Craton (data from Colvine et al.. 1988: Golding et al.. 1989: Gebre-Mariam et al.. 1993. 1995: McCuaig and Kerrich. 1994: Oberthür et al.. 1996).

hydrothermal fluids may have leached heavy carbon isotopes from 2.0 Ga carbonate-bearing metasediments or seafloor altered metavolcanic rocks.

3.12 SOURCE OF THE MINERALIZING FLUIDS

3.12.1 Scheelite $\delta^{18}O$ - $^{87}Sr/^{86}Sr$ correlation diagram

Correlations between stable and radiogenic isotopes are of particular importance because they come about through totally different mechanisms (Rollinson. 1993). In hydrothermal systems. oxygen isotopes measure the changes (temperature. mixing. and water/rock ratios) in the fluid. whereas strontium isotopes generally monitor processes that affect the dissolved constituents (Norman and Landis. 1983). Scheelite does not incorporate Rb into its lattice and thus preserves its initial $^{87}Sr/^{86}Sr$ ratios at the time of formation (Mueller et al.. 1991: Kent et al.. 1995: Anglin et al.. 1996: Voicu et al.. 1997b). Using the initial strontium composition of scheelite as a measure of the isotopic composition of the mineralizing fluid allows direct comparison with the stable isotopes.

The $\delta^{18}O_{fluid}$ during scheelite deposition was calculated using the scheelite-water fractionation equation (Wesolowski and Ohmoto. 1986). The $\delta^{18}O$ vs $^{87}Sr/^{86}Sr$ diagram (Fig. 3.16) can be used to delineate magmatic. meteoric. seawater. and mantle-derived waters. The seawater box was defined using the variation of Sr through time relative to Bulk Earth (Rollinson. 1993). The box for the 2.0 Ga limestones was located using the $\delta^{18}O$ values from Melezhik et al. (1997). The mantle-derived water box was located using the $\delta^{18}O$ mean value of 6‰. constant through time for the Earth (Taylor. 1980: Rollinson. 1993). and the $^{87}Sr/^{86}Sr$ composition of the mantle array as defined by Zindler and Hart (1986). Meteoric and magmatic water boxes are less constrained. due to the small number of available Sr isotope analyses for the Guiana Shield.
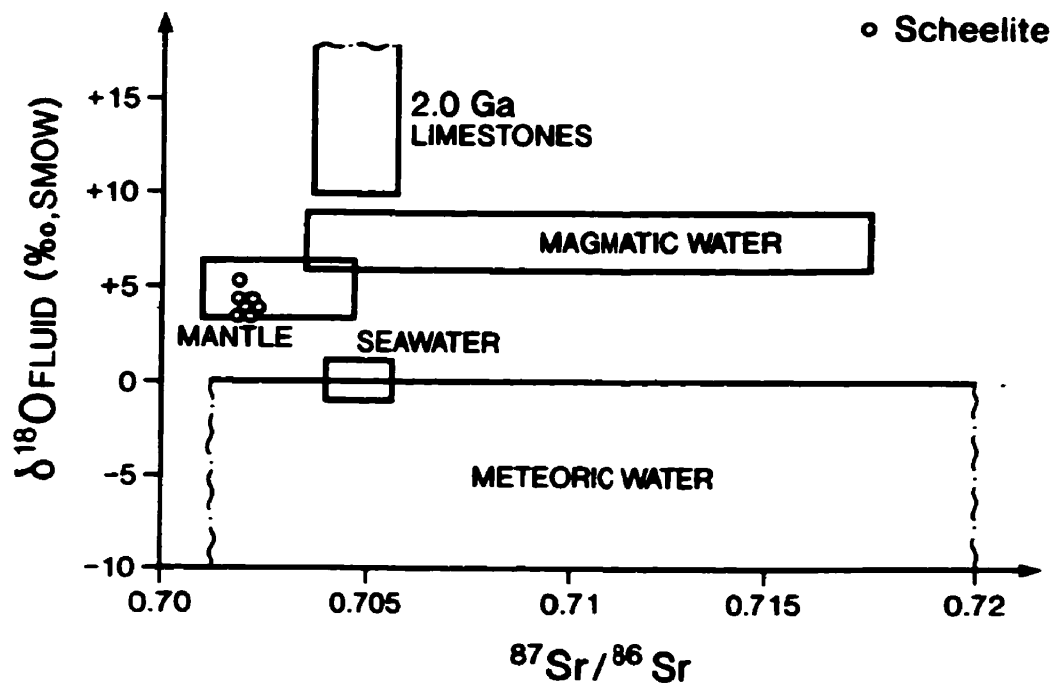
Figure 3.16   Correlation diagram between radiogenic ($^{87}Sr/^{86}Sr$) and stable ($\delta^{18}O$) isopic compositions of scheelite-bearing hydrothermal fluid from the Omai deposit. See text for discussion of data sources.

Meteoric waters probably would have circulated through Paleoproterozoic igneous and sedimentary rocks, which have a large $^{87}Sr/^{86}Sr$ variation range (e.g. 0.7007-0.7015 for Guyana limestones, Gibbs et al., 1986; 0.7015-0.7025 for mafic/ultramafic metavolcanic rocks, Gibbs and Barron, 1993; 0.7042-0.7744 for the gneissic rocks in French Guiana, Gruau et al., 1985). The $\delta^{18}O$ values for the meteoric water were considered at low latitudes (based on paleomagnetic evidence from northern South America and western Africa for the 2.1-1.5 Ga period; Onstott et al., 1984; Caen-Vachette, 1988), generally varying between 0 and -10‰. The magmatic box was defined using the values of Taylor (1977) for O isotopes and the $^{87}Sr/^{86}Sr$ values determined for several granitoid intrusions in Guyana and French Guiana (Snelling and McConnell, 1969; Teixeira et al., 1989; Gibbs and Barron, 1993).

The interpretation of the Sr isotope data alone is ambiguous, due to fact that radiogenic isotope values can be derived by flow path rock leaching. The low $^{87}Sr/^{86}Sr$ ratios of the Omai scheelites are similar to those of the Barama-Mazaruni basalts (Gibbs and Barron, 1993). Therefore, the narrow range of non-radiogenic Sr isotopes of the scheelites could reflect equilibration with the local tholeiitic basalts. On the other hand, if the Pb-Pb (Norcross et al., 1998), Sm-Nd and Sr isotopic systems have not been reset by late tectonic events and the vein-forming ages reflect a real post-peak metamorphic emplacement, other deep-seated (magmatic or metamorphic) or surface (seawater or meteoric water) regional sources are needed to explain the Sr values. Plotting Sr isotopes vs $\delta^{18}O$ data help establish the nature of this source, because oxygen isotopes are little affected by rock-fluid interaction in fluid-dominated systems. The correlation diagram suggests that the fluids responsible for scheelite deposition were possibly derived from mantle or deep crustal parts of the greenstone sequence. However, mixing of these deep-seated fluids with seawater (= meteoric water) cannot be ruled out. Lack of reliable Sr

data from the plutonic bodies occurring near Omai does not allow an estimate of the presence of a magmatic component in the mineralizing fluids.

3.12.2 The source of carbon

The possible reservoirs for carbon have distinct isotopic values: 1) seawater and marine carbonates range between -1 and +2‰ (Rollinson. 1993). but values as high as ~12.9‰ have been reported from several 2.0 Ga old limestones and marbles of different regions (Baker and Fallick. 1989: Veizer et al.. 1992: Melezhik et al.. 1997): 2) sedimentary organic carbon and reduced carbon in metamorphic rocks is strongly depleted in $\delta^{13}C$. with a mean value of ~ -25‰ (Hoefs. 1989): 3) magmatic carbon. with an average value of -3‰ (Burrows et al.. 1986: Colvine et al.. 1988): and 4) mantle-derived carbon. with an average value of -6‰ (Rollinson. 1993).

Carbonates associated with Archean gold deposits range from +2 to -9‰ (mean of ~ -4‰: e.g. Burrows et al.. 1986: Groves et al.. 1988: Nisbet and Kyser. 1988: Golding et al.. 1989: de Ronde et al.. 1992). In the Paleoproterozoic Ashanti gold belt. the hydrothermal carbonates have an average value of -14‰ (Oberthür et al.. 1996). whereas the Loulo gold deposit in Mali yielded values ranging between -13.5 and -4.5‰ (Fouillac et al.. 1993). This range in carbon isotopes has been interpreted either as reflecting a magmatic origin of the carbonate-bearing mineralizing fluids (e.g. Burrows et al.. 1986). or as the result of the metamorphic dissolution of mantle-related CO_2 along crustal-scale fault systems (e.g Groves et al.. 1988: Golding et al.. 1989: Oberthür et al.. 1996).

At Omai. carbon isotopes of hydrothermal carbonates show a variation range (+1.3 to +4.7‰) that is different from reported values of typical Precambrian orogenic gold deposits. On the other hand. a huge disparity exists at Omai between $\delta^{13}C$ values

in carbonates and those analyzed in fluid inclusions in quartz (between -13 and +0.5‰: Elliott. 1992). The $\delta^{13}C$ values of fluids under the normal conditions of the hydrothermal systems should closely approximate the $\delta^{13}C$ values of carbonates in equilibrium with the fluid (Ohmoto. 1986). The possibility that fluids responsible for carbonate and quartz deposition were not coeval is not supported by the textural aspects of the veins.

Heavy carbon isotope compositions of carbonates at Omai can result from fluid-rock interaction between hydrothermal fluids and seafloor-altered metabasalts or limestones of the surrounding greenstone sequence. However, this interpretation cannot explain carbon isotope values as high as +4.7‰. considering a maximum value of --1‰ for marine carbonates in altered mafic volcanic rocks (Kerrich. 1990) and +2‰ for seawater. A possible explanation is given by Burrows et al. (1986) and Wood et al. (1986), who consider that seawater-derived carbonates would lead to an enrichment in $\delta^{13}C$ by 3-5‰ with respect to their starting isotopic composition. due to decarbonatization during lower greenschist grade metamorphism. Thus. within greenstone belt sequences. the seawater-derived $\delta^{13}C$ isotopes would vary between +3 and +7‰. Another explanation could be related to the heavy carbon isotopic composition (average of +6‰) of 2.0 Ga old limestones (Baker and Fallick. 1989: Veizer et al.. 1992: Melezhik et al.. 1997). which seems to be a worldwide excursion in the carbon isotope composition at this time. The dissolution of marine carbonates would have yielded CO_2 gas having $\delta^{13}C$ values comparable to those of the protolith (an average $\delta^{13}C$ ratio of +6‰). However. the small volume of Paleoproterozoic limestones identified to date in Guyana reduces the likelihood of generating large volumes of CO_2-bearing fluids. even though extensive limestone units occur in the time-equivalent sequences of the Birimian greenstone belt of West Africa (Leube et al.. 1990: Milési et al.. 1992).

The disparity of the $\delta^{13}C$ values between carbonates and fluid inclusions in quartz can be explained by the gradual contamination of deep-seated fluids of metamorphic or magmatic origin (as indicated by radiogenic isotopes) by seawater-derived fluids. Mixing between deep-seated fluids with negative $\delta^{13}C$ values and surface-derived fluids which have leached heavy carbon isotopes from seafloor metavolcanic rocks or 2.0 Ga old limestones is reflected by the gradual decrease of temperature of the ore-bearing fluids. As temperature is the most important factor affecting the isotopic fractionation. the wide variation of $\delta^{13}C_{fluid}$ (-13 to +3.3‰) and $\delta^{18}O_{fluid}$ (-2.7 to +5.3‰) reflects in fact the gradual change of both chemical and physical parameters of the hydrothermal solutions.

3.13 GENETIC MODEL FOR THE GOLD MINERALIZATION

The Omai deposit represents a typical example of granitoid- (Fennell pit) and greenstone-hosted (Wenot pit) orogenic gold deposit.

The genetic model for the Omai deposit must integrate several geological constraints including: 1) the close spatial relationship between gold mineralization and felsic-intermediate intrusive/subvolcanic rocks. as well as the presence of gold-bearing veins in the basalt/andesite and pelite sequences: 2) low grade metamorphism of the country rocks: 2) several gold-bearing vein sets. characterized by crack-seal. breccia. and fracture-filling textures: 3) syn- to late-tectonic mineralization controlled by shallow crustal brittle to brittle-ductile structures: 4) mineralization spatially hosted within a regional structural break (Makapa-Kuribrong shear zone). but. at a local scale. associated with subsidiary rather than major structures: 5) a complex vein mineralogy precipitated during several hydrothermal pulses. and characterized by a paragenesis characteristic of

both orogenic and epithermal gold deposits: 6) a possible deeply-seated source of the fluids. which have interacted with local mafic volcanic rocks and surface-derived waters.

The mixing of two different fluid sources. one of mantle and/or lower crustal origin and the second surface-derived. imply that Omai is not a typical epithermal (i.e. formed by deep circulation of surface waters principally) nor a typical mesozonal orogenic deposit (i.e formed by advection of mantle/magmatic/metamorphic fluids principally). These overlapping features of the Omai deposit match conditions of the shallow crustal level of the continuum model proposed by Groves (1993) for Archean orogenic deposits. This type of gold deposit has been classified as orogenic epizonal (Gebre-Mariam et al.. 1995; Groves et al.. 1998).

The exact source of the deep-seated fluids at Omai remains uncertain because the interaction with the local mafic lavas or mixing with seawater/meteoric fluids can obscure initial radiogenic isotope compositions. The scheelite Sr vs O isotope diagram and low radiogenic Nd ratios (see Chapter IV) suggest a deep-seated origin for the early hydrothermal fluids. formed either by degassing or by exsolution from mantle-derived silicate magmas (cf. Colvine et al.. 1988). Therefore. as in most Archean deposits (Barley and Groves. 1990). the deeply seated ore solution is best considered as the result of a crustal-scale fluid and heat flux. derived both from the upper mantle and different levels in the crustal profile.

The stable isotope composition of the Omai ore fluid plots outside both metamorphic and magmatic water boxes which. however. does not preclude a possible metamorphic/magmatic origin of the fluids. Granulitization of the lower crust seems to be an unlikely mechanism for the generation of CO_2. since the greenstone terranes of Guyana (and generally most of the Guiana Shield) are underlain by juvenile crust (Gruau et al.. 1985; Voicu et al.. 1997a). Phillips and Powell (1993) have emphasized the

importance of hydrothermal fluids of metamorphic origin in transporting Au. They suggested that the fluids resulted from dehydration of mafic or sedimentary rocks during greenschist to amphibolite facies metamorphism.This observation agrees with the fact that regions hosting epizonal gold deposits lack previously metamorphosed cratonic crust and include thick mafic sequences and interlayered greywackes (Mitchell. 1996). However. the inferred age of mineralization at Omai is younger than the greenstone belt deposition. peak-metamorphism. and the granitoid emplacement. The best explanation is related to a late lower/middle crustal metamorphic event related to the continuation at depth of the Trans-Amazonian orogeny. There are only scarce data at Omai to prove the existence of a late deeper crustal metamorphism or a temporal relationship with gold emplacement. but such a tectono-magmatic evolution of the Guiana Shield could be envisaged. The span of time between the regional peak of metamorphism and gold mineralization at Omai can thus be explained by late thermal events related to episodic magmatic underplating of the lower crust.

On the other hand. the presence of W. Te. Mo. and Bi. associated with low concentrations of Cu-Zn-Pb. is consistent with a granitoid influence. However. orthomagmatic models invoke that ore fluids are typically saline. and result in metal zonation (Cassidy et al.. 1998). features which have not been recorded at Omai. Furthermore. the span of time between deposition of supracrustal rocks. crystallization of the Omai stock and mineralization indicates that gold is not related to the emplacement of the Omai stock. It is difficult to consider that the Sm-Nd and Pb-Pb systems have been reset in undeformed veins emplaced after the regional metamorphism/deformation and which have no major feature showing ductile fabric. A magmatic origin of the mineralizing fluids cannot explain the similar mineral assemblage (except tellurides) in veins from both Omai stock and volcano-sedimentary rocks from Wenot pit.

Although the host Omai stock is not the preferred source of the ore fluids. it cannot be ruled out the possible influence of the syn-mineralization emplacement of the Tigri granodiorite. located at ~6 km SW of Omai. which could have acted as a heat source needed to generate fluid movement.

In summary. it is suggested that the steeply dipping Makapa-Kuribrong shear zone has tapped deep-seated hydrothermal fluids which advected towards shallow crustal levels. Mixing between these fluids and downward circulating. cooler seawater/meteoric water. together with chemical interaction with wallrocks resulted in gold deposition in subsidiary brittle shear zones. chiefly within the Omai stock and brittle felsic dikes. The predominant occurrence of ore-bearing veins within felsic intrusive/subvolcanic rock types is related to the competency contrasts with surrounding volcano-sedimentary rocks. Only the thick gold-bearing veins. created by large fluid volumes were able to cut through lithological contacts. whereas thinner veins were emplaced in brittle felsic bodies forming vein swarms and stockworks.

3.14 COMPARISON WITH OTHER PRECAMBRIAN GOLD DEPOSITS

The features of the Omai deposit are compared to Precambrian gold deposits in Table 3.4. A small number of Late Archean deposits are hosted within epizonal. shallow-level. or low metamorphic grade terranes (Tremlow. 1984: Colvine et al.. 1988: Gebre-Mariam et al.. 1993: Hagemann et al.. 1994: McCuaig and Kerrich. 1994). These deposits have transitional features between epi- and mesothermal gold mineralization. They are located in prehnite-pumpellyite to lower greenschist volcanic and intrusive metamorphic rocks. within major regional breaks. although their late-orogenic emplacement was controlled chiefly by subsidiary brittle±ductile shear zones. Ore paragenesis is more similar to that of epithermal deposits. whereas vein-forming gangue minerals and alteration patterns are typical of mesothermal deposits. The ore-bearing

Table 3.4   Geological characteristics of the Omai deposit compared with other Paleoproterozoic and Late-Archean gold deposits

	Omai deposit	Late-Archean shallow-level	Late-Archean mesothermal	Paleoproterozoic
Examples	1, 2, 3, and this study	Wiluna, Racetrack, Commoner, Shamva	Sigma, Camflo, Kerr Addison, Mt Charlotte, Golden Mile, Victory	Ashanti, Loulo, Hiré, Poura, Loulonic, Adieu-Vat
References	1, 2, 3, and this study	4, 5, 6, 7	8, 9, 10, 11, 12, 13	14, 15, 16
Associated rocks	Granitoid, quartz porphyries, rhyolites, andesites, basalts. Metasedimentary rocks	Basalts, komatiites, dolerites	Granitoids, quartz porphyries, various volcanic and metasedimentary rocks	Granitoids, various volcanic and metasedimentary rocks
Metamorphic grade of host rocks	Prehnite-pumpellyite to lower greenschist	Prehnite-pumpellyite to lower greenschist	Greenschist to lower amphibolite	Lower greenschist, prehnite-pumpellyite
Structural setting	Brittle shear zones	Brittle-(ductile) shear zones	Ductile-brittle shear zones	Brittle-(ductile) shear zones
Structural timing of mineralization	Late-orogenic	Late-orogenic	Late-orogenic	Late-orogenic
Age of host lithologies	2.10 - 2.12 Ga	2.69 to 2.70 Ga	2.69 to 2.66 Ga (Yilgarn), 2.69-2.67 Ga (Abitibi)	2.18 to 2.17 Ga, 2.11 to 2.08 Ga
Age of mineralization	1.99 Ga	2.62 Ga	2.65 to 2.60 Ga (Yilgarn); 2.63 to 2.40 Ga (Abitibi)	2.08-1.95 Ga
Major ore and gangue minerals	Pyrite, galena, chalcopyrite, sphalerite, tellurides, molybdenite. Pyrrhotite, quartz, carbonate, scheelite. K-mica, chlorite	Pyrite, arsenopyrite, stibnite, galena, arsenopyrite, chalcopyrite, sphalerite, tetrahedrite, cassiterite, albite, carbonate. K-mica, chlorite	Pyrite, arsenopyrite, pyrrhotite, galena, sphalerite, chalcopyrite, tellurides, quartz, carbonate, scheelite, albite, tourmaline	Pyrite, arsenopyrite, chalcopyrite, galena, tellurides, quartz, carbonate, muscovite, tourmaline
Hydrothermal alteration	Fe-sulfides, K-mica, silicification, carbonation, chloritization	Fe-sulfides, K-mica, Na-feldspar, carbonation, silicification, chlorite	Fe-sulfides, K-mica, carbonation, silicification, chloritization, biotization	Fe-sulfides, K-mica, carbonation, silicification, Na-feldspar
Fluid temperature	120-260 C	150-325 C	250-400 C	120-340 C
Ore fluid characteristics	Salinity: 0-1.8 eq wt% NaCl, Mole CO_2:5%	Salinity: 3.7 eq wt% NaCl, Mole CO_2: 17%	Salinity: 0-6 eq wt%NaCl; Mole CO_2; 10-15%	Salinity: 3 eq wt%NaCl; Mole CO_2; <20%
Depth (inferred)	<5 km	<5 km	5 to 10 km	5 to 10 km
$^{87}Sr/^{86}Sr$ in scheelite	0.7019-0.7021	No data	0.7014-0.7028 (Yilgarn), 0.7015-0.7022 (Canadian Shield)	No data
$^{143}Nd/^{144}Nd$ in scheelite	0.5122 to 0.5138	No data	0.5133 to 0.5159 (Yilgarn); 0.5127 to 0.5151 (Canadian Shield)	No data
$\delta^{18}O_{fluid}$ (‰SMOW)	-2.7 to +5.6‰	-2.8 to +7.2‰	+5 to +8‰	+6 to +10‰
$\delta^{13}C_{carb}$ (‰PDB)	+1.4 to +4.6‰	-4.3 to -1.9‰	-8.5 to -2.5‰	-9 to -16‰

Principal references: 1-Bertoni et al. (1991a); 2- Elliott (1992); 3- Norcross (1997); 4- Gebre-Mariam et al. (1993); 5- Hagemann et al (1994); 6- Tremlow (1984); 7- Kerrich and Cassidy (1994); 8- Golding et al. (1989); 9- Hodgson (1990); 10- Mueller et al (1991); 11- Kent et al (1996); 12- Groves et al (1998); 13- Anglin et al (1996). 14- Milési et al (1992). 1995; 15- Fouillac et al. (1993); 16- Oberthur et al (1996).

fluids have low salinity. low CO_2 content. temperatures between $150°$ and $325°C$. and pressures of -1 kbar. The hydrothermal systems are dominated by fluids from deep crustal levels. which advected along major crustal faults into shallow-level. brittle zones. where they mixed with surface waters. Typical examples include Wiluna. Racetrack (Western Australia). Commoner. and Shamwa (Zimbabwe).

Some Paleoproterozoic gold deposits in the West African and Guiana Cratons share many characteristic features of the Omai mineralization. The comparison between Omai and these deposits includes the structural. textural. and mineralogical features. Only few data are available for stable and radiogenic isotopes in West African gold deposits (Fouillac et al.. 1993: Marcoux and Milési. 1993: Oberthür et al.. 1996).Isotopic data are missing for most Guiana Shield mineralizations. except for some Pb-Pb ages on galenas from a few French Guiana deposits (Marcoux and Milési. 1993).

Las Cristinas gold deposit in Venezuela is characterized by localized vein systems and stockworks related to intrusive rocks and more persistent gold-quartz veins that cut both granitic and volcanic rocks (Gray et al... 1993: Day et al.. 1995). The deposit is located in weakly metamorphosed rocks and controlled by brittle shear systems. The alteration envelopes comprise an inner albite-quartz-carbonate assemblage. and an outer zone of ferroan dolomite or sericite. Ore mineralogy comprises pyrite. chalcopyrite. and molybdenite. The Loulouie and Adieu-Vat gold occurrences in French Guiana are similar. but have a more complex ore paragenesis (pyrite. galena. chalcopyrite. sphalerite. pyrrhotite. molybdenite. Bi minerals. and tellurides: Milési et al.. 1995). Galena from Loulouie yielded a Pb-Pb age of 2.01 Ga.

In the Birimian greenstone belt of West Africa. similar gold deposits to Omai such as Hiré. Poura. Sabodala. and Banora. are described as late-orogenic mesothermal Au-quartz veins with rare polymetallic sulfides (Milési et al.. 1992). They formed during

the last brittle to brittle-ductile stages of the Eburnian orogeny and yielded a Pb-Pb model age of 2.0 Ga. The ore systems are located in weakly metamorphosed igneous and sedimentary rocks, within regional tectonic corridors. The mineralized bodies consist of veins, lenses or stockworks and are characterized by a Au-Cu-Pb-Zn-Ag-Bi metallic assemblage, in a predominantly quartz-carbonate gangue.

This brief comparison between Omai and other Precambrian gold deposit shows that they have common metallogenic features that are characteristic of epizonal orogenic deposits. Paleoproterozoic epizonal deposits seem to occur more frequently compared to their Archean counterparts, although the exploration conditions in West Africa and Guiana Cratons did not allow until now a more detailed description of the gold occurrences. The increased frequency of the Paleoproterozoic epizonal deposits could be explained by more favorable conditions for the preservation of the upper parts of the mineralized systems, due either to less post-mineralization tectonic activity or to thick anorogenic sedimentary sequences which covered most of the terrains containing this type of deposits. Certain Paleoproterozoic greenstone belts like Ashanti were more deeply eroded and exhibit intermediate or lower levels of the mineralized systems, but most deposits seem to be preserved at their upper mineralized levels. Thus, Paleoproterozoic greenstone terrains of the Guiana and West Africa Shields represent first order targets for epizonal orogenic gold deposits.

3.15 SUMMARY AND CONCLUSIONS

The granitoid- and greenstone-hosted Omai deposit represents a first example of a Paleoproterozoic orogenic epizonal gold deposit. Its metallogenic features are shared between classical epithermal and mesozonal orogenic deposits. Typical low-temperature features include: 1) association with brittle rather than ductile structures; 2) vein sets and stockwork-style mineralization; 3) breccia textures; 4) the local presence of open spaces

and vugs within the veins: 5) the presence of argillic alteration: and 6) the metal inventory (Au-Ag-Te-Hg-Pb-Zn-Cu). Typical features of mesozonal orogenic deposit include: 1) the presence of lode gold-type veins: 2) very low metallic/gangue mineral ratio: 3) ribbon and shear textures formed by the crack-seal growth mechanism: 4) the style of hydrothermal alteration: 5) local association with brittle=ductile structures (in the Wenot area): and 6) partially. the metal inventory (Au-W-Mo-Bi).

Crosscutting relationships. geochronological data. and the general evolution of the Omai mine shows that the mineralized veins and their host structures were formed late in the evolution of the Guyana greenstone belt. Vein emplacement post-dates the development of the volcano-sedimentary belt. the tilting of the volcanic sequence and the intrusion of porphyry/rhyolite dikes. regional low-grade metamorphism. as well as the emplacement of the unmetamorphosed Omai stock. but is probably contemporaneous with or slightly post-dates the deeper crustal metamorphism related to continuation at depth of the Trans-Amazonian orogeny. The isotope data suggest deep-seated mineralizing fluids of metamorphic or magmatic origin which interacted with the local mafic volcanic rocks and with surface-derived fluids.

Omai can be considered as a Paleoproterozoic equivalent of the Archean epizonal gold deposits described in the Yilgarn and Zimbabwe Cratons. Several Paleoproterozoic gold deposits similar to Omai have been described in Guiana and West African Cratons (Las Cristinas. Loulouie. Adieu-Vat. Hiré. Poura. Sabodala. and Banora).

The upper part of the mineralizing system at Omai is preserved. Therefore. this part of the Guiana Shield represents an excellent exploration area for orogenic epizonal gold deposits. hosted especially by felsic rocks emplaced within mafic volcano-

sedimentary sequences altogether lying within the Makapa-Kuribrong crustal scale shear zone.

3.16 REFERENCES

Anglin. C.D.. Jonasson. I.R.. and Franklin. J.M.. 1996. Sm-Nd dating of scheelite and tourmaline: Implications for the genesis of Archean gold deposits. Val d'Or. Canada. Economic Geology. v. 91. p. 1372-1392.

Baker. A.J.. and Fallick. A.E.. 1989. Evidence from the Lewisian limestones for isotopically heavy carbon in two-thousand-million-year-old sea water. Nature. v. 337. p. 352-354.

Barley. M.E.. and Groves. D.I.. 1990. Mesothermal gold mineralization in the Yilgarn Craton. Western Australia. the result of late Archean convergent tectonics?. Chronique de la recherche minière. v. 498. p. 3-13.

Beli. K.. Anglin. C.D.. and Franklin. J.M.. 1989. Sm-Nd and Rb-Sr isotope systematics of scheelites: Possible implications for the age and genesis of vein-hosted gold deposits. Geology. v. 17. p. 500-504.

Bertoni. C.H.. Shaw. R.P.. Singh. R.. Minamoto. J.. Richards. J.M.. and Belzile. E.. 1991a. Geology and gold mineralization of the Omai property. Guyana: In Brazil gold '91: The economics geology geochemistry and genesis of gold deposits. Edited by E.A. Ladeira. Balkema. Rotterdam. p. 767-773.

Bertoni. C.H.. Shaw. R.P.. Singh. R.. Belzile. E.. Minamoto. J.. Richards. J.M.. and Morgan. R.. 1991b. Geology and gold mineralization of the Omai property. Guyana. Unpublished report. 111 p.

Bottinga. Y.. 1969. Calculated fractionation factors for carbon and hydrogen exchange in the system calcite-CO_2-graphite-methane-hydrogen and water vapour. Geochimica et Cosmochimica Acta. v. 33. p. 49-64.

Bowers. T.S.. and Taylor. H.P.Jr.. 1985. An integrated chemical and stable-isotope model of the origin of mid-ocean ridge hot spring systems. Journal of Geophysical Research. v. 90. p. 12583-12606.

Burrows. D.R.. Wood. P.C.. and Spooner. E.T.C.. 1986. Carbon isotope evidence for a magmatic origin for Archean gold-quartz vein ore deposits. Nature. v. 321. p. 851-854.

Caen-Vachette. M.. 1988. Le craton ouest-africain et le bouclier guyanais: un seul craton au Protérozoïque inférieur?. Journal of African Earth Sciences. v. 7. p. 479-488.

Cassidy. K.F.. Groves. D.I.. and McNaughton. N.J.. 1998. Late-Archean granitoid-hosted lode-gold deposits. Yilgarn Craton. western Australia: Deposit characteristics. crustal architecture and implications for ore genesis. Ore Geology Reviews. v. 13. p. 65-102.

Clayton. R.N.. O'Neil. J.R.. and Mayeda. T.K.. 1972. Oxygen isotope exchange between quartz and water. Journal of Geophysical Research. v. 77. p. 3057-3067.

Colvine. A.C.. Fyon. J.A.. Heather. K.B.. Marmont. S.. Smith. P.M.. and Troop. D.G.. 1988. Archean lode gold deposits in Ontario: Ontario Geological Survey Miscellaneous Paper. v. 139. 210 p.

Cooke. D.R.. McPhail. and D.C.. Bloom. M.S.. 1996. Epithermal gold mineralization. Acupan. Baguio district. Philippines: Geology. mineralization. and the thermochemical environment of ore deposition. Economic Geology. v. 91. p. 243-272.

Day. W.C.. Tosdal. R.M.. Acosta. E.L.. Aruspon. J.C.. Carvajal. L.. Cedeño. E.. Lowry. G.. Martinez. L.F.. Noriega. J.A.. Nuñez. F.J.. Rojas. J.. and Prieto. F.. 1995. Geology of the Lo Increíble mining district and U-Pb age of the early Proterozoic Yuruari Formation of the Pastora Supergroup. Guayana Shield. Venezuela. U.S. Geological Survey Open-File-Report 2124. p. E1-E13.

Elliott. R.G.. 1992. The geology and geochemistry of the Omai goldfield. Guyana. Unpublished Ph.D. thesis. Oxford Brookes University. 230 p.

Fouillac. A.M.. Dommanget. A.. and Milési. J.P.. 1993. A carbon. oxygen. hydrogen and sulfur isotopic study of gold mineralization at Loulo. Mali. Chemical Geology. v. 106. p. 47-62.

Gebre-Mariam. M.. Groves. D.I.. McNaughton. N.J.. Mikucki. E.J.. and Vearncombe. J.R.. 1993. Archean Au-Ag mineralization at Racetrack. near Kalgoorlie. Western Australia: A high crustal-level expression of the Archean lode-gold continuum. Mineralium Deposita. v. 28. p. 375-387.

Gebre-Mariam, M., Hagemann, S.G., and Groves, D.I., 1995. A classification scheme for epigenetic Archaean lode-gold deposits. Mineralium Deposita, v. 30, p. 408-410.

Gibbs, A.K., and Olzsewski, W.J., 1982. Zircon U-Pb ages of Guiana greenstone-gneiss terrane. Precambrian Research, v. 17, p. 199-214.

Gibbs, A.K., and Barron, C.N., 1993. Geology of the Guiana Shield. Oxford Monographs on Geology and Geophysics v. 22, Oxford, Clarendon Press, 246 p.

Gibbs, A.K., Montgomery, C.W., O'Day, P.A., and Erslev, E.A., 1986. The Archean-Proterozoic transition: Evidence from the geochemistry of metasedimentary rocks of Guyana and Montana. Geochimica et Cosmochimica Acta, v. 50, p. 2125-2141.

Golding, S.D., McNaughton, N.J., Barley, M.E., Groves, D.I., Ho, S.E., Rock, N.M.S., and Turner, J.V., 1989. Archean carbon and oxygen reservoirs: Their significance for fluid sources and circulation paths for Archean mesothermal gold deposits. Economic Geology Monograph 6, p. 376-388.

Gray, F., Cox, D.P., Orris, G.J., Page, N., Wynn, J.C., Brooks, W.E., and Bliss, J.D., 1993. Mineral resource assessment of the Venezuelan Guayana Shield: Low-sulfide gold-quartz veins. In Geology and mineral resource assessment of the Venezuelan Guayana Shield. Edited by U.S. Geological Survey and Corporation Venezolana de Guayana, Técnica Minera, C.A., U.S. Geological Survey Bulletin 2062, p. 63-69.

Groves, D.I., 1993. The crustal continuum model for late-Archean lode-gold deposits of the Yilgarn Block, Western Australia. Mineralium Deposita, v. 28, p. 366-374.

Groves, D.I., and Foster, R.P., 1991. Archean lode gold deposits. In Gold Metallogeny and Exploration. Edited by R.P. Foster, Blackie, p. 63-103.

Groves, D.I., Golding, S.D., Rock, N.M.S., Barley, M.E., and McNaughton, N.J., 1988. Archean carbon reservoirs and their relevance to the fluid source for gold deposits. Nature, v. 331, p. 254-257.

Groves, D.I., Goldfarb, R.J., Gebre-Mariam, M., Hagemann, S.G., and Robert, F., 1998. Orogenic gold deposits: A proposed classification in the context of their crustal distribution and relationship to other gold deposit types. Ore Geology Reviews, v. 13, p. 7-27.

Gruau. G.. Martin. H.. Leveque. B.. and Capdevilla. R.. 1985. Rb-Sr and Sm-Nd geochronology of Lower Proterozoic granite-greenstone terrains in French Guiana. South America. Precambrian Research. v. 30. p. 63-80.

Hagemann. S.G.. Gebre-Mariam. M.. and Groves. D.I.. 1994. Surface-water influx in shallow-level Archean lode-gold deposits in Western Australia. Geology. v. 22. p. 1067-1070.

Hallbauer. D.K.. 1994. Geochemical trace element analysis for ionic species by capillary electrophoresis. Mineralogical Magazine. v. 58A (VM Goldsmidt Conference Abstracts). p. 362-363.

Hallbauer. D.K.. and Voicu. G..1998. A geochemical assessment of the hydrothermal systems at the Omai gold mine. Guyana. from the composition of fluid inclusions in ore minerals and gangue. Geocongress'98. The Geological Society of South Africa. 8-10 July 1998. Extended Abstracts. p. 213-215.

Hoefs. J.. 1987. Stable isotope geochemistry. Spriger Verlag. Berlin. 241 p.

Kent. A.J.R.. Campbell. I.H.. and McCulloch. M.T.. 1995. Sm-Nd systematics of hydrothermal scheelite from the Mount Charlotte mine. Kalgoorlie. Western Australia: An isotopic link between gold mineralization and komatiites. Economic Geology. v. 90. p. 2329-2335.

Kerrich. R.. 1990. Carbon isotope systematics of Archean Au-Ag vein deposits in the Superior Province. Canadian Journal of Earth Sciences. v. 27. p. 40-56.

Kerrich. R.. and Cassidy. K.F.. 1994. Temporal relationships of lode gold mineralization to accretion. magmatism. metamorphism and deformation - Archean to present: A review. Ore Geology Reviews. v. 9. p. 263-310.

Leube. A.. Hirdes. W.. Mauer. R.. and Kesse. G.O.. 1990. The Early Proterozoic Birimian Supergroup of Ghana and some aspects of its associated gold mineralization. Precambrian Research. v. 46. p. 139-165.

Marcoux. E.. and Milési. J.P.. 1993. Lead isotope signature in Early Proterozoic ore deposits in Western Africa: comparison with gold deposits in French Guiana. Economic Geology. v. 88. p. 1862-1879.

Matthews. A.. and Katz. A.. 1977. Oxygen isotope fractionation during the dolomitization of calcium carbonate. Geochimica et Cosmochimica Acta. v. 41. p. 1431-1438.

McCuaig. T.C.. and Kerrich. R.. 1994. P-T-t-deformation-fluid characteristics of lode gold deposits: Evidence from alteration systematics: *In* Alteration and alteration processes associated with ore-forming systems. *Edited by* D.R. Lentz. Geological Association of Canada. Short Course Notes. v. 11. p. 339-379.

Macdonald. J.R.. 1968. A guide to mineral exploration in Guyana. Geological Survey of Guyana. Bulletin 38. Georgetown. 91 p.

Melezhik. V.A.. Fallick. A.E.. and Clark. T.. 1997. Two billion year old isotopically heavy carbon: evidence from the Labrador Trough. Canada. Canadian Journal of Earth Sciences. v. 34. p. 271-285.

Milési. J-P.. Ledru. P.. Feybesse. J-L.. Dommanget. A.. and Marcoux. E.. 1992. Early Proterozoic ore deposits and tectonics of the Birimian orogenic belt. West Africa. Precambrian Research. v. 58. p. 305-344.

Milési. J-P.. Egal. E.. Ledru. P.. Vernhet. Y.. Thiéblemont. D.. Cocherie. A.. Tegyey. M.. Martel-Jantin. B.. and Lagny. P.. 1995. Les minéralisations du Nord de la Guyane française dans leur cadre géologique: Chronique de la recherche minière. v. 518. p. 5-58.

Mitchell. A.H.G.. 1996. Distribution and genesis of some epizonal Zn-Pb and Au provinces in the Carpathian-Balkan region. Trans. Instn. Min. Metall. (Sect. B: Appl. earth sci.). v. 105. p. B127-B138.

Mueller. A.G.. de Laeter. J.R.. and Groves. D.I.. 1991. Strontium isotope systematics of hydrothermal minerals from epigenetic Archean gold deposits in the Yilgarn block. Western Australia. Economic Geology. v. 86. p. 780-809.

Nisbet. E.G.. and Kyser. T.K.. 1988. Archean carbon and gold. Nature. v. 331. p. 210-211.

Norcross. C.. 1997. U-Pb geochronology of the Omai intrusion-hosted Au-quartz vein deposit and host rocks. Guiana Shield. South America. Unpublished M.Sc. thesis. University of Toronto. 65 p.

Norcross. C.E.. Davis. D.W.. and Spooner. E.T.C.. 1998. U-Pb geochronology of the Omai intrusion-hosted Au-quartz vein deposit and host rocks. Guyana. South America : GSA Annual Meeting. Oct. 26-29. 1998. Toronto. Abstracts with Programs. p. A-127.

Norman. D.I.. and Landis. G.P.. 1983. Source of mineralizing components in hydrothermal ore fluids as evidenced by $^{87}Sr/^{86}Sr$ and stable isotope data from the Pasto Bueno deposit. Peru. Economic Geology. v. 78. p. 451-465.

Oberthür. T.. Schmidt Mumm. A.. Vetter. U.. Simon. K.. and Amanor. J.A.. 1996. Gold mineralization in the Ashanti belt of Ghana: Genetic constraints of the stable isotope geochemistry. Economic Geology. v. 91. p. 289-301.

Ohmoto. H.. 1986. Stable isotope geochemistry of ore deposits. *In* Stable Isotopes in High Temperatures Processes. *Edited by* J.W. Valley. H.P.Jr. Taylor and J.R. O'Neil. Mineralogical Society of America. Reviews in Mineralogy. v. 16. p. 1-40.

O'Neil. J.R.. Clayton. R.N.. and Mayeda. T.K.. 1969. Oxygen isotope fractionation in divalent metal carbonates. Journal of Chemical Physics. v. 51. p. 5547-5558.

Onstott. T.C.. Hargraves. R.B.. York. D.. and Hall. C.. 1984. Constraints on the motions of South American and African shields during Proterozoic: I. $^{40}Ar/^{39}Ar$ and paleomagnetic correlations between Venezuela and Liberia. Geol. Soc. Am. Bull.. v. 95. p. 1045-1054.

Phillips. G.N.. and Powell. R.. 1993. Link between gold provinces. Economic Geology. v. 88. p. 1084-1098.

Rollinson. H.. 1993. Using geochemical data: evaluation. presentation. interpretation. John Wiley and Sons. New York. 352 p.

de Ronde. C.E.J.. Spooner. E.T.C.. de Wit. M.J.. and Bray. C.J.. 1992. Shear zone-related Au quartz vein deposits in the Barberton greenstone belt. South Africa: Field and petrographic characteristics. fluid properties. and light stable isotope geochemistry. Economic Geology. v. 87. p. 366-402.

Robert. F.. and Brown. A.C.. 1986. Archean gold-bearing quartz veins at the Sigma Mine. Abitibi greenstone belt. Quebec: Part II. Vein paragenesis and hydrothermal alteration. Economic Geology. v. 81. p. 593-616.

Rye. R.O.. 1993. The evolution of magmatic fluids in the epithermal environment: The stable isotope perspective. Economic Geology. v. 88. p. 733-753.

Shelton. K.L.. So. C-S.. Haeussler. G.T.. Chi. S-J.. and Lee. K-Y.. 1990. Geochemical studies of the Tongyoung gold-silver deposits. Republic of Korea: Evidence of meteoric water dominance in a Te-bearing epithermal system. Economic Geology. v. 85. p. 1114-1132.

Shieh. Y.N.. and Zhang. G.X.. 1991. Stable isotope studies of quartz-vein type tungsten deposits in Dajishan Mine. Jiangxi Province. Southeast China. *In* Stable isotope geochemistry: A tribute to Samuel Epstein. *Edited by* H.P. Taylor. J.R. O'Neil and I.R. Kaplan. The Geochemical Society. Special Publication 3. p. 425-435.

Snelling. N.J.. and McConnell. R.B.. 1969. The geochronology of Guyana. Geologie en Mijnbouw. v. 48. p. 201-213.

Taylor. H.P.Jr.. 1977. Water/rock interactions and the origin of H_2O in granitic batholiths. Journal Geological Society of London. v. 133. p. 509-558.

Taylor. H.P.Jr.. 1980. The effects of assimilation of country rocks by magmas on $^{18}O/^{16}O$ and $^{87}Sr/^{86}Sr$ systematics in igneous rocks. Earth and Planetary Science Letters. v. 47. p. 243-254.

Teixeira. W.. Tassinari. C.C.G.. Cordani. U.G.. and Kawashita. K.. 1989. A review of the geochronology of the Amazonian Craton: Tectonic implications. Precambrian Research. v. 42. p. 213-227.

Tremlow. S.G.. 1984. Archean gold-telluride mineralization of the Commoner mine. Zimbabwe: *In* Gold'82. *Edited by* R.P. Foster. Balkema. Rotterdam. p. 469-492.

Veizer. J.. Clayton. R.N.. and Hinton. R.W.. 1992. Geochemistry of Precambrian carbonates: IV. Early Paleoproterozoic (2.25 ± 0.25 Ga) seawater. Geochimica et Cosmochimica Acta. v. 56. p. 875-885.

Voicu. G.. Bardoux. M.. Stevenson. R.. and Jébrak. M.. 1997a. The Omai deposit. Guyana. Determination of age and source of gold using Nd-Sr isotopes of hydrothermal scheelite and its spatially-related lithologies. Ottawa 97. GAC/MAC Annual Meeting. Ottawa. Canada. May 21-23. 1997. Program with Abstracts. v. 22. A-154.

Voicu. G.. Bardoux. M.. Harnois. L.. Stevenson. R.. and Crépeau. R.. 1997b. Geochemical evolution of the Paleoproterozoic volcanic and plutonic rocks from Omai area. Guyana. South America: Implications for tectonic history and source regions: 30th International Geological Congress. Beijing. China. August 1-12. 1996. v. 2. 1. p. 101-114.

Voicu. G.. Bardoux. M.. Harnois. L.. and Crépeau. R.. 1997c. Lithological and geochemical environment of igneous and sedimentary rocks at the Omai gold mine. Guyana. South America. Exploration and Mining Geology. v. 6. no. 2. p. 153-170.

Walrond. G.W.. 1980. A metallogenetic scheme for the Guyana Shield. *In* Metalogenesis en Latinoamerica: Simposium Internacional. *Edited by* J.L.L. Moreno. Mexico. p. 141-164.

Walrond. G.W.. 1987. Geological map of Guyana. scale 1: 1 million. Guyana Geology and Mines Commission.

Wesolowski. D.. and Ohmoto. H.. 1986. Calculated oxygen isotope fractionation factors between water and the minerals scheelite and powellite. Economic Geology. v. 81. p. 471-477.

Wood. P.C.. Burrows. D.R.. and Spooner. E.T.C.. 1986. The Hollinger-McIntyre Au-quartz vein system. Timmins. Ontario. Canada: Geologic characteristics. fluid properties and light stable isotope geochemistry. *In* Proceedings Gold '86: *Edited by* A.J. Macdonald. Willowdale. Canada. Konsult International. p. 56-80.

Zindler. A.. and Hart. S.R.. 1986. Chemical geodynamics. Annual Review Earth Planetary Science. v. 14. p. 493-571.

CHAPTER IV

THE SOURCE OF THE OMAI GOLD DEPOSIT, GUIANA SHIELD: EVIDENCE FROM Nd-Sr ISOTOPIC DATA OF SCHEELITE AND HOST ROCKS

4.1 INTRODUCTION

Radiogenic isotope studies of orogenic gold deposits (Cox and Singer, 1986; Hodgson, 1990; Gray et al., 1993; Groves et al., 1998) and host rocks can provide information on the source of solutes such as Nd and Sr, which are frequently associated with gold and other metallic and non-metallic components. Determination of the source of the mineralizing fluids is generally limited by lack of paragenetically gold-related minerals. An exception is scheelite, which is frequently present as an accessory mineral in Precambrian to Tertiary gold deposits. Where present, scheelite predates or is contemporaneous to gold deposition (Hodgson, 1990; Mueller et al., 1991; Darbyshire et al., 1996; Anglin et al., 1996).

Previous studies of Nd isotopes in gold-related scheelite used this method to date the mineralizing fluids (Bell et al., 1989; Anglin, 1990; Darbyshire et al., 1996; Anglin et al., 1996; Eichhorn et al., 1997) or to trace the source of the gold (Kent et al., 1995). The Sr isotopic composition of scheelite has been used to constrain the path and source of the Archean gold-bearing hydrothermal fluids (Mueller et al., 1991; Kent et al., 1995). The isotopic variation of scheelite has been studied on a regional (several scheelite-bearing gold deposits of a mining district; Bell et al., 1989; Anglin, 1990; Mueller et al., 1991; Darbyshire et al., 1996; Anglin et al., 1996) and a mine scale (Mount Charlotte deposit, Yilgarn Craton; Kent et al., 1995). Geologically meaningful scheelite isochrons were obtained at the regional scale, indicating that the method is a suitable geochronometer for gold deposits. At the mine scale, the isotopic data can be used to constrain the source of ore-forming components. However, the only previous Nd-Sr isotope study of scheelites dealing with the source of gold (Kent et al., 1995) did not report the isotopic composition of the mine host rocks, which may have an important influence on the isotopic composition of hydrothermal fluids. Evidence for the source

of the fluids can be obscured by interaction during ascent with local rocks and it is plausible that the final isotopic composition represents mixing of several distinct sources (Cassidy et al.. 1998). Therefore. a comparison between the Nd and Sr isotopic compositions of scheelite and their local host rocks should provide reliable information regarding the path and source of ore-forming fluids. This information. correlated with the timing of emplacement of host rocks and gold mineralization. have important implications for models of Precambrian orogenic gold deposits. Kerrich and Cassidy (1994) provided a review of various models proposed for the orogenic gold deposits. which can be classified into two main categories : "early gold" and "late gold" models. "Early gold" models explicitly relate mineralization to processes resulting from terrane accretion and are generally based on geochronological. structural. and metamorphic observations. "Late gold" models are based on non-concordant younger mineralization ages. involving either delayed thermal rebound or younger mid-crust tectono-magmatic events.

The principal aim of this study is to constrain the source of the host rocks of the Omai deposit and the path and source of the mineralizing fluids using Sm-Nd and Sr isotope systematics. A second aim is to review briefly the implications of source of mineralizing fluids and their time of emplacement upon the genetic models proposed for the Precambrian gold deposits.

4.2 GEOLOGICAL SETTING

The Omai gold mine is a large open pit operation in the Potaro district of Guyana. 200 km southwest of the capital Georgetown. Gold in this area was discovered more than a century ago. It was sporadically explored and exploited by several mining companies. but the ore reserves have been classified as uneconomical. Since 1990. a joint

venture between Cambior Inc. and Golden Star Resources have exploited the deposit. At the present time. gold is produced from two separate open pit mining operations (Fennell pit in the Omai stock and country volcanic rocks and Wenot pit in the volcano-sedimentary sequence). The combined mineable reserves for both open pits and alluvial deposits are 83 Mt at 1.6 g/t Au. containing 4.2 million ounces of gold.

The Omai gold deposit is located in the northern part of the Guiana Shield. which consists of a greenstone belt sequence of Paleoproterozoic metavolcanic and metasedimentary rocks known as the Barama-Mazaruni Supergroup (Gibbs and Barron. 1983. 1993: Gibbs. 1987: Renner and Gibbs. 1987: Walrond. 1987: Elliott. 1992). The volcano-sedimentary sequence has been metamorphosed from prehnite-pumpellyite to amphibolite facies and it has been intruded by large masses of post-volcanic to post-tectonic granitoids referred to as the Granitoid Complex/Trans-Amazonian Granitoids (Fig. 4.1). Subsequently. during the Mesoproterozoic and Permo-Triassic. the region was intruded by several generations of gabbro and diabase sills and dikes. Uplift and erosion under humid tropical conditions created a thick weathered profile. which is mostly covered by the Tertiary continental-deltaic Berbice Formation (Bertoni et al.. 1991: Voicu et al.. 1997a.b).

The Omai area is underlain by a southward-younging sequence of at least 2 km of polygenic conglomerate that is locally intruded by vesicular basalt sills several meters thick. These rocks are overlain by a mafic-intermediate volcanic sequence that is in fault contact along the Wenot shear zone with fine grained clastic sedimentary rocks (mudstones. siltstones. and sandstones) (Fig. 4.2). The lowermost part of the volcanic pile is characterized by a sequence of massive to pillowed tholeiitic basalts. intruded by hornblende pyroxenite and gabbro bodies. The tholeiites are overlain by calc-alkaline
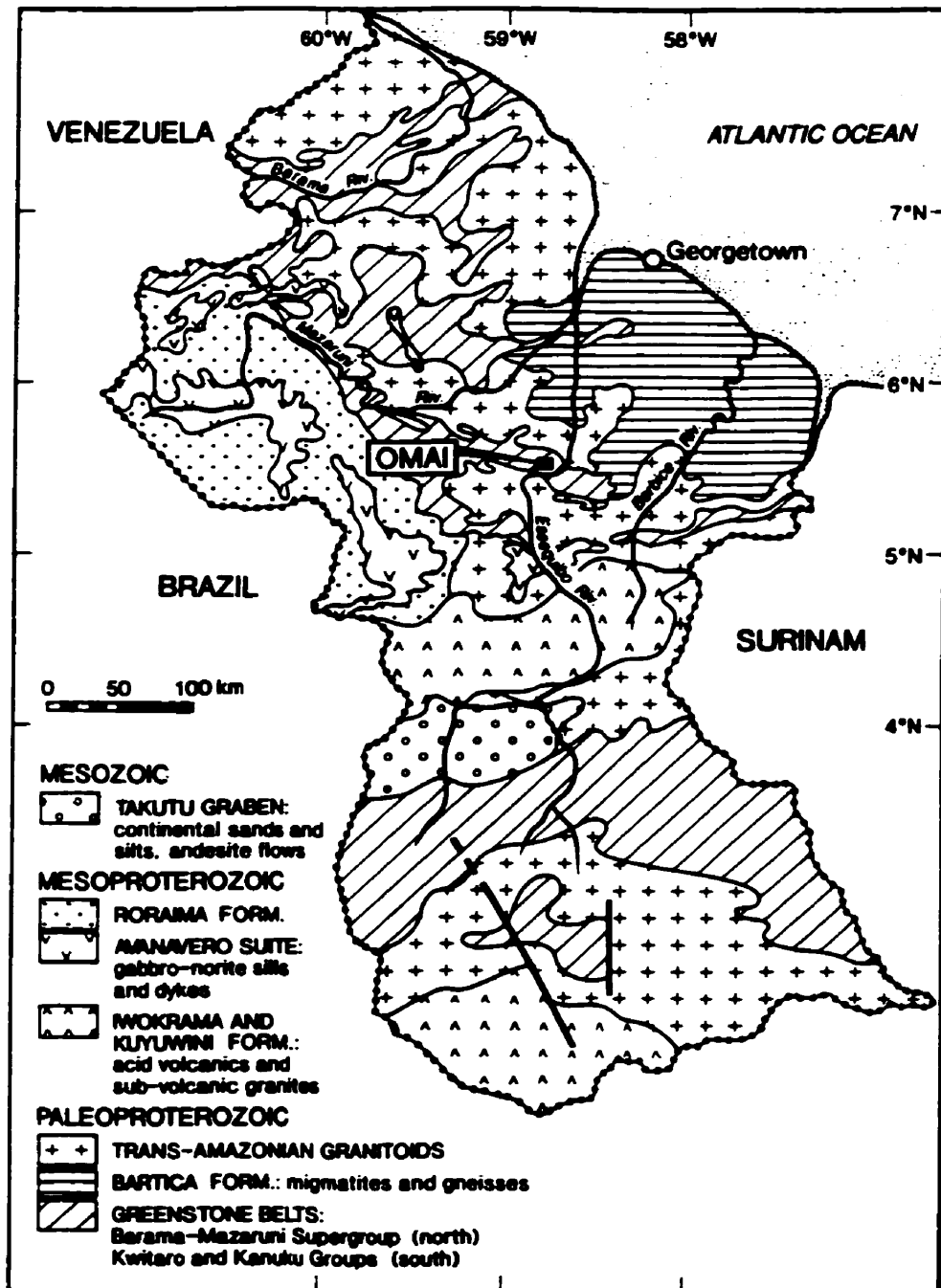
Figure 4.1   Simplified geological map of Guyana (modified from Walrond. 1987:
              Gibbs and Barron. 1993) showing the location of the Omai area.

PERMIAN-TRIASSIC
APATOE SUITE: dolerite dykes
MESOPROTEROZOIC
AMANAVERO SUITE: Tumatumari-Omai sill: gabbro, hornblende pyroxenite, granophyre
PALEOPROTEROZOIC
(Barama-Mazaruni Supergroup)
OMAI STOCK
Quartz monzodiorite, granodiorite
Hornblendite, diorite
Intrusion breccia
VOLCANO-SEDIMENTARY COMPLEX
Basalt
Andesite
Porphyritic andesite
Volcanic breccia
Amygdaloidal basalt
Silicified andesite
Pillowed andesite
Quartz-feldspar porphyry, rhyolite
Tuffaceous greywacke, tuff
Pelite (siltstone, sandstone, mudstone)
Volcanic conglomerate
MAFIC-ULTRAMAFIC COMPLEX
Microgabbro
Pyroxene hornblendite
Hornblende porphyry

Bedding
Foliation
Geological contact
Shear zone
Fault
(--) (suspected)
Open pit limits
A-A',B-B' Vertical cross-sections

Figure 4.2   Simplified geological map of the Omai area.

pillowed andesites interlayed with minor tuffs and intruded by early syn-tectonic quartz-feldspar porphyry and rhyolite dikes.

The volcano-sedimentary sequence has been metamorphosed to prehnite-pumpelleyite and lower greenschist facies. An undeformed granitoid intrusive (Omai stock) intrudes across the contact between the calc-alkaline andesitic and tholeiitic basaltic volcanic suites. The Omai stock is composed of fine to coarse grained quartz monzodiorite. granodiorite. diorite. and hornblendite.

Several unmetamorphosed post-mineral sills and dikes occur in the Omai area. The Mesoproterozoic Tumatumari-Omai leucogabbro sill (Avanavero Suite) outcrops north of the Fennell pit. This sill strikes WNW-ESE. dips $30°SW$ and truncates all other rock types and cross cutting associated veins.

Gold at Omai is present in undeformed quartz $\pm$ carbonate $\pm$ chlorite $\pm$ scheelite veins and stockworks in two areas. referred to as Fennell and Wenot pits. Fennell represents a granitoid (Omai stock)-hosted deposit. whereas Wenot is a greenstone-hosted gold deposit. The thickness of the veins varies between several mm and 1.8 m. They are principally hosted within the felsic rocks (Omai stock and porphyry/rhyolite dikes) and. to a lesser extent. in adjacent andesites/basalts and pelites of the volcano-sedimentary sequence (Bertoni et al.. 1991: Elliott. 1992: Voicu et al.. 1997a.b). Six gold-bearing undeformed subhorizontal and subvertical vein sets can be distinguished in the Fennell and Wenot pits. The structural relationships between the vein sets suggest that they are contemporaneous. The veins can be classified as extensional (including crack and seal tensional and shear veins). breccia veins. and fracture-filling veins. The formation of most veins can be summarized by two filling stages and a late fracture-filling stage related to a protracted hydrothermal process. Vein mineralogy comprises

quartz. ankerite. calcite. sericite. chlorite. pyrite. epidote. chalcopyrite. galena. scheelite. hematite. molybdenite. tellurides. and native gold. Scheelite is one of the first mineral phase deposited within the crack and seal tension veins hosted by the Omai stock and exhibits a widespread but erratic distribution. It occurs as coarse-grained. euhedral crystals ranging in size from 0.5 to 10 cm. usually attached directly to the walls of veins. It is considered to be contemporaneous with the vein gold deposition (Bertoni et al.. 1991: Bhatt. 1995: Voicu et al.. 1998). The scheelite-bearing veins which occur within the Omai stock are the focus of this study. Several analysed scheelites include native gold or contain gold-bearing fractures. providing evidence of the Au-W paragenetic relationship (Fig. 4.3).

Omai represents a shallow-level or epizonal orogenic gold deposit (terminology from Gebre-Mariam et al.. 1993. 1995: Hagemann et al.. 1994: Groves et al.. 1998). but. overall. has characteristics of both epi- and mesothermal gold mineralization (Voicu et al.. 1997: Hallbauer and Voicu. 1998).

4.3 GEOCHRONOLOGICAL DATA

Geochronological studies of the granite-greenstone belt and hydrothermal veins at Omai are summarized in Table 4.1. Precise U-Pb and Pb-Pb geochronology for the Omai rocks and vein-forming hydrothermal minerals are provided by Norcross (1997) and Norcross et al. (1998). Zircons from quartz-feldspar porphyry dikes that intrude the pillowed andesite sequence in Wenot pit gave a U-Pb age of 2120±2 Ma. whereas zircons from the Omai stock gave ages of 2094±1Ma (for quartz monzodiorite) and 2096+11/-10 Ma (for diorite). Titanite and apatite analyses from the hornblendite rim of the Omai stock yielded a Pb-Pb age of 2096±2 Ma.
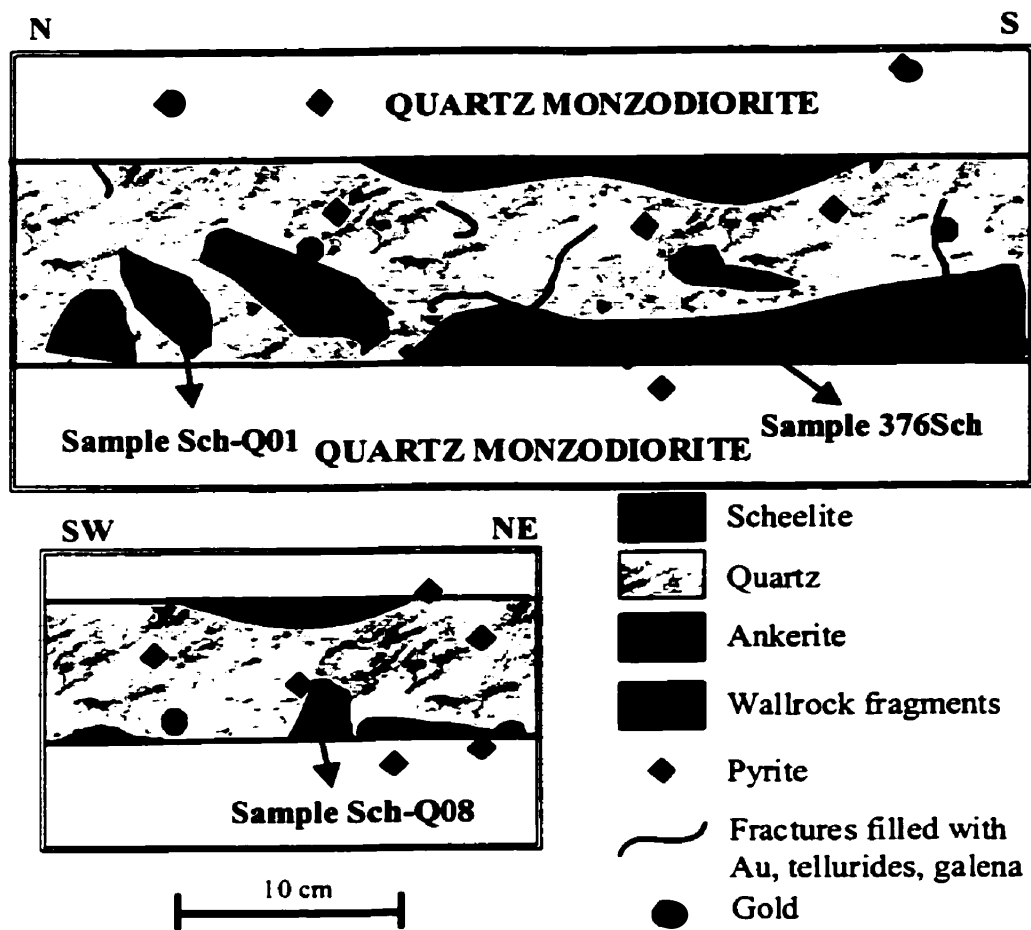
Figure 4.3   Sketches of veins within the Omai stock, Fennell pit. Locations of samples Sch-Q08, Sch-Q01, and 376Sch are shown. Note that scheelites form coarse crystal aggregates, generally directly attached to the walls of veins. Visible gold occurs within quartz and scheelite as milimeter-scale blebs or associated with galena and tellurides in fractures that cut across the vein-forming minerals.

Table 4.1   Ages of granite-greenstone terranes and gold deposits in the Guiana
Shield

Location	Age±2σ. Ma	Method Mineral	Lithology	Reference
Barama-Mazaruni Supergroup. Guyana	2250±104	U-Pb. zircon	Issineru metagraywacke	Gibbs and Olszewski. 1982
	2227±39	U-Pb. zircon	Bartica gneiss	
	2120±2	U-Pb. zircon	Omai. Wenot pit. dacite (quartz-feldspar porphyry)	Norcross. 1997
	2094±1	U-Pb. zircon	Omai stock (quartz diorite)	
	2096+11'-10	U-Pb. zircon	Omai stock (diorite)	
	2096±2	Pb-Pb. titanite. apatite	Omai stock (homblendite)	
	1945±100	K-Ar	Tigri granitoid	Snelling and McConnell. 1969
	2015±80	K-Ar	Granite	
Pastora Supergroup. Venezuela	2131±10	U-Pb. zircon	felsic metavolcanic rocks	Day et al.. 1995
Paramaca Series. French Guiana	2110±90	Sm-Nd	mafic metavolcanic rocks	Gruau et al.. 1985
	2146±2	U-Pb. zircon	St-Élie. Dévis rhyolite	Lafrance. 1997
	2174±7	U-Pb. zircon	Trondhjemite	Milési et al.. 1995
	2093±8	U-Pb. zircon	Granite	
	2083±39	Pb-Pb	Granite	Teixeira et al.. 1989
	2030±65	Rb-Sr	Granite	
Omai gold deposit. Guyana	1999±6	Pb-Pb. rutile. titanite	hydrothermal veins and wallrocks in the Omai stock	Norcross. 1997
Yaou. Loulouie. Dorlin. Adieu-Vat gold deposits. French Guiana	1955-2068*	Pb-Pb. galena		Marcoux and Milési. 1993

* - Pb model ages

Hydrothermal rutile and titanite from the Omai veins and wallrocks gave a Pb-Pb model age of 1999±6 Ma and likely represents the age of mineralization. The structural relationships between the undeformed mineralized veins and deformed porphyry dikes clearly suggests that the vein systems post-date the emplacement and deformation of the dikes. Furthermore. one of the vein systems crosscuts the whole width of the Omai stock. as well as its contacts with the mafic volcanic rocks. Locally. near the contact between the Omai stock and surrounding andesites. the breccia-texture veins within the stock contain andesite fragments. suggesting that the flow direction of the mineralizing fluid was from country rocks towards the Omai stock. These observations suggest that the Omai stock represents the host rock. but does not necessarily have a temporal relationship with the emplacement of the mineralized veins. The resetting of the Pb-Pb system at Omai at ~2000 Ma by a later tectono-magmatic event is not reflected in the field. where post-mineralization brittle faulting. sporadic mafic magmatism (Tumatumari-Omai sill was dated at 1789±2 Ma. Norcross et al.. 1998). and erosion have only slightly modified the geometry of the mineralized zones by causing minor offsets and incision. Therefore. it is considered that the Pb-Pb age for rutile/titanite (Norcross et al.. 1998) constrain the emplacement of the gold-bearing veins at about 2000 Ma. This age suggests that gold emplacement is between 90 to 120 Ma younger than the host igneous rocks. Gold mineralization also post-dates the peak of regional metamorphic activity due to the Trans-Amazonian orogeny constrained between 2120 (the age of deformed porphyry dikes) and 2094 Ma (the age of the undeformed Omai stock).

Detrital zircons from the metasedimentary rocks at Issineru. type-locality of the Barama-Mazaruni belt yield a U-Pb age of 2250±104 Ma (Gibbs and Olszewski. 1982). which represents a maximum age for the source rocks. Therefore. the volcano-sedimentary sequence at Omai could be considered younger than 2.35 Ga (detrital zircons. Gibbs and Olszewski. 1982) and older than 2.12 Ga (porphyry age at Omai.

Norcross et al.. 1998). The age of the greenstones at Omai can be roughly estimated at 2200±100 Ma. which is consistent with field evidence indicating that mafic volcanic and sedimentary rocks are older than cross-cutting quartz-feldspar porphyry dikes.

4.4 ANALYTICAL METHODOLOGY

Scheelite from quartz-carbonate stockwork veins were cleaned and crushed. Each sample was sieved and the < 70 mesh fractions were placed in methylene iodide in standard 250 ml separating funnels to isolate the heavy mineral fraction. Scheelite grains were handpicked under a binocular microscope and viewed under UV light to ensure homogeneous chemical composition. Cleaned fractions were then crushed in an agate mortar and weighed into Teflon dissolution vessels along with a mixed $^{149}Sm/^{150}Nd$ isotopic tracer solution. Samples were treated with hydrochloric acid. following 20 minutes in an ultrasonic bath in order to remove the protective coating of tungstic acid and thus aid dissolution. Hydrofluoric acid was added for 24h and the samples were dried on a hot plate at 100°C. Aqua regia was then added for 48h and the samples were dried at 100°C. Hydrochloric acid was added a second time and the solutions were centrifuged for 10 minutes. Rare-earth elements and Sr were extracted using cation-resin exchange columns and Nd and Sm were separated on Di(2-ethylhexyl) phosphate-coated Teflon resin columns. Rb contents were not measured. but extremely low Rb/Sr ratios previously reported for scheelites (<0.001. Bell et al.. 1989: Mueller et al.. 1991) implies that correction for Rb decay is probably unnecessary.

Whole-rock samples were cleaned. crushed and powdered in preparation for dissolution and chemical separation. Sample weights for dissolution varied from 200 mg for felsic compositions to 400 mg for mafic compositions. Samples were dissolved for one week in an HCl/HF acid mixture in pressurized bombs. Isotopic compositions were

measured at the Université du Québec à Montréal GEOTOP laboratory on a VG-Sector 54 multicollector mass spectrometer. using Ta-Re double filaments (for Nd and Sm) and single Re filaments (for Sr). Sm-Nd isotopic compositions were normalized to $^{146}Nd/^{144}Nd = 0.7219$ and Sr isotope ratios to $^{86}Sr/^{88}Sr = 0.1194$. The values of La Jolla and NBS-987 $SrCO_3$ standards for the laboratory were: La Jolla = 0.511848 (2σ = 0.000018. n = 27): NBS-987 = 0.710266 (2σ = 0.000035. n = 30). Given the reproducibility of measurements. an estimate of the uncertainty of the initial Nd value is better than ±0.5 epsilon units. Errors in the Sm/Nd ratio are 0.5%. A decay constant for ^{147}Sm of 6.54×10^{-12} y^{-1} was used for the age calculations. The present-day CHUR values used for the initial Nd calculation are $^{143}Nd/^{144}Nd = 0.512638$ and $^{147}Sm/^{144}Nd = 0.1967$.

4.5 RESULTS

Sm-Nd concentrations and isotope data for gold-related scheelites and igneous rocks from the Omai area are presented in Table 4.2. Sr isotopes were analysed only in scheelites. The range of Sr isotopes in the mafic volcanic rocks and dolomitic limestones from the northern part of the Barama-Mazaruni Supergroup (Gibbs et al.. 1986: Gibbs and Barron. 1993) and the range of Nd and Sr isotope data for the Paramaca Series and Arawa-Degrad gneisses in French Guiana (Gruau et al.. 1985) are also shown for comparison. Most of the scheelite samples are from the Omai stock. In the Wenot zone. only one scheelite grain (sample 643/40) was recovered from a quartz-carbonate vein within quartz-feldspar porphyry. Its anomalous Sm-Nd isotopic composition suggests either a completely different geological history (compared to scheelites from the Omai stock) or it is the result of an analytical error arising from incomplete sample dissolution.

Table 4.2   Sm-Nd and Sr isotopic and concentration data for scheelite and the host rocks from Omai, Guyana

Sample No.	Mineral/Rock	Nd (ppm)	Sm (ppm)	Sm/Nd	$^{147}Sm/^{144}Nd$[a]	$^{143}Nd/^{144}Nd$[b]	f Sm/Nd[c]	ε_{Nd}(T)[d]	ε_{Nd}(0)[d]	$^{87}Sr/^{86}Sr$
Sch-Q01	Scheelite	56.02	14.82	0.26	0.1598	0.512230 ± 16	-0.18	+1.50	-7.95	0.70202±12
Sch-Q08	Scheelite	92.25	31.01	0.34	0.2032	0.512856 ± 17	+0.03	+2.60	+4.25	0.70203±10
350Sch	Scheelite	71.06	33.01	0.46	0.2808	0.513817 ± 11	+0.42	+1.47	+23.00	0.70204±16
376Sch	Scheelite	23.09	8.45	0.36	0.2211	0.513028 ± 11	+0.12	+1.37	+7.61	0.70198±13
Sch-Q07	Scheelite	76.31	22.81	0.30	0.1806	0.512522 ± 12	-0.08	+1.87	-2.25	0.70210±11
Sch	Scheelite	109.62	32.35	0.30	0.1784	0.512447 ± 15	-0.09	+0.96	-3.72	0.70196±16
643/40	Scheelite	204.56	162.55	0.79	0.4806	0.515070 ± 11	+1.44	-25.38	+47.44	0.70214±15
Sch-Q05	Scheelite									0.70201±11
Omai stock										
310	Quartz monzodiorite	33.74	5.85	0.17	0.1048	0.511394 ± 12	-0.46	+1.14	-24.25	
349B	Quartz monzodiorite	27.02	4.71	0.17	0.1054	0.511490 ± 14	-0.46	+3.07	-22.38	
351	Quartz monzodiorite	33.92	5.95	0.17	0.1060	0.511499 ± 11	-0.46	+3.07	-22.21	
AD3	Granodiorite	31.56	5.29	0.17	0.1014	0.511432 ± 17	-0.48	+3.05	-23.52	
QD2	Diorite	34.51	6.99	0.20	0.1224	0.511675 ± 09	-0.37	+1.89	-18.78	
D10	Diorite	26.24	5.51	0.21	0.1270	0.511741 ± 10	-0.35	+1.92	-17.48	
111	Hornblendite	13.90	3.28	0.23	0.1426	0.512002 ± 20	-0.27	+2.65	-12.39	
622\123	Quartz-feldspar porphyry	4.13	0.83	0.20	0.1217	0.511614 ± 11	-0.38	+0.92	-19.96	
Volcanic rocks										
419	Tholeiitic basalt	11.92	3.02	0.25	0.1532	0.512233 ± 13	-0.22	+4.23	-7.89	
B10	Tholeiitic basalt	6.26	2.04	0.32	0.1965	0.512848 ± 20	-0.001	+4.17	-4.11	
B4	Tholeiitic basalt	14.81	4.10	0.28	0.1675	0.512309 ± 10	-0.15	+1.72	-6.42	
c1	Tholeiitic basalt	6.84	2.21	0.32	0.1960	0.512733 ± 14	-0.003	+2.06	+1.86	
349	Calc-alkaline andesite	7.80	1.72	0.22	0.1335	0.511895 ± 12	-0.32	+3.11	-13.49	
359	Calc-alkaline andesite	7.30	1.62	0.22	0.1342	0.511876 ± 12	-0.32	+2.54	-14.86	
Barama-Mazaruni[e]	Volcanic rocks									0.7015-0.7025
Barama-Mazaruni[f]	Limestone									0.7007-0.7015
Paramaca[g]	Andesites				0.1033-0.1264	0.511440-0.511722				-23 - -18
Paramaca[g]	Tholeiites				0.2021-0.2046	0.512781-0.512825				+3 - +4
Paramaca[g]	Komatiites				0.1467-0.1805	0.512070-0.512505				-11 - -3
Arawa-Degrad[g]	Gneisses									0.7042-0.7744

[a] Analytical errors are ±0.5%. [b] Uncertainties are 2σ and refer to last significant digit. [c] f Sm/Nd = ($^{147}Sm/^{144}Nd$ sample/0.1967 chondrite) - 1. [d] ε_{Nd} calculated at T = 1994 Ma for scheelite, T = 2102 Ma for Omai stock, T = 2120 for quartz-feldspar porphyry, and T = 2200 Ma for mafic volcanic rocks. [e] Data for Barama-Mazaruni volcanic rocks from Gibbs (1987) and Gibbs and Barron (1993). [f] Data for Cuyuni (Barama-Mazaruni) limestone from Gibbs et al. (1986). [g] Data for Paramaca Series, French Guiana, from Gruau et al. (1985).

A similar Sr isotope ratio to those of scheelite samples from Omai stock would rather favor the latter possibility.

The U-Pb and Pb-Pb ages of Norcross et al. (1998) were used for the calculation of initial Nd isotopic values.

Sm and Nd concentrations in the mafic volcanic rocks vary from 1.6 to 4.1 ppm and from 6.3 to 14.8 ppm. respectively. similar to other Paleoproterozoic rocks of the Guiana Shield (Gruau et al.. 1985: Gibbs and Barron. 1993). The volcanic rocks have Sm/Nd ratios from 0.22 to 0.32 and $f^{(Sm/Nd)}$ values. calculated as a measure of $^{147}Sm/^{144}Nd$ enrichment relative to a bulk silicate Earth. from -0.32 to -0.001. The ϵ_{Nd} values have been calculated for an age of 2200 Ma and range from about +1.7 to +4.2.

Sm and Nd concentrations in the Omai stock vary from 3.3 to 7 ppm and 13.9 to 34.5 ppm. respectively. The $^{147}Sm/^{144}Nd$ ratios increase from a low of 0.10 in the more felsic central part of the stock to a high of 0.14 in more mafic compositions near the contact with the volcanic rocks. Lower $^{147}Sm/^{144}Nd$ ratios in the felsic compositions are consistent with magmatic differentiation (cf. Stevenson. 1995). The ϵ_{Nd} values have been calculated using the U-Pb age of 2094 Ma (Norcross et al.. 1998). They vary between +0.5 and +2.3.

Scheelites have an initial $^{143}Nd/^{144}Nd$ ratio of 0.510141 ($\epsilon_{Nd(i)}$ = +1.7). The initial $^{143}Nd/^{144}Nd$ and $^{87}Sr/^{86}Sr$ ratios of scheelites are believed to reflect the initial ratios of the hydrothermal fluids. Although the Sm-Nd system is normally resistant to alteration and low grade metamorphism. some studies (see discussion in Poitrasson et al.. 1995) suggest that alteration and fractionation of the Sm/Nd ratio subsequent to

crystallization could influence calculated initial Nd values. However, oxygen isotope data of the scheelites and other hydrothermal minerals (Voicu et al.. 1997a) demonstrate that the isotopic systems were not affected by subsequent resetting.

Sm (8.5 - 33 ppm) and Nd (23.1 -109.6 ppm) concentrations of scheelites are highly variable. but compare well to scheelites from Yilgarn. Canadian and Zimbabwe deposits (Bell et al.. 1989: Anglin. 1990: Kent et al.. 1995: Darbyshire et al.. 1996: Anglin et al.. 1996). This large variation is also reflected in the $^{147}Sm/^{144}Nd$ ratios which range from 0.16 to 0.28. however no consistent correlation is observed between REE contents vs $^{147}Sm/^{144}Nd$ ratios. Likewise. the fractionation factor $f^{(Sm/Nd)}$ also shows a wide range of variation from +0.4 to -0.2. The $\epsilon_{Nd}^{(1999\,Ma)}$ values vary from about +1 to −2.6.

The scheelites define a linear array on a $^{143}Nd/^{144}Nd$ vs $^{147}Sm/^{144}Nd$ plot corresponding to an age of 1994±140 Ma. (MSWD = 9.7). Although this age overlaps the rutile/titanite Pb-Pb age of 1999±6 Ma (Norcross et al.. 1998). the large error also overlaps with the U-Pb ages of the host igneous rocks.

Sr isotopic ratios for scheelite have a narrow range and low values (0.7019 - 0.7021). They compare well with $^{86}Sr/^{87}Sr$ ratios of the gold-related scheelite from Archean deposits of the Canadian Shield (Bell et al.. 1989). but are slightly higher compared to those from the Yilgarn and Zimbabwe Cratons (Mueller et al.. 1991: Kent et al.. 1995: Darbyshire et al.. 1996).

4.6 DISCUSSION

4.6.1 Source of Nd in the Omai igneous rocks

The ϵ_{Nd} values of mafic volcanic rocks (tholeiites and andesites) plot between the Depleted Mantle reservoir growth curve (De Paolo. 1988. 1991) and CHUR. The initial $^{143}Nd/^{144}Nd$ ratios obtained for these rock types correspond to $\epsilon_{Nd}^{(2200\ Ma)}$ values between +4.2 and +1.7. In general. there is no correlation between lithology and ϵ_{Nd} values. since the isotopic compositions of calc-alkaline andesites overlap those of tholeiitic basalts. The range of the ϵ_{Nd} values suggests the magmas were derived from a depleted mantle with limited interaction. if any. with an older. LREE-enriched continental crust. However. magmatism was active long enough to allow an advanced degree of differentiation to occur. The presence of highly siliceous rocks at Omai (rhyolite and quartz-feldspar porphyry) does not necessarily imply a continental tectonic setting. but simply indicates that the magmas were chemically evolved (cf. Samson et al.. 1995).

Voicu et al. (1997a.b) proposed that the major and trace element geochemistry of the juvenile tholeiitic basalts and the thick conglomerate sequence north of Fennell pit could be interpreted as a back-arc basin environment. but one which was strongly affected by a volcanic arc signature. Indeed. the calc-alkaline andesites and fine-grained sedimentary rocks shares many features of an immature island arc. These observations could be reconciled if the region was subjected to alternating periods of extension and compression resulting in the migration of volcanic loci and corresponding changes in the chemical character of the magmas. Evidence for this process can be found at both the local (e.g. Omai) and regional scale in Guyana greenstone belts (Gibbs. 1987: Renner and Gibbs. 1987: Elliott. 1992). Thus. the dominant tholeiitic volcanism at Omai may

have formed in a back-arc basin during extensional periods. whereas the calc-alkaline eruptions reflect compressional periods and arc volcanism.

The Sm-Nd isotopic compositions are consistent with an overall volcanic arc setting. Furthermore. the isotopic signature of the mafic volcanic rocks suggests that at least this part of the Guiana Shield was likely a site of new crustal addition during the Paleoproterozoic time. which was not affected by older (Archean) reworked continental crust. These observations agree with the interpretation of the Sm-Nd and Rb-Sr data from French Guiana (Gruau et al.. 1985) and confirm the lack of Archean crust in the central and eastern parts of the Guiana Shield. However. the possibility of contamination by slightly older Paleoproterozoic crustal material cannot be totally ruled out.

The $\epsilon_{Nd}^{(2094 \text{ Ma})}$ values of the Omai stock range from +2.3 to +0.6 and plot between the Depleted Mantle reservoir growth curve and CHUR. These positive values indicate derivation of the magmas from a reservoir with an isotopic signature similar to depleted mantle. This could imply an origin through melting of young mantle-derived rocks such as the basalts or differentiation from a more mafic magma at depth. The emplacement of the Omai stock after the peak of regional metamorphism is more consistent with an origin through magmatic differentiation with subsequent assimilation of crustal rocks leading to variable isotopic compositions.

4.6.2 Source of Nd in hydrothermal fluids

The Nd data for scheelites and the isotopic evolution of Omai stock and volcanic rocks are shown in Fig. 4.4. All the ϵ_{Nd} values (+2.6 to +1) of the scheelites calculated at 1999 Ma lie within the field of the tholeiitic basalts. They are generally more positive than the values of the Omai stock. andesites and quartz-feldspar porphyry calculated at
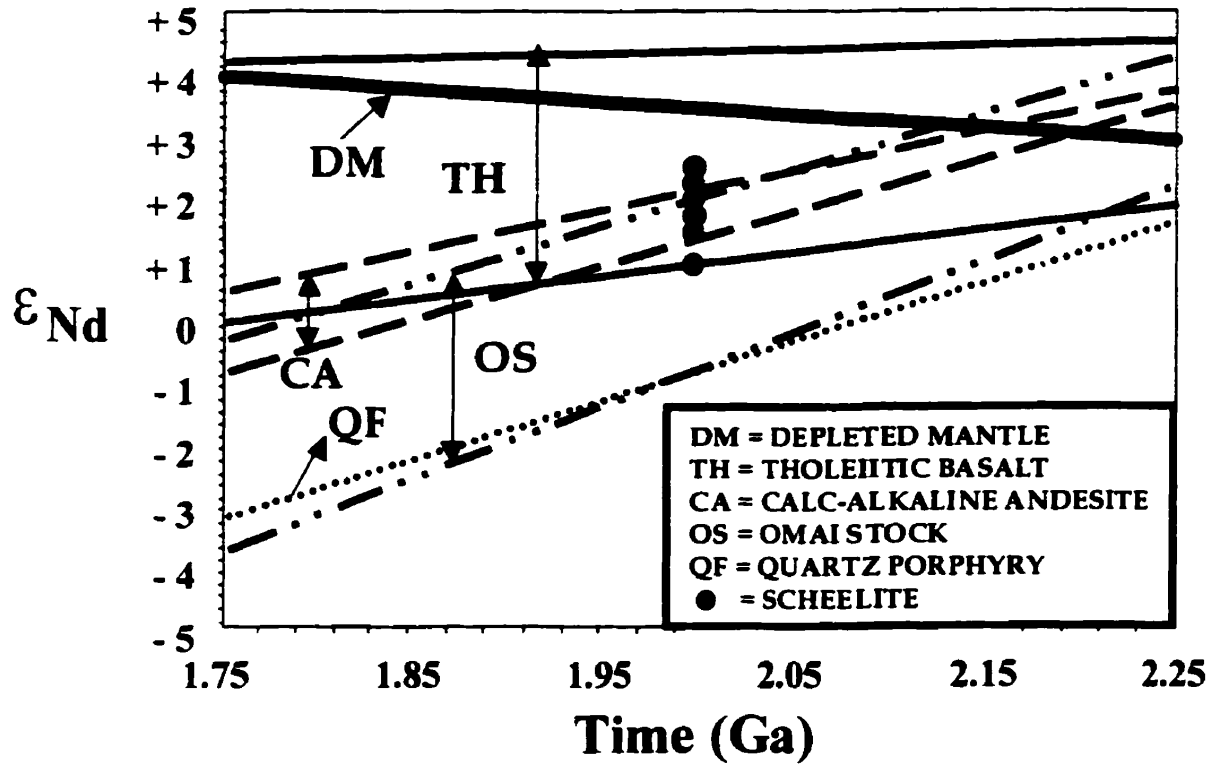
Figure 4.4   The evolution of ε_{Nd} with time for the Omai rock types and scheelite; ε_{Nd} values calculated at T = 1999 Ma; Depleted Mantle growth curve from DePaolo et al. (1991).

the same age (1999 Ma). However, scheelites with lower positive ϵ_{Nd} values also overlap the Omai stock and andesite array. These data could imply that at least a portion of the mineralizing fluids that deposited scheelite originated from the tholeiitic basalts, possibly with limited contamination from less radiogenic Nd-bearing rocks.

In order to better constrain the fluid source, several possible mixing compositions between the tholeiitic basalts (representing a mantle juvenile source) and other rock types from the Omai area are presented in Fig. 4.5. The calculations have been performed using an equation for simple mixtures (DePaolo, 1988):

$$\epsilon_{Nd}^{scheelite} = \frac{X^{TH} \times C_{Nd}^{TH} \times \epsilon_{Nd}^{TH} + X^{L} \times C_{Nd}^{L} \times \epsilon_{Nd}^{L}}{X^{TH} \times C_{Nd}^{TH} + X^{L} \times C_{Nd}^{L}}$$

where X^{TH}, C_{Nd}^{TH} and X^{L}, C_{Nd}^{L} represent the weight fractions and the concentration of total Nd for tholeiitic basalts and other rock types (the probable contaminants), respectively. The sum $X^{TH} + X^{L}$ is always equal to 1. The Nd concentrations and the ϵ_{Nd} values used for the mixing calculation represent the average for each rock type. The diagram allows for several observations:

1. Scheelites (except sample Sch) plot within the ϵ_{Nd} variation range of the tholeitiic basalts (calculated at 1999 Ma). The average ϵ_{Nd} of the scheelites is 1.0 ϵ_{Nd} unit lower than that of the tholeiitic basalts. This suggests that mixing between tholeiitic basalts and one or more local components is not necessarily needed to decipher the fluid source. The variability of the Nd isotopic ratios in scheelites could represent the direct effect of variable Nd ratios in the tholeiitic basalts. This observation seems to be confirmed by
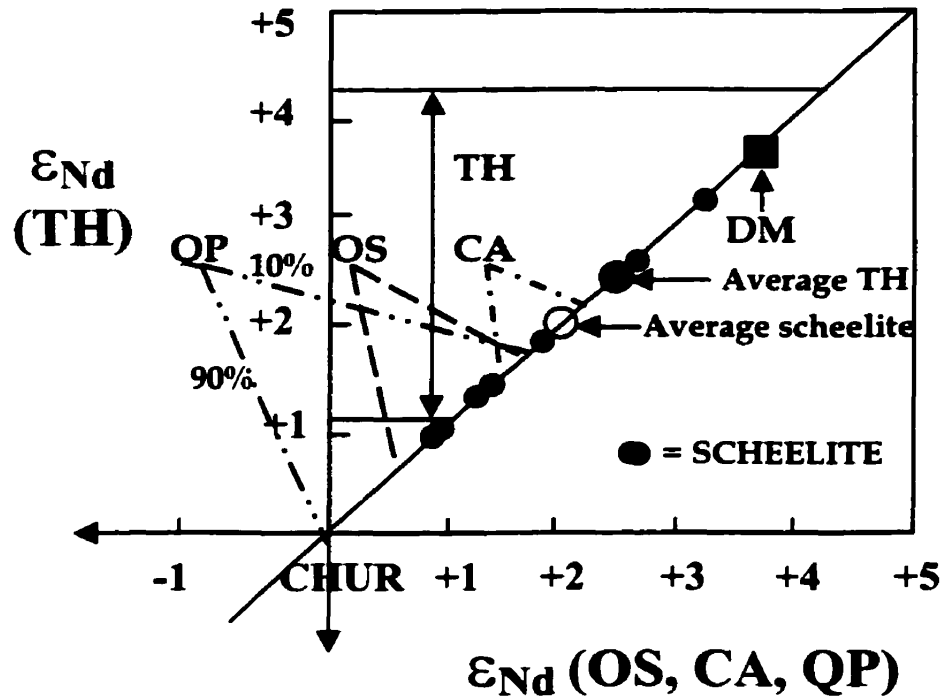
Figure 4.5 ε_{Nd} (TH) *vs* ε_{Nd} (OS, CA, QP) plot showing possible mixing combinations between the tholeiitic basalts (TH), considered the most likely local source for the highly radiogenic Nd in scheelite, and other lower radiogenic Nd-bearing rock types (OS = Omai Stock; CA = calc-alcaline andesites; QP = quartz-feldspar porphyry). Only the mixing values of 10% and 90% are shown. The ε_{Nd} values used in the diagram represent the average of each rock type calculated at 1999 Ma, the age of the hydrothermal activity (average ε_{Nd} for OS = +0.6; for CA = +1.4; for QP = -0.8); average ε_{Nd} value for TH at 1999 Ma = +2.6; average ε_{Nd} for scheelites at 1999 Ma = +1.6; DM (Depleted Mantle) at 1999 Ma after DePaolo et al. (1991).

the Sr isotopic ratios (see below). However. limited contamination. if any. of the hydrothermal fluids by fluids from the Omai stock. andesite or quartz-feldspar porphyry cannot be ruled out. Any mixing combination between tholeiitic basalts and 10-70% Omai stock. 10-90% andesite and/or 10-40% quartz porphyry results in a range of ϵ_{Nd} values which are similar to that of most scheelites. Because most of the scheelite-bearing mineralized veins discussed in this study are hosted by the Omai stock. a possible influence by fluids derived from the Omai stock is likely.

2. Two scheelites from gold-rich veins in the southwestern part of the Fennell pit have ϵ_{Nd} values which plot between the Depleted Mantle curve and the average ϵ_{Nd} value for the tholeiitic basalts. The hydrothermal fluids responsible for precipitation of these scheelites were. thus. strongly juvenile. with little or no contamination by other rock types. The remaining scheelite samples show a direct paragenetic relationship between scheelite and typical granitoid-related ore minerals (tellurides. molybdenite). but contain less gold. This observation could be interpreted in terms of a gradual dilution of the gold content in the mineralizing fluids due to the addition of fluids derived from the Omai stock. This would imply that the gold was likely precipitated from juvenile fluids by dilution/contamination while traveling and interacting with fluids from the more felsic rocks such as the quartz monzodiorite.

The relationship between dilution and contamination cannot be clearly assessed. but a possible explanation could be the gradual dilution of the juvenile fluids due to interaction and contamination with more diluted gold-bearing fluids from the host Omai stock. Juvenile fluids. initially rich in gold. formed. by precipitation. the high-grade ore zones. whereas fluids affected by contamination with fluids from the Omai stock became diluted. led to the formation of lower-grade ore zones.

However. the Omai stock is an unlikely source or heat engine for the mineralizing fluids because it predates gold mineralization by about 90 Ma and is not metamorphosed. Younger granitoid batholiths. possibly contemporaneous with gold mineralization. occur as close as 6 km south-east of Omai. The Tigri batholith. for example. is dated at 1940±100 Ma (K-Ar method. Snelling and McConnell. 1969) and. thus. could have acted as the heat source needed to generate fluid movement.

The isotopic signature at Omai is similar to (but not as depleted as) that observed in scheelites from the Mount Charlotte deposit of the Kalgoorlie gold field. Western Australia (Kent et al.. 1995) and Val d'Or gold camp. Abitibi Subprovince (Anglin et al.. 1996). Kent et al. (1995) concluded that ore fluids were also derived from a juvenile source. represented by the Kalgoorlie-Kambalda komatiites. mixed with fluids released from the doleritic host rocks of the deposit. This conclusion is in agreement with a number of studies which have suggested that komatiitic lavas are potential source rocks for Archean gold deposits. Anglin et al. (1996) suggested that the ϵ_{Nd} values of the Val d'Or scheelites also indicated a depleted mantle reservoir source such as mafic/ultramafic rocks (i.e.. basalts/komatiites). In the Guiana Shield. however. only sparse komatiitic compositions lacking spinifex textures have been described in the central belt of French Guiana and in central Guyana (Gruau et al.. 1985: Gibbs. 1987: Gibbs and Barron. 1993). As in other Paleoproterozoic greenstone belts. komatiites in the Guiana Shield probably represent less than 1% of the rock assemblages. and it is unlikely that these small volumes of rocks would be the major source of gold. Kent et al. (1995) observed that the hydrothermal fluids appeared to be mainly derived from rock types (komatiites) with the lowest concentration of Nd. Although the Omai fluids also appear to be derived from juvenile mafic rocks (the basalts). they are generally characterized by greater Nd concentrations than the associated calc-alkaline andesites.

However. the question remains: do the mafic/ultramafic rocks represent regional or local fluid source(s). or. in other words. is (are) the source(s) of the fluids homogeneous or heterogeneous? A homogeneous source could imply a major introduction of gold into the greenstone belt. whereas a heterogeneous source indicates possible remobilization of earlier gold. Anglin et al. (1996) suggested that the absence of evidence for the mixing of two or more isotopically distinct sources favors a homogeneous. lower crustal/depleted mantle source or. at least. material recently derived from a depleted mantle. whereas mixing would indicate the influence of local sources upon deeper crustal fluids. This observation is only partially valid at Omai for two reasons:

1. At 1999 Ma. the ϵ_{Nd} values of the tholeiitic basalts overlap those of the scheelites. Thus. although the scheelites indicate a juvenile source. this source could be up to 120 Ma old.

2. The 90 Ma gap between the peak of regional metamorphism and gold mineralization rules out the local mafic volcanic rocks as the only source of the ore fluids. Another magmatic or metamorphic deep-seated source characterized by similar isotopic compositions to the local tholeiitic basalts is needed to explain the post-peak metamorphism emplacement of the gold-bearing veins at Omai. Mixing between two sources can be envisaged. but characterized by isotopically similar. not distinct. features. The most plausible explanation is mixing between fluids derived by devolatilization of a tholeiitic type lower crust. advected along major crustal faults. and local fluids of similar isotopic composition derived from the upper greenstone tholeiitic basalts. released during alteration and gold mineralization. In this case. the Omai deposit contains both primary and remobilized gold.

Possible mechanisms for gold remobilization are described by Keays and Scott (1976). who demonstrated that basalts containing abundant magmatic Fe-Ni-Cu sulfides might be expected to contain abundant Au. This observation seems applicable to the Omai deposit. where tholeiitic basalts are enriched in magmatic pyrrhotite (often nickeliferous). pentlandite. and chalcopyrite. and have whole-rock gold contents up to 2 ppm (Voicu et al.. 1997a). Furthermore. massive gold-bearing stringers are found locally in tholeiites at Omai. Pillowed tholeiitic basalts are particularly good source rocks because during spilitic alteration Au has been found to migrate to interpillow positions or into fractures and. due to their high permeability. the gold could be easily remobilized by later fluids (Hutchinson. 1987: Nesbitt et al.. 1987). Thus. widespread spilitization of the Omai basalts may have led to a preconcentration of the gold. making it available for ore formation during any subsequent metamorphic and/or deformational events in which elements would be mobilized and concentrated in rheologically favorable sites.

4.6.3 Source of Sr in hydrothermal fluids

The small range and low $^{87}Sr/^{86}Sr$ isotopic ratios of the Omai scheelites (0.7019 - 0.7021) support observations from vein textures and mineral paragenesis that early stage of mineralization at the Omai deposit resulted from deposition of a largely juvenile-derived fluid. The Sr isotopic compositions are much lower than those reported for orthogneisses of the Paramaca Series (0.704-0.774: Gruau et al.. 1985). suggesting that the hydrothermal fluids responsible for Au deposition at Omai were not derived from a similar high-grade metamorphic complex. On the other hand. the scheelites have higher Sr isotopic compositions than dolomitic limestones of Barama-Mazaruni Supergroup (0.7007-0.7015: Gibbs et al.. 1986). However. since the gold-bearing veins were formed at least 120 Ma after the deposition and diagenesis of the limestones belonging to the volcano-sedimentary sequence. it is unlikely that the mineralizing fluids

were derived from diagenetic fluids. Meteoric water probably did not have an important role because its Sr isotopic composition would have reflected leaching of Sr from the overlying metasedimentary sequences and would have certainly been more radiogenic than the compositions observed in the scheelites. The low $^{87}Sr/^{86}Sr$ ratios of the scheelites are similar to those of the Barama-Mazaruni basalts (Gibbs and Barron. 1993). This is consistent with models suggesting a major component of metamorphic fluid. released during the devolatilization of mafic rocks at depth. Thus. the Sr isotope data are in agreement with the Nd isotopes. which also suggest a juvenile source.

The limited variation of the Sr isotope ratios is also consistent with studies which indicate that hydrothermal fluids rapidly reach equilibrium with host rocks over short distances. Sr isotopes indicate that the travel distance of mineralizing fluids approach isotopic equilibrium with host rocks over distances varying from a few hundred metres to up to about 2 km (Böhlke and Kistler. 1986: Farmer and DePaolo. 1987: Mueller et al.. 1991). Therefore the narrow range of Sr isotopes of the scheelites and their similarity to the isotopic compositions of mafic volcanic rocks could reflect equilibration of the fluids with the host basalts. and not that of the source. Thus. the isotopic composition of the veins could reflect mixing between a regional. lower crustal source. and a local source represented by tholeiitic basalts. both characterized by similar isotopic features. which produced non-radiogenic Sr isotope ratios. However. the Sr isotope ratios do rule-out contributions from more radiogenic Sr isotope sources. such as felsic intrusives or high-grade metamorphic gneisses (e.g Snelling and McConnell. 1969. Gruau et al.. 1985).

4.7 GENETIC SIGNIFICANCE OF Nd-Sr ISOTOPIC DATA

The difference in age between mineralizing fluids and the host rocks at Omai is similar to that observed for other Precambrian gold-related scheelites and host rocks. For example. gold mineralization is about 70 Ma younger than host rocks in the Val d'Or district (Anglin. 1990: Anglin et al.. 1996). 50 to 320 Ma younger in the Porcupine district of the Abitibi subprovince (Bell et al.. 1989). 70 Ma at Mount Charlotte. Yilgarn Craton (Kent et al.. 1995). and up to 200 Ma in the Zimbawbe Craton (Darbyshire et al.. 1996). Kerrich and Cassidy (1994) argued that these ages reflect selective resetting related to secondary fluid events. Anglin et al. (1996) suggested that the similarity in ages between hydrothermal activity in the Val d'Or district and deep crustal metamorphism postdating the stabilization of the upper crustal belts may indicate a related process. The Pb-Pb ages of hydrothermal minerals at Omai are broadly contemporaneous with the ages of high-grade metamorphic rocks in Guyana. Suriname. and French Guiana. Granulite belt in Suriname yielded a U-Pb age of 2026 ± 20 Ma (Bosma et al.. 1983). whereas the Arawa and Degrad gneisses from northern French Guiana yielded 2000 ± 70 Ma (Rb-Sr method. Gruau et al.. 1985). Both metamorphism and mineralization significantly postdate the stabilization of the upper crustal greenstone belts. The granulitic and gneissic rocks could be representative of the lower crust underlying the volcano-sedimentary sequence. as has been suggested for the Abitibi greenstone belt (Jemielita et al.. 1990: Anglin et al.. 1996). Although there are only sparse data at Omai to suggest the existence of late deep crustal metamorphism or a temporal relationship with gold emplacement. the span of time between the peak of regional metamorphism and gold mineralization seems best explained by late thermal events related to the continuation of the Trans-Amazonian orogeny at deeper crustal levels.

The isotopic characteristics of the hydrothermal fluids and host rocks from Omai can be used to discriminate between various models proposed for orogenic gold deposits.

"Early gold" models :

- *Magmatic model*. Nd and and especially Sr isotopes from Omai rule out the granitoid intrusives as the main source for the hydrothermal fluids. Field relationships suggest that the vein emplacement post-dates the Omai stock. Furthermore, a genetic link between the Omai stock and the mineralized veins cannot explain the greenstone-hosted Wenot mineralization. Although the Tigri granitoid could be contemporaneous with the Omai mineralization and theoretically could represent the source of fluids, it is difficult to explain the presence of the mineralized veins in the Omai area and not within the Tigri batholith.

- *Gold-shoshonite association*. To date there is no shoshonitic magmatism identified in the Omai area.

- *Cratonization and Crustal continuum*. These models are based on close relationships between the thermal and rheological features of gold deposits relative to their host environment, although they have no implications about fluid sources. These models agree with field data at Omai, where the hydrothermal alteration assemblage mirrors the greenschist metamorphic grade affecting the country rocks. However, this relationship does not necessarily imply a genetic and temporal link between hydrothermal events and regional peak of metamorphism.. Because the emplacement of the mineralized veins at Omai occur at shallow-crustal levels, the alteration assemblages could mimic low-grade metamorphic conditions of country rocks. This implies that the mineralized system is close to equilibrium with the country rocks, although it is not a

requirement that the ore system be integral an part of the ambient tectono-magmatic conditions.

"Late gold" models :

- *Delayed dehydration*. This model envisages a direct relationship between post-collisional thermal rebound and mineralization that would be emplaced up to 100 Ma after collision. Peak temperatures are attained at increasing crustal depths at progressively later times. However. because the Omai deposit occurs at shallow crustal level 90 Ma after peak metamorphism. a genetic link between thermal rebound and mineralization is unlikely.

- *Late deep metamorphic activity*. This model is based on non-concordant younger mineralization ages and suggests that late gold mineralization is related to fluids which have been ascribed to mafic magmatic underplating (Krogh. 1990: Corfu. 1993: Zweng et al.. 1993) or to lower crustal extension and passive upwelling of the lithosphere (Corfu. 1993) under the Archean Superior Craton. At Omai it is difficult to envisage the selective resetting of the Pb-Pb and Sm-Nd systems affecting hydrothermal minerals. whereas the Pb-Pb system in magmatic minerals (in hornblendite) has not been affected by later thermal events. Moreover. values of $\delta^{18}O$ on scheelite. quartz and carbonate and $^{87}Sr/^{86}Sr$ on scheelite are tightly clustered (Voicu et al.. 1998). signifying that mineral phases are neither secondary nor reset. Therefore. there is no selective resetting of the Pb-Pb and Sm-Nd systems. which is consistent with the coherent stable and Sr isotope data. Therefore. Pb-Pb and Sm-Nd data should be considered as truly reflecting the timing of primary mineralization. The isotopic data suggest that fluids derived from devolatilization of the lower part of the greenstone sequences may have been focused along regional-scale structural breaks and advected towards shallow crustal levels. where

they interacted with local sources. represented in this case by tholeiitic basalts. There is geological evidence of mafic magmatic underplating in north-central Guyana. represented by several gabbro-anorthosite complexes. Athough there are no precise geochronological data for these complexes. field relationships suggest that their emplacement post-dates collisional tectonism (Walrond. 1987). Moreover. there is an agreement in age between granulitization and vein emplacement at Omai. which could reflect related processes. Although Kerrich and Cassidy (1994) include granulitization in the "early gold" models. the evolution of the Precambrian belts shows that high-grade granulitic metamorphism is associated with the final stages of the orogenic evolution. Low radiogenic Sr isotope signatures from Omai may be consistent with a genetic link between granulites. characterized in the Guiana Shield by low radiogenic Sr values (Bosma et al.. 1983). and gold mineralization.

The age of the Omai deposit compares well with the ages of gold deposits of similar characteristics in the Guiana and West African Shields. Galenas from French Guiana deposits (Loulouie and Adieu-Vat) yielded a model age of 2014 Ma (Marcoux and Milési. 1993: Milési et al.. 1995). whereas the West African deposits (Hiré and Poura) yielded a Pb-Pb age of 2000±17 Ma (Milési et al.. 1989. 1992). Thus. on a regional scale. these deposits represent a late feature with respect to the general tectonic and metallogenic evolution of the two Paleoproterozoic shields. Although there are no radiogenic isotope data which could suggest the source of fluids at a regional scale. the age of 2000 Ma can be considered as a major (craton-wide) hydrothermal event related to the continuation at lower crustal level of Trans-Amazonian and Eburnian (West Africa) orogenies.

4.8 CONCLUSIONS

In the Omai area. Nd and Sr isotopes can distinguish between different possible sources of the mineralizing fluids and host rocks. offering a potential tool for isotopic tracing in 'gold-only' type deposits. Isotopic ratios of scheelite and country rocks suggest that the mineralizing fluid is largely derived from a radiogenic Nd source. but a non-radiogenic Sr source. The timing and composition of the fluids can be interpreted in terms of mixing of fluids derived from a deep-seated. juvenile tholeiitic type source with local shallow-level fluids derived from the tholeiitic basalts during gold mineralization and alteration. Evidence for the mixing of two isotopically similar sources at Omai favors a heterogeneous fluid. which contains both primary and remobilized gold. Given the field relationships and isotope data. it is proposed that Omai classifies as a good example of a "late gold" deposit related to deep metamorphic activity during the last phases of the Paleoproterozoic Trans-Amazonian orogeny.

4.9 REFERENCES

Anglin, C.D.. 1990. Sm/Nd isotopic analyses of scheelite and tourmaline from Val d'Or gold deposits [abs.]: In NUNA Conference on greenstone gold and crustal evolution. Val d'Or. May 1990. p. 129-131.

Anglin. C.D.. Jonasson. I.R.. and Franklin. J.M.. 1996. Sm-Nd dating of scheelite and tourmaline: Implications for the genesis of Archean gold deposits. Val d'Or. Canada. Economic Geology. v. 91. p. 1372-1392.

Bell. K.. Anglin. C.D.. and Franklin. J.M.. 1989. Sm-Nd and Rb-Sr isotope systematics of scheelites: Possible implications for the age and genesis of vein-hosted gold deposits. Geology. v. 17. p. 500-504.

Bertoni. C.H.. Shaw. R.P.. Singh. R.. Minamoto. J.. Richards. J.M.. and Belzile. E.. 1991. Geology and gold mineralisation of the Omai property. Guyana. In Brazil gold '91: The economics geology geochemistry and genesis of gold deposits. Edited by E.A. Ladeira. Balkema. Rotterdam. p. 767-773.

Böhlke. J.K.. and Kistler. R.W.. 1986. Rb-Sr. K-Ar. and stable isotope evidence for the ages and sources of fluid components of gold-bearing quartz veins in the Northern Sierra Nevada Foothills metamorphic belt. California. Economic Geology. v. 81. p. 296-322.

Bosma. W.. Kroonenberg. S.B.. Maas. K.. and De Roever. E.W.F.. 1983. Igneous and metamorphic complexes of the Guiana Shield in Suriname. Geologie en Mijnbouw. v. 62. p. 241-254.

Cassidy. K.F.. Groves. D.I.. and McNaughton. N.J.. 1998. Late-Archean granitoid-hosted lode-gold deposits. Yilgarn Craton. Western Australia : Deposit characteristics. crustal architecture and implications for ore genesis. Ore Geology Reviews. v. 13. p. 65-102.

Corfu. F.. 1993. The evolution of the southern Abitibi greenstone belt in light of precise U-Pb geochronology. Economic Geology. v. 88. p. 1323-1340.

Cox. D.P.. and Singer. D.A.. eds.. 1986. Mineral deposits models. U.S Geological Survey Bulletin 1693. 379 p.

Darbyshire. D.P.F.. Pitfield. P.E.J.. and Campbel. S.D.G.. 1996. Late Archean and Early Proterozoic gold-tungsten mineralization in the Zimbabwe Archean craton: Rb-Sr and Sm-Nd isotope constraints. Geology. v. 24. p. 19-22.

Day. W.C.. Tosdal. R.M.. Acosta. E.L.. Aruspon. J.C.. Carvajal. L.. Cedeño. E.. Lowry. G.. Martinez. L.F.. Noriega. J.A.. Nuñez. F.J.. Rojas. J.. and Prieto. F.. 1995. Geology of Lo Increíble mining district and U-Pb ages of the early Proterozoic Yuruari Formation of the Pastora Supergroup. Guayana Shield. Venezuela. U.S. Geological Survey Open File Report 2124. p. E1-E13.

De Paolo. D.J.. 1988. Neodymium isotope geochemistry. An introduction. Minerals and Rocks. v. 20. Springer Verlag. Berlin. New York. Tokyo. 187 p.

De Paolo. D.J.. Linn. A.M.. and Schubert. G.. 1991. The continental crustal age distribution: Methods of determining mantle separation ages from Sm-Nd isotopic data and application to the Southwestern United States. Journal of Geophysical Research. v. 90 (B2). p. 2071-2088.

Eichhorn. R.. Höll. R.. Jagoutz. E.. and Schärer. U.. 1997. Dating scheelite stages: A strontium. neodymium. lead approach from the Felbertal tungsten deposit. Central Alps. Austria. Geochimica et Cosmochimica Acta. v. 61. no. 23. p. 5005-5022.

Elliott. R.G.. 1992. The geology and the geochemistry of the Omai goldfield. Guyana. Unpublished Ph.D. thesis. Oxford Brookes University. 230 p.

Farmer. G.L.. and DePaolo. D.J.. 1987. Nd and Sr isotope study of hydrothermally altered granite at San Miguel. Arizona: Implications for element migration paths during the formation of porphyry copper ore deposits. Economic Geology. v. 82. p. 1142-1151.

Gebre-Mariam. M.. Groves. D.I.. McNaughton. N.J.. Mikucki. E.J.. and Vearncombe. J.R.. 1993. Archean Au-Ag mineralization at Racetrack. near Kalgoorlie. Western Australia: A high crustal-level expression of the Archean lode-gold continuum. Mineralium Deposita. v. 28. p. 375-387.

Gebre-Mariam. M.. Hagemann. S.G.. and Groves. D.I.. 1995. A classification scheme for epigenetic Archaean lode-gold deposits. Mineralium Deposita. v. 30. p. 408-410.

Gibbs. A.K.. 1987. Proterozoic volcanic rocks of the northern Guyana Shield. South America. In Geochemistry and mineralisation of Proterozoic volcanic suites. Edited by T.C. Pharaoh. R.D. Beckinsale. and D. Rickard. Geological Society of London Special Publication. v. 33. Oxford. Blackwell. p. 275-288.

Gibbs. A.K.. and Olszewski. W.J.Jr.. 1982. Zircon U-Pb ages of Guiana greenstone-gneiss terrane. Precambrian Research. v. 17. p. 199-214.

Gibbs. A.K.. and Barron. C.N.. 1983. The Guiana Shield reviewed. Episodes. v. 2. p. 7-14.

Gibbs. A.K.. and Barron. C.N.. 1993. Geology of the Guiana Shield. Oxford Monographs on Geology and Geophysics. v. 22. Oxford. Clarendon Press. 246 p.

Gibbs. A.K.. Montgomery. C.W.. O'Day. P.A.. and Erslev. E.A.. 1986. The Archean-Proterozoic transition: Evidence from the geochemistry of metasedimentary rocks of Guyana and Montana. Geochimica et Cosmochimica Acta. v. 50. p. 2125-2141.

Gray. F.. Cox. D.P.. Orris. G.J.. Page. N.. Wynn. J.C.. Brooks. W.E.. and Bliss. J.D.. 1993. Mineral resource assessment of the Venezuelan Guayana Shield: Low-sulfide gold-quartz veins. In Geology and mineral resource assessment of the Venezuelan Guayana Shield. Edited by U.S. Geological Survey and Corporation Venezolana de Guayana. Técnica Minera. C.A.. U.S. Geological Survey Bulletin 2062. p. 63-69.

Groves. D.I.. Goldfarb. R.J.. Gebre-Mariam. M.. Hagemann. S.G.. and Robert. F.. 1998. Orogenic gold deposits: A proposed classification in the context of their crustal distribution and relationship to other gold deposit types. Ore Geology Reviews. v. 13. p. 7-27.

Gruau. G.. Martin. H.. Leveque. B.. and Capdevilla. R.. 1985. Rb-Sr and Sm-Nd geochronology of Lower Proterozoic granite-greenstone terrains in French Guiana. South America. Precambrian Research. v. 30. p. 63-80.

Hagemann. S.G.. Gebre-Mariam. M.. and Groves. D.I.. 1994. Surface-water influx in shallow-level Archean lode-gold deposits in Western Australia. Geology. v. 22. p. 1067-1070.

Hallbauer. D.K.. and Voicu. G.. 1998. A geochemical assessment of the hydrothermal systems at the Omai gold mine. Guyana. from the composition of fluid inclusions in ore minerals and gangue. Geocongress'98. The Geological Society of South Africa. 8-10 July 1998. Extended Abstracts. p. 213-215.

Hodgson. C.J.. 1990. An overview of the geological characteristics of gold deposits in the Abitibi subprovince. University of Western Australia Geology Department Extension Publication v. 24. p. 63-100.

Hutchinson. R.W.. 1987. Metallogeny of Precambrian gold deposits: Space and time relationships. Economic Geology. v. 82. p. 1993-2007.

Jemielita. R.A.. Davis. D.W.. and Krogh. T.E.. 1990. U-Pb evidence for Abitibi gold mineralization postdating greenstone magmatism and metamorphism. Nature. v. 34. p. 831-834.

Keays. R.R.. and Scott. R.B.. 1976. Precious metals in ocean-ridge basalts: Implications for basalts as source rocks for gold mineralization. Economic Geology. v. 71. p. 705-720.

Kent. A.J.R.. Campbell. I.H.. and McCulloch. M.T.. 1995. Sm-Nd systematics of hydrothermal scheelite from the Mount Charlotte mine. Kalgoorlie. Western Australia: An isotopic link between gold mineralization and komatiites. Economic Geology. v. 90. p. 2329-2335.

Kerrich. R.. and Cassidy. K.F.. 1994. Temporal relationships of lode gold mineralization to accretion. magmatism. metamorphism and deformation - Archean to present: A review. Ore Geology Reviews. v. 9. p. 263-310.

Krogh. T.E.. 1990. Direct evidence for tectonic underplating in an Archean granulite-greenstone terrane. Am. Geophys. Union Trans. v. 71. p. 617.

Lafrance. J.. 1997. Métallogénie et contexte tectonique de l'indice St-Élie. Guyane française. Unpublished M.Sc. thesis. Université du Québec à Montréal. 123 p.

Marcoux. E.. and Milési. J.P.. 1993. Lead isotope signature in Early Proterozoic ore deposits in Western Africa: comparison with gold deposits in French Guiana. Economic Geology. v. 88. p. 1862-1879.

Milési. J-P.. Feybesse. J-L.. Ledru. P.. Dommanget. A.. Ouedraogo. M.F.. Marcoux. E.. Prost. A.. Vinchon. C.. Sylvain. J.P.. Johan. V.. Tegyey. M.. Calvez. J.Y.. and Lagny. P.. 1989. West African gold deposits in their Lower Proterozoic setting. Chronique de la Recherche Minière. v. 497. 98 p.

Milési. J-P.. Ledru. P.. Feybesse. J-L.. Dommanget. A.. and Marcoux. E.. 1992. Early Proterozoic ore deposits and tectonics of the Birimian orogenic belt. West Africa. Precambrian Research. v. 58. p. 305-344.

Milési. J-P.. Egal. E.. Ledru. P.. Vernhet. Y.. Thiéblemont. D.. Cocherie. A.. Tegyey. M.. Martel-Jantin. B.. and Lagny. P.. 1995. Les minéralisations du Nord de la Guyane française dans leur cadre géologique. Chronique de la Recherche Minière. v. 518. p. 5-58.

Mueller. A.G.. de Laeter. J.R.. and Groves. D.I.. 1991. Strontium isotope systematics of hydrothermal minerals from epigenetic Archean gold deposits in the Yilgarn block. Western Australia. Economic Geology. v. 86. p. 780-809.

Nesbitt. B.E.. St. Louis. R.M.. and Muehlenbachs. K.. 1987. Distribution of gold in altered basalts of D.S.D.P. hole 504B. Canadian Journal of Earth Sciences. v. 16. p. 201-209.

Norcross. C.. 1997. U-Pb geochronology of the Omai intrusion-hosted Au-quartz vein deposit and host rocks. Guiana Shield. South America. Unpublished M.Sc. thesis. University of Toronto. 65 p.

Norcross. C.E.. Davis. D.W.. and Spooner. E.T.C.. 1998. U-Pb geochronology of the Omai intrusion-hosted Au-quartz vein deposit and host rocks. Guyana. South America : GSA Annual Meeting. Oct. 26-29. 1998. Toronto. Abstracts with Programs. p. A-127.

Poitrasson. F.. Pin. C.. and Duthou. J-L.. 1995. Hydrothermal remobilization of rare earth elements and its effect on Nd isotopes in rhyolite and granite. Earth and Planetary Science Letters. v. 130. p. 1-11.

Renner. R.. and Gibbs. A.K.. 1987. Geochemistry and petrology of metavolcanic rocks of the early Proterozoic Mazaruni greenstone belt. northern Guyana. *In* Geochemistry and mineralization of Proterozoic volcanic suites. *Edited by* T.C. Pharaoh. R.D. Beckinsale. and D. Rickards. Geological Society Special Publication 33. Blackwell. Oxford. p. 289-314.

Samson. S.D.. Hibbard. J.P.. and Wortman. G.L.. 1995. Nd isotopic evidence for juvenile crust in the Carolina terrane. southern Appalachians. Contributions to Mineralogy and Petrology. v. 121. p. 171-184.

Snelling. N.J.. and McConnell. R.B.. 1969. The geochronology of Guyana. Geologie en Mijbouw. v. 48. p. 201-213.

Stevenson. R.. 1995. Crust and mantle evolution in the Late Archean: Evidence from a Sm-Nd isotopic study of the North Spirit Lake greenstone belt. northwestern Ontario. Canada. Geological Society of America Bulletin. v. 107. p. 1458-1467.

Voicu. G.. Bardoux. M.. Harnois. L.. Stevenson. R.. and Crépeau. R.. 1997a. Geochemical evolution of the Paleoproterozoic volcanic and plutonic rocks from Omai area. Guyana. South America: Implications for tectonic history and source regions: 30th International Geological Congress. Beijing. China. August 1-14. 1996. v. 2. 1. p. 101-114.

Voicu. G.. Bardoux. M.. Harnois. L.. and Crépeau. R.. 1997b. Lithological and geochemical features of igneous and sedimentary rocks at the Omai gold mine. Guyana. South America. Exploration and Mining Geology. v. 6. 2. p. 153-170.

Walrond. G.W.. 1987. Geological map of Guyana. scale 1: 1 million: Guyana Geology and Mines Commission. Georgetown. Guyana.

Zweng. P.L.. Mortensen. J.K.. and Dalrymple. G.B.. 1993. Thermochronology of the Camflo gold deposit. Malartic. Quebec: Implications for magmatic underplating and the formation of gold-bearing quartz veins. Economic Geology. v. 88. p. 1700-1721.

CHAPTER V

MINERALOGICAL NORM CALCULATIONS APPLIED TO TROPICAL WEATHERING PROFILES

5.1 INTRODUCTION

The special climatic and geomorphologic conditions prevailing in tropical regions have a direct influence on the supergene alteration processes. The mineralogical composition of the tropical weathering products is very different from that of the initial unaltered rock or from the equivalent weathering products in the temperate and cold climatic regions. The various methods proposed for the calculation of the normative mineralogy of the igneous and metamorphic fresh rocks are based only on primary minerals, without considering the mineral phases resulted by alteration processes. For tropical profiles, characterized by various degree of mineral weathering leading to the formation of mixtures of relict primary and neoformed secondary phases, these methods cannot be applied. A calculation method formulated for bauxitic laterites, but which is not useful for determining the mineralogical norm of other types of saprolite and laterite profiles, has been proposed by Nyobe (1991).

The purpose of the present paper is to present a new algorithm leading to the conversion of the whole-rock chemical analyses into normative mineralogical percentages, which can be used for various tropical weathering components. The algorithm gives good results and the normative minerals are closer to the real mineralogy of the weathered profile when the rocks are intensively altered, with the chemical index of alteration (CIA: Nesbitt and Young, 1982; Fedo et al., 1995) greater than 80. This value corresponds to a mineralogical index of alteration (MIA, proposed in this paper) greater than 60. Geologic systems, however, are not simple, and a single calculated value may not adequately reflect their complexities. Due to the highly variable mineralogy and, sometimes, to the poor crystallinity of the neoformed mineral phases, the present norm calculations only illustrate trends in the weathering profile composition. The algorithm used for norm calculations is based on a number of simplifications and assumptions. The main simplification is that the minerals used in the norm have their stoichiometrically

ideal compositions. excluding any substitutions (except Al-goethite). The ubiquitous occurrence of pure and mixed amorphous phases of Al. Si. Mn. and Fe. which cannot be reported by X-ray diffraction and are rarely considered. yet abundant in some saprolite profiles. are integrated in the calculations of their crystallized equivalents (kaolinite. gibbsite. pyrolusite. etc.) and as amorphous silica. The main assumption is that the mineralogical index of alteration of a sample is the same for all its mineralogical pairs used for the partition of a chemical element between a primary and its equivalent secondary mineral. The norm computations may give interesting indications of the changes in mineralogy with depth in the composition of a weathering profile. may help to determine local zones depleted/enriched in certain chemical elements. or may give a warning of unusual compositions. which should be followed up by detailed mineralogical analysis. In this paper. the examples used for the application of the mineralogical norm calculations are constrained by semi-quantitative/qualitative XRD analyses. The similarity between the two sets of results provides additional credence to the normative calculations.

The algorithm has been used in MINNOR. a WINDOWS application which performs mineralogical norm calculations and plots frequency histograms of the normative minerals.

5.2 WEATHERING PROFILE

The terminology used for tropical regolith represents the subject of many recent studies (Lecomte. 1988: Butt and Zeegers. 1989. 1992: Bàrdossy and Aleva. 1990: Tardy. 1992: Lawrance. 1994). The multitude of terms used to describe each horizon. makes it difficult to apply a uniform scheme for the description and terminology of the lateritic profiles. For the purposes of this paper. we have used the terminology of Butt and Zeegers (1992) and Bàrdossy and Aleva (1990).

Although the supergene processes are integrated and complex. specific supergene alteration horizons are produced within the regolith. Some of these horizons are characterized by secondary mineral formation. associated with important isovolumetric changes. but with preservation of primary rock fabric by weathering products (Lawrance. 1994). These horizons define the saprolith. which generally comprises at least 2/3 of the whole weathering profile. It can be subdivided in two zones: at the base. the saprock. which represents slightly weathered rock. with an arbitrary upper limit of 20% weatherable minerals altered (Trescases. 1992). The upper part of the saprolith is defined as saprolite. which can be subdivided into coarse (containing remnants of unweathered bedrock) and fine (without remnants of unaltered bedrock) saprolite. The algorithm for the norm calculation proposed in this paper cannot be used for saprock and coarse saprolite.

The upper part of the regolith. affected by surface oxidation associated with volumetric changes. and characterized by total extinction of the parent rock fabric and the development of new fabric. is defined as pedolith or laterite *sensu stricto*. At the lower part. the pedolith consists of a mottled clay zone. characterized by localized spots. patches. and streaks of Fe oxides and oxy-hydroxides in an argillaceous matrix. The middle part is defined as duricrust. which represents a highly indurated zone. composed of ferruginous. aluminous. siliceous or calcareous material. with a pisolithic. botryoidal or massive fabric. The ferruginous duricrust is a highly weathered material consisting mainly of Fe oxides and oxy-hydroxides. with variable amounts of Al hydroxides. silica and phyllosilicates. It is normally referred to as ironstone or ferricrete. The aluminous duricrust is characterized by a major enrichment of free Al hydroxide minerals and it is refered to as bauxitic laterite. This term may include also aluminous mottled clay zone and even alumina-rich saprolite. The siliceous (or silcrete) and calcareous (or calcrete) duricrust represent strongly silicified/carbonatized indurated material formed by *in situ*

cementation/replacement of pre-existing regolith. The upper part of the pedolith is affected by surface physical and chemical reworking of the duricrust. which may separate pisoliths from their matrix. resulting in a lateritic gravel. Thin residual soils can also develop at the surface. containing secondary and resistent primary minerals.

5.3 NORMATIVE MINERALS

The minerals used in weathering norm are represented by three primary minerals. six secondary minerals. four primary/secondary mineral pairs. and five minerals which can have both primary and secondary origin. These minerals have been selected on the basis of their frequency in the published mineralogical data for supergene alteration profiles and of chemical and mineralogical data obtained for the weathering profile of Omai. Guyana. Most of the abbreviations for these minerals are from Cross et al. (1903) and Kretz (1983). The complete list of the minerals used in normative calculations and their symbols is presented in Table 5.1.

5.3.1 Primary minerals

Ilmenite (FeOxTiO$_2$) occurs as an inherited heavy mineral in weathering profiles derived from igneous and metamorphic rocks. especially from the more mafic types (Allen and Hajek. 1989). Its average content is less than 1%. exceptionally 5%. In supergene environments. ilmenite frequently transforms first to pseudorutile and then to anatase within porous leucoxene grains.

Magnetite (FeOxFe$_2$O$_3$). All magnetite reported from the weathering profiles is a relict mineral. inherited from the parent rock. It generally represents less than 2% in bauxitic laterite and saprolith. and up to 8% in the ferruginous horizons and over

Table 5.1   Symbols for the weathering profile-forming minerals

Minerals	Symbols	Minerals	Symbols
Albite	Ab	Ilmenite	Ilm
Anatase	Ant	Kaolinite	Kln
Anorthite	An	Magnetite	Mag
Apatite	Ap	Montmorillonite	Mnt
Boehmite	Bhm	Orthoclase	Or
Calcite	Cal	Pyrolusite	Pyt
Chlorite	Chl	Quartz	Qtz
Corundum	Crn	Sericite	Ser
Gibbsite	Gbs	Amorphous silica	Sil
Al-Goethite	Al-Gt	Epidote	Ep
Hematite	Hem	Pyroxene	Px

BIFs. Partial or complete oxidation of the magnetite leads to the formation of its isostructural form. maghemite (γ-Fe_2O_3). frequently described in the superficial horizons. The normative magnetite calculated in this paper represents the total amount of magnetite + maghemite.

Apatite ($CaOxP_2O_5$). Phosphate minerals make up only a very small percentage of the weathering profiles. Their direct determination is difficult because P_2O_5 is only a minor constituent. ranging from 0.02 to 0.5%. A large fraction of it is organic (Lindsay et al.. 1989). Apatite is the most commonly listed inorganic soil phosphate. but it usually represents less than 0.5%. The P_2O_5 content remained unused in some samples after the normative apatite calculation may be considered as representing organic phosphorus.

5.3.2 Secondary minerals

Pyrolusite (MnO_2) is used as a general mineralogical term for the Mn oxide and hydroxide minerals decribed in the supergene environments. The mineralogy of Mn is complicated by the large number of chemical substitutions. resulting in the formation of continuous series of compositions from MnO to MnO_2. within which a number of stable and metastable arrangements of atoms form a variety of minerals. As Mn is generally leached in weathering profiles. the amount of the Mn-bearing minerals is usually less than 0.5%. However. the Mn oxides can be enriched (up to 5%. Séa et al.. 1994) in profiles developed on Mn-rich parent rocks or on certain ultramafic rocks.

Al-Goethite [($Fe_{1.60}Al_{0.40})_{\Sigma 2.0}O_3xH_2O$] is considered the most widespread Fe mineral in ferruginous (up to 50-60%) and bauxitic (between 1 to 30%) laterites. The amount of Al substitution for Fe in the goethite structure is often considerable. varying between 4 to 30% (Allen and Hajek. 1989). Higher Al substitution has been observed in

goethite from extremely weathered profiles. comparatively to the goethite formed in reductomorphic environments. A synthesis of the published data for Al substitution in goethite in various weathered profiles (Allen and Hajnek. 1989: Bárdossy and Aleva. 1990: Oliveira and Campos. 1991) indicates a mean value of 20%. which has been used for the Al-goethite normative calculations.

Kaolinite ($2SiO_2xAl_2O_3x2H_2O$) is the most frequent silicate mineral formed in all types of weathering profiles. It has been commonly described as a weathering product of almost all primary silicate minerals. including mainly feldspar. muscovite and biotite. Minor isomorphous substitution of Fe^{3-} in the octahedra of kaolinite has been sometimes reported in poorly crystallized kaolinites. but the substitution ratio do not justify the Fe consideration in the chemical formula. Halloysite. another 1:1 phyllosilicate. and its dehydrated form. metahalloysite. are also frequently reported in the weathering profiles. but not as common as kaolinite. The halloysite stability under weathering conditions has been subdivided (Allen and Hajek. 1989) into an initial stage of hydrated halloysite followed by a more stable metahalloysite stage. As metahalloysite and kaolinite have the same stoichiometric formula. the normative kaolinite calculated in this paper may be interpreted as representing the total amount of these two minerals.

Gibbsite ($Al_2O_3x3H_2O$) is a product of extremely advanced weathering. formed by the desilication of kaolinite or by direct weathering of feldspar and biotite. It is the main alumina mineral in the lateritic bauxites (Bàrdossy and Aleva. 1990). where the amount of gibbsite generally ranges from 40 to 70%. but values up to 90% are not uncommon. Gibbsite may also be present in minor amount in coarse saprolite. close to the contact with the bedrock. or in the upper saprolite. interlayered with kaolinite-rich horizons (Tardy. 1992).

Boehmite ($Al_2O_3xH_2O$) forms in some bauxitic profiles. particulary those located close to the edge of a plateau and in an horizon close to the soil surface (Tardy. 1992). When this occurs. goethite disappears and hematite becomes the single iron mineral present. Boehmite has been not described in saprolite or ferruginous laterites.

Amorphous silica (SiO_2xH_2O). Amorphous phases represent a major problem of the weathering profiles and are not entirely confined to silica. Amorphous Al oxy-hydroxides may comprise over 30% of some bauxitic laterites. and amorphous Al silicates. with variable Al/Si ratios. are abundent in some saprolites and soils. especially over the felsic rocks. They "crystallize" to a mixture of poorly ordered kaolinite and amorphous silica. The amorphous silica (opal) can also have an organic origin. especially in soils and in the upper parts of the weathering profiles. The few published data on the amorphous silica in the supergene environments do not give a good idea about its occurence in different weathering horizons.

5.3.3 Primary/secondary mineral pairs

Chemical weathering strongly affects the mineralogy and major-element geochemistry of the unaltered bedrock. The degree of weathering. which must yield distinct values for different weathered materials. can be evaluated by quantitative measures. using the whole-rock cheminal analyses. These values. representing the average weathering index for each analyzed system (sample). can also be applied for the determination of the weathering index of each separate mineralogical component of the system. Several primary/secondary mineral pairs can be considered as reflecting the degree of weathering of the entire system. The principal condition is to consider the system as closed. without mass transfer (loss or gain). This mineralogical index of

weathering can be further used in normative calculations for the partitioning of the chemical elements between several pairs of primary and their equivalent altered minerals.

The first step is represented by the calculation of the chemical index of alteration (CIA; Nesbitt and Young, 1982; Fedo et al., 1995) for each analyzed sample, using the following equation:

$$CIA = [Al_2O_3/(Al_2O_3 + CaO + Na_2O + K_2O)] \times 100 \quad (1)$$

The equation yields values between 50 and 60 for incipient weathering, between 60 and 80 for intermediate weathering, and more than 80 for intense to extreme weathering. Usually, the lower part of the weathering profile has CIA values between 60 and 90, and the upper part more than 80, frequently between 95 and 100.

Because CIA values range between 50 and 100 and can not be directly applied to the normative calculations, a second calculation is requested using the mineralogical index of alteration (MIA):

$$MIA = 2 \times (CIA - 50) \quad (2)$$

The mineralogical index of alteration evaluates the degree of mineralogical weathering, i.e. the transformation ratio of a primary mineral into its equivalent alteration mineral. MIA yields values between 0 and 100, and reflects incipient (MIA<20), intermediate (MIA=20-60), and intense to extreme (MIA>60) mineralogical transformation. The value of 100 means complete transformation of a primary mineral into its equivalent alteration product. The calculated MIA values are further used for partitioning the major oxides between the pairs of primary/ secondary minerals. As an example, MIA value of 60 means that for the albite/montmorillonite pair, 60% of the

Na_2O content is used for the normative montmorillonite calculation (secondary mineral) and 40% for the normative albite calculation (primary mineral).

Anorthite ($CaOx2SiO_2xAl_2O_3$)/Epidote ($4CaOx3Al_2O_3x6SiO_2xH_2O$) pair represents minor Ca-bearing mineral phases reported only in saprolite. Their total amount does not exceed 1%. Anorthite in supergene environments is greatly dependant on the presence or absence of plagioclases in the parent rock. It weathers out rapidly even in temperate regions. Epidote is considered as a secondary mineral formed by weathering of calcic plagioclase. Its stability in supergene conditions is comparable to that of quartz. ilmenite and sphene (Allen and Hajek. 1989).

Orthoclase ($K_2Ox6SiO_2xAl_2O_3$)/Sericite($K_2Ox6SiO_2x3Al_2O_3x2H_2O$) pair represents the main K-bearing minerals in the weathering profile. especially in the saprolite. Locally , the saprolite formed over K-rich parent rocks. may contain up to 25% sericite. For the purposes of the present paper. the sericite represents the mixture of more or less altered muscovite. phlogopite and biotite. In the bauxitic laterite. further potassium leaching has as result partial or total transformation of these minerals first into illite and then into kaolinite.

Pyroxene ($2MgOx2SiO_2$)/Chlorite ($5MgOx3SiO_2xAl_2O_3x4H_2O$) pair represents an important indicator of the intensity of weathering. In normative calculation. Mg-bearing orthopyroxene (enstatite) is used. For the saprolite formed over the olivine-rich ultrabasic rocks. enstatite can be replaced by forsterite. which have the same stoichiometric formula. If the primary minerals are represented by amphiboles instead of pyroxenes. the normative enstatite represents in fact antophyllite-cummingtonite mixture. but the calculated content must be considered as semi-quantitative/qualitative. Chlorite is considered as an alteration product of pyroxenes/ amphiboles and it is

calculated as its Mg-bearing form (clinochlore). Even if chlorite is the main Mg-mineral phase in the saprolite. other Mg-bearing alteration minerals (serpentine. talc) can form. especially over ultramafic rocks. In this situation. the calculated amount of normative chlorite represents in fact a mixture of serpentine/talc. Because there are differences between their stoichiometric formulas. the normative serpentine/talc content must be considered as a semi-quantitative/qualitative value. Mg-bearing minerals are almost completely leached from the upper part of the saprolite and overlying horizons. Only small amounts of chorite have been reported from the mottled clay zone and the ferruginous/bauxitic laterites. The amount of Mg increases in the saprolite towards the parent rock.

Albite $(Na_2Ox6SiO_2xAl_2O_3)$/Montmorillonite $(Na_2OxAl_2O_3x5SiO_2xH_2O)$ pair. Because only few soil smectites have the ideal stoichiometric composition and most are not completely dioctahedral or trioctahedral. montmorillonite is used for the normative calculation purposes as a generic term for the smectite group. including beidellite and nontronite. These Na-bearing minerals are confined to the lower part of the saprolite. Albite content increases and montmorillonite content decreases with depth in weathering profiles. presumably due to a diminution in alteration intensity. Rare and insignificant quantities of these minerals have been described in feruginous and bauxitic laterite.

5.3.4 Primary and secondary minerals

Calcite $(CaCO_3)$ represents a primary mineral in the lower part of the saprolite and a secondary one in the upper part of the lateritic profile and bauxite deposits. Usually it is less than 1%. The amount of calcite drastically increases in the calcareous

laterite (up to 80%). The calcite resulted by using MINNOR is greatly dependant on the accuracy of the CO_2 analytical determination.

Anatase (TiO_2). Most of the titanum oxide is present as neoformed anatase. with average content between 1-4%. but primary rutile is also reported. usually less than 1%. Brookite. the third titanum oxide polymorph. is a very rare inherited mineral in bauxitic laterite. Because in the mineralogical norm calculations it is impossible to make the distinction between the three polymorphs. the anatase calculated using MINNOR represents in fact the total quantity of the three titanum oxides.

Hematite (Fe_2O_3) represents a common iron oxide in the mottled clay zone. duricrust and bauxitic laterite (Boeglin and Mazaltarim. 1989: Bàrdossy and Aleva. 1990: Zang and Fyfe. 1993). It is a rare mineralogical phase in saprolite. where generally goethite/hematite ratio is greater than 5. Most of the hematite has a secondary origin. but it has been also reported as a inherited primary mineral. Aluminium can replace iron in the hematite structure. but to a lesser extent than in goethite. The degree of substitution ranges from 1 to 10 mol% Al_2O_3. most frequently from 2 to 5 mol%. Because Al substitution in the hematite structure is missing in many weathering profiles. we have prefered for the normative calculations to use the stoichiometric formula of hematite.

Corundum (Al_2O_3) has been reported as associated with magnetite and maghemite from the upper part of the bauxitic laterite deposits. In saprolite and mottled clay zone it represents a relict mineral inherited from the parent rock. In duricrust. corundum may reach up to 10% and it is associated with iron oxy-hydroxides. A decrease in water activity at a constant temperature or an increase in temperature at a constant water activity may induce gibbsite and/or boehmite dehydration. resulting in the formation of secondary corundum (Nahon and Tardy. 1992).

Quartz (SiO_2) is very common in most lateritic regoliths. In bauxitic laterite. the quartz represents a relict mineral inherited from silicic sedimentary and igneous parent rocks. It can also be abundant as a secondary mineral in lateritic regoliths formed over ultramafic rocks in most climatic environments. and over most lithologies. especially felsic. in arid environments.

5.4 CALCULATION PROCEDURES OF THE WEATHERING NORM (WN) AND COMMENTS

The calculation procedures of the WN include several steps as follows:

(1) Form the molecular proportions by dividing the weight percent of each analyzed oxide by its molecular weight.

(2) Calculate the chemical index of alteration (CIA).

(3) Calculate the mineralogical index of alteration (MIA).

(4) If CaO>0. go to (5). If CaO=0. go to (9).

(5) If CO_2>0. form calcite and then go to (6). Remaining CaO becomes CaO^1. If CO_2=0. go to (6).

The amount of calcite is greatly dependent on the accuracy of the CO_2 analytical determination. Missing data for CO_2 do not affect the program running. but calcite is not calculated. influencing the norms of other Ca-bearing minerals (anorthite. apatite. epidote). However. the error in this case is less than 0.5%. If the samples are from a calcrete horizon. the CO_2 content must be absolutely analyzed.

(6) If $P_2O_5 > 0$. form apatite and go to (7). Remaining CaO^1 becomes CaO^2. If $P_2O_5 = 0$. go to (8).

(7) If $CaO^2 > 0$. go to (8). If $CaO^2 = 0$. go to (9).

(8) Form the anorthite/epidote pair using for partitioning the MIA values. and then go to (9). Remaining SiO_2. Al_2O_3. and H_2O become SiO_2^1. $Al_2O_3^1$. and H_2O^1. respectively.

(9) If $FeO > 0$. form ilmenite and then go to (10). Remaining FeO and TiO_2 become FeO^1 and TiO_2^1. respectively. If FeO=0. go to (11).

Certain analytical technics do not distinguish between the ferric and ferrous iron content. Because their proportions have an important effect on the norm calculations. the program provides two different ways of allocating the iron:

(a) If the FeO and Fe_2O_3 values are reported in the chemical analyses. the program uses these values as entered.

(b) The second procedure can be used only if the weathering profile is considered as a closed system. FeO and Fe_2O_3 are initially recalculated following the method used for unaltered rocks suggested by Irvine and Baragar (1971):

$$FeO^* = (0.863 \times Fe_2O_3T) - 0.0065 \quad (3)$$

$$Fe_2O_3^* = (0.152 \times Fe_2O_3T) - 0.0073 \quad (4)$$

where FeO^* and $Fe_2O_3^*$ represent the iron content in the hypotetical unaltered protolith.

Further. the following equations are used in order to allocate the iron:

$$FeO = FeO^* \times (100 - MIA)/100 \quad (5)$$

$$Fe_2O_3 = (FeO^* - FeO) \div Fe_2O_3^* \quad (6)$$

These equations have been tested on hundreds of published chemical analysis of the weathering profiles. with both FeO and Fe_2O_3 reported. The differences between calculated and reported contents do not exceed 2%.

(10) Form magnetite from FeO^1 and Fe_2O_3 and go to (11). Remaining Fe_2O_3 becomes $Fe_2O_3^{1}$.

(11) Form anatase from TiO_2^{1} and go to (12).

(12) Form the orthoclase/sericite pair from K_2O. SiO_2^{1}. $Al_2O_3^{1}$. and H_2O^{1} using the MIA values and go to (13). Remaining oxides become SiO_2^{2}. $Al_2O_3^{2}$. and H_2O^{2}.

(13) Form the pyroxene/chlorite pair from MgO. SiO_2^{2}. $Al_2O_3^{2}$. and H_2O^{2} using the MIA values and go to (14). Remaining oxides become SiO_2^{3}. $Al_2O_3^{3}$. and H_2O^{3}.

(14) Form the albite/montmorillonite pair from Na_2O. SiO_2^{3}. $Al_2O_3^{3}$. and H_2O^{3}. using the MIA values and go to (15). Remaining oxides become SiO_2^{4}. $Al_2O_3^{4}$. and H_2O^{4}.

(15) Form pyrolusite and go to (16).

(16) Form Al-goethite from $Fe_2O_3^1$. $Al_2O_3^4$ and H_2O^4. and go to (17). Remaining oxides become $Fe_2O_3^2$. $Al_2O_3^5$. and H_2O^5.

(17) Form hematite from $Fe_2O_3^2$ and go to (18).

Hematite forms only when $Fe_2O_3^2$ is in excess comparatively to H_2O^5 after the Al-goethite formation. It is usually the case of the ferruginous laterite profiles. where the iron content is relatively high in respect to the water content.

(18) Form kaolinite from SiO_2^4. $Al_2O_3^5$. and H_2O^5 and go to (19). Remaining oxides become SiO_2^5. $Al_2O_3^6$. and H_2O^6.

Kaolinite forms until one of the three oxides is entirely consumed. For the bauxitic laterite. characterized by weak silica content. SiO_2 is the first entirely consumed oxide. For the ferruginous laterite. the water is first consumed due to the important quantity used in the Al-goethite calculation. For the saprolite and the siliceous/ calcareous laterite. any of these oxides may be first totally used.

(19) If $Al_2O_3^6 \le H_2O^6$. form boehmite and return to (16). Cancel goethite and kaolinite and go to (17). Form hematite and go to (19). Recalculate the normative boehmite and go to (21). Remaining H_2O becomes $H_2O^7_{(Bhm)}$. If $Al_2O_3^6 > H_2O^6$. go to (20).

As mentioned earlier. boehmitic profiles of the bauxitic laterites are characterized by the lack of kaolinite and the exclusive presence of hematite. instead of Al-goethite-hematite association described in the gibbsitic profiles. The procedure used in (19) allocates all available iron to hematite when the alumina/water ratio allows the boehmite formation.

(20) Form gibbsite and go to (21). Remaining oxides become $Al_2O_3^-$ and $H_2O^-_{(Gibs)}$.

(21) Form amorphous silica from SiO_2^{-5} and $H_2O^-_{(Bhm)}$ or from SiO_2^{-5} and $H_2O^-_{(Gibs)}$ and go to (22). Remaining silica becomes SiO_2^6.

(22) Form corundum from $Al_2O_3^7$ and go to (23).

(23) Form quartz from SiO_2^6.

(24) Calculate the normative weight percents by multiplying the molecular proportions of each mineral by its molecular weight.

5.5 THE MINNOR PROGRAM DESCRIPTION

MINNOR is an application for WINDOWS written in Visual Basic for IBM-compatible computers. The program requires Microsoft WINDOWS 3.1x and runs from the hard-disk. It can be installed using Setup.exe command. The program allows a user to create a file by clicking the 'Create File' button. The user must give a file name (which automatically registers with .trs suffix) and the number of analysed samples. The program opens a table with a number of rows equal with the number of samples. The table contains sample name and twelve major oxides. For the calculation of calcite. CO_2 values are requested. If both FeO and Fe_2O_3 are analyzed. and FeO=0. the user must enter 0.01. in order to avoid the allocating of iron. Missing analytical data for one or more oxides does not affect the program running. but. given the interdependence of variables in normative calculations. the obtained results are erroneous. The file can be saved using the 'Save File' button. 'Close' button close the file without saving it.

In order to see or to add more analysed samples in an already existing file. the user must click the 'Open File' button.

'Run using...' button allows to perform mineralogical norm calculations. The user must choose the file (from hard-disk or floppy-disk) and. after clicking the 'Open File' button. the program plots the percentages of the normative minerals from the first sample. By clicking 'Forwards' and 'Backwards' buttons. the user can see the mineralogical norm for each sample of the file. By clicking the downpage buttons. the program plots histograms for each normative mineral from all samples of the file.

5.6 APPLICATIONS

In order to test the program. three different types of tropically weathered profiles have been choosen: a bauxitic laterite deposit from Cameroon (Nyobe. 1991). a ferruginous laterite profile from Burkina Faso (Boeglin and Mazaltarim. 1989) and a complete weathered profile from Omai. Guyana (Voicu and Bardoux. 1995).

Bauxitic laterite deposit. The chemical analyses of eight bauxitic laterite samples (data from Nyobe. 1991) are stored in the Cameroon.trs file. Because the iron is reported as Fe_2O_3 total. the program has automatically allocated the iron content between Fe_2O_3 and FeO. CO_2 has not been analysed. The comparison between the results obtained for the normative minerals using MINNOR and chemical calculations of Nyobe (1991) are presented in Table 5.2. The two methods give similar results. but the calculations using MINNOR are developed for a wider range of normative mineral phases. The normative mineral assemblages are constrained by qualitative modal estimates obtained by X-ray powder diffraction.

Table 5.2   Comparison between the normative mineral calculations for bauxitic laterite from Fongo Tongo deposit, Cameroon, using the method of Nyobe (1991) and MINNOR

Mineral

Sample	Ab	Ant	An	Ap	Bhm	Cal	Chl	Crn	Gbs	Al-Gt(□)	Hem	Ilm	Kln	Mag	Mnt	Or	Pyl	Qtz	Ser	Sil	Ep	Px
1*	0.00	1.76	0.00	nc	nc	nc	0.00	1.94	78.31	12.71	nc	nc	4.39	nc	nc	nc	0.00	0.00	nc	nc	nc	nc
1**	0.00	1.72	0.00	0.15	0.00	0.00	0.43	0.49	78.40	11.88	2.28	0.06	3.53	0.00	0.15	0.00	0.04	0.00	0.25	0.00	0.13	0.00
2*	0.00	1.82	0.00	nc	nc	nc	0.56	0.00	78.31	10.02	nc	nc	8.78	nc	nc	nc	0.00	0.00	nc	nc	nc	nc
2**	0.00	1.80	0.00	0.10	0.00	0.00	0.68	0.00	76.62	9.49	1.82	0.02	8.23	0.00	0.07	0.00	0.05	0.00	0.25	0.00	0.08	0.00
3*	0.52	1.19	0.00	nc	nc	nc	0.00	4.79	80.65	5.52	nc	nc	7.22	nc	nc	nc	0.00	0.00	nc	nc	nc	nc
3**	0.00	1.17	0.00	0.06	0.00	0.00	0.32	4.13	80.65	5.15	0.98	0.02	6.78	0.00	0.38	0.00	0.02	0.00	0.33	0.00	0.08	0.00
4*	0.00	1.84	0.00	nc	nc	nc	0.00	4.08	80.96	7.35	nc	nc	4.90	nc	nc	nc	0.00	0.00	nc	nc	nc	nc
4**	0.00	1.84	0.00	0.03	0.00	0.00	0.46	3.27	81.02	7.24	1.39	0.00	4.28	0.00	0.15	0.00	0.02	0.00	0.08	0.00	0.02	0.00
5*	0.00	1.84	0.00	nc	nc	nc	0.00	0.92	80.65	9.13	nc	nc	6.97	nc	nc	nc	0.09	0.00	nc	nc	nc	nc
5**	0.00	1.82	0.00	0.03	0.00	0.00	0.49	0.00	80.51	8.56	1.64	0.02	6.25	0.00	0.15	0.00	0.10	0.00	0.25	0.00	0.02	0.00
6*	0.00	1.61	0.00	nc	nc	nc	0.00	3.06	81.74	8.01	nc	nc	4.90	nc	nc	nc	0.00	0.00	nc	nc	nc	nc
6**	0.00	1.59	0.00	0.03	0.00	0.00	0.33	2.20	81.82	7.59	1.45	0.02	4.25	0.00	0.15	0.00	0.04	0.00	0.16	0.00	0.02	0.00
7*	0.00	1.26	0.00	nc	nc	nc	0.00	4.08	73.94	14.95	nc	nc	5.93	nc	nc	nc	0.18	0.00	nc	nc	nc	nc
7**	0.00	1.23	0.00	0.03	0.00	0.00	0.27	2.43	74.07	13.57	2.60	0.04	5.26	0.00	0.07	0.00	0.14	0.00	0.25	0.00	0.02	0.00
8*	0.00	1.13	0.00	nc	nc	nc	0.00	6.12	56.16	12.64	nc	nc	22.70	nc	nc	nc	0.18	0.00	nc	nc	nc	nc
8**	0.00	1.11	0.00	0.03	0.00	0.00	0.33	4.66	56.31	11.90	2.28	0.02	21.93	0.00	0.07	0.00	0.17	0.00	0.25	0.00	0.02	0.00

nc = not considered; (□) = Al-goethite has been calculated by Nyobe (1991) as goethite; (*) = normative minerals using the method of Nyobe (1991); (**) = normative minerals using MINNOR

Ferruginous lateritic profile. The mean values of 224 chemical analyses (Boeglin and Mazaltarim. 1989) of ironstones of the Gaoua area in Burkina Faso are stored in the Burkina.trs file. Because the iron content is reported as Fe_2O_3 total. the program has allocated the iron using the equations (3)-(6). The mineralogical composition of each sample has been determined by X-ray powder diffraction. The peak characteristics have allowed a quantitative estimation of the principal ironstone-forming minerals. Accesory minerals have not been considered. The comparison between the quantitative composition determined by XRD of the principal minerals and the same minerals using the normative calculations is presented in Table 5.3. The results obtained by these two different approaches are similar. It is to note that the composition of all normative minerals is in the standard deviation limits reported by Boeglin and Mazaltarim (1989).

Complete weathered profile. Nine selected whole-rock chemical analyses of all distinctive horizons of the weathering profile from Omai. Guyana. South America (Voicu and Bardoux. 1995: Voicu et al.. 1996) are shown in Table 5.4. They are stored in the Guyana.trs file. The iron. reported as Fe_2O_3 total. has been partitioned between the two iron oxides. CO_2 content has not been analysed. The weathering norm (WN) for each sample is presented in Table 5.5. Mineralogical norm values are concordant with the semi-quantitative XRD determinations. Normative mineral histograms plotted with MINNOR for goethite. kaolinite. sericite and quartz are shown in Fig. 5.1. The variation of the normative mineralogy observed in the same horizon or between the different horizons of the weathering profile suggests that the supergene alteration processes have been greatly influenced by the protolith composition and by locally enhanced permeability created by structural discontinuities including faults joints and lithologic contacts. These discrete structures. frequently observable at Omai. may initially weather and erode rapidly. creating favorable conditions to focus meteoric waters and to become

Table 5.3 Comparison between the mineralogical compositions of ironstones of the Gaoua area in Burkina Faso determined by semi-quantitative XRD method and normative mineralogical compositions using MINNOR

Samples Minerals (in wt%)	20-25% (n=1)	25-30% (n=5)	30-35% (n=19)	35-40% (n=25)	40-45% (n=48)	45-50% (n=76)	50-55% (n=43)	55-60% (n=7)
Qtz(*)	51	42	37	25	17	11	6	3
Qtz-Sil(**)	52.05	41.96	37.93	26.26	19.27	13.39	7.45	4.02
Kln(*)	22	26	26	30	32	33	34	31
Kln(**)	18.42	20.21	20.78	26.14	27.53	28.78	28.37	27.03
Gt-Hem(*)	27	32	38	43	49	55	59	66
Al-Gt-Hem-Mag(**)	27.23	31.82	46.26	42.47	47.96	53.03	57.44	61.27
Gbs(*)	0	0	0	2	1	1	0	0
Gbs(**)	0	0	0	0	0	0	0	0

Sample names represent their iron content: n = number of analysed samples: (*) = mineralogical composition determined by semi-quantitative XRD method (data from Boeglin and Mazaltarim, 1989, Table III) - only the principal mineralogical phases are determined: (**) = normative mineralogical composition using MINNOR - only the same minerals determined by XRD method are shown

Table 5.4   Chemical analyses for the weathering profile from Omai, Guyana

Sample	S2	S6	702	738	1423	3432	1cw	1dw	1aw
Oxides	Saprolite	Saprolite	Saprolite	Saprolite	Mottled clay zone	Mottled clay zone	Mottled clay zone	Siliceous duricrust	Pisolith
SiO_2	70.21	51.36	45.70	69.30	48.86	56.67	56.20	61.34	65.88
TiO_2	1.28	1.27	2.32	0.62	1.89	1.16	1.72	0.86	1.38
Al_2O_3	19.85	19.71	33.88	19.92	33.12	18.59	27.92	10.71	20.63
Fe_2O_3	0.65	17.98	4.52	1.44	2.78	11.09	2.01	22.29	4.51
FeO	0.17	0.35	0.01	0.42	0.05	2.40	0.06	0.21	0.01
MgO	0.13	0.13	0.07	0.14	0.07	1.45	0.10	0.00	0.01
CaO	0.21	0.15	0.01	0.01	0.00	0.13	0.00	0.00	0.02
Na_2O	2.35	0.07	0.05	0.25	0.05	1.42	0.02	0.00	0.02
K_2O	0.30	0.01	0.02	2.81	0.34	0.63	0.51	0.06	0.24
MnO	0.01	0.06	0.01	0.01	0.01	0.02	0.01	0.01	0.01
P_2O_5	0.02	0.03	0.07	0.02	0.05	0.08	0.06	0.09	0.05
H_2O	4.25	9.80	13.91	5.25	13.03	6.53	11.25	5.22	7.80
CO_2	na	na	na	na	na	na	na	na	na
Total	99.55	100.79	100.65	100.27	100.33	100.15	100.77	100.82	100.77
MIA	74.81	97.69	99.58	73.29	97.61	79.00	96.27	98.88	97.32

na = not analysed; MIA = mineralogical index of alteration, calculated using the equation (2) (see text);
FeO calculated using the equations (3) - (6) (see text)

Table 5.5   Mineralogical norm of the weathering profile at Omai. Guyana

Sample	S2	S6	702	738	1423	3432	1cw	1dw	1aw
Minerals	Saprolite	Saprolite	Saprolite	Saprolite	Mottled clay zone	Mottled clay zone	Mottled clay zone	Siliceous duricrust	Pisolith
Ab	5.00	0.01	0.00	0.56	0.01	2.52	0.00	0.00	0.00
Ant	1.09	0.88	2.30	0.14	1.83	0.00	1.65	0.62	1.26
An	0.26	0.01	0.00	0.01	0.00	0.13	0.00	0.00	0.00
Ap	0.02	0.04	0.00	0.02	0.03	0.11	0.00	0.00	0.06
Bhm	0.00	0.00	0.00	0.00	0.00	0.00	0.00	0.00	0.00
Cal	0.00	0.00	0.00	0.00	0.00	0.00	0.00	0.00	0.00
Chl	0.26	0.34	0.19	0.28	0.18	3.15	0.26	0.00	0.02
Crn	4.71	0.00	0.00	0.00	0.00	0.00	0.00	0.00	0.00
Gbs	0.00	0.00	0.00	0.00	0.00	0.00	0.00	0.00	0.00
Al-Gt	0.67	18.71	4.70	1.49	2.89	8.40	2.09	17.12	4.69
Hem	0.12	3.59	0.90	0.28	0.55	1.61	0.40	9.12	0.90
Ilm	0.35	0.73	0.02	0.88	0.01	2.20	0.12	0.44	0.21
Kln	25.33	43.01	83.83	29.75	79.85	32.12	65.72	21.29	48.65
Mag	0.00	0.00	0.00	0.00	0.00	4.37	0.00	0.00	0.00
Mnt	13.68	0.53	0.38	1.42	0.37	8.73	0.14	0.00	0.15
Or	0.44	0.00	0.00	4.43	0.04	0.78	0.11	0.00	0.03
Pyt	0.01	0.05	0.01	0.01	0.01	0.02	0.01	0.01	0.01
Qtz	44.79	24.93	0.73	43.04	5.33	29.73	18.01	49.95	40.81
Ser	1.89	0.08	0.16	17.42	2.80	4.20	4.15	0.50	1.97
Sil	0.00	7.34	7.21	0.26	6.14	0.89	7.07	1.61	1.76
Ep	0.42	0.39	0.00	0.01	0.02	0.27	0.00	0.00	0.05
Px	0.08	0.00	0.00	0.09	0.00	0.75	0.00	0.00	0.00
Total	99.21	100.72	100.48	100.16	100.22	100.05	99.79	100.69	100.63

Figure 5.1   Frequency histograms of the Omai samples for kaolinite, Al-goethite, quartz, and sericite. Data are plotted using MINNOR program. The order of samples is the same as in Tables 5.4 and 5.5.

zones of sesquioxide accumulation and induration. Sample S6 is such an example. On the other hand. some local zones are depleted in Fe oxy-hydroxides but enriched in other chemical elements (samples S2. 702. 738). For the mottled clay zone. the normative mineralogical composition reflects the variations of the argillaceous matrix/ ferrugineous spot ratio and the presence of weathered quartz veins. The result is a wide range in the mineralogical composition of this horizon. The mineralogical composition of the analyzed pisolith (sample 1aw) can help to define its formation. Low normative Al-goethite/hematite and high normative quartz and kaolinite content mean that only a thin cortex is formed by Fe oxy-hydroxides. which have precipitated from aqueous solutions around a central nucleus represented by a probably residual quartz grain and Al-Si-rich material.

5.7 CONCLUSIONS

A new petrochemical calculation algorithm is proposed for the conversion of the whole-rock chemical analyses into specific minerals of the tropically weathered terrains. The algorithm can be used on several types of lateritic profiles. The minerals used in calculations have been selected on the basis of published mineralogical data from the weathering profiles of the intertropical belt (South America. Africa. Australia. and Southern Asia). This algorithm has been used in MINNOR. a user-friendly application for WINDOWS. which performs the weathering norm (WN) calculations and plots histograms for each normative mineral from the analysed samples. The MINOR program is available for distribution free to interested user: those desiring copies are asked to send one formatted 3'5" disk to the first author.

5.8 REFERENCES

Allen. B.L.. and Hajek. B.F.. 1989. Mineral occurrence in soil environments. *In* Minerals in Soil Environments. 2nd Edition. *Edited by* J.B. Dixon and S.B. Weed. Soil Science Society of America. Madison. p. 199-278.

Bàrdossy. G.. and Aleva. G.J.J.. 1990. Lateritic bauxites. Developments in Economic Geology. v. 27. Elsevier. Amsterdam. 624 pp.

Boeglin. J-L.. and Mazaltarim. D.. 1989. Géochimie. degrés d'évolution et lithodépendance des cuirasses ferrugineuses de la région de Gaoua au Burkina Faso. Sciences Géologiques Bulletin. v. 42. p. 27-44.

Butt. C.R.M.. and Zeegers. H.. 1989. Classification of geochemical exploration models for tropically weathered terrains. Journal of Exploration Geochemistry. v. 32. p. 65-74.

Butt. C.R.M.. and Zeegers. H.. eds.. 1992. Regolith exploration geochemistry in tropical and subtropical terrains. Handbook of Exploration Geochemistry. v. 4. Elsevier. Amsterdam. 607 p.

Cross. W.. Iddings. J.P.. Pirsson. L.V.. and Washington. H.S.. 1903. Quantitative classification of igneous rocks. University of Chicago Press. 57 p.

Fedo. C.M.. Nesbitt. H.W.. and Young. G.M.. 1995. Unraveling the effects of potassium metasomatism in sedimentary rocks and paleosols. with implications for paleoweathering conditions and provenance. Geology. v. 23. p. 921-924.

Irvine. T.N.. and Baragar. W.R.A.. 1971. A guide to the chemical classification of the common volcanic rocks. Canadian Journal of Earth Sciences. v. 8. p. 523-548.

Kretz. R.. 1983. Symbols for rock-forming minerals. American Mineralogist. v. 68. p. 277-279.

Lawrance. L.. 1994. Supergene ore deposit geochemistry. One Day Short Course. The Geological Society of Zimbabwe. Harare. 70 p.

Lecomte. P.. 1988. Stone line profiles: Importance in geochemical exploration. Journal of Geochemical Exploration. v. 30. p. 35-61.

Lindsay. W.L.. Vlek. P.L.G.. and Chien. S.H.. 1989. Phosphate minerals. *In* Minerals in Soil Environments. 2nd Edition. *Edited by* J.B. Dixon and S.B. Weed. Soil Science Society of America. Madison. p. 1089-1130.

Nahon D.. and Tardy. Y.. 1992. The ferruginous laterites. *In* Handbook of Exploration Geochemistry. 4. Regolith Exploration Geochemistry in Tropical and Subtropical Terrains. *Edited by* C.R.M. Butt and H. Zeegers. Elsevier. Amsterdam. p. 41-56.

Nesbitt. H.W.. and Young. G.M.. 1982. Early Proterozoic climate and plate motions inferred from major element chemistry of lutites. Nature. v. 299. p. 715-717.

Nyobe. J.B.. 1991. Application of normative calculations in quantitative comparative mineralogical studies of bauxite. Ore Geology Rewiews. v. 6. p. 45-50.

Oliveira. S.M.B.. and Campos. E.G.. 1991. Gold-bearing iron duricrust in Central Brazil. Journal of Geochemical Exploration. v. 41. p. 309-323.

Séa. F.. Trudel. P.. and Tanguay. M.G.. 1994. Géochimie des horizons d'oxydes ferro-manganésifères noirs enrichis en or dans la latérite de Misséni. au Mali. Canadian Journal of Earth Sciences. v. 31. p. 1791-1805.

Tardy. Y.. 1992. Diversity and terminology of lateritic profiles. *In* Weathering. Soils & Paleosoils. *Edited by* I.P. Martini and W. Chesworth. Developments in Earth Surface Processes 2. Elsevier. Amsterdam. p. 379-406.

Trescases. J.-J.. 1992. Chemical weathering. *In* Handbook of Exploration Geochemistry. 4. Regolith Exploration Geochemistry in Tropical and Subtropical terrains. *Edited by* C.R.M. Butt and H. Zeegers. Elsevier. Amsterdam. p. 25-40.

Voicu. G.. and Bardoux. M.. 1995. Petrography. geochemistry and tectonic transitions in the evolution of the Omai zone. Guyana. South America. Unpublished report. 175 p.

Voicu. G.. Bardoux. M.. Jébrak. M.. and Voicu. D.. 1996. Normative mineralogical calculations for tropical weathering profiles. Winnipeg'96. GAC/MAC Annual Meeting. Winnipeg. Canada. 27-29 May 1996. Program with Abstracts. v. 21. A-99.

Zang. W. and Fyfe. W.S.. 1993. A three-stage genetic model for the Igarapé lateritic gold deposit. Carajas. Brazil. Economic Geology. v. 88. p. 1768-1779.

CONCLUSIONS

Omai represents a first example of Paleoproterozoic granitoid- and greenstone-hosted epizonal orogenic gold deposit. To date. this type of deposit has been described only in the Archean Yilgarn and Zimbabwe Cratons. The main features of the Omai deposit are:

1) Gold-bearing veins occur mainly in felsic bodies hosted within a thick greenstone sequence consisting of mafic volcanics and sedimentary rocks of the Paleoproterozoic Barama-Mazaruni Supergroup. metamorphosed under prehnite-pumpellyite to lower greenschist facies during the Trans-Amazonian orogeny (2.25-1.9 Ga). Lode gold occurs also within a unmetamorphosed and undeformed granitoid intrusive (Omai stock).

2) Volcanic and intrusive rocks at Omai have calc-alkaline and tholeiitic affinities. They were probably formed in a back-arc/immature island arc setting. during alternating periods of tectonic extension and compression. Radiogenic isotope data suggest that this part of the Guiana Shield was a site of new crustal formation during the Paleoproterozoic. uncontaminated by Archean reworked crust.

3) Sm-Nd isochron on scheelite yielded an age of 1994 ± 140 Ma. Although the mineralization age error overlaps U-Pb ages of the Omai stock and country volcanic rocks. the structural and textural relationships suggest that the gold is younger than the crystallization age of the stock and the volcanic rocks.

4) Gold at Omai is contained in quartz veins located mainly within felsic intrusive and subvolcanic rocks (Omai stock and porphyry/rhyolite dikes). The veins

were emplaced in predominantly brittle structures at a local scale and within a major tectonic corridor (Makapa-Kuribrong crustal structure) at a regional scale. Two vein types occur: subhorizontal and subvertical. subdivided in six vein sets. The structural relationships between the vein sets suggest that they are contemporaneous. The textural evidence (crack and seal tension and shear veins. breccia veins. and fracture-filling veins) suggests that the veins formed by one or more episodes of a protracted pulsative hydrothermal system. The formation of most veins can be summarized by two filling stages (I and II) and a late fracture-filling stage (III).

5) Omai is a low-sulphide type deposit. The metallic minerals represent less than 2% of the vein volume. Quartz is the main vein-forming mineral and is associated with minor ankerite. calcite. albite. sericite. chlorite. epidote. and tourmaline. Metallic minerals are sulphides (pyrite. pyrrhotite. galena. chalcopyrite. sphalerite. molybdenite). tellurides (petzite. calaverite. hessite. tellurobismuthite. altaite. coloradoite. and melonite). tungstates (scheelite). and native elements (Au. Cu. and possibly Bi). Gold is free or occurs as inclusions associated with sulphides/tellurides in pyrite.

6) The presence of tellurides associated with other mineral phases during the three depositional stages allowed the characterization of the physico-chemical conditions of ore deposition. The mineralizing solutions are characterized by relatively narrow ranges in S. Te. and O fugacities (log values between -17 and -11. -14 and -10.5. and -43 and -36. respectively). and a weakly acidic pH (between 4 and 5.4). During the early hydrothermal stage. W and Na were transported as sodium tungstate and later precipitated as scheelite and albite. whereas subsequent S- and Te-rich fluids played an important role in gold. sulphide. and telluride transport and deposition. Possible mechanisms of gold deposition have been fluid cooling. chemical composition of wallrocks. phase immiscibility. and high efficiency of fluid/rock interaction.

7) Comparison between the Sm-Nd isotopic ratios of gold-related scheelites and the host rocks suggests that high radiogenic Nd in scheelites resulted by mixing between fluids derived from two different sources. but with similar isotopic characteristics. Ore fluids derived probably by devolatilization of the lower crust during deeper metamorphic processes mixed with local fluids with similar isotopic characteristics derived from local mafic volcanic rocks. released during alteration and gold mineralization. However. limited interaction with a local. less radiogenic Nd local source such as the Omai stock or other felsic/intermediate igneous rocks. cannot be ruled out. although the tight clustering of the Sr isotope ratios (0.7019 - 0.7021) indicates only a low radiogenic mafic source.

8) Stable isotope data allowed to characterize the mineralizing fluids. which have $\delta^{18}O$ values between +5.3 and -2.7‰ and the δD values between -52 and +18‰. The isotopic composition of the hydrothermal fluids plots outside both magmatic and metamorphic water boxes. The carbon isotopes of carbonates range between +1.7 and +4.7‰. suggesting possible mixing with surface-derived fluids. Isotopic and cationic temperatures show that the Omai deposit formed between 170°C and 266°C.

9) The Omai deposit is the first Paleoproterozoic gold mineralization which can be described as epizonal. with features of both classic epithermal and mesozonal orogenic deposits. which suggest that its emplacement occurred at a high crustal level. in a near surface environment. The main epithermal characteristics are: the chemical composition of the mineralizing fluids (low salinity. low CO_2 content. slightly acidic to neutral pH. moderate O and S fugacities. high Te fugacity): surface-water involvement: presence of dominant brittle ore-hosting structures: $\delta^{18}O/\delta D$ depleted/$\delta^{13}C$ enriched nature of the ore fluids and. partially. the mineral paragenesis. mesozonal features are: the alteration style: geodynamic setting: late-orogenic emplacement: the presence of

deeply sourced fluids and: partially. the mineral paragenesis. The location of the Omai deposit in a low-grade metamorphic terrane is a specific epizonal feature. Epizonal deposits represent the upper crustal end-member of a spectrum of deeper-seated gold mineralizations (continuum model).

10) The comparison between the Omai deposit and the Archean gold deposits shows that they have common metallogenic features. suggesting that the models used for Archean deposits can be applied to Paleoproterozoic deposits.

11) Several gold occurrences of the Guiana Shield share many characteristics with the Omai mineralization. Unfortunately. most of them are lacking detailed geologic and metallogenic descriptions and isotopic data are missing altogether. Most of the gold in Guyana is described to occur within the Makapa-Kuribrong structural break. a crustal-scale shear zone trending sub-parallel to the southeast-trending Barama-Mazaruni greenstone belt. which can be traced for over 200 km longitudinally. The felsic/intermediate rock types located within this major tectonic structure represent potential exploration targets. The fact that the shallow-level Omai mineralization was preserved. suggests that the depth of erosion is less than 5 km. If this erosion level is preserved along the Makapa-Kuribrong crustal structure. it probably represents one of the most important exploration target for large tonnage/low grade epizonal gold deposits in the Precambrian greenstone belts.

This thesis represents one of the first integrated research project of a gold deposit in the Guiana Shield. However. the mineral potential of the Guiana Shield deserves further research in order to unfold the complex geologic and metallogenic features of the mineral deposits and their host rocks. Several recommendations follow:

- detailed structural analysis during each exploration project. in order to achieve a regional scale image of the main structural trends within the greenstone belts and associated intrusive rocks;

- petrographical and geochronological systematic investigation especially of the felsic rock types. which represent the best lithological control for the emplacement of the mineralized veins. Precise U-Pb geochronology is needed in order to clarify the discrepancies related to the ages of intrusives. Hydrothermal minerals should be dated by the Pb-Pb. Ar-Ar and Sm-Nd methods. More Nd. Sr. and Pb isotope data are necessary to constrain the sources of the mineralizing solutions.

- detailed chemical and mineralogical studies of the hydrothermal alteration associated with gold occurrences and of their unaltered host rocks. in order to clarify the relationship between regional peak metamorphism and mineralization processes.

- gold deposits in Guyana lack stable isotope studies. The isotope data of Omai should be compared with data obtained from other gold occurrences in order to better define the nature of hydrothermal fluids. as well as their physico-chemical conditions and mechanisms of ore transport and deposition.

APPENDIX 1

A GEOCHEMICAL ASSESSMENT OF THE HYDROTHERMAL SYSTEMS AT THE OMAI GOLD MINE, GUYANA, FROM THE COMPOSITION OF FLUID INCLUSIONS IN ORE MINERALS AND GANGUE

The Omai deposit is located in the Proterozoic greenstone belt of Guyana. South America. and associated with shallow intrusions and shear zones. The deposit is spatially. but not temporally. associated mainly with an epizonal quartz monzodioritic intrusion (Omai stock. Fennell pit) and with quartz-feldspar porphyry/ rhyolite dikes. and subordinately with mafic volcanic flows and metasedimentary rocks (Wenot pit). Two contemporaneous vein types formed under a NW-SE trending principal strain direction occur at Omai: 1) Vein swarms are confined to fracture zones within felsic/intermediate lithologies. as a result of their brittle response to the regional scale deformation and to the rheological contrasts with the country volcanic/sedimentary rocks: 2) Lode-type veins. which crosscut all lithologies. except post-mineralization mafic dikes and sills. Both vein types have two distinct textural aspects (ribbon and breccia). suggesting a sequential open and fill history of the fractures. due to several stages of a pulsative hydrothermal system. Although the metallic minerals represent less than 1% of vein volume. their mineralogy is complex. consisting of various native elements. sulphides. tellurides and sulphosalts. The gangue minerals are represented mainly by quartz. with subordinate carbonates. scheelite. albite. sericite. chlorite and epidote.

In support of other mineralogical and geochemical investigations into the hydrothermal history of the Omai deposit. a project was initiated to study compositional variations of fluid in key vein-forming minerals. The aim of the project was to model the evolution of hydrothermal systems within the deposit. 45 clean mineral separates including silicates. carbonates. epidote. sulfides and gold were prepared and the fluids extracted by crushing and leaching and then analyzed by capillary electrophoresis (CE) (Hallbauer. 1994).

Crush-Leach Procedures: Specific procedures have been designed for the leaching of fluid inclusions. based on detailed investigations into the behaviour of

inclusions and the adsorption and consequent loss of ionic species onto fresh fracture surfaces (Bottrell et al. 1988). In particular, acidified dilute $LaCl_3$ solution had been used for the extraction of cations, the $LaCl_3$ addition intended as adsorbate to free negative charges on silica surfaces, created during crushing. However, the operating conditions for CE (Jandik and Bonn, 1993) are adversely affected by such additions. Several tests were therefore carried out to investigate tetrabutylammonium hydroxide (TBA) as a cation exchange molecule using K, Na and Ca adsorbed onto crushed, hydrothermal quartz samples. It could be shown that TBA could replace $LaCl_3$ in the leach solution, clearing the way for a simpler leach procedure with only one analyte for all determinations.

For the preparation of electrolytes, sample dilution, preparation of standards as well as for cleaning of containers and vials only de-ionised water (MQ) was used exclusively. The Water blank was routinely checked for contamination and, at present, varies between 0.5 and 1ppb K, Na and Ca contamination. Standard solutions are prepared from 1000 ppm stock solutions made from pure chemicals.

The specimens were prepared for an extraction of fluids as indicated in Table 1. Wet crushing was chosen as non-oxidizing and also more efficient crushing. The MQ-TBA leach water was degassed before use. A mortar and pestle of sintered corundum was used to crush quartz samples and an agate mortar was employed for samples of softer minerals as well as for sulfides. An average of about 1-2 g of sample was crushed for fluid extraction. The final crush-leach procedure was timed and could be completed

(bottling of leach fluid) in less than two minutes. This also minimized the risk of oxidation for reduced sulfur species and Fe^{2+}.

Table 1   Method of preparation for crush-leach analysis of mineral specimens

•	Coarse crush to 1 to 4 mm in diameter
•	Wash with de-ionized and de-gassed (Ar saturated) water (MQ - 50 μM TBA). dry at 110 °C
•	Hand-pick clean grains of same generation and mineral species
•	Wash with MQ (- 50 μM TBA) . dry and weigh
•	Crush and leach in 5 ml of MQ water (-TBA)
•	Pass through membrane filter (0.47 μm). wash water max. 10 ml
•	Store in air tight polypropylene container (20 ml size)
•	Analyze for ionic species by CE or other technique
•	Data reduction and report

Chemical and Instrumental Parameters: CE analyses were carried out with a WATERS Quanta 4000 electrophoresis instrument. A digital to analogue converter and vendor-provided software assured a smooth sampling of data and their storage on an IBM compatible PC. Using the information from Elliott (1992) the results were calculated for an average fluid salinity of S=1.

Results and Discussion: The anionic species detected (in sequence of separation by CE) were $S_2O_3^{2-}$. Cl^-, SO_4^{2-}. NO_3^-. WO_4^{2-}. F^-. HCO_3^-. acetate and propionate. Cationic species included NH_4^+. K^+. Na^+. Ca^{2+}. Sr^{2+}. Mg^{2+}. Mn^{2+}. Li^+. Zn^{2+}. and Cu^{2+} (Table 2). Fluids containing thiosulfate anions were restricted to sulfide minerals and gold and reached concentrations of 600 to 1000 ppm. This supports proposals made in the literature that thiosulfate could have been an important ligand in the hydrothermal transport of gold. The S_2O_3 anion was accompanied by larger amounts of sulfate (2550 to 4000 ppm). Although most inclusion fluids contained sulfate. the amounts were small

in all other minerals except for albite. which showed about the same level of sulfate anions as the sulfides. The distribution of chloride showed an average of about 1000 to 1500 ppm for quartz and other gangue minerals. Most mineral fluids contained varying amounts of NO_3. A broad correlation exists between NO_3 and the contents of NH_4. This points to an equilibrium in the fluids between the nitrogen species as predicted by chemical considerations. NH_4 contents were generally higher in fluids from sulfides. indicating and supporting a reducing environment in these fluids. Except for one quartz specimen. WO_4 anions were only found in fluids from scheelite. In this case a good correlation could be observed between Na and WO_4 (Fig. 1). indicating hydrothermal transport of tungsten as sodiumtungstate and later precipitation as scheelite. Except for fluids in scheelite and in sulfides. all other minerals showed HCO_3 contents of between 3000 and 5000 ppm. Also of interest are the contents of acetate and propionate in many
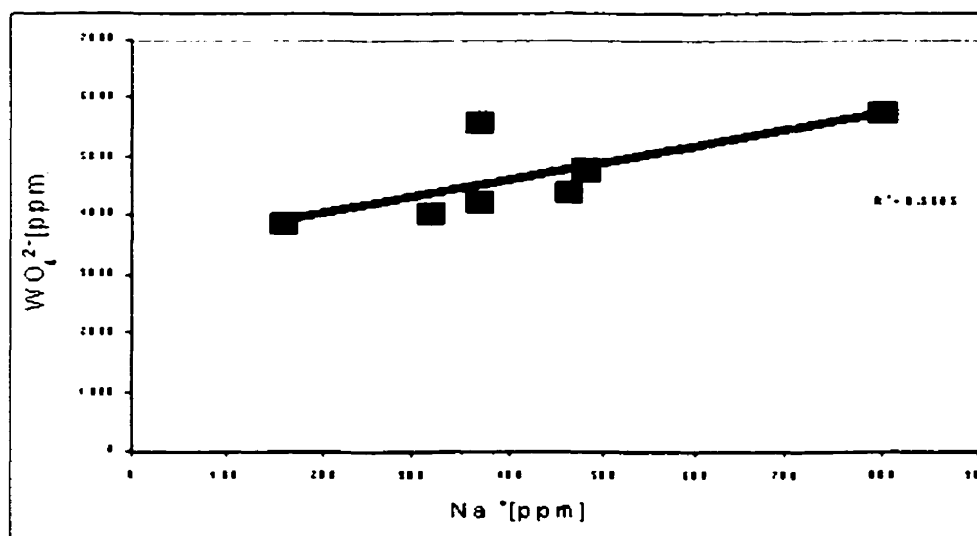
Figure 1   Plot of WO_4^{2-} vs Na^- showing a correlation that indicates hydrothermal transport of tungsten as sodium tungstate.

fluids. This is interpreted as influence of meteoric water or seawater. The presence of seawater in the fluids is also indicated by the normalization of the Na-Ca-Cl data to seawater using the approach of Davisson and Criss (1996) which showed a position for all samples close to the seawater position in the Na-deficit/Ca excess plot.

The cationic components show a strong dominance of Na and Ca. Mg only occurs in significant amounts in fluids from carbonates. while the average amount in fluids does not exceed 200 ppm. The cations have also been useful in estimating the filling temperature of the inclusions. using the empirical Na-K-Ca geothermometer designed by Fournier and Truesdell (1973). There is good agreement with fluid inclusion data from Elliott (1992). According to the geothermometer. the temperatures for fluids in quartz range from 150 to 200 °C while the temperatures for sulfide fluids are scattered from 170 to 260 °C. Temperatures for fluids in epidote range from 210 to 250 °C (Table 3).

The data obtained from the analysis of fluid inclusions supports other results from field investigations as well as from isotope analyses. It also supports the pulsating nature of the hydrothermal system and the mixing of deep-sourced initial fluid and seawater. A transport of tungsten species in hydrothermal fluids as sodiumtungstate is clearly indicated. There is also a strong pointer to a transport of gold as thiosulfate complex. The presence of acetate and/or propionate in the majority of sampled fluids is a further indicator of a mixing of surficial water (Giordano and Kharaka. 1994) and water from a deep seated source.

References

Bottrell. S.H.. Yardley. B.W.D. and Buckley. F.. 1988. A modified crush-leach method for the analysis of fluid inclusion electrolytes. Bulletin Mineralogy. v. 111. p. 279-290.

Davisson. M.L. and Criss. R.E.. 1996. Na-Ca-Cl relations in basinal fluids. Geochimica et Cosmochimica Acta. v. 60. 15. p. 2743-2752.

Elliott. R.G.. 1992. The geology and geochemistry of the Omai goldfield. Guyana. Unpublished Ph.D. thesis. Oxford Brookes University. 230 p.

Fournier. R.O. and Truessdell. A.H.. 1973. An empirical Na-K-Ca geothermometer for natural waters. Geochimica et Cosmochimica Acta. v. 37. p. 1255-1275.

Giordano. T.H. and Kharaka. Y.K.. 1994. Organic ligand distribution and speciation in sedimentary basin brines. diagenetic fluids and related ore solutions. In: Geofluids : Origin. Migration and Evolution of Fluids in Sedimentary Basins. (J. Parnell. Ed.) Geological Society Special Publication No 78. London. p. 175-202.

Hallbauer. D.K.. 1994. Geochemical trace element analysis for ionic species by capillary electrophoresis. Mineralogical Magazine. v. 58A (V. M. Goldschmidt Conference Abstracts). p. 362-363.

Jandik. P. and Bonn. G.. 1993. Capillary Electrophoresis of Small Molecules and Ions. VCH Publishers. Weinheim. 298 p.

Table 2   Chemical composition (in ppm) of the fluid inclusions of vein-forming minerals from Omai

No.	Mineral	Sample	NH_4^+	K^+	Na^+	Ca^{2+}	Sr^{2+}	Mg^{2+}	Mn^{2+}
1	Epidote	EP	43	133	275	1397	Tr.	217	Tr.
2	Epidote	Q-EP1	39	177	814	2401	19	61	Tr.
3	Epidote	QCEC1	28	105	260	1803	Tr.	63	Tr.
4	Epidote	405	38	134	407	2389	Tr.	116	Tr.
5	Quartz	405	27	68	368	1320	Tr.	326	Tr.
6	Quartz	SCH-Q04	39	99	726	920	Tr.	193	30
7	Quartz	SCH-Q06	78	117	806	2780	30	188	Tr.
8	Quartz	Q8-CB3	136	160	1624	1693	Tr.	172	Tr.
9	Quartz	9	43	91	998	2540	Tr.	116	Tr.
10	Quartz	SCH-Q08	64	173	1538	1487	Tr.	123	Tr.
11	Quartz	1003	34	49	783	2398	Tr.	122	Tr.
12	Quartz	Qu11	21	123	383	1780	14	96	Tr.
13	Quartz	MZ1 Qu	194	115	1320	750	Tr.	73	Tr.
14	Quartz	G2 Qu	119	130	2204	573	Tr.	45	Tr.
15	Quartz	QA1	48	74	962	1853	20	42	17
16	Quartz	Q-EP 1	21	43	479	2713	Tr.	22	Tr.
17	Quartz	SCH-Q1	73	66	1139	1918	Tr.	48	Tr.
18	Quartz	SCH-Q05	55	83	1027	1773	Tr.	46	Tr.
19	Quartz	SCH-Q07	85	144	1815	819	Tr.	34	Tr.
20	Scheelite	SCH-Q08	9	19	368	1531	20	28	n.d.
21	Scheelite	SCH-Q06	67	134	367	2853	51	79	n.d.
22	Scheelite	SCH	15	34	161	2096	37	24	n.d.
23	Scheelite	SCH-Q1	38	75	462	1773	53	43	n.d.
24	Scheelite	SCH-Q07	32	91	479	1330	16	99	n.d.
25	Scheelite	SCH-Q04	23	67	800	938	17	26	n.d.
26	Scheelite	SCH-Q05	14	53	317	1854	33	22	n.d.
27	Pyrite	OR1	84	179	550	2620	Tr.	57	Tr.
28	Pyrite	Q1	120	308	855	1290	Tr.	136	Tr.
29	Pyrite	PY1	138	272	711	1614	Tr.	110	Tr.
30	Pyrite	124	16	53	299	2353	21	102	Tr.
31	Pyrite	641 138	187	278	1624	1230	Tr.	98	Tr.
32	Pyrite	3-428	184	364	1898	815	Tr.	63	Tr.
33	Chalcopyrite	G2	54	198	1197	1680	212	267	Tr.
34	Galena	G3	77	119	1068	2192	Tr.	84	Tr.
35	Galena	G1	42	79	772	2452	81	35	Tr.
36	Chalcopyrite	CPY1	105	189	1355	1310	Tr.	58	Tr.
37	Gold	Au	79	222	1801	1192	Tr.	42	Tr.
38	Ankerite	114	40	81	288	2657	85	175	n.d.
39	Ankerite	CB-01	15	18	289	1680	21	884	n.d.
40	Ankerite	Q8-CB3	10	54	359	2272	35	1085	n.d.
41	Ankerite	641 138	13	32	135	1644	13	892	Tr.
42	Calcite	Q-CB2	27	54	325	1783	34	674	n.d.
43	Calcite	CB-07	38	88	640	2062	51	205	n.d.
44	Calcite	Carbo11	20	18	871	2199	127	136	Tr.
45	Albite	114	38	108	362	2285	43	326	Tr.

Tr = trace (0.1-2 ppm); n.d. = not detected (<0.1 ppm)

Table 2   Chemical composition (in ppm) of the fluid inclusions of vein minerals from
Omai (cont.)

No.	Mineral	Sample	Ba^{2-}	Li^-	Co^{2-}	Zn^{2-}	Cu^{2-}	$S_2O_3^{2-}$	Br^-
1	Epidote	EP	n.d.	n.d.	n.d.	n.d.	n.d.	Tr.	n.d.
2	Epidote	Q-EP1	Tr.	n.d.	n.d.	n.d.	n.d.	n.d.	n.d.
3	Epidote	QCEC1	n.d.	n.d.	n.d.	n.d.	n.d.	n.d.	n.d.
4	Epidote	405	n.d.	n.d.	n.d.	n.d.	n.d.	n.d.	n.d.
5	Quartz	405	Tr.	n.d.	n.d.	Tr.	Tr.	n.d.	n.d.
6	Quartz	SCH-Q04	Tr.	n.d.	n.d.	Tr.	Tr.	n.d.	n.d.
7	Quartz	SCH-Q06	n.d.	Tr.	n.d.	Tr.	Tr.	n.d.	n.d.
8	Quartz	Q8-CB3	Tr.	n.d.	n.d.	Tr.	Tr.	n.d.	Tr.
9	Quartz	9	n.d.	n.d.	n.d.	Tr.	n.d.	n.d.	n.d.
10	Quartz	SCH-Q08	n.d.	n.d.	n.d.	n.d.	n.d.	n.d.	n.d.
11	Quartz	1003	n.d.	n.d.	n.d.	n.d.	n.d.	n.d.	n.d.
12	Quartz	Qu11	185	n.d.	n.d.	n.d.	Tr.	n.d.	n.d.
13	Quartz	MZ1 Qu	Tr.	Tr.	n.d.	Tr.	Tr.	n.d.	n.d.
14	Quartz	G2 Qu	Tr.	Tr.	n.d.	Tr.	n.d.	n.d.	n.d.
15	Quartz	QA1	n.d.	n.d.	n.d.	Tr.	n.d.	n.d.	n.d.
16	Quartz	Q-EP 1	n.d.	n.d.	n.d.	n.d.	n.d.	n.d.	n.d.
17	Quartz	SCH-Q1	Tr.	n.d.	n.d.	n.d.	n.d.	n.d.	Tr.
18	Quartz	SCH-Q05	Tr.	n.d.	n.d.	n.d.	n.d.	n.d.	n.d.
19	Quartz	SCH-Q07	Tr.	n.d.	n.d.	n.d.	n.d.	n.d.	n.d.
20	Scheelite	SCH-Q08	Tr.	5	n.d.	n.d.	n.d.	n.d.	Tr.
21	Scheelite	SCH-Q06	Tr.	10	n.d.	n.d.	132	n.d.	n.d.
22	Scheelite	SCH	n.d.	14	n.d.	n.d.	n.d.	n.d.	Tr.
23	Scheelite	SCH-Q1	n.d.	34	n.d.	n.d.	n.d.	n.d.	Tr.
24	Scheelite	SCH-Q07	n.d.	5	n.d.	n.d.	n.d.	n.d.	n.d.
25	Scheelite	SCH-Q04	n.d.	Tr.	n.d.	n.d.	n.d.	n.d.	n.d.
26	Scheelite	SCH-Q05	Tr.	7	n.d.	n.d.	n.d.	n.d.	n.d.
27	Pyrite	OR1	n.d.	n.d.	n.d.	n.d.	Tr.	957	n.d.
28	Pyrite	Q1	Tr.	n.d.	n.d.	Tr.	Tr.	150	n.d.
29	Pyrite	PY1	n.d.	n.d.	n.d.	Tr.	Tr.	470	n.d.
30	Pyrite	124	n.d.	n.d.	n.d.	n.d.	n.d.	1132	n.d.
31	Pyrite	641/138	n.d.	n.d.	n.d.	n.d.	Tr.	971	n.d.
32	Pyrite	3-428	n.d.	n.d.	n.d.	n.d.	Tr.	721	n.d.
33	Chalcopyrite	G2	130	n.d.	34	n.d.	Tr.	344	Tr.
34	Galena	G3	n.d.	n.d.	n.d.	63	138	Tr.	n.d.
35	Galena	G1	Tr.	n.d.	n.d.	n.d.	Tr.	53	Tr.
36	Chalcopyrite	CPY1	Tr.	n.d.	n.d.	n.d.	n.d.	181	Tr.
37	Gold	Au	n.d.	n.d.	n.d.	Tr.	Tr.	Tr.	n.d.
38	Ankerite	114	n.d.	n.d.	n.d.	18	15	n.d.	n.d.
39	Ankerite	CB-01	n.d.	n.d.	n.d.	n.d.	n.d.	n.d.	n.d.
40	Ankerite	Q8-CB3	89	n.d.	n.d.	n.d.	n.d.	n.d.	n.d.
41	Ankerite	641/138	n.d.	n.d.	n.d.	n.d.	39	n.d.	n.d.
42	Calcite	Q-CB2	Tr.	n.d.	n.d.	Tr.	57	n.d.	n.d.
43	Calcite	CB-07	Tr.	n.d.	n.d.	Tr.	n.d.	n.d.	n.d.
44	Calcite	Carbo11	n.d.	n.d.	n.d.	n.d.	n.d.	n.d.	n.d.
45	Albite	114	153	n.d.	n.d.	n.d.	Tr.	n.d.	n.d.

Tr = trace (0.1-2 ppm); n.d. = not detected (<0.1 ppm)

Table 2   Chemical composition (in ppm) of the fluid inclusions of vein minerals from
Omai (cont.)

No.	Mineral	Sample	Cl⁻	SO₄²⁻	NO₂	NO₃⁻	Oxalate⁻	WO₄²⁻	F
1	Epidote	EP	1437	188	Tr.	219	n.d.	n.d.	183
2	Epidote	Q-EPI	2840	492	n.d.	78	Tr.	n.d.	35
3	Epidote	QCECI	825	181	Tr.	166	Tr.	n.d.	108
4	Epidote	405	1345	104	Tr.	121	Tr.	n.d.	114
5	Quartz	405	1487	120	Tr.	37	Tr.	n.d.	936
6	Quartz	SCH-Q04	1693	109	Tr.	Tr.	Tr.	n.d.	416
7	Quartz	SCH-Q06	1400	91	Tr.	41	n.d.	483	224
8	Quartz	Q8-CB3	2495	264	n.d.	Tr.	Tr.	n.d.	186
9	Quartz	9	1397	93	Tr.	41	Tr.	Tr.	65
10	Quartz	SCH-Q08	2251	107	Tr.	58	Tr.	n.d.	125
11	Quartz	1003	1279	125	Tr.	Tr.	Tr.	Tr.	Tr.
12	Quartz	Qu11	1165	694	Tr.	171	128	Tr.	35
13	Quartz	MZ1 Qu	830	451	Tr.	405	Tr.	n.d.	116
14	Quartz	G2 Qu	2730	202	n.d.	272	Tr.	Tr.	42
15	Quartz	QA1	1011	147	n.d.	173	Tr.	n.d.	Tr.
16	Quartz	Q-EP 1	856	74	n.d.	147	Tr.	Tr.	21
17	Quartz	SCH-Q1	888	262	Tr.	367	Tr.	Tr.	Tr.
18	Quartz	SCH-Q05	591	327	Tr.	505	Tr.	Tr.	Tr.
19	Quartz	SCH-Q07	1610	315	Tr.	492	n.d.	Tr.	Tr.
20	Scheelite	SCH-Q08	895	46	n.d.	Tr.	n.d.	5595	11
21	Scheelite	SCH-Q06	804	156	n.d.	154	n.d.	4271	154
22	Scheelite	SCH	658	57	n.d.	25	n.d.	3883	4
23	Scheelite	SCH-Q1	1113	94	Tr.	70	n.d.	4426	Tr.
24	Scheelite	SCH-Q07	573	79	n.d.	100	Tr.	4808	Tr.
25	Scheelite	SCH-Q04	322	71	n.d.	107	Tr.	5771	Tr.
26	Scheelite	SCH-Q05	450	77	n.d.	105	n.d.	4042	Tr.
27	Pyrite	ORI	1018	3566	n.d.	117	n.d.	Tr.	116
28	Pyrite	QI	1648	4436	Tr.	208	n.d.	Tr.	192
29	Pyrite	PYI	1150	4443	n.d.	138	n.d.	Tr.	Tr.
30	Pyrite	124	176	2227	n.d.	143	Tr.	249	19
31	Pyrite	641/138	380	1017	Tr.	842	67	Tr.	91
32	Pyrite	3-428	415	1713	n.d.	979	Tr.	Tr.	95
33	Chalcopyrite	G2	3388	1147	n.d.	160	n.d.	n.d.	Tr.
34	Galena	G3	622	548	Tr.	509	119	n.d.	441
35	Galena	GI	1374	306	n.d.	257	29	n.d.	46
36	Chalcopyrite	CPYI	1175	662	Tr.	706	Tr.	n.d.	Tr.
37	Gold	Au	419	563	Tr.	878	Tr.	n.d.	117
38	Ankerite	114	199	216	n.d.	151	Tr.	Tr.	95
39	Ankerite	CB-01	489	44	n.d.	99	Tr.	n.d.	11
40	Ankerite	Q8-CB3	468	93	n.d.	33	23	n.d.	20
41	Ankerite	641/138	338	109	Tr.	50	13	n.d.	123
42	Calcite	Q-CB2	262	144	n.d.	164	Tr.	n.d.	129
43	Calcite	CB-07	400	536	n.d.	309	Tr.	n.d.	109
44	Calcite	Carbo11	2313	74	n.d.	28	n.d.	n.d.	8
45	Albite	114	844	2996	n.d.	481	n.d.	n.d.	Tr.

Tr = trace (0.1-2 ppm); n.d. = not detected (<0.1 ppm)

Table 2   Chemical composition (in ppm) of the fluid inclusions of vein minerals from Omai (cont.)

No.	Mineral	Sample	Formate	HPO₄²⁻	HCO₃⁻	Acetate	Propionate
1	Epidote	EP	Tr.	n.d.	5908	Tr.	Tr.
2	Epidote	Q-EP1	71	n.d.	2760	122	91
3	Epidote	QCEC1	Tr.	n.d.	6461	Tr.	Tr.
4	Epidote	405	Tr.	n.d.	5231	Tr.	Tr.
5	Quartz	405	Tr.	n.d.	5310	Tr.	Tr.
6	Quartz	SCH-Q04	Tr.	n.d.	5807	Tr.	Tr.
7	Quartz	SCH-Q06	Tr.	n.d.	3732	Tr.	Tr.
8	Quartz	Q8-CB3	Tr.	n.d.	3269	Tr.	Tr.
9	Quartz	9	Tr.	n.d.	4616	Tr.	Tr.
10	Quartz	SCH-Q08	Tr.	n.d.	4074	Tr.	Tr.
11	Quartz	1003	134	n.d.	5077	n.d.	Tr.
12	Quartz	Qu11	164	232	4728	82	n.d.
13	Quartz	MZ1 Qu	Tr.	n.d.	4291	720	735
14	Quartz	G2 Qu	Tr.	n.d.	3046	374	262
15	Quartz	QA1	Tr.	n.d.	5269	195	190
16	Quartz	Q-EP 1	21	n.d.	5508	Tr.	94
17	Quartz	SCH-Q1	Tr.	n.d.	4280	653	304
18	Quartz	SCH-Q05	Tr.	n.d.	4945	414	235
19	Quartz	SCH-Q07	n.d.	n.d.	3378	709	599
20	Scheelite	SCH-Q08	15	n.d.	1457	n.d.	n.d.
21	Scheelite	SCH-Q06	n.d.	n.d.	767	n.d.	Tr.
22	Scheelite	SCH	13	n.d.	2977	n.d.	n.d.
23	Scheelite	SCH-Q1	Tr.	n.d.	1818	n.d.	Tr.
24	Scheelite	SCH-Q07	Tr.	17	2043	133	194
25	Scheelite	SCH-Q04	Tr.	19	1619	134	84
26	Scheelite	SCH-Q05	Tr.	7	2865	78	75
27	Pyrite	OR1	Tr.	n.d.	531	87	118
28	Pyrite	Q1	Tr.	n.d.	550	105	Tr.
29	Pyrite	PY1	198	n.d.	406	123	227
30	Pyrite	124	23	n.d.	2728	213	245
31	Pyrite	641 138	130	n.d.	1243	1442	401
32	Pyrite	3-428	204	n.d.	1152	1147	250
33	Chalcopyrite	G2	134	n.d.	805	133	115
34	Galena	G3	88	n.d.	2853	721	357
35	Galena	G1	49	n.d.	4000	265	160
36	Chalcopyrite	CPY1	Tr.	n.d.	3197	930	151
37	Gold	Au	112	n.d.	2551	1420	603
38	Ankerite	114	64	n.d.	5590	147	182
39	Ankerite	CB-01	29	n.d.	6235	109	48
40	Ankerite	Q8-CB3	24	75	5361	n.d.	n.d.
41	Ankerite	641 138	134	n.d.	6467	n.d.	n.d.
42	Calcite	Q-CB2	50	n.d.	5901	200	195
43	Calcite	CB-07	204	n.d.	3995	524	838
44	Calcite	Carbo11	18	n.d.	4077	n.d.	n.d.
45	Albite	114	146	n.d.	2218	Tr.	Tr.

Tr = trace (0.1-2 ppm); n.d. = not detected (<0.1 ppm)

Table 3   Temperatures of mineralizing fluids calculated using the Na-Ca-K cationic composition of the fluid inclusions

Mineral	Sample	T	Mineral	Sample	T	Mineral	Sample	T
Epidote	EP	244	Quartz	SCH-Q1	147	Chalcopyrite	CPY1	199
Epidote	Q-EP1	210	Quartz	SCH-Q05	162	Galena	G3	177
Epidote	QCEC1	228	Quartz	SCH-Q06	177	Galena	G1	166
Epidote	405	221	Scheelite	SCH-Q08	127	Gold	Au	198
Quartz	405	190	Scheelite	SCH-Q06	224	Ankerite	114	203
Quartz	SCH-Q04	189	Scheelite	SCH	178	Ankerite	CB01	176
Quartz	SCH-Q06	184	Scheelite	SCH-Q1	185	Ankerite	Q8-CB3	173
Quartz	Q8-CB3	181	Scheelite	SCH-Q07	197	Ankerite	641/138	184
Quartz	9	164	Scheelite	SCH-Q04	165	Calcite	Q-CB02	179
Quartz	SCH-Q08	188	Scheelite	SCH-Q05	179	Calcite	CB07	180
Quartz	1003	143	Pyrite	OR1	226	Calcite	Carbo11	187
Quartz	Qu11	221	Pyrite	PY1	251	Albite	114	213
Quartz	MZ1 Qu	177	Pyrite	124	248			
Quartz	G2 Qu	168	Pyrite	641/138	178			
Quartz	QA1	158	Pyrite	3-428	216			
Quartz	Q-EP1	151	Chalcopyrite	G2	204			

T = temperature. in Celsius degrees

APPENDIX 2

MINERAL RESOURCES OF GUYANA

ORE DEPOSITS

Despite the disappointing history of past exploration in Guyana, it had become apparent that the hopes that had long been held for extensive mineral development in the country could at last be approaching realization. The best example is the Omai gold mine, which, after tens of years of exploration (frequently using inadequate methods) and artisanal exploitation, started to produce in 1992. The advancement of the knowledge of the mineral resources of Guyana can be applied for the whole Guiana Shield. It is well known from mining experience the regional extend of the metallogenetic provinces in other Precambrian terrains.

Although Guyana is rich in a wide variety of mineral resources, identification and location of known mines and occurrences in the literature is uneven and incomplete. Gold, diamonds, and bauxite are the major exploited resources and are better documented than other commodities. Only a few major deposits are discussed with any detail, and maps are extremely rare. Notably absent in the mining record are occurrences of primary nickel, PGE, and base metals (copper, lead, and zinc).

The mineral resources of Guyana were divided into metallogenic provinces, based on the specific tectono-magmatic evolution of each major lithostratigraphical unit, which could represent the host rocks for different ore deposit models (Fig. 1). Six major metallogenic provinces have been considered: 1. low/intermediate grade metamorphic greenstone belt (Barama-Mazaruni Supergroup); 2. high grade metamorphic greenstone belt (Kanuku and Kwitaro Groups); 3. granitoid-related metallogenetic province; 4. mafic/ultramafic rock (not related to the greenstone belts) province; 5. intra-cratonic sedimentary rocks (Roraïma Formation); 6. hot spot-related alkaline and carbonatite massifs.
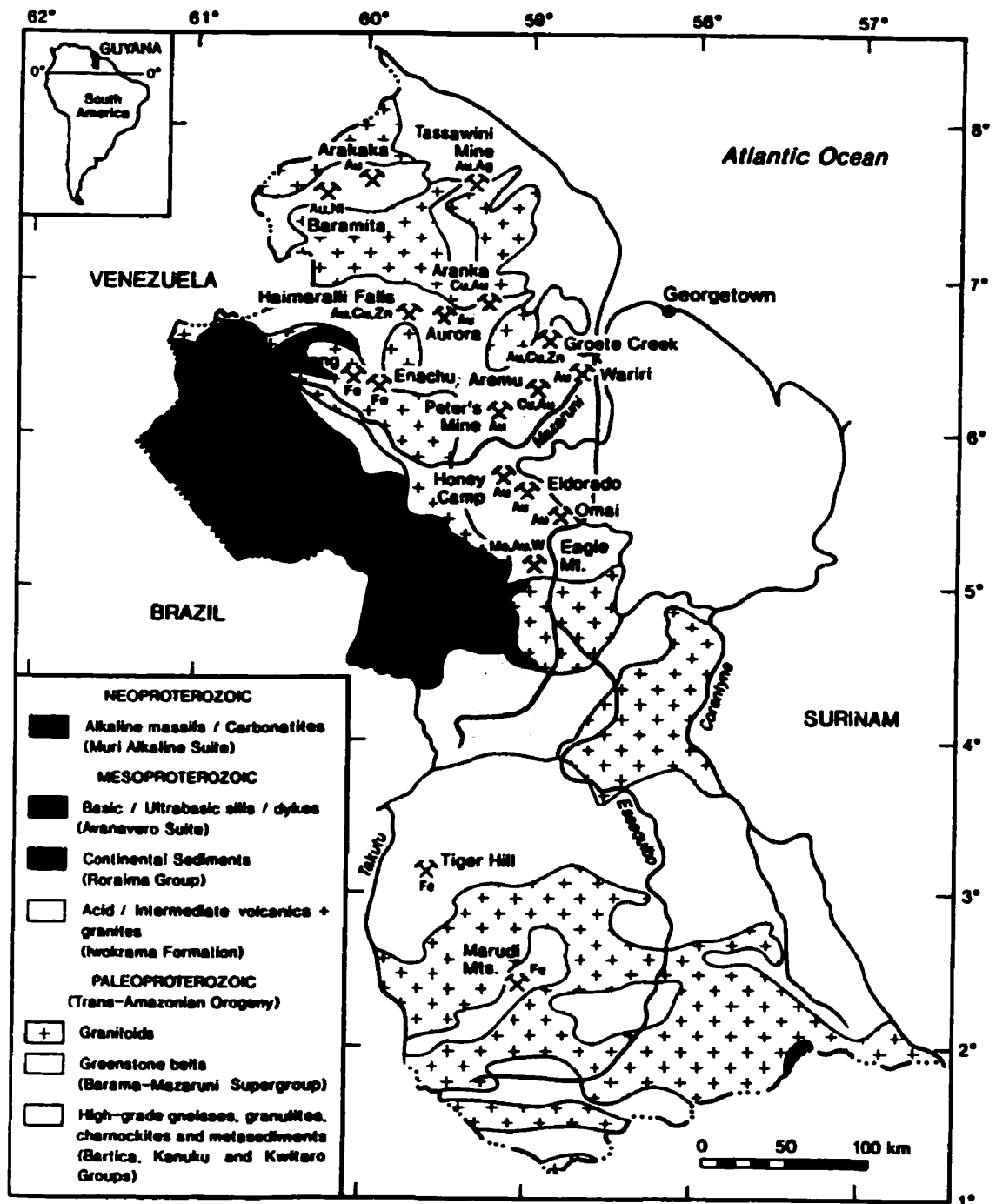
Figure 1   Metallogenic   map of Guyana showing the principal mineral
            occurrences

1. Low/intermediate metamorphic grade greenstone-related province

The low-grade metamorphic Barama-Mazaruni Supergroup represents the principal metallogenetic province of Guyana. Because of its close chemical relationship with the Canadian Archean greenstone belts (Gibbs and Barron, 1993), it has been argued that a similar mineral endowment could be expected. However, gold is the only commodity characteristic of Archean greenstone belts which has so far been produced from their Guyana analogues.

In Guyana, there are no known volcanic-sedimentary base metal sulphide deposits (model 4D), which are prevalent in the Abitibi greenstone belt or in Paleoproterozoic greenstone belts of the Baltic Shield. But the records of the gold mines and diamond drilling data clearly indicate that frequently gold is associated with a number of sulfides. In addition to ubiquitous pyrite, variable amounts of chalcopyrite, pyrrhotite, arsenopyrite, sphalerite, galena, and molybdenite have been recorded. At places, a few of these sulfides occur in sufficiently significant quantities to deserve consideration for further exploration and possible economic exploitation. For example, the Groete Creek deposit has a proven strike length of 1,525 m, with a pitch for 410 m, and has a mineralized width of 10 m at 0.6% Cu and 0.05oz/ton Au (Walrond, 1980). The reported mineral paragenesis is typical of VMS deposits (gold, auriferous pyrite, chalcopyrite, pyrrhotite, galena, and sphalerite). The persistence of chalcopyrite has been proved by diamond drilling and a genetic relationship of the gold mineralization with this sulfide may be established. The deposit is zoned, with the upper massive horizon being typified by pyrite-sphalerite, followed at lower levels by chalcopyrite-galena, which in turn passes to a lower stringer ore zone of pyrrhotite-chalcopyrite. A similar genetic relationship is described for the base metal deposits in the Noranda area, Abitibi subprovince (Kerr and Gibson, 1993; Lacroix et al., 1993). The VMS deposits typically

occur as clusters. with a preferred alignment with major tectonic zones. In the northern part of Guyana. a north-westerly trending lineament has been identified by magnetic data. which corresponds to the relatively straight alignment of the highly mineralized Groete Creek. Wariri. Aremu. and Peter's Mine deposits (Fig. 1). Another major north-easterly alignment (Makapa-Kuribrong shear zone) seems to correspond to Omai. Honey Camp. Eldorado. Haimaralli Falls. and Baramita gold ± base metal sulfide deposits. This tectonic zone extends westward in Venezuela in the El Callao and Lo Increible districts (known for for their important gold deposits) and eastward in Suriname. Recent discovery of an important VMS deposit in equivalent greenstone belts of Brazil (Salobo deposit). as well as the base metal occurrences (Paul Isnard) reported in Paramaca (equivalent of Barama-Mazaruni Supergroup) Formation of French Guiana. strongly support the supposition that the Guiana Shield has an excellent potential for highly mineralized massive sulfide deposits.

Gold represents the main economic mineralization to date. In most occurrences. it is associated with quartz-carbonate veins. with minor amount of pyrite. chalcopyrite. sphalerite. galena. and molybdenite. At Omai. native gold is also associated with Au-Ag-Bi-Pb-Ni-Hg tellurides. pyrrhotite. and scheelite. The vast majority of the vein-gold deposits and prospects can be classified as belonging to the model 6B. but a few occurrences have several characteristics common of models 6C (epithermal or Hemlo gold) or 4B (Au- or Mo-rich porphyry type). However. lack of detailed descriptions of most occurrences makes impossible their assessment with a genetic model. At Eagle Mountain. 70 km south-west of Omai. the native gold is associated with quartz veins. but important molybdenite disseminations (up to 0.14% Mo) are reported from a granite-porphyry which intrudes the Barama-Mazaruni metavolcanic rocks. Cassiterite. scheelite. and native cooper have been also reported. The deposit is described by Banerjee and Moorhead (1970) as mesothermal and by Macdonald (1968) as a typical porphyry-Mo.

However. the presence of cassiterite. scheelite and molybdenite assemblage is characteristic for post-tectonic S-type granites. In this case one could think of two different mineralization epochs. the first related to a compressive tectonic regime (gold-bearing quartz veins. model 6B) and the second related to an extensive regime (molybdenite-cassiterite-scheelite association. models 7A and 7B). Another special case is the Omai deposit. where gold-bearing quartz-carbonate-scheelite veins are characterized by a mineral paragenesis which are typical for the model 6B associated with a low-temperature/pressure paragenesis. as described for the Hemlo deposit (model 6C). Hydrothermal alteration is similar with that reported at the Las Cristinas deposit in Venezuela (Gray et al.. 1993) and the Loulouie deposit in French Guiana (Milési et al.. 1995).

Other possible mineral occurrences related to this metallogenic province include Ni-Cu (model 2C. 2E). Cu (model 4A). Cu-Pb-Zn (model 4D). and Zn-Pb-Ag (model 5).

2. High metamorphic grade rock-related province (Kanuku and Kwitaro Groups, Southern Guyana)

The Kwitaro Group is represented by a mixture of metapelites and metarenites. with intercalations of felsic volcanics. metamorphosed at the amphibolitic facies. Its stratigraphic and tectonic features are poorly understood. and only one mineral occurrence (Fe. Marudi Mts.. Fig. 1) has been reported. The Kwitaro environment appears similar to the stratiform sediment-hosted Pb-Zn-Ag (model 5). to the sediment-hosted Cu (model 4A) and to the Superior-type Iron Formation (model 1A). World-class Pb-Zn-Ag and Cu deposits are connected with exhalative emanations in predominant metapelitic-metaarenitic horizons associated with felsic flows and tuffs. which perhaps

reinforces the analogy. More structural information is definitely required especially with regard to the identification of deep seated faulted surfaces which must have acted as conduits for mineralizing fluids. The main exploration strategy for these types of mineral deposit models would be reconnaissance stream geochemistry for Cu. Pb. Zn. Co. Ag. combined with detailed geological mapping in areas of interest. Superior-type Fe occurrence of the Marudi zone is poorly described and comprises ferruginous (and occasionally manganiferous) quartzites. which have not yet shown any material of possible ore grade. The presence of gold associated to this iron-formation at Marudi (Macdonald. 1968) should rather suggest a Homestake Au model (6A).

The Kanuku Group is represented by high-grade gneisses. granulites. and charnockites. which usually are considered as being a poorly favorable environment for major mineral deposit preservation. The only mineral occurrence is Tiger Hill. described as an iron formation ($\pm$Cu) of Algoma-type. hosted by migmatites and acid plutonic rocks. Considering other similar geological environments in the world. the Kanuku Group could represent a regional metallotect for Ti (model 3). Cu-Pb-Zn (model 4D). and Fe (model 1B).

3. Granitoid-related metallogenic province

Granitoid rocks in Guyana are poorly understood. The lack of geochronological data has led to several speculations about the relationships between the different granitoid generations and the volcano-sedimentary terranes. In general. they can be divided into compression-related granitoids (I-type granitoids. of calc-alkaline affinity) and extension-related granitoids (S-type. of high-K calc-alkaline or alkaline affinities). The only known mineral occurrences related to the I-type granitoids are Putareng and Enachu. where magnetite-hematite bodies occur within hornblende granitoids (Fig. 1).

The deposits are estimated to be tens of millions of tons, with significant amounts of titanium (TiO_2 up to 18%). The mineralization characteristics and the geological environment seem to be similar to model 1D. Other possible mineralizations in I-type granitoid rocks include Au (models 6B, 6C), and Cu $\pm$ Mo $\pm$ Au (model 4B).

S-type granitic rocks are described in French Guyana and Brazil, but not yet in Guyana. They represent favorable environments for Sn-W $\pm$ Mo (models 7A and 7B), U-Th, and pegmatite-related Nb-Ta-Be-Li deposits.

4. Mafic/ultramafic rock-related metallogenic province

Mafic/ultramafic rocks (not related to greenstone belts) are represented by some Paleoproterozoic intrusives, Avanavero Suite (Mesoproterozoic), and Apatoe Suite (Permian-Triassic). They represent shallow-level gabbroic to ultramafic bodies or tholeiite dikes and sills, which occur scattered throughout the Paleoproterozoic basement. No mineral occurrence related to these mafic rocks is reported, but detailed studies are missing. Even if these mafic bodies are of small sizes (up to 20 km in diameter), their petrographical characteristics are similar to the large batholiths known in other Precambrian regions (Bushveld, Sudbury, Stillwater, etc). Thus, the mafic/ ultramafic bodies of Guyana Shield could represent interesting targets for several metallic associations, as Cu-Ni (models 2A, 2B, 2C, and especially 2D), Fe-Ti-V (model 1C), Ti (model 3), and Cr. However, more petrographic and geochronological studies are required, in order to achieve a better understanding of the relationships between the different mafic/ultramafic rock generations, as well as their evolution in relation to the tectono-magmatic events of the Guiana Shield.

5. Intra-cratonic sedimentary rock-related metallogenic province

The Roraïma Group consisting of flat-lying. unmetamorphosed rudites and pelites of continental origin are thought to be the source of most of the alluvial diamonds in Guyana (Keats. 1973). More recently. Meyer and McCallum (1993) have described in the Guaniamo area of Venezuela a second source for diamonds. in primary Proterozoic kimberlite-type rocks. However. the characteristics of the two diamond types are different. and a common source is unlikely. In Guyana. the possibility of finding kimberlites to the northeast of the Pakaraima Mountains (or even within them) is considered as good. although no real evidence of their occurrence has yet been found. except for the occurrence of pyrope garnet in the heavy mineral suite of rutile. tourmaline. and gorceixite.

The lower part of the Roraïma Group. consisting of pebbly sandstones and conglomerates which overlie unconformably the volcanic flows and metasediments of the Barama-Mazaruni Supergroup. represents favorable metallotect for Au-U deposits (model 6D).

6. Hot-spot alkaline/carbonatite rock-related metallogenetic province

In Guyana. the only known alkaline rocks/carbonatite massifs. called the Muri Suite. is situated in its southern part. near the brazilian border. No mineral occurrences are reported. but these petrographic types represent important metallotects for a wide variety of economic metals. Alkaline rocks (nepheline-syenites. essexites. ijolites. urtites. etc.) may contain economic grades of REE. Nb. Ta. Th. U. Fe. Cu. Mo. F. and Ba (model 8A). Brecciated alkali granites. affected by hydrothermal processes. represent the host rocks for the Olympic Dam-type Cu-U-Au deposits (model 4C). Carbonatites are

characterized by the presence of economic concentrations of Nb. Ta. REE. P. Ti. Zr. and U (model 8A). Alkaline breccias (kimberlites and lamproites) are the source for gem- and industrial-grade diamonds (model 8B). The presence of alkaline carbonatite ring plutons with interesting Nb. Ta. P. U. and REE grades in Venezuela and Brazil clearly indicates the economic potential of this metallotect in Guyana.

Table 1   Summary of ore deposit models

Chemical element	Deposit model	Model number
Fe	Superior type	1A
	Algomatype	1B
	Bushveld Fe-Ti-V type	1C
	Volcanic-hosted magnetite	1D
Ni	Stillwater Ni-Cu	2A
	Duluth Ni-Cu	2B
	Komatiitic Ni-Cu and Dunitic Ni-Cu	2C
	Synorogenic-synvolcanic Ni-Cu	2D
Ti	Anorthosite Ti	3 (see also 1C)
Cu	Basaltic Cu and Sediment-hosted Cu	4A
	Porphyry Cu±Mo±Au	4B
	Olympic Dam Cu-U-Au	4C
	Volcanogenic massive sulfides (VMS)	4D (see also 2A. 2B. 2C. 2D)
Zn. Pb	Stratiform sediment-hosted Zn-Pb-Ag	5 (see also 4D)
Au	Homestake Au or Iron Formation-hosted Au	6A
	Low-sulfide Au-quartz veins or Orogenic Au	
	Hemlo type or Epithermal Au or Sulfidic	6B
	Schist type	6C
	Quartz pebble conglomerate Au-U	6D (see also 4B. 4C)
Sn	Sn greisen	7A
	Sn±W vein type	7B
Nb-Ta-REE-P-U	Carbonatite and Alkaline rock-related	8A
C (diamond)	Diamond-bearing kimberlite/lamproite pipes	8B

ORE DEPOSIT MODELS

CHEMICAL ELEMENT: Fe
DEPOSIT MODEL: SUPERIOR TYPE

OCCURENCES - WORLD Krivoy Rog (Russia). Quadrilatero Ferrifero (Brazil). Negaunee (USA). Penge (South Africa). Hamersley (Australia). Gunflint (Canada). Mesabi Range (USA). Labrador Iron Province (Canada)

OCCURENCES - GUIANA SHIELD Le Pao (Venezuela). Cerro Altamira (Venezuela). Amapa (Brazil). Cerro Bolivar (Venezuela). Tiger Hill (Guyana). Wichibai (Guyana). Paloemeu River (Suriname). Los Barrancos (Venezuela)

TONNAGE and GRADE 11 Mt (min). 2400 Mt (max). 170 Mt (ave). 30% Fe (min). 66% Fe (max). 53% Fe (ave)

GEOLOGICAL ENVIRONMENT Banded iron-rich sedimentary rocks. interpreted as chemical precipitates from sea or lake waters not affected by volcanism or hydrothermalism. generally of great lateral extend. typically layered on centimeter scale with siliceous (chert) beds (itabirites): Petrography: chert. jasper. shale. dolomite. limestone. argilite. slate: Sedimentary textures typical of shalllow-water deposition in tectonically stable regions: mostly Archean and Paleoproterozoic (1.8-2.2 Ga). less commonly Meso- and Neoproterozoic

TECTONIC SETTING Advanced stages of rifting. "mid-plate" or "passive" (Atlantic-type) margin and or oceanic platforms

METALLOGENESIS Mineralogy: hematite. magnetite. siderite. subordonated pyrite. chalcopyrite. stilpnomelane: Structure: very fine grained. always banded at centimeter scale: Alteration: none related to ore deposition: Ore controls: no primary controls of local importance: Genesis: 1) sedimentary origin: Fe has been brought in from the land during the period of precipitation or it accumulated in the world ocean over a long period of time. from various sources: 2) hydrothermal-exhalational origin: in this hypothesis. the difference between "Algoma type". interpreted as "exhalational" from the beginning. and "Superior type" becomes only quantitative: 3) biogenetic origin: iron-oxidizing microorganisms played a key role in concentrating and precipitating iron

ASSOCIATED DEPOSIT TYPES Sedimentary manganese deposits may occur interbedded with iron formations

WEATHERING Alteration of original iron minerals to Fe-hydroxides and hematite. resulting in high-grade supergene ore. In tropical regions. the BIF are capped by thick indurated ferrugineous laterites. resulting in proeminent topography. easily observable in airborne radar (SLAR) imagery

GEOCHEMICAL SIGNATURE Fe$\pm$Mn enrichment

EXPLORATION METHODS Geophysical data (gravimetry. magnetometry). basin analysis. structural and tectonic study of major rift and graben zones

CHEMICAL ELEMENT: Fe
DEPOSIT MODEL: ALGOMA TYPE

OCCURENCES - WORLD Vermillion (USA). Adams Mine (Canada). Wawa region (Canada).

Serra dos Carajas (Brazil). Buzuluk (Ukraina). Anshan district (China). Kittila-Pahtavaara (Finland). Uele River (Zaire). Ituri River (Zaire). Atlantic City (USA)

OCCURENCES - GUIANA SHIELD Cuadrilatero Ferrifero de San Isidro (Venezuela)

TONNAGE and GRADE 11 Mt (min). 2400 Mt (max). 170 Mt (ave). 30% Fe (min). 66% Fe (max). 53% Fe (ave)

GEOLOGICAL ENVIRONMENT Mafic to felsic submarine volcanic rocks and deep-water poorly-sorted volcanoclastic sediments: frequently associated to pillowed greenstones. intermediate to felsic tuffs and agglomerates and clastic sediments. In setting and composition. these BIF are closely comparable with the Phanerozoic "Lahn-Dill type" of iron ores. interpreted as submarine-exhalational. The BIF is hosted by a chert units. often metamorphically recrystallized into quartzite. The BIF contacts against the regionally predominant meta-volcanic or meta-sedimentary host rock tend to be sharp. bedding-conformable (stratiform) and depositional. Gradational contacts of the BIF against an altered or metasomatized (silicified. carbonatized. hematitized) wallrock have also been recorded. The BIF located in temperate/cold regions are unmodified by supergene processes and are. as a consequence. of low to very low grade. In the tropical regions. the mined BIF are entirely weathering enriched. so only the supergene products and relics of strongly altered "primary" rocks can be examined in outcrop.

TECTONIC SETTING Advanced stages of rifting and tectonically active submarine volcanic belts

METALLOGENESIS Mineralogy: hematite. magnetite. siderite $\pm$ Fe-Mg silicates $\pm$ pyrite $\pm$ pyrrhotite $\pm$ stilpnomelane: Structure: banded on centimeter scale with volcanic rocks and chert beds: Alteration: no syngenetic alteration: rare post-depositional metasomatism (silicification: carbonatization): Ore controls: low sediment and volcanic input is probably a key factor

ASSOCIATED DEPOSIT TYPES Kuroko massive sulfides and Homestake Au deposits

WEATHERING Alteration of original iron minerals to Fe-hydroxides and hematite. resulting in high-grade supergene ore

GEOCHEMICAL SIGNATURE Fe enrichment

EXPLORATION METHODS Geophysical data (gravimetry. magnetometry). basin analysis. aiborne radar imagery. geological mapping (ferrugineous laterites). geochemical sampling

1C

CHEMICAL ELEMENT: Fe
DEPOSIT MODEL: BUSHVELD Fe-Ti-V TYPE

OCCURENCES - WORLD Bushveld (South Africa). Sudbury (Canada). Stillwater (USA). Muskox (Canada). Munni Munni (Australia). Koillismaa (Finland). Kiglapaid (Canada). Rincon del Tigre (Bolivia). Chinei (Russia). Liganga (Tanzania). Cunene (Angola-Namibia). Kaffirskraal (South Africa)

OCCURENCES - GUIANA SHIELD Not known

TONNAGE and GRADE Until recently. because of the high cost of recovery and separation of Fe and Ti from the ore. only the intervals anomalously enriched in V qualified as ore. so their reserves were calculated: 14 Bt Fe. 1.5 Bt Ti. 200 Mt V

GEOLOGICAL ENVIRONMENT Layered mafic-ultramafic (norite. gabbro. dunite. peridotite. anorthosite. troctolite) circular to elliptical intrusions. with cumulte textures. locally with poikilitic matrix. intruded into granitic gneiss or into volcanic-sedimentary terranes: the intrusions are unmetamorphosed. and they were controlled by intersection of lineaments. and driven by mantle diapirism: three crystallization phases have been observed: 1) the primary or cumulus stage: 2) the post-cumulus stage

(related to ore forming): 3) the subsolidus stage: the intrusions are characterized by two regionally coexisting suites of concentrated metals: the basaltophile Fe-Ti-V-Cr-PGE suite and the granophile Sn-F-W-(Mo. Cu) suite: layers (around 30) of Fe-Ti-V are widespread in the ferrogabbro member of the Upper Zone: the layers are remarkably persistent. having been traced for 175 km along strike: a series of pipe-like pegmatoid bodies of various types occur at different levels within the complex. and some of them are host ore deposits: generally Archean (2.7 Ga) and Paleoproterozoic (2.1 Ga)

TECTONIC SETTING Intracontinental hotspot-related layered mafic-ultramafic complexes or a meteorite impact origin (for Sudbury)

METALLOGENESIS Mineralogy: V-bearing magnetite. ±ülvospinel. ±ilmenite. ±chromite ±sulphides (traces) (pentlandite. pyrrhotite. chalcopyrite. cubanite. mackinavite): Structure: massive. cumulus texture: Alteration: metasomatic reactions with wallrocks. during the second crystallization stage: Ore controls: the presence of immiscible liquids. which crystallized at different intrusion levels: enriched mineralized layers near top of intrusion

ASSOCIATED DEPOSIT TYPES Bushveld Cr. Stillwater Ni-Cu. Merensky Reef PGE

WEATHERING Blocks of magnetite in soils and alluvium

GEOCHEMICAL SIGNATURE Fe. Ti. V. ± Cr. ± Ni. ± Co. ± PGE

EXPLORATION METHODS Magnetic anomalies. geochemical studies. airborne radar imagery. and surface mapping

1D

CHEMICAL ELEMENT: Fe
DEPOSIT MODEL:VOLCANIC-HOSTED MAGNETITE

OCCURENCES - WORLD Kirunavaara area (Sweden). Svappavaara area (Sweden). Gällivare area (Sweden). Pea Ridge (USA). Bourbon (USA). Pilot Knob (USA). Bafq-Saghand (Iran). Anhui Province (China)

OCCURENCES - GUIANA SHIELD Cuchivero area (?) (Venezuela)

TONNAGE and GRADE 3.5 Mt (min). 450 Mt (max). 40 Mt (ave). 38% Fe (min). 64% Fe (max). 58% Fe (ave)

GEOLOGICAL ENVIRONMENT Massive concordant and discordant magnetite ore bodies in intermediate to alkalic volcanic and igneous rocks (andesite. trachite. quartz porphyry. monzonite. and diorite): porphyroaphanitic to medium-grained equigranular textures: subvolcanic plutons are intruded in continental volcanic rocks and clastic sediments: the contacts of magnetite ore bodies range from knife-sharp. wedded. through ductile sheaths of chlorite-rich phyllonite. into gradational transitions of massive magnetite to a mixed (rock/ore) and a non-ore (rock) breccia: Mesoproterozoic (1.3-1.5 Ga) in Sweden. China. and USA-Missouri. Phanerozoic in other areas

TECTONIC SETTING Continental margin. subducted-related volcanic terrane. associated with late-orogenic high-K volcanic rocks and/or hotspot related magmatism (?)

METALLOGENESIS Mineralogy: magnetite. apatite ± hematite ± pyrite. ± chalcopyrite. ± chalcocite: Structure: fine. granoblastic: Alteration: diopside. andradite. biotite. quartz. albite. K-feldspar. scapolite. epidote. carbonates: Ore controls: magnetite in massive replacement. breccia filling and stockwork veins. related to cupolas of deeper plutons: Genesis: initially considered as injected plutonic rest-magma. they have been reinterpreted as exhalative-sedimentary and as subaerial-volcanogenic

ASSOCIATED DEPOSIT TYPES Sedimentary Fe in associated clastic rocks. Olympic Dam type

WEATHERING None
GEOCHEMICAL SIGNATURE Fe. P. V
EXPLORATION METHODS Strong magnetic anomalies. geochemical prospection

2A

CHEMICAL ELEMENT: Ni
DEPOSIT MODEL: STILLWATER Ni - Cu

OCCURENCES - WORLD Bushveld (South Africa). Sudbury (Canada). Stillwater (USA). Muskox (Canada). Munni Munni (Australia). Koillismaa (Finland). Kiglapaid (Canada). Rincon del Tigre (Bolivia). Chinei (Russia). Liganga (Tanzania).Cunene (Angola-Namibia). Kaffirskraal (South Africa)

OCCURENCES - GUIANA SHIELD Not known

TONNAGE and GRADE 375 Mt. 0.25% Ni. 0.25% Cu (ave)

GEOLOGICAL ENVIRONMENT Layered mafic-ultramafic (norite. gabbro. dunite. peridotite. anorthosite. troctolite) intrusions with cumulte textures and locally poikilitic matrix: intruded into granitic gneiss or into volcanic-sedimentary terrane: the complexes are substantially thrust- and block-faulted anf locally sheared and metamorphosed. but their great competency has prevented tight folding. penetrative deformation and wholesale metamorphic recrystallization: the complexes are usually divided into several series. with different metallogenetic characteristics(Fe-Ti-V. Cr. Cu-Ni. PGE enriched zones): Ni-Cu ores are generally localized in the Basal Series represented by a sheet of cumulate and non-cumulate mafic rocks. contaminated by the floor meta-sediments: similar geological environment as Bushveld Fe-Ti-V model: mostly Archean (2.7). but also Paleo- and Mesoproterozoic

TECTONIC SETTING Hotspot in anorogenic settings

METALLOGENESIS Mineralogy: pyrrhotite. chalcopyrite. pentlandite. Co-sulfides. PGE minerals: Structure: massive to disseminated: Alteration: none related to ore: Ore controls: basins in basal contact of intrusion with rapidly varying lithologies: fractures in footwall country rock

ASSOCIATED DEPOSIT TYPES Bushveld Fe-Ti-V and Cr. Merensky Reef PGE

WEATHERING Gossan

GEOCHEMICAL SIGNATURE Cu. Ni. Co. PGE

EXPLORATION METHODS Airborne and ground magnetometry. radar imagery. geochemical prospection

2B

CHEMICAL ELEMENT: Ni
DEPOSIT MODEL: DULUTH Ni - Cu

OCCURENCES - WORLD Duluth (USA). Noril'sk-Talnakh (Russia). Pechenga (Russia). Thompson Belt (Canada). Ungava Belt (Canada). Limpopo Belt (Botswana)

OCCURENCES - GUIANA SHIELD Not known

TONNAGE and GRADE 3.96 Bt. 0.66% Cu. 0.2% Ni (ave)

GEOLOGICAL ENVIRONMENT Large layered ultramafic intrusions (peridotite. harzburgite. anorthosite. troctolite). with cumulate to ophitic texture. associated with pyritic shale (source of sulfur).

mostly Paleoproterozoic (1.9-2.1 Ga): intruded during rifting into metasedimentary and metavolcanic rocks: the Ni-Cu sulphide orebodies are localized at the lower part of the intrusions. near the contact with underlying sedimentary/volcanogenic formations: ages vary from Paleoproterozoic to Neoproterozoic. rarely Paleozoic

TECTONIC SETTING Early stage of continental rifting

METALLOGENESIS Mineralogy: pyrrhotite. pentlandite. chalcopyrite. cubanite. ± PGE minerals: Structure: massive. disseminations. blebs. ore-cemented wallrock breccias. and small masses: Alteration: local hydrothermal remobilization: Ore controls: source of external sulfur: syn-intrusion faulting: basal portion of layered intrusion

ASSOCIATED DEPOSIT TYPES Bushveld Fe-Ti-V. Stillwater Ni-Cu

WEATHERING Not known

GEOCHEMICAL SIGNATURE Cu. Ni. Co. PGE. Ti: non-magmatic sulfur in isotopic analyses

EXPLORATION METHODS Extensive sampling and chemical/isotopic analyses

2C

CHEMICAL ELEMENT: Ni
DEPOSIT MODEL: KOMATIITIC Ni - Cu and DUNITIC Ni - Cu

OCCURENCES - WORLD Kambalda (Australia). Mt. Edwards (Australia). Mt. Keith (Australia). Damba (Zimbabwe). Langmuir (Canada). McWatters (Canada). Hitura (Finland). Rankin Inlet (Canada). O'Toole (Brazil). Bon Accord (South Africa). Windarra (Australia). Scotia Mine (Australia). Mt. Martin (Australia). Thompson (Canada)

OCCURENCES - GUIANA SHIELD Not known

TONNAGE and GRADE 0.2 Mt (min). 17 Mt (max). 1.6 Mt (ave). 0.71% Ni. 0.0056% Cu (min). 3.4% Ni. 0.28% Cu (max). 1.5% Ni. 0.094% Cu. 0.085% Co. 0.078 g/t Au. 580 ppb Pd. 1 10 ppb Ir. 190 ppb Pt (ave)

GEOLOGICAL ENVIRONMENT Ni-Cu sulphides associated with komatiitic volcanic and subvolcanic rocks (komatiite. komatiitic basalt. basalt. peridotite. dunite). with MgO content between 15 - 40%. with spinifex structures. with bladed olivine and pyroxene with skeletal and dendritic appearance: komatiitic sequences are often more than 1 km thick. often include cyclic units of ultramafic flows alternating with variously structured komatiitic basalts: flow-top breccias often grade into thin hyaloclastite (palagonite) tuffs which. in turn. may pass into grey. green. or black arenitic to pelitic volcanoclastics: also included are chemical sediments and alterites (silicites. carbonates): subvolcanic dykes. sills. and irregular bodies are often associated to the volcanic komatiites: in areas where thick komatiitic sequences are developed. the lowermost. highly magnesian flows with few interflow sediments are mineralized: related to Archean (mainly) and Paleoproterozoic greenstone belts

TECTONIC SETTING Arc and back-arc related metallogeny

METALLOGENESIS Mineralogy: pyrite. pyrrhotite. chalcopyrite. pentlandite. ± PGE minerals: Structure: lenticular. irregular elongate to tabular. pipe-like Ni-Cu sulphides. and disseminated at the upper part of the deposit: Alteration: none related to ore: Ore controls: zones of increased spinifex development. active faulting. presence of sulphide-bearing chert and argilite: Genesis: magmatic origin of the Ni-Cu sulphides (separation of the sulfide phase before melt solidification and its gravity accumulation along the base of a flow) or exhalational origin

ASSOCIATED DEPOSIT TYPES Synorogenic-synvolcanic Ni-Cu

WEATHERING Gossan. indurated iron-rich laterites

GEOCHEMICAL SIGNATURE Mg. Ni. Cu. PGE

EXPLORATION METHODS Geochemical studies of the chemical nature of the mafic-ultramafic volcanic subvolcanic flows. detailed geological mapping in known komatiitic dunitic areas

2D

CHEMICAL ELEMENT: Ni
DEPOSIT MODEL: SYNOROGENIC-SYNVOLCANIC Ni-Cu

OCCURENCES - WORLD Selebi (Botswana). Vammala (Finland). Empress (Zimbabwe). Carr Boyd (Australia). Kenbridge (Canada). Lorraine (Canada). Lynn Lake (Canada). Macassa (Canada). Phoenix (Botswana). Hosangen (Norway).

OCCURENCES - GUIANA SHIELD Not known

TONNAGE and GRADE 0.26 Mt (min). 17Mt (max). 2.1 Mt (ave). 0.35% Ni. o.13% Cu (min). 1.6% Ni. 1.3% Cu (max). 0.77% Ni. 0.47% Cu. 0.017% Co. 0.035 ppm Au. 63 ppb Pd. 16 ppb Pt (ave)

GEOLOGICAL ENVIRONMENT Small to medium sized gabbroic (gabbro. norite. peridotite. anorthosite) intrusions in greenstone belts. with cumulate texture. intruded synvolcanically or during orogenic development of a metamorphic terrane containing volcanic and sedimentary rocks: most gabbroic-hosted deposits are in structurally complex settings and some are controlled by ductile shears (ore mylonite or ball ore. with durchbewegung fabrics): the orebodies consist of several folded sheets and lenses. occuring along gabbroid contacts: mostly in Archean and Paleoproterozoic greenstone belts or higher-level metamorphic belts

TECTONIC SETTING Arc and back-arc related metallogeny

METALLOGENESIS Mineralogy: pyrrhotite. pentlandite. magnetite. chalcopyrite. ± ilmenite. ± rutile: Structure: lenses of disseminated to massive mineralization. commonly highly deformed and metamorphosed: Alteration: none: Ore control: more ultramafic parts of the intrusion. near its basal contacts

ASSOCIATED DEPOSIT TYPES Komatiitic and Dunitic Ni-Cu

WEATHERING Ni-rich laterites

GEOCHEMICAL SIGNATURE Ni. Cu. Co. PGE

EXPLORATION METHODS Detailed geological mapping. geochemical anomalies. drilling. magnetic anomalies

3

CHEMICAL ELEMENT: Ti
DEPOSIT MODEL: ANORTHOSITE Ti

For Bushveld Fe-Ti-V model see IC:

OCCURENCES - WORLD Sanford Lake (USA). Laramie Range (USA). Pluma Hidalgo (Mexico). Grenville Province (Canada). Nain Province (Canada). Kunene (Angola-Namibia). Luanping (China). Dolginovo (Russia). Roseland (USA). Tsaga (Russia). Karelich (Bielarus). Iron Mountain (USA). Sanford Lake (USA)

OCCURENCES - GUIANA SHIELD Kaburi (Guyana). Tampoc (?) (French Guyana)

TONNAGE and GRADE Between 125 and 300 Mt. between 18%o and 32%o Ti. and 36%o to 49%o Fe. Locally. V enrichment (up to 0.76% V)

GEOLOGICAL ENVIRONMENT Anorthosite. "alkalic" anorthosite and ferrodiorite (gabbro, charnockite) massifs intruded in the lower crust granulite metamorphic terranes. under hot. dry conditions. They are so-called "massif anorthosite". petrographically and tectonically different of "layered" anorthosite (Bushveld). and "Rapakivi" anorthosite: many of the anorthosite massifs have been involved in high-grade metamorphic events. but those of the Nain Province are virtually unaffected by postemplacement metamorphism and deformation. The anorthosite massifs are distributed irregularly. as single independent bodies or clusters in a broad. loosely defined belt: mostly ages range from 0.9 to 1.5 Ga (Neo- to Mesoproterozoic). but older (Archean) and younger (Paleozoic) anorthosites do exist

TECTONIC SETTING Some anorthosite massifs are considered high-level (at depths less than 12 km) and others are solidified in the lower crust: both types are related to the taphrogenic (pull-apart. rift) and collisional regimes within the continental crust

METALLOGENESIS Most anorthosites contain local accumulations of Ti-Fe oxides and there is some difference in ore mineralogy and in the style of mineralization. depending on the petrographic variety of anorthosite. Mineralogy: ilmenite+Ti-magnetite $\pm$ ulvospinel (in anorthosite); ilmenite $\pm$ apatite (in ferrodiorite); ilmenite $\pm$ rutile (in "alkalic" anorthosite); minor sulphide (pyrrhotite. pentlandite. chalcopyrite) quantities in all anorthosite types. Structure: four types of Ti-Fe oxide emplacement have been distinguished: 1) extensive low-grade stratiform disseminated ore bodies conformable with the magmatic layering: 2) conformable sheets and lenses of massive Ti-magnetite- plagioclase hybrids: 3) injected peneconcordant to discordant lenses and sheets of massive Ti-magnetite: 4) Ti-Fe oxide fracture veinlets: the disseminations and veinlets are usually located along anorthosite margins. whereas concordant layers (tabular zones or irregular lenses) are frequently located within or at base of ferrodiorite: Alteration: none related to ore: Ore controls: high-temperature metasomatism between Ti-Fe oxides-rich country rock and anorthosite and/or immiscible Ti-P liquid in ferrodioritic magma. forming cumulate-like bodies

ASSOCIATED DEPOSIT TYPES Not known

WEATHERING Ti $\pm$ Fe $\pm$ P enrichment in weathering zone

GEOCHEMICAL SIGNATURE Ti. P. Zr. V

EXPLORATION METHODS Ground/airborne magnetometry and gravimetry. geochemical sampling. airborne radar (SLAR) imagery (circular features)

4A

CHEMICAL ELEMENT: Cu
DEPOSIT MODEL: BASALTIC Cu and SEDIMENT-HOSTED Cu

For Stillwater Ni-Cu see 2A; for Duluth Ni-Cu see 2B; for Komatiitic Ni-Cu see 2C; for Synorogenic-synvolcanic Ni-Cu see 2D;

OCCURENCES - WORLD (Only Precambrian) Redstone (Canada). Copper Harbour (USA). Stoer (Scotia). Ugui (Russia). Santa Barbara (Brazil). Pandura (Australia). Waterberg (South Africa). Zaïre Copperbelt. Coppermine River (Canada). Gabozero (Russia). Mamainse Point (Canada). White Pine (USA).

OCCURENCES - GUIANA SHIELD Not known

TONNAGE and GRADE Variable. between 5Mt and 135 Mt. between 0.6°o Cu and 5°o Cu - Ag. ± Co · U ± Ba ± Pb ± Zn

GEOLOGICAL ENVIRONMENT Subaerial to shallow marine flood (plateau) basalt flows. breccias and tuffs. red-bed sandstone. conglomerate. limestone. and black shale: frequently. the sedimentary rocks are pigmented red to brownish red by powdery hematite coating clasts and dispersed in the matrix ("red beds"). Because of the prevalent deposition of red beds in the tectonically active area. additions of volcanic material are common. They range in intensity from a minor epiclastically derived volcanic detritus to dominantly volcanic (mainly basaltic) sequences with minor sediments (" volcanic red beds"): frequently. sedimentary/volcanic deposition cycles are reported: the metallogeny is much influenced by the basement composition and by permeability (the amygdaloidal basalt units. scoriaceous and brecciated flowtops. porous interflow sediments as conglomerates and sandstones. faults. breccia zones and shears represent the most important host rocks for mineralization): disseminated native cooper in the upper parts of thick sequences of subaerial basalt. and cooper sulphides in overlying and interbedded sedimentary rocks: the age ranges from Paleoproterozoic to Tertiary

TECTONIC SETTING Intracontinental and continental margin rift. aulacogen-failed arm of triple junction of plate spreading. major growth faults and grabens

METALLOGENESIS Mineralogy: native cooper. native silver. chalcocite. bornite. chalcopyrite. pyrite ± barite. ± pechblende. ± thorite ± monazite: Structure: flow-top breccia and amygdules filling in basalt. fine grains in clastic rocks. and replacement of carbonates in limestones: Ore control: flow-top breccia. amygdules. and fractures in basalts. highly permeable sedimentary rocks. organic shale and limestone. reducing low-pH environment. synsedimentary faulting. major crustal faults in intracontinental zones: Genesis: syngenetic. epigenetic. remobilizations.

ASSOCIATED DEPOSIT TYPES Kipushi Cu-Pb-Zn. Sandstone U. Evaporite deposits. Volcanogenic Mn. Sedimentary-exhalative Pb-Zn

WEATHERING Dispersed cooper nuggets in streams draining basalts and in situ chalcocite/bornite-covelline enrichment

GEOCHEMICAL SIGNATURE Cu. Ag. Zn. Cd. Pb

EXPLORATION METHODS Radiometry (weak radioactivity in some deposits). geochemical sampling. basin analysis

4B

CHEMICAL ELEMENT: Cu
DEPOSIT MODEL: PORPHYRY Cu ± Mo ± Au

OCCURENCES - WORLD (Only Precambrian) Malanjkhand (India). Zhongtiaoshan (China). Coppin Gap (Australia). Boddington (Australia). Tallberg (Sweden). Pearl Lake (Canada). Don Rouyn (Canada). Haib River (Namibia). Kopsa (Finland). Goren (Burkina Faso). Gaoua (Burkina Faso). Grandroy (Canada)

OCCURENCES - GUIANA SHIELD Eagle Mountain (Guyana)

TONNAGE and GRADE 19 Mt (min). 1100 Mt (max). 140 Mt (ave). 0.31°o Cu. 0.0072°o Mo. 0.2 g t Au (min). 0.94°o Cu. 0.035% Mo. 0.72 g/t Au (max). 0.54% Cu. 0.016% Mo. 0.38 g/t Au (ave)

GEOLOGICAL ENVIRONMENT The Precambrian porphyry deposits are either monometallic end-members. or mixtures of two or more anomously concentrated metals in various proportions: some correspond reasonably to the Phanerozoic model porphyries. but other are genetically uncertain:

disseminated. stringer or stockwork ore accumulations in intrusive or pseudointrusive host rocks that mimic some aspects of their Phanerozoic counterparts: some "stockwork Mo" and "plutonic gold-only porphyry" deposits could be considered in this "porphyry Cu–Mo–Au" model: in terms of relative age, two varieties can be distinguished among porphyries emplaced into greenstone metavolcanics: 1. early porphyries, affiliated to synvolcanic intrusions; 2. late porphyries, usually associated with late orogenic to postorogenic intrusions emplaced into a previously deformed and metamorphosed greenstone belt suite: the host rocks to these intrusions include a wide variety of lithologies, consisting of high-level tonalite to monzogranite or syenitic porphyries intruding granitic, volcanic, calcareous sedimentary, and other rocks: porphyry has closely spaced phenocrysts in a microaplitic groundmass frequently associated with abundant dykes, breccia pipes, and faults: a considerable proportion of Precambrian porphyries are partially or entirely sheared and converted into sericite and chlorite schists

TECTONIC SETTING Rift zones contemporaneous with Andean or island-arc volcanism along convergent plate boundaries

METALLOGENESIS Mineralogy: chalcopyrite, pyrite, ± molybdenite, ± native Au, ± magnetite, ± bornite ± scheelite ± marcasite ± pyrrhotite ± Bi–Au–Ag–Pb tellurides and selenides: Structure: stockwork veinlets and disseminated sulphide grains: Alteration: from innermost zones outward: sodic-calcic, potassic, phyllic, argillic to propylitic: Ore controls: stockwork veins in porphyry, along porphyry contact, and in favorable country rocks (carbonate rocks, mafic and older granitic rocks): the metallization is centered on the K-silicate alteration facies: Genesis: magmatic origin for all the essential components of porphyry deposits, with variable superimposed meteoric–hydrothermal activity

ASSOCIATED DEPOSIT TYPES Base-metal skarn. Porphyry-Cu skarn related. Epithermal veins

WEATHERING Green and blue Cu carbonates and silicates, secondary chalcocite, hematitic limonite

GEOCHEMICAL SIGNATURE Cu ± Mo ± Au ± Ag ± W

EXPLORATION METHODS Strong color anomalies (in arid areas), geochemical prospecting techniques (in vegetated areas), distinctive fluid inclusion assemblages, geophysical prospection (ground magnetometry, I.P)

4C

CHEMICAL ELEMENT: Cu
DEPOSIT MODEL: OLYMPIC DAM Cu-U-Au

OCCURENCES - WORLD Olympic Dam (Australia), Vergenoeg (South Africa), Great Bear Lake (?) (Canada), Redbank (?) (Australia), Bayan Obo (?) (China)

OCCURENCES - GUIANA SHIELD Not known

TONNAGE and GRADE 2000 Mt, 1% Cu, 0.06% U, 0.6 g/t Au, 3.5 g/t Ag (ave)

GEOLOGICAL ENVIRONMENT Alkali granite with granophyric texture, brecciated and forming clasts in matrix-rich breccia: the granite breccia forms an annulus between the surroundind granite and polymict, hematite-rich, bedded, and intrusive breccias in the more central portions of the complexes: the granite appears to be typical anorogenic: the highest grade mineralization is found in the breccias of most varied lithology: also felsic volcanic breccias and tuffs are reported: genesis is not yet well understood: the brecciation, alteration, and extensive iron introduction, followed by emplacement of U, Cu, and Au, are attributed to a hydrothermal system active at the near-surface level, and spilling-over into the subaerial environment: the system has been imagined as a vented maar (diatreme) or hydrothermal upwelling controled by steep faults: age is Mesoproterozoic (1.5 Ga)

TECTONIC SETTING Graben transcurrent to broad arch related to anorogenic magmatism (hotspot)

METALLOGENESIS Mineralogy: the copper minerals comprise bornite, chalcopyrite, and

chalcocite. occuring either as clastic fragments in the breccia matrices or as replacements and open-space fillings: U is present as uraninite ± coffinite ± brannerite: REE-minerals (bastnaesite. florencite) and thin veins containing fluorite. barite. and siderite also occur: Structure: ore minerals in breccia matrix and in veins: the textures of the breccia are extremely variable. commonly consisting of subangular to subrounded fragments. in a fine-grained. rock-flour matrix: clast-supported breccias are rare: the brecciated granites consit of highly disrupted and hydrothermally altered wall-rock granite: diffuse foliation or layering and replacement textures are locally described in breccias: Alteration: dominated by hematite-chlorite-sericite assemblages. with locally intense silicification: close to the deposit. hematitization becomes more abundant and appears to overprint early sericitization: hematite alteration grades into hematite replacement and intense iron metasomatism. particulary toward the centre of the deposit: quartz (associated with higher average gold) and intense chlorite alteration of granite below ore bodies: Ore controls: the mineralization was broadly contemporaneous with formation of the host breccias: matrix polymictic breccia and fractures parallel to long axis of graben

ASSOCIATED DEPOSIT TYPES Sediment-hosted Cu. Algoma type Fe

WEATHERING Not known

GEOCHEMICAL SIGNATURE Cu. U. Co. Au. F. Ba

EXPLORATION METHODS Trace of graben can be detected in post-ore cover rocks as photo lineaments: geophysical techniques (radiometry. magnetometry). geochemical sampling

4D

CHEMICAL ELEMENT: Cu
DEPOSIT MODEL: VOLCANOGENIC MASSIVE SULFIDES (VMS) or KUROKO-TYPE or NORANDA- TYPE

OCCURENCES - WORLD (Only Precambrian) Amulet (Canada). Corbet (Canada). Flin Flon (Canada). Mt. Lyell (Australia). Kidd Creek (Canada). Mobrun (Canada).

OCCURENCES - GUIANA SHIELD Paul Isnard (French Guyana). Groete Creek(?)(Guyana)

TONNAGE and GRADE 0.12 Mt (min). 18 Mt (max). 1.5 Mt (ave). 0.45% Cu (min). 3.5% Cu (max). 1.3% Cu. 1.9% Pb. 2% Zn. 0.16 g/t Au. 13 g/t Ag (ave)

GEOLOGICAL ENVIRONMENT VMS occur in two principal geological settings: 1. areas dominated by mafic volcanic rocks. and 2) areas containing subequal amounts of mafic volcanic rocks and sedimentary strata: 1): these deposits can be divided into: a) associated with sequences of primarily massive to pillowed mafic flows: and b) associated to mafic and felsic amygdaloidal and scoriaceous flows and pyroclastic rocks. volcanic breccia and epiclastic strata: both types of deposits occur in volcanic sequences that have subvolvanic intrusions near their base: trondhjemites predominate. but also layered mafic intrusions are reported: 2) deposits associated to relatively monotonous. regular sequences of volcanic (dominant mafic) and sedimentary (dominant pelitic) strata: these terranes are typically highly deformed. making identification of primary tectonic relationships difficult: they are very rare in Precambrian greenstone belts: age ranges from Archean to Tertiary

TECTONIC SETTING Arc-related metallogeny. Local extensional tectonic activity

METALLOGENESIS Mineralogy: upper massive zone (black ore): pyrite. sphalerite. chalcopyrite. galena. tetraedrite: lower massive zone (yellow ore): pyrite. chalcopyrite. sphalerite. pyrrhotite. magnetite: stringer (stockwork): pyrite. chalcopyrite: Structure: massive. disseminated or sulphide-matrix breccia: Alteration: there are two diffrent types: a) alteration pipes. occuring immediately below the MS zone. comprising a chloritic core surrounded by a sericite ± talc ± magnetite ± phlogopite rim: and 2) lower

semi-conformable alteration zones. occuring several hundreds of metres below the MS deposit. comprising quartz-epidote and. locally. carbonate zones that are hundreds of meters thick: Ore controls: an impermeable cap to the hydrothermal reaction zone is the most important factor in the formation of VMS: the more felsic top of volcanic or volcanic-sedimentary sequences: near center of felsic volcanism: related to the pyritic shales: redeposited ore in paleo depressions in the sea floor: Genesis: VMS deposits form from hydrothermal fluids as syngenetic accumulations on or near the sea floor: the sources of fluids are circulating seawater and magmatic water

ASSOCIATED DEPOSIT TYPES Algoma Fe. Superior Fe. Volcanogenic Mn

WEATHERING Variable colored gossans

GEOCHEMICAL SIGNATURE Pb. Au. Mg. Zn. Hg. Cu. Ba. As. Ag

EXPLORATION METHODS Geophysics (airborne electromagnetic surveys). mapping and geochemical analyses (VMS are associated in time and space with bimodal basalt-dacite. rhyolite suites. generated from strongly fractionated magma bodies. reflected in the REE patterns: Hg leakage haloes: paleomorphological reconstructions. study of the alteration zones

5

CHEMICAL ELEMENTS: Zn and Pb
DEPOSIT MODEL: STRATIFORM SEDIMENT-HOSTED Zn-Pb-Ag SULPHIDES or SEDEX TYPE

For Volcanogenic massive sulfides see **4D**:

OCCURENCES - WORLD (Only Precambrian) Sullivan (Canada). Broken Hill (Australia). Singhbum (India). Balmat-Edwards (USA). Kholodnina (Russia). Big Syn (South Africa). Black Mountain (South Africa). Century (Australia). Dariba (India). Rosh Pinah (Namibia). Lady Loretta (Australia). Balaria (India). Mochia (India)

OCCURENCES - GUIANA SHIELD Not known

TONNAGE and GRADE 1.7 Mt (min). 130 Mt (max). 15 Mt (ave). 2.4% Zn. 1% Pb (min). 13% Zn. 7.7% Pb (max). 5.6% Zn. 2.8% Pb (ave)

GEOLOGICAL ENVIRONMENT Euxinic marine sedimentary rocks including black shale. siltstone. sandstone. chert. and minor bimodal volcanic rocks: slump breccias and conglomerates are associated with synsedimentary faults: the sulphide and sulphate minerals are interbedded with the sedimentary volcanic rocks: the deposits are formed from the discharge of hydrothermal fluids onto the sea floor: the bulk of the ore is contained in a stratiform sulphide body. which can usually be divided into three principal facies: bedded ore facies. distal sedimentary facies and vent complex: the strata that host SEDEX deposits are commonly characterized by abrupt facies or thickness changes. horst and graben development. basaltic volcanic rocks and sills. syndepositional fault-derived resedimented material. and local unconformities: some SEDEX deposits (ex. Broken Hill) are located in medium to high-grade metamorphic terranes. being characterized by the presence of granite sills synchronous with ore deposition and by the association with continental evaporites coeval with hydrothermal activity: Precambrian Zn-Pb deposits are hosted in high-grade metamorphic terranes: age ranges from Paleoproterozoic to Paleozoic. but the most important deposits are Mesoproterozoic (1.7-1.4 Ga)

TECTONIC SETTING Advanced stages of rifting. in marine epicratonic and intracratonic basins. with smaller second- and third-order basins

METALLOGENESIS Mineralogy: sphalerite. galena. pyrite. pyrrhotite ± barite. ± chalcopyrite: Structure: stratiform accumulation of finely crystalline and disseminated sulphides: Alteration: silicification. tourmalization. albitization. and chloritization: some deposits have no reported alteration:

Ore controls: small local basins form the morphological trap. euxinic facies. synsedimentary faults representing the feeder zones: Genesis: 1. submarine hydrothermal ore deposition associated with volcanism: 2. ore deposition in a clastic sedimentary sequence: 3. replacement of a pre-existing Mn-rich horizon by fluids derived from post-tectonic granites

ASSOCIATED DEPOSIT TYPES Volcanogenic Massive Sulphide deposits. Mississippi Valey-type deposits

WEATHERING Gossans containing carbonate. sulphates. and silicates of Zn. Pb. and Cu

GEOCHEMICAL SIGNATURE Cu. Pb. Zn. Ba

EXPLORATION METHODS Gravimetric determination of major rift graben/horst zones. basin analysis. applied geochemistry. exploration geophysics. and drilling

6A

CHEMICAL ELEMENT: Au
DEPOSIT MODEL: HOMESTAKE Au or IRON-FORMATION-HOSTED Au

For Olympic Dam Cu-U-Au see 4C:

OCCURENCES - WORLD Homestake (USA). Dome Mine (Canada). Barberton (South Africa). Ida (Australia). McWatters (Canada). Passagem (Brazil). Morro Velho (Brazil). Vulbachikwe (Zimbabwe). Cauê (Brazil). Kolar (India)

OCCURENCES - GUIANA SHIELD Not known

TONNAGE and GRADE 0.093 Mt (min). 12 Mt (max). 0.94 Mt (ave). 4.4 g/t Au (min). 19 g/t Au (max). 9.2 g t Au (ave)

GEOLOGICAL ENVIRONMENT Strabound to stratiform gold deposits in iron-rich and carbonate-rich sediments. mostly in Archean terranes: regionally (greenschist to amphibolite. rarely granulite facies) metamorphosed mafic and felsic volcanic rocks. komatiites and volcaniclastic sediments. interlayered with BIF. intruded by felsic plutonic rocks (granites. quartz-porphyries. syenite porphyries): the ore zones consist of multiple. interbedded. sulphide-rich and sulphide-poor horizons ranging in thickness from a few cm to almost 2m: usually. the rocks that host the gold deposits have been deformed into a set of complex folds: Au mineralization represents submarine hot-spring activity related to volcanism or later hydrothermal activity related to intrusive rocks

TECTONIC SETTING Arc and back-arc related metallogeny in the Archean-Paleoproterozoic greenstone belts

METALLOGENESIS Mineralogy: native Au. pyrite. pyrrhotite. arsenopyrite. magnetite ± scheelite ± molybdenite ± fluorite: Structure: narrow thinly laminated beds. scattered grains and blebs. veins. or lenses. overlying stringers: Alteration: quartz. siderite. tourmaline. chlorite. prismatic cummingtonite: oxide-facies BIF replaced by pyrite and pyrrhotite: Ore controls: Fe-rich siliceous or carbonate-rich chemical sediment. discordant quartz-carbonate veins with Au: Genesis: syngenetic. epigenetic. and multistage or remobilization

ASSOCIATED DEPOSIT TYPES Algoma Fe. Superior Fe. Volcanogenic Massive Sulphides. Low-sulphide gold-quartz veins

WEATHERING Fe-rich gossans

GEOCHEMICAL SIGNATURE As. Au. Ag. Fe. Bi. Hg

EXPLORATION METHODS Regional airborne magnetic surveys (positive magnetic anomalies

for Fe-oxides and negative anomalies when Fe-oxides are replaced by pyrite and pyrrhotite). electromagnetic (EM). self-potential (SP). induced polarization and resistivity surveys (for detecting sulphide concentrations). geological mapping (association of gold with siliceous. sulphide-bearing carbonate iron formation). geochemical sampling (strong As anomalies)

6B

CHEMICAL ELEMENT: Au
DEPOSIT MODEL: LOW-SULFIDE Au-QUARTZ VEINS or MESOTHERMAL QUARTZ VEINS or SHEAR-ZONE Au or OROGENIC Au

OCCURENCES - WORLD (Only Precambrian) Hollinger-McIntyre (Canada). Kalgoorlie (Australia). Sigma (Canada). Kirkland Lake (Canada). Lamaque (Canada). Ashanti (Ghana). Fazenda Brazileiro (Brazil)

OCCURENCES - GUIANA SHIELD El Callao (Venezuela). Botanamo (Venezuela). Las Cristinas (Venezuela). Omai (Guyana). Alex Hill (Guyana). Loulouie (French Guyana). Adieu-Vat (French Guyana). Changement (French Guyana). Lawa region (Suriname). Aurora (Guyana). Peter's Mine (Guyana). Loksie Hatti (Suriname). Lo Increible (Venezuela). Vuelvan Caras (Venezuela). Ste. Élie (French Guyana)

TONNAGE and GRADE 0.001 Mt (min). 0.91 Mt (max). 0.03 Mt (ave). 1.5 g/t Au (min). 43 g/t Au (max). 16 g/t Au (ave)

GEOLOGICAL ENVIRONMENT Gold in massive persistent quartz-carbonate veins in metamorphosed (greenschist facies) volcanic rocks. volcanic sediments. and late granitoid batholiths: generally. the deposits having significant tonnage and grade are in areas underlain by greenstone: the veins may occupy ductile. high-angle shear zones. and major geologic terrane boundaries of regional extent: deposits in higher-level. more brittle. sheared environments form stockwork and disseminated systems in and adjacent to plutonic bodies: age ranges from Archean to Tertiary.

TECTONIC SETTING Back-arc and arc related metallogeny

METALLOGENESIS These veins differ from other auriferous veins in that they characteristically contain only a few percent sulphide minerals. commonly pyrite: ore zones are lenticular. tabular or irregular shaped bodies. composed of veins. breccia zones. and/or stockworks: the ore zones are localized by: a) zones of anomalously high strain within a deformation zone: b) pre-existing structural anisotropies: c) a preffered lithology. where a strong competency contrast exists between adjacent rock types: d) fold limbs and fold noses: Mineralogy: native Au. quartz. pyrite. subordonated galena. sphalerite. chalcopyrite. arsenopyrite. scheelite. tellurides: abundent Ca. Mg. and Fe carbonates: Structure: ribbon quartz. open-space filling: locally. stockworks in intrusive rocks: plutonic porphyry Au: Alteration: quartz. siderite. albite. sericite: locally. concentric alteration zones. similar to porphyry types: Ore controls: high-angle faults. ductile to brittle tectonic zones. joint sets. rheological contrasts between different lithotypes

ASSOCIATED DEPOSIT TYPES Homestake Au. VMS

WEATHERING Abundant quartz chips in soil. auriferous laterite. Au-bearing saprolite. and extensive placer Au deposits

GEOCHEMICAL SIGNATURE Au. As. W. Ag. Pb. Cu

EXPLORATION METHODS Regionally. delineation of fault/shear zones: within the shear systems. both intersecting shears and felsic intrusions commonly represent the locus of Au concentration: at the property scale. two characteristics may assist exploration of a specific occurrence: a) virtually all ore zones are elongate and plunging: b) careful documentation of the mineralogy and alteration in drilling may also

present a guide to ore. Geochemical and geological mapping paying special attention to the quartz veins and blocks (in soils)

CHEMICAL ELEMENT:Au
DEPOSIT MODEL: HEMLO TYPE or EPITHERMAL Au or SULPHIDIC SCHIST TYPE

OCCURENCES - WORLD (Only Precambrian) Hemlo (Canada). Shamva (Zimbabwe). Big Bell (?) (Australia). Ariab (Sudan)

OCCURENCES - GUIANA SHIELD Not known

TONNAGE AND GRADE 60 - 80 Mt. 7.2 g/t Au (ave)

GEOLOGICAL ENVIRONMENT These gold deposits are characterized by a dominance of sulphide mineralization over quartz veins and by a paraconcordant position within their host volcanic-sedimentary sequence: ores typically comprise disseminated and vein pyrite in sericite schists which are the result of potassium metasomatism: these deposits are relatively inconspicupous so difficult to recognize: the host rocks are metamorphosed in middle greenschist and lower amphibolite facies. and are strongly modified by ductile tectogenesis, by several phases of hydrothermal alteration. and by thermal metamorphism at the fringe of granitization front: age is Archean

TECTONIC SETTING Arc and back-arc related metallogeny in greenstone belts

METALLOGENESIS Mineralogy: native gold. pyrite. molybdenite. arsenopyrite. stibnite. sphalerite. galena. chalcopyrite. cinnabar. gold-bearing tellurides. pyrrhotite. niccolite. gold-silver selenides. barite: many extremely rare minerals. indicating low-pressure. low-temperature epithermal association: Structure: subparallel ore zones (up to 30 m wide): in between are often numerous thin discontinous ore-bearing layers: local varieties include bands to massive lenses of granular gold-bearing pyrite: Alteration: strong K and Ba enrichment. and Na. Ca.. and Mg depletion: Ore controls: there is not complete unity in ideas about the factors which control the gold deposition: Genesis: pre or post-metamorphic ore emplacement: syngenetic or epigenetic: epithermal. mesothermal. or both (multiple phases of mineralization): poorly constrained model

ASSOCIATED DEPOSIT TYPES Mesothermal gold. Homestake gold. Volcanogenic Massive Sulphides. Polymetallic (Cu-Pb-Zn) veins (?)

WEATHERING Strong yellowish limonitic alteration

GEOCHEMICAL SIGNATURE Au. Ba. Fe. Hg. As. Sb. Te. Se

EXPLORATION METHODS Mapping of regional ductile zones: anomalous mineralogical paragenesis: geochemical studies

CHEMICAL ELEMENT: Au
DEPOSIT MODEL: QUARTZ PEBBLE CONGLOMERATE Au-U

OCCURENCES - WORLD Witwatersrand (South Africa). Elliot Lake (Canada). Jacobina (Brazil). Tarkwa (?) (Ghana). James Bay (Canada). Krugersdorp (South Africa). Fortescue (Australia). Medicine Bow (USA). Padlei (Canada)

OCCURENCES - GUIANA SHIELD Stone Creek (Suriname). Tafelberg (Suriname). Emma Range (Suriname). Wilhelmina Mountains (Suriname). Käyser Mountains (Suriname). Montagne Tortue (in Upper Detrital Formation. French Guyana). Trois Pitons (French Guyana). Montagne Genevieve (French Guyana). Santa Elena de Uairen (Venezuela)

TONNAGE and GRADE Between 150 Mt and 1000 Mt. 6.3 g/t and 9.2 g/t Au. 188 G t and 477 g t U

GEOLOGICAL ENVIRONMENT Thick (up to 16 km) oligomictic successions of clastic sedimentary rocks dominated by thick quartzose arenite units that range chemically. mineralogically. and texturally from submature to supermature: major portions of these variably micaceous and feldspathic quartzite units. including very coarse-grained members containing pyritic (or hematitic) quartz-pebble beds. contain trough and planar cross-beds with unimodal dip directions: these units are interpreted as having been deposed under fluvial conditions. in brained-stream systems within broad valleys. and . most importantly. on huge alluvial fans: in addition. some deposits contain volcanic rocks. quartz arenites with bimodal cross-bedding. siltstones and argillites. carbonate rocks. and iron-formations: major deposits are Archean to Paleoproterozoic

TECTONIC SETTING 1. Intracontinental. related to the early stages of rifting: slow subsidence of Archean craton. followed by moderate uplift and erosion to remove Phanerozoic strata and retain Paleoproterozoic rocks: 2. filling of a foreland basin. in an Andean-type volcanic arc

METALLOGENESIS Mineralogy: gold. pyrite. uraninite. brannerite. zircon. chromite. monazite. Os-Ir alloys. platinum: Proterozoic occurences have only traces of pyrite and no uraninite: Structure: pyrite may occur as rounded grains. and concentrically layered concretions: gols is in small angular grains. up to 0.1 mm in diameter: Alteration: none related to mineralization: Ore controls: braided stream channels in broad unconformity surfaces in alluvial fans: gold concentrates at base of mature conglomerate beds deposited on an erosion surface: carbonaceous layers resembling algal mats deposited at low-energy base of fan contain U and fine Au: Genesis: polygenetic processes: physical reworking. entrapment of hydrothermally introduced gold by clastic (placer) pyrite: pyrite formation by hydrothermal sulphidation of detrital magnetite with simultaneous gold precipitation: and selective Au and U precipitation in a permeable horizon (conglomerate) . from downward-percolating groundwaters

ASSOCIATED DEPOSIT TYPES Recent gold placer deposits: Low-sulphide gold quartz veins: Homestake Au in basement rocks: Superior Fe in overlying sequences

WEATHERING Residual Au in saprolite/laterite profile

GEOCHEMICAL SIGNATURE Au. U. PGE

EXPLORATION METHODS Anomalous radioactivity: geological mapping (thick mature conglomerate sequences): basin analysis

7A

CHEMICAL ELEMENT: Sn
DEPOSIT MODEL: Sn GREISEN

OCCURENCES - WORLD (Only Precambrian) Irish Creek (USA). Encruzilhada (Brazil). Euraji (Finland). Sabaloka (Sudan). Jabal As Silsilah (Saudi Arabia). Georgetown Inlier (Australia). Ahvenisto (Finland). Eurajoki (Finland). Bushveld (South Africa - granites associated to mafic ultramafic layered intrusions). Kitelya (Russia)

OCCURENCES - GUIANA SHIELD Morro Potosi (Brazil). Cariri (Brazil). Sao Domingos (Brazil). Pitinga (Brazil)

TONNAGE and GRADE 0.8 Mt (min). 65 Mt (max). 7.2 Mt (ave). 0.17°o Sn (min). 0.47°o Sn (max). 0.28°o Sn (ave)

GEOLOGICAL ENVIRONMENT Specialized biotite and or muscovite leucogranite (A-type). formed by partial melting of felsic granulites in the lower mantle. with distinctive accessory minerals topaz. fluorite. tourmaline and beryl: the greisens are generally post-magmatic and associated with late fractionated melt: granites are nonfoliated (usually postdate major folding). with aplitic and porphyric textures: most granites are probably emplaced at high- to medium levels. into rocks of the basement complex. into the meta-sedimentary sequences of orogens. or into the genetically related volcanics (rhyolite. rhyodacite): age ranges from Archean to Tertiary: in the Guiana Shield. the tin granites belong to two main age groups. corresponding to the Uatuma (1.97 to 1.8 Ga) and post-Uatuma (1.53 to 0.97 Ga) events

TECTONIC SETTING Anorogenic granites intruded in stable cratonic areas (hot spots). or related to accreted margins

METALLOGENESIS Mineralogy: general zonal development of cassiterite. molybdenite. arsenopyrite. beryl. wolframite. bismuthinite. Cu-Pb-Zn sulphide minerals. fluorite. quartz. calcite: Structure: varied. the most common being disseminated cassiterite in massive greisen. and quartz veinlets and stockworks (in cupolar or overlying rocks): less common are pipes. lenses. and tectonic breccias: Alteration: consists of a coarse-grained assemblage developed during late magmatic or deuteric stages of crystallization: incipient greisen: muscovite. chlorite. fluorite. tourmaline: advanced greisenizaton: quartz. muscovite. topaz. fluorite: massive greisen: quartz. muscovite. topaz: Ore controls: cupolas and ridges developed on the roof or along margins of granitoids: faults and fractures: Genesis: syngenetic (endogranitic greisen). and epigenetic (exogranitic greisen)

ASSOCIATED DEPOSIT TYPES Sn ± W veins

WEATHERING Red alteration close to greisen veins: placer deposits (cassiterite) formed by weathering and erosion: concentration of cassiterite by tropical weathering processes is an important factor in the economics of tin recovery

GEOCHEMICAL SIGNATURE Cassiterite. topaz. and tourmaline in streams: muscovite biotite granites may have high contents of SiO_2 (> 73%). and K_2O (> 4%): enrichment in Sn. F. Rb. Be. W. Mo. Pb. Cs. REE. and depleted in CaO. TiO_2. MgO. total FeO. Ni. Cu. Co. V. Sc. and Sr

EXPLORATION METHODS Linear arrays exhibited by the host granites have implications in terms of exploration: geochemical studies (silica and potassium-rich granites). geochemical anomalies (Sn. F. W. Be. Rb). LANDSAT photographs (usually ring complexes)

7B

CHEMICAL ELEMENT: Sn ± W
DEPOSIT MODEL: Sn ± W VEIN TYPE

OCCURENCES - WORLD Kibaran Tin Belt (Rwanda. Uganda and Burundi). Agargaon (India). Hamme (USA). Pedra Petra (Brazil). Novo Trento (Brazil). Wankie (Zimbabwe). Lake Ladoga area (Russia)

OCCURENCES - GUIANA SHIELD Oriento Novo (Brazil). Queimadfa (Brazil). Pedra Petra (Brazil). Jorka Creek (Suriname). Alto Paragua (Venezuela)

TONNAGE and GRADE 0.012 Mt (min). 4.5 Mt (max). 0.24 Mt (ave). 0.56% Sn. 0.6% WO_3 (min). 2.3% Sn. 1.4% WO_3 (max). 1.3% Sn. 0.91% WO_3 (ave)

GEOLOGICAL ENVIRONMENT The Sn-W veins have closed spatial relation to multiphase granitoids (biotite and or muscovite leucogranite. monzodiorite. syenite). intruding sandstone. shale. and metamorphic equivalents: the host rocks have commonly phanerocrystalline textures. but minor pegmatitic bodies and porphyroaphanitic dykes are present: Sn veins are usually related to mesozonal to hypabissal plutons. with extrusive rocks generally absent. with thermally metamorphosed roof rocks. but frequently crosscut by dykes and dyke swarms: the Sn veins often grade into cassiterite- and Sn-Ta-Nb-mineralized pegmatites: W veins are related to the tensional fractures in epizonal granitic plutons and their wallrocks: usually. country rocks are metamorphosed in greenschist facies: ages range from Paleoproterozoic to Tertiary: few Archean occurences are reported

TECTONIC SETTING Foldbelts and accreted margins with late orogenic to postorogenic granitoids which may. in part. be anatectic

METALLOCENESIS Mineralogy: extremely varied: cassiterite. wolframite. molybdenite. bismuthinite. pyrite. pyrrhotite. arsenopyrite. scheelite. hematite. stannite. beryl. fluorite: although variations and overlaps are ubiquitous. many deposits show an inner zone of cassiterite-wolframite fringed with Pb. Zn. Cu. and Ag sulphide minerals: Structure: massive quartz veins with minor vugs. brecciated bands. filled fissures. replacement. open cavities: sometimes. the veins grade into stockwork: Alteration: deepest zones: pervasive albitization: upper zones: vein selvages of muscovite-zinnwaldite. sericite. tourmaline. chlorite (greisen development): an idealized zonal relation might consist of quartz-tourmaline-topaz-zinnwaldite. quartz-sericite-chlorite. quartz-chlorite. chlorite: Ore controls: W: swarms of parallel veins cutting granitic rocks: Sn: within or above the apices of granitic cusps and ridges. variations in vein structure. lithologic and structural changes. vein intersections. dykes. and cross-faults

ASSOCIATED DEPOSIT TYPES Sn-W pegmatites. Sn skarn. Replacement Sn deposits

WEATHERING Cassiterite and wolframite in stream gravels. placer tin deposits. wolframite in soils (stolzite and tungstite may be weathering products)

GEOCHEMICAL SIGNATURE Sn. W. As. Mo. Bi. B. and elements characteristic of specialized granites (F. Rb. Be. Nb. Cs. REE)

EXPLORATION METHODS Geochemical sampling. tectonic setting studies (late to post-granitoids). geological mapping (blocks of pegmatites and quartz veins in soils)

8A

CHEMICAL ELEMENTS: Nb + Ta + REE + P + Th + U + Mo + Fe
DEPOSIT MODEL: CARBONATITE and ALKALINE ROCK - RELATED DEPOSITS

OCCURENCES - WORLD (Only Precambrian) Palabora (South Africa). Bukusu (Uganda). Quagssiarssuk (Greenland). Mountain Pass (USA). James Bay (Canada). Pechenga (Russia). Newania (India). Mabounie (Gabon). Mount Weld (Australia). Juquia (Brazil). Pilansberg (South Africa). Meponda (Mozambique). Nemegosenda (Canada)

OCCURENCES - GUIANA SHIELD Cerro Impacto (Venezuela). La Churuata (Venezuela). Kaituma (Guyana). Morro dos Seis Lagos (Brazil). Muri Mountains (Guyana). Acarai Mountains (Suriname). Bakhiu area (?) (Suriname)

TONNAGE and GRADE 16 Mt (min). 220 Mt (max). 60 Mt (ave): 0.18% Nb (min). 1.9% Nb (max). 0.58% Nb. 0.60% REE (ave)

GEOLOGICAL ENVIRONMENT Generally, elliptical concentric complexes consisting of sovites. ankerite carbonatites. fenites. ijolites. pyroxenites. dunites (carbonatites) and nepheline sodalite syenites. essexites. monzonites. alkali granites. diorites. hornblendites. pyroxenites (alkaline rocks): the complexes are the result of multiple stages of magmatic. deuteric and metasomatic crystallization: usually. the mafic ultramafic phases were emplaced during the early evolutionary stages: post-crystallization felsic (albitites. quartz porphyries) and mafic (camptonites. vogesites. monchiquites. tinguaites) dykes and sills are also reported: the complexes are from unmetamorphosed to high-grade metamorphic facies: sometimes. diatreme(?) breccia bodies of alkaline-carbonatite affiliation are reported in different parts of the Precambrian cratons. but their relationship with the ring complexes is not yet well understood: another category is represented by the "linear" carbonatites. which are schistosity-conformable sheets or screens enveloped by metamorphics that show evidence of alkaline metasomatism: they tend to be controlled by high-strain zones and could be either ductile deformed intrusive carbonatites or metamorphosed alkaline front metasomatites: age of the carbonatite/alkaline complexes ranges from Paleoproterozoic to Tertiary
TECTONIC SETTING Intracontinental hotspots. anorogenic magmatism
METALLOGENESIS Mineralogy: in carbonatites: apatite. magnetite. pyrochlore. barite. bastnaesite. pariste. chlorite. columbite-tantalite. monazite: in alkaline complexes: calcite. pyrrhotite. ilmenite. thorite. molybdenite. galena. sphalerite. hematite. zircon. rutile. monazite. orthite: Structure: disseminated and banded: Alteration: fenitization (widespread alkali metasomatism of quartzo-feldspathic rocks: mostly K-feldspar with some aegirine. barkevicite. sphene. apatite) near contact of carbonatite /alkaline intrusion: locally. chloritization. epidotization: Ore controls: commonly restricted to carbonatite/alkaline ring complexes. dykes. sills. breccias. sheets. and veins: Genesis: magmatic. metasomatic or both
ASSOCIATED DEPOSIT TYPES None. but the same tectonic environment as the diamond pipes (diatremes)
WEATHERING May result in goethite-rich laterites and aluminous laterites
GEOCHEMICAL SIGNATURE Anomalous values of Th. U. P. Nb. Y. Ce. La. Sm. Ba. Eu. Ti. Zn. Mo. Pb
EXPLORATION METHODS Radiometric anomalies. magnetic anomalies. high gravity anomalies: satelite imagery (ring complexes)

8B

CHEMICAL ELEMENT: C (DIAMOND)
DEPOSIT MODEL: DIAMOND-BEARING KIMBERLITE/ LAMPROITE PIPES

OCCURENCES - WORLD South African deposits. Ukukit (Russia). Seguela (Ivory Coast). West Australian deposits. Wyoming (USA). Lac Doré (Canada)
OCCURENCES - GUIANA SHIELD Guaniamo (Venezuela) and placer diamonds. The source of the diamonds is considered: 1. Roraïma Formation in Venezuela and Guyana: 2. Rosebel Formation/Upper Detritic Formation in Suriname and French Guyana. respectively: 3. from the Precambrian kimberlites in West Africa
TONNAGE and GRADE 2.5 Mt (min). 260 Mt (max). 26 Mt (ave). 0.072 carats/t (min). 0.88 carats/t (max). 0.25 carats/t (ave)
GEOLOGICAL ENVIRONMENT Kimberlite. olivine and leucite-bearing lamproites: breccias with inclusions of many rocks from mantle. basement and overlying sequences: lapilli tuff locally fills upper levels of diatreme: the rocks are believed to be hybrid ultramafic rocks of upper mantle origin:

diamond-related minerals in kimberlites are: pyrope. Mg-ilmenite. ulvospinel. Ti-rich phlogopite. yimengite. diopside. monticellite: the pipes have porphyritic igneous texture: age ranges from Archean (2.5 Ga) to Tertiary

TECTONIC SETTING Most pipes intrude cratonal areas: some intrude folded cover rocks that overlie deformed cratonal margins: pipes are not correlated with orogenic events but occur in areas of epeirogenic warping or doming and along major basement fracture zones

METALLOGENESIS Mineralogy: diamond. bort. and carbonado/amorphous carbonado: rarely troilite. pyrrhotite. pentlandite. mackinawite. and chalcopyrite: Structure: diamonds are sparsely disseminated as phenocrysts or xenocrysts in breccia: mined kimberlites yield from 0.1 to 0.6 ppm diamond: Alteration: serpentinization resulting in "blue clay" zones: silicification and carbonate alteration of country rock near pipe: rarely. alkalic metasomatism forming K-feldspar and Na-amphiboles: Ore controls: diamond distribution is irregular and restricted to kimberlite lamproite pipes and upward-flaring crater zones: Genesis: diamonds form in ultrapotassic upper mantle magmas (200 km depth). which are so rapidly transported to earth's surface that the diamonds do not revert to more normal surface forms of carbon. such as graphite. even with the reduction in pressure and temperature

ASSOCIATED DEPOSIT TYPES Diamond placers

WEATHERING Pipes weather rapidly to form circular topographic depressions

GEOCHEMICAL SIGNATURE Cr. Ti. Mn. Ni. Co. PGE. heavy minerals pyrope. phlogopite. and Mg-ilmenite indicate nearby pipes: lamproite pipes lack ilmenite

EXPLORATION METHODS LANDSAT or SLAR (determination of regional zones of tectonic weakness). detailed geochemical and mineralogical studies

REFERENCES

Banerjee. A.K.. and Moorhead. G.A.. 1971. Gold and Sulfide Mineralization in Guiana Shield. Guyana Geology and Mines Commission Report. 23 p.

Beurlen. H.. and Cassedanne. J-P.. 1981. The Brazilian mineral resources. Earth Science Reviews. v.17. p. 177-206.

Bliss. J. D.. 1992. Developments in mineral deposit modeling. U. S. Geological Survey Bulletin 2004. 168 p.

Bosma. W.. Kroonenberg. S.B.. Van Lissa. R.V.. Maas. K.. and De Roever. E.W.F.. 1984. An explanation to the geology of Suriname. Contributions to the geology of Suriname 8. Geologisch Mijnbouwkundige Dienst van Suriname. Medeling 27. p. 31-82.

Choubert. B.. 1974. Les precambriens des Guyanes. Mem. Bur. Rech. Géol. Min.. Paris. 81. 213 p.

Cox. D.P.. and Singer. D.A. (eds.). 1986. Mineral Deposit Models. U.S. Geological Survey Bulletin 1693. 379 p.

de Vletter. D.R.. 1984. Economic Geology and Mineral Potential of Suriname. Geologisch Mijnbouwkundige Dienst van Suriname. Mededeling 27. p. 91-129.

Gaal. G.. and Teixeira. J.B.G.. 1988. Brazilian Gold: Metallogeny and Structures. Krystalinikum. v. 19. p. 43-58.

Gibbs. A.K.. and Barron. C.N.. 1993. Geology of the Guiana Shield. Oxford Monographs on Geology and Geophysics no. 22. Oxford. Clarendon Press. 246 p.

Gray. F.. Cox. D.P.. Orris. G.J.. Page. N.. Wynn. J.C.. Brooks. W.E.. and Bliss. J.D.. 1993. Mineral resource assessment of the Venezuelan Guayana Shield. *In* Geology and mineral resource assessment of the Venezuelan Guayana Shield. *Edited by* U.S. Geological Survey and Corporation Venezolana de Guayana. Técnica Minera. C.A.. U.S. Geological Survey Bulletin 2062.

Groves. D.I.. Goldfarb. R.J.. Gebre-Mariam. M.. Hagemann. S.G.. and Robert. F.. 1998. Orogenic gold deposits: A proposed classification in the context of their crustal distribution and relationship to other gold deposit types: Ore Geology Reviews. v. 13. p. 7-27.

Hutchinson. R.W.. 1987. Metallogeny of Precambrian Gold Deposits: Space and Time Relationships. Economic Geology. v. 82. p. 1993-2007.

Kerr. D.J.. and Gibson. H.L.. 1993. A comparison of the Horne volcanogenic massive sulphide deposit and intracauldron deposits of the Mine sequence. Noranda. Quebec. Economic Geology. v. 88. 6. p. 1419-1442.

Kirkham. R.V.. Sinclair. W.D.. Thorpe. R.I.. and Duke. J.M. (eds.). 1993. Mineral Deposit Modeling. Geological Association of Canada Special Paper 40. 770 p.

Lacroix. J.. Daigneault. R.. Chartrand. F.. and Guha. J.. 1993. Structural evolution of the Grevet Zn-Cu massive sulphide deposit. Lebel-sur-Quevillon area. Abitibi Subprovince. Quebec. Economic Geology. v. 88. 6. p. 1559-1577.

Laznicka. P.. 1993. Precambrian empirical metallogeny. Precambrian lithologic associations and metallic ores. Developments in Economic Geology. v. 29. 1622 p.

MacDonald. J.R.. 1968. Guide to Mineral Exploration in Guyana. Geological Survey of Guyana Report. 91 p.

Meyer. H.O.. and McCallum. M.E.. 1993. Diamonds and their sources in the Venezuelan portion of the Guiana Shield. Economic Geology. v. 88. p. 989-998.

Milési. J-P.. Egal. E.. Ledru. P.. Vernhet. Y.. Thiéblemont. D.. Cocherie. A.. Tegyey. M.. Martel-Jantin. B.. and Lagny. P.. 1995. Les minéralisations du Nord de la Guyane française dans leur cadre géologique. Chronique de recherche minière. v. 518. p. 5-58.

Sawkins. F.J.. 1990. Metal Deposits in Relation to Plate Tectonics. Minerals and Rocks 17. Springer Verlag. Berlin. New York. 460 p.

Walrond. G.W.. 1980. A metallogenetic scheme for the Guyana Shield. In: Moreno. J.L.L. (ed.): Metalogenesis en Latinoamerica: Simposium Internacional. Mexico. p. 141-164.